Master Thesis, Department of Geosciences

Basin Modelling: HC Generation Modelling of the Åre, Melke and Spekk Formations, Haltenbanken Area

Amdad Ali

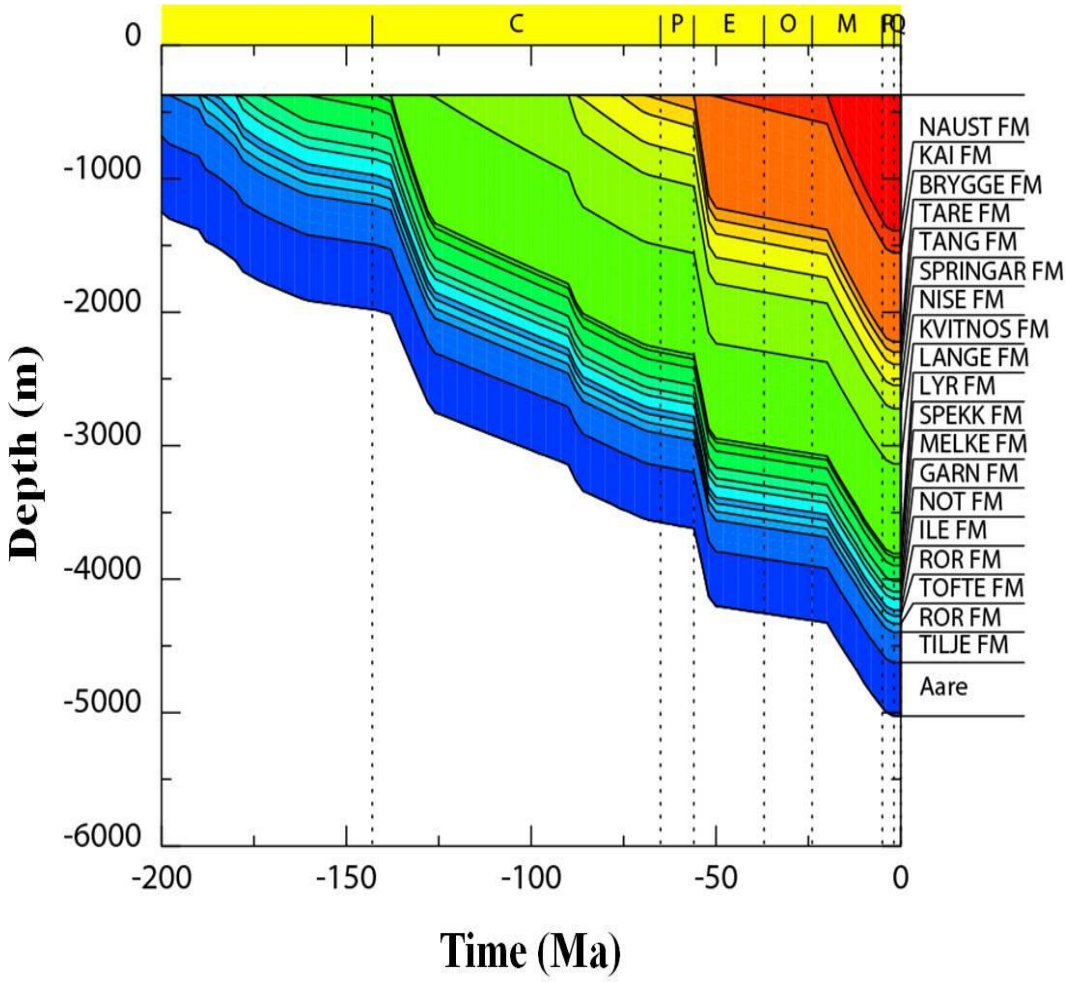

UNIVERSITY OF OSLO

FACULTY OF MATHEMATICS AND NATURAL SCIENCES

Basin Modelling: HC Generation Modelling of the Åre, Melke and Spekk Formations, Haltenbanken Area

Amdad Ali

Master Thesis in Geosciences

Discipline: PEGG

Department of Geosciences

Faculty of Mathematics and Natural Sciences

University of Oslo

February, 2012

Tutor (s): **Dag Arild Karlsen (UiO), Magnus Wangen (IFE)**
This work is published digitally through DUO – Digitale Utgivelser ved UiO
http://www.duo.uio.no
It is also catalogued in BIBSYS (http://www.bibsys.no/english)

Keywords: Basin Modeling, HC Generation, Haltenbanken, Kinetic Models, Burial History, Thermal History, HC Potential.

“All models are wrong but some are useful” - George Box

Abstract

The present study involves 1D basin modelling of two (2) wells from the Haltenbanken Area (the Midgard well 6407/4-1 and the Smørbukk well 6506/12-9S), by employing BAS software. The core objective is to estimate the minimum critical moments (timing of oil and gas generation and expulsion) for the Åre, Melke and Spekk formations, at these two locations, by reconstructing the burial and thermal histories, utilizing the formation thicknesses, age of horizons, geothermal gradients and other relevant parameters. It is furthermore, a target to evaluate if two common modelling tools in use provide the same or different time estimates. This study utilized two different kinetic modelling approaches i.e. the Pepper & Corvi model (1995) and the Tissot & Espitalie (1969 & 1975) model for the kerogen transformation. These modelling approaches are based on realistic source rocks' pre-exponential factors and distribution of activation energies.

It was found that both kinetic modelling techniques yielded similar results concerning the critical moments and the remaining potentials for the source rocks, but that the two models differ quite considerably concerning results for the expelled quantities of oil and gas.

According to modelling results (Case-1, Case-2, Case-3 *see section 5.9*), the Åre Formation started HC generation at the depth of 3200 m and is recently at the depth of approximately 5000 m. The time for oil generation in this formation was ca. 92 Ma b.p. at the Midgard location and 87 Ma at the Smørbukk location, which corresponds to Turonian – Late Cretaceous. Gas from this formation is estimated to start from ca. 30 Ma b.p. (Rupelian – Early Oligocene) for the Midgard location and at ca. 50 Ma (Ypresian – Early Eocene) for the Smørbukk location.

Furthermore, modelling results for the Melke Formation suggests HC generation at the depth of ca. 3200 m. This formation is currently at the depth of ca. 4200 m & 4100 m in the Midgard and the Smørbukk regions respectively. This formation is modelled to have started oil generation at ca. 47 Ma b.p. (at Midgard) and ca. 48 Ma b.p. (at Smørbukk), which corresponds to Lutetian – Middle Eocene time. Similarly, gas generation from this formation is estimated at ca.13 Ma b.p. (Serravallian – Middle Miocene) for the Midgard region and ca.20 Ma b.p. (Burdigalian – Early Miocene) for the Smørbukk region.

The current study suggests that the Spekk Formation has started HC generation at the depth of ca. 2900m, while at present this formation is at the depth of ca. 4200 m at the location of

the Midgard and the Smørbukk fields. This formation started oil generation at ca. 40 Ma b.p. that corresponds to the Bartonian – Middle Eocene time, in the Midgard field, while oil generation from the shales in the Smørbukk field took place at ca. 55 Ma b.p. (Ypresian – Early Eocene). Early Gas generation from the shales of this formation is estimated to have been initiated at ca. 10 Ma b.p. (Tortonian – Late Miocene) at the Midgard field and at ca. 25 Ma b.p. (Chattian – Late Oligocene) for the Spekk Formation at the Smørbukk field.

Another objective of the present work was to estimate the remaining source rock potential of these wells today. This study estimates 5% remaining potential for the Åre Formation while 40% - 50% reactive kerogen is computed to be left within the Melke Formation. Similarly, the present modelling argues that Spekk Formation has 40% - 55% remaining potential in the areas under investigation.

Bearing in mind the fact that both Midgard and the Smørbukk fields have received petroleum charges from down flank regions, which are buried deeper than the investigated formations in the trap themselves therefore, the current results provide minimum times for actual reservoir filling. Still, the relative time difference for HC generation in these three formations may still be applicable to the deeper “oil and gas kitchens”. It is outside the scope of this thesis, but still of interest that this residual potential may affect the cap rock properties of the structures, as continued generation of HC compounds could tentatively act to hinder the influx of petroleum products from the main reservoir.

Acknowledgements

I would like to acknowledge my supervisors Dr. Dag A. Karlsen and Dr. Magnus Wangen for their productive comments and necessary advices whose help, guidance, inspiration, and supervision from preliminary to concluding levels make this study possible. I am very grateful for their remarkable help and support.

During my Master studies at department of geosciences, I am grateful to all my lecturers in the section of Petroleum geology and Petroleum geophysics, most especially, Johan Peter, Knut Bjørlykke, Faleide Inge, Roy Gabrielson, Leiv Gelius, Jern, Nazmul Mondol, Jens Jahren and Michael Heeremans for their support, fruitful feedback and recommendations. I would always be indebted to you all.

I am grateful to IFE (Institute of Energy Technology), Kjeller for providing basin modelling software BAS (Basin Simulator) and Dr. Magnus for his Technical support. NPD (Norwegian Petroleum Directorate) is highly appreciated for free access to well and geochemical data.

At last, I would like to thank my family for their encouragement and all my friends at Geosciences department who backed to many interesting social and academic discussions, especially Waqas Ahmed (store Bror), Mujtaba Mongat (baby), Ahmed Salman (Salu bhai) and Muhammad Shafiq Goraya.

Technical Abbreviations Used in this Thesis

TOC = Total Organic Matter

HI = Hydrogen Index

OI = Oxygen Index

HC = Hydrocarbon

1, 2, 3-D = Dimensional

TTI = Time- Temperature Index

PVT = Pressure, Volume and Temperature

VR (%) = Vitrinite Reflectance

NPD = Norwegian Petroleum Directorate

GOGI = Gas Oil Generation Index

OM = Organic Matter

LLNL = Lawrence Livermore National Laboratory

S2 = Reactive Kerogen Content

GDE = gross depositional environment

GOR = Gas to Oil Ratio

Ma = Million Years Before Present

x = The amount of the reactant

t = Time

k = The Reaction Rate

K = The Reaction Rate Constant

A = The Pre-Exponential Factor or Frequency Factor

(Units are reciprocal time for uni-molecular reactions)

E = The Activation Energy

R = The Universal Gas Constant (1.987 cal/mol•K)

T = The Absolute Temperature (Kelvins)

Table of Contents

Chapter 1

Introduction

1.1 Basin Modelling – An Overview

Basin modelling is the forward modelling of geological processes of sedimentary basins in time and space. Basin modelling techniques are used to reduce petroleum exploration risk; commercially available basin modelling simulators are used to evaluate charge risk by integrating geological and engineering data into models of one or multiple petroleum systems active in the area of exploration. Basin simulations may be done from a single well to whole basin using multiple wells and pseudo wells (Welte et al., 1997).

1-D basin modelling deals with the single point in a basin such as a drilled well to determine the maturity history of one or several source rocks at the well location. However, 1-D basin modelling is unable to imply lateral variation in lithology, fluid flow, petro-physical parameters and calculation of charge volumes in a basinal sense, as no lateral parameter information is available. Nevertheless, assumptions can be made concerning the lateral variations in source rocks. On the other hand, 1-D modelling is easy to calibrate, easy to run and comparatively much economical (Hantschel & Kauerauf, 2009). 2D basin modelling is related to model a geological section (two wells minimum) which provides more detail than 1D modelling. 3D basin modelling is based on grid modelling. It is the most advanced form of basin simulations and is only used where enough data is available. It allows to areas based on structural constraint, 3D models allow calculating charge volumes and assessments of fetch or drainage area which is important in understanding charge at the prospect scale. 3D basin modelling is the most sophisticated approach for determining migration of HC (Hantschel & Kauerauf, 2009). 4D Basin Modelling (Space and Time) is a new development in basin modelling using space and time frame concept. Integrating space/time framework and 3D restoration modernizes basin modelling (Dutranois et al., 2010).

Every modelling approach has its own merits and demerits. Which modelling approach should be used either 1D, 2D or 3D entirely depends on time, budget, and data available and problem under consideration. For example 3D basin modelling is necessary if there is a need to model the flow of oil (Throndsen and Wangen, 1998; Wangen and Throndsen, 2003).

Organic basin modelling tries to address the hydrocarbon generation as resulting from heat effect on kerogen. The type of kerogen found in rocks is determined by the characteristics of the organic input to the paleo-basinal setting and the Eh and Ph conditions at the water/sediment interface. Key parameters of major significance to the modelling of generated oil and gas include total organic carbon content (TOC), the quality of the kerogen measured as hydrogen index (HI), kerogen type, primary & secondary cracking kinetics, activation energy distributions and adsorption coefficients etc. Petroleum Geochemistry is the application of geochemical practices in Hydrocarbon exploration, development and recovering oil and gas by studying origin, migration, accumulation and alteration (water washing, biodegradation, thermal alteration and deasphalting) of petroleum (Hunt,1996). Petroleum Geochemistry plays a significant role in understanding and modelling of organic facies and the resultant petroleum system. It serves to address various issues of basin modelling such as knowing the thermal maturation history of HCs and calibrating it with numerous geochemical and petrographic parameters on rocks as vitrinite reflectance data, rock eval data, apatite fission track data, fluid inclusion data and oils with biomarkers maturity parameters (Waples, 1994)

During current thesis project, 1D basin modelling is performed by using two wells from the Haltenbanken area of the Norwegian Continental shelf. In this study the modelling is also focused on geochemical aspects of petroleum generation. It is of great interest to know when oil and gas was generated in these regions. These two modelled wells are as mentioned taken from the Haltenbanken (Mid Norwegian Continental Shelf) area and represent the central part of the Halten Terrace. This region (Figure 2.1) is separated from the Trøndelag Platform to the East by the Kristiansund–Bodø Fault Zone and to the West the Haltenbanken High separates the deeper Møre–Vøring basin from the Halten Terrace. To the North the Halten terrace converts into a narrower Dønna Terrace and towards the South lies the narrow Klakk Fault Complex (Ehrenberg et al., 1992).

Basin modelling deals with simulation of geological processes that tend to unravel the geological history of a sedimentary basin. The starting point for the simulation is to account for the whole sequence of layers that have been deposited within the basin, through geological time, by forward modelling. Important geological processes include deposition, compaction, heat flow analysis, petroleum generation, expulsion, phase dissolution, migration, and accumulation (Hantschel & Kauerauf., 2009).

Basin modelling techniques have the capacity to calculate and model the following parameters but it is not limited to these:

• Timing of generation and expulsion of petroleum i.e. HC phases.

• Primary and secondary migration modelling.

• Probabilistic charge risking by estimating generated volumes of petroleum compared to lost volumes during migration and the trap sizes. Thus, a central question includes if generated volumes are enough to fill traps or not.

• Identification of key charge volume uncertainties.

• Source rock identification and quality assessment.

• Hydrocarbon phase prediction.

• Burial history and uplift modelling.

• Integration of geochemical, geophysical and geological datasets into the wider exploration work-scope.

1.2 Brief Review on History of Basin Modelling

1D basin modelling is generally referred to as maturity modelling (Waples, 1998). Maturity modelling started from the development of Tissot's kinetic model (1969), and Lopatain's TTI model (1971) was the initial step in integrating chemical and geochemical data with geology which leads to the prediction of maturity and HCs generation. Modelling of source rock maturity, often from mere a single seismic section and assumptions about source rock characteristics from – say onshore outcrop sections, delivers to geologists a new powerful tool for analysis of geological processes and in particular oil exploration. Using these methods, geologists were able to reconstruct the thermal and burial histories which further helped to understand the geological events from past to the present (Waples, 1998). During 1980's these methods lead to the most sophisticated 1D basin modelling further facilitated by advancement in computing capabilities (Waples, 1998).

The first basin modelling simulators (computer based) were developed in about 1980 (Yukler et al., 1978). The core idea included multiple 1D heat flow simulations and related geochemical models to evaluate source rock maturity for the purpose of constructing petroleum generation and expulsion maps. An imperative task was to evaluate and calibrate

the thermal histories during the geological basin's formation. Heat flow evaluation is one of the most researched problems in applied geo-engineering. After deducing the paleo-temperatures, chemical kinetics equations could be utilized to estimate the generation rate for petroleum generation. Another important aspect was the estimation of pore fluid pressures while thermal conductivities were determined by making use of compaction curves of sedimentary basin and their related porosity models. During this time, practical studies were done using 1D simulator, from singular wells as computational abilities were restricted and multiphase fluid flow for migration and accumulation of petroleum could not be applied. Hydrocarbon generation and expulsion was determined by using source rock maturity profiles utilizing temperature data from multiple wells. 1D modelling concepts are still in use, in particular when limited data is available during early exploration phases and when the project needs initial and quick interpretations (Hantschel & Kauerauf., 2009).

During the early 1980s, there were four schools of thoughts involved in developing basin modelling; the German, French, South Carolina and the Illinois schools (Hermanrud et al., 1991). The petroleum industry was introduced to the new generation of basin modelling simulators during 1990s. The most important features included the application of sophisticated fluid flow models with three phases: gas, liquid petroleum and water. Map based flow-path analysis and 2D Darcy flow models were appreciated in basin modelling commercial packages (Ungerer et al., 1990; Hermanrud, 1993). During this time, another important addition in basin modelling was the application of special geological processes such as halokinesis, refined fault behavior, diffusion, cementation, fracturing and igneous intrusions (Hantschel & Kauerauf, 2009).

During the post-1998 years, owing to rapidly increasing computing powers and reduced costs of computers a new generation of basin modelling simulators changed the work flow of basin modelling studies once again. Lots of new features were included related to reservoir characterization and petroleum migration. Simulators were more focused on 3D functions with upgraded model building and simulator tool performance. Three-phase-Darcy models were now available in 3D, while pore pressure and heat flow calculations were executed in full 3D which required the interpretation and mapping of complete set of horizons instead of just the top of horizons. Application of multi-component models resolved the problem of petroleum phases and development of fast thermodynamics PVT (Pressure, Volume and Temperature) controlled fluid analysis based on flash calculation for these components

became possible. Traditional two component (oil-gas) black model was replaced by four and fourteen fluid components (chemical species), which improved the understanding of reservoir composition and petroleum quality. Consequently, computing time was considerably reduced by combining computer hardware as PC clusters with parallelized simulators. Additionally, data for calibration, risk analysis for quantification of possibility for success or failure and the deliberation of extensional and compressional tectonics significantly increased the applicability of basin modelling. Integrated exploration workflow that incorporates basin modelling became a standard practice of the industry (Hantschel. & Kauerauf, 2009).

1.3 Future Trends in Basin Modelling

Basin modelling is a comparatively new discipline however, there is still room for improvements and more research. Some future trends in basin modelling will include further refinement and application of geological processes, development for incorporation of stress and strain data into basin modelling simulator that will improve the understanding of compaction and pore-pressure processes. Other important development in future basin modelling simulators could incorporate the use of seismic sections more directly into basin models. Direct incorporation of seismic data will decrease chances of error and improve the quality of models. Principles of up-scaling and attribute analysis should be developed (Hantschel & Kauerauf, 2009).

1.4 Software (Simulator)

BAS is combined tool for 1-D, 2-D and 3-D basin simulator for heat flow, time-dependent and paleo-fluid flow. It can compute sedimentary basin temperatures if basin is placed on the basement. BAS simulator calculate the following variables at each time step forward in time: Fluid flow potential , Fluid pressure , Hydrostatic fluid pressure, Excess pressure, Sediment pressure (effective vertical stress), Bulk pressure (lithostatic pressure), Porosity (as a function of pressure and temperature) , Volume fraction cement, Fluid flow (Darcy velocity), Temperature (in basin and/or basement), Heat flux , Absolute permeability, Heat conductivity, Vitrinite reflection (Lopatin and %Easy Ro) and Kerogen maturation etc.

BAS accounts for the varying sedimentation rate and laterally varying lithologies together with laterally varying boundary conditions such as surface temperature, surface fluid potential and basin/basement temperature or basin/basement heat flux. Geological processes like hiatus, erosion and sediment deposition are allowed at the top of basin simultaneously. In the model,

heat conductivity and permeability are porosity dependent that's why a variety of porosity, heat conductivity and permeability functions are implemented. BAS works forward in time and formation thicknesses are given as primary input data which can be reproduced from computed porosities combined with computed net thicknesses (Wangen, 2002).

1.5 Aim of Study

This master thesis project is a 1D basin modelling study of two (2) wells from the Haltenbanken Area, by employing BAS (Basin Simulator, IFE) software. Modelling work and software training was done at the Institute of Energy Technology (IFE), Kjeller. The purpose of this study includes:

i) To learn and understand the basics of basin modelling with respect to HC generation.

ii) To accomplish1-D modelling of two wells (the Midgard 6407/4-1 and the Smørbukk 6506/12-9S) from the Haltenbanken by reconstructing the burial and the thermal histories utilizing the formation thicknesses, age of horizons, geothermal gradients and other relevant parameters.

iii) Estimation of critical moments (timing of HC generation and expulsion) for each source rock (Åre Formation, Melke Formation & Spekk Formation) are investigated based on realistic source rocks' pre-exponential and activation energy distributions.

iv) To estimate the remaining hydrocarbons potential for each source rock in the study area.

v) Analysis of the critical moments for the Spekk, the Melke and the Åre formations in two wells to constrain the differences in source rock maturation at both locations. Besides estimating the critical moment for each formation, analysis is also carried out to examine the differences in timing of HC generation for the Smørbukk and the Midgard areas.

vi) This study utilized two different kinetic modelling approaches i.e. the Pepper & Corvi (1995), and the Tissot kinetic modelling approach as adopted by Forbes et al. (1991). The target is to evaluate if these two methodologies results in similar or significantly different results. This necessitates a comparison between the results obtained from two methods with already published data.

In the previous studies, the Melke Formation was not considered as a major source rock in the Haltenbanken Petroleum Province (Heum et al., 1986), and it is generally ignored despite its overall high TOC content. However, it may have provided some contribution in the prevalent petroleum system (Mo et al., 1989 & Forbes et al., 1991 etc). This formation is reasonably organic rich, with ca. 1-4% TOC as per NPD (Norwegian Petroleum Directorate in the two wells under investigation, the Midgard 6407/4-1 & the Smørbukk 6506/12-9S). TOC (%) value greatly exceeds the 0.5% value traditionally cited as minimum for world class source rocks (Tissot and Welte, 1984). Thus, TOC value of the Melke Formation within this range is classified as "good to very good" source rock (Peters and Cassa, 1994). It is possibly correct to say that the significance of the Melke Formation had been overlooked to some extent due to presence of the very prolific Spekk Formation, and that this formation may have contributed to reservoir charges or petroleum in the migration avenues. During the present study, based on considerable TOC (%) content the Melke Formation has been modelled separately for hydrocarbon generation.

Similar is the role of the coals (coals contain minimum 50% TOC) in the Åre Formation debated in terms of oil and gas genesis (Karlsen et al., 1995; 2004, Karlsen and Skeie, 2006), but it is more than likely that the coals could have contributed at least gas plus condensate to the overall migration system and traps. The main question is when, and to what extent?

1.6 Organization of the Study

The present study has been divided into seven parts (chapters 1-7 and finally conclusions) (Figure 1.2). All these parts are mutually connected and they together lead to the final conclusion in assessing the timing of HC generation for each source rock, its remaining potential and comparison between both locations by making use of different kinetic models simultaneously.

Chapter 1 deals with the introduction to basin modelling and the aim of the present study (Figure 1.2). Chapter 2 encompasses a review on geology of the study area (the Haltenbanken Petroleum Province). A general review of the petroleum system of Haltenbanken Area together with the petroleum system event chart based on the current study is dealt with in the chapter 3 (Figure 1.2).

Chapter 4 comprises of the burial and thermal history modelling along with their main data input. Additionally, this chapter also deals with the VR (%) calibration that was carried out to

adjust the modelled results according to the published data. Similarly, geochemical and kinetic input data that has been used to infer the timing of HC generation is explained in chapter 5 (Figure 1.2).

An uncertainty analysis has been discussed in chapter 6. The various results have been dealt with in detail and finally conclusions based on these results are presented in chapter 7 (Figure 1.2).

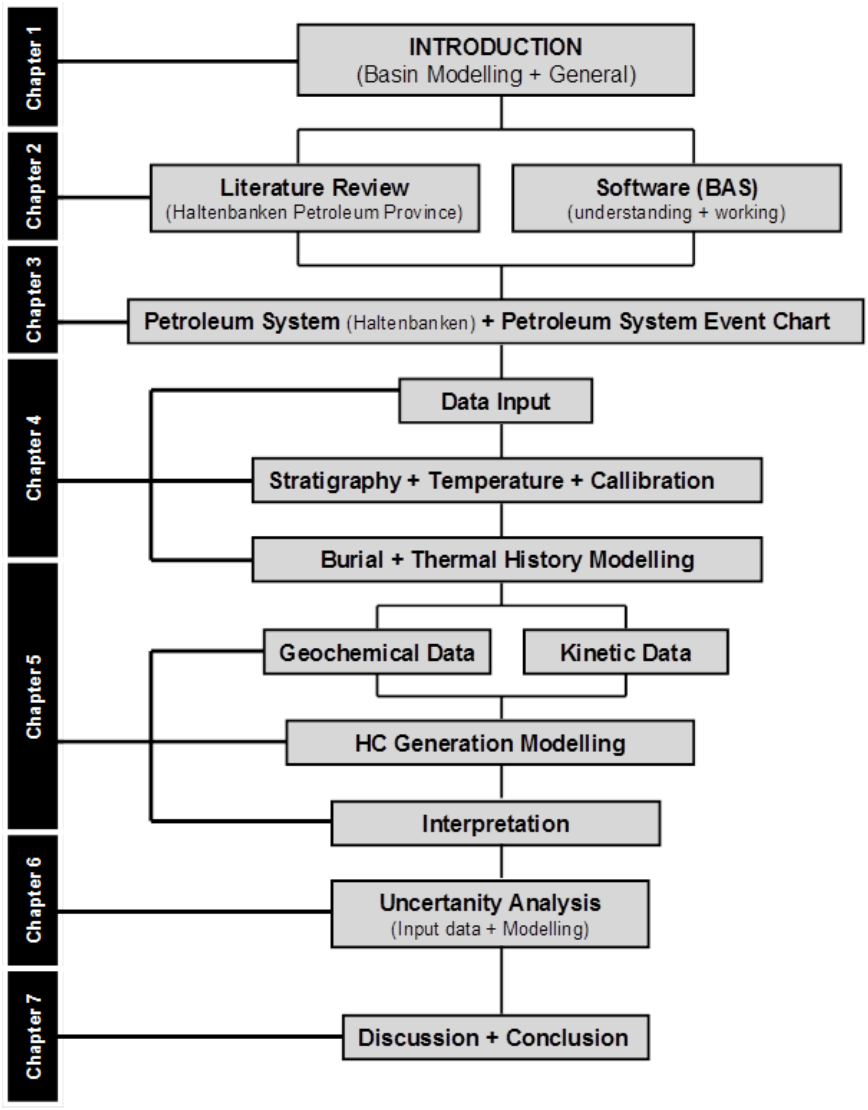

Figure 1.2: Organization chart for the current study representing sections and subsections which together constitute chapters of this study (chapter 1 - 7).

Chapter 2

Geological Settings

2.1 Brief Exploration History of the Haltenbanken

The study area is located in the Haltenbanken Petroleum Province on the mid Norwegian Continental Shelf. During the fifth concession round in 1980, two exploration licences (blocks 6507/11 and 6507/12) were opened for exploration in this area and Saga Petroleum (Statoil) made the first discovery (6507/11-1, gas/condensate, the Midgard field) in 1981 (Ehrenberg et al., 1992; Karlsen et al., 1995). Three more exploration licenses 6407/1, 6407/2 and 6507/10 were awarded in 1982 for exploration.

In 1979, a seismic grid with 2km line spacing was acquired which covered block 6506/12 (Smørbukk field lies within this block). After data processing, this particular area was evaluated in 1980 and then revaluation was carried out in 1983 by the Statoil. This block however, was awarded in March 1984 under the eighth concession round. In 1984, a second seismic survey was shot with 1km line spacing in order to fill in the gaps of the previous survey. Data from the older survey was reprocessed to coincide with new data in order to have the final grid spacing of 1 km. During 1988, a 3D seismic survey was carried out over a structure later to be named the Smørbukk field, which resulted in gas/condensate discovery from multiple reservoir intervals (Ehrenberg et al., 1992). Today, the Halten terrace and the Dønna region is one of the mature and highly productive HC provinces on the Norwegian Continental Shelf.

2.2 Tectonic Framework and Structural Settings

The central part of the Haltenbanken region, the Halten Terrace is separated from Trøndelag Platform to the East by the Kristiansund–Bodø Fault Zone. Towards the West, the Haltenbanken High separates deeper Møre–Vøring basin from the Halten Terrace and the Halten terrace converts into a narrower Dønna Terrace in the North. Towards the South lies the narrow Klakk Fault Complex (Figure 2.1) (Ehrenberg et al., 1992).

The Haltenbanken region is a highly faulted, tectonically induced basin with major faults showing oblique–slip (Figure 2.1) (Gabrielsen et al., 1984; Bøen et al., 1984; Bugge et al., 1984; Buckovics and Ziegler 1985; Karlsen et al., 1995). Structurally, the Haltenbanken province is — made up of N-S to NNE-SSW striking faults with NNW-SSE trending faults

making horst and graben structures (Figure 2.1) (Hollander et al., 1984). The Haltenbanken Petroleum Province is situated on a passive rifted continental margin which is overprinted on the older structural elements formed during the Caledonian Orogeny between Greenland and Fennoscandian cratons (Buckovics and Ziegler 1985; Karlsen et al., 1995).

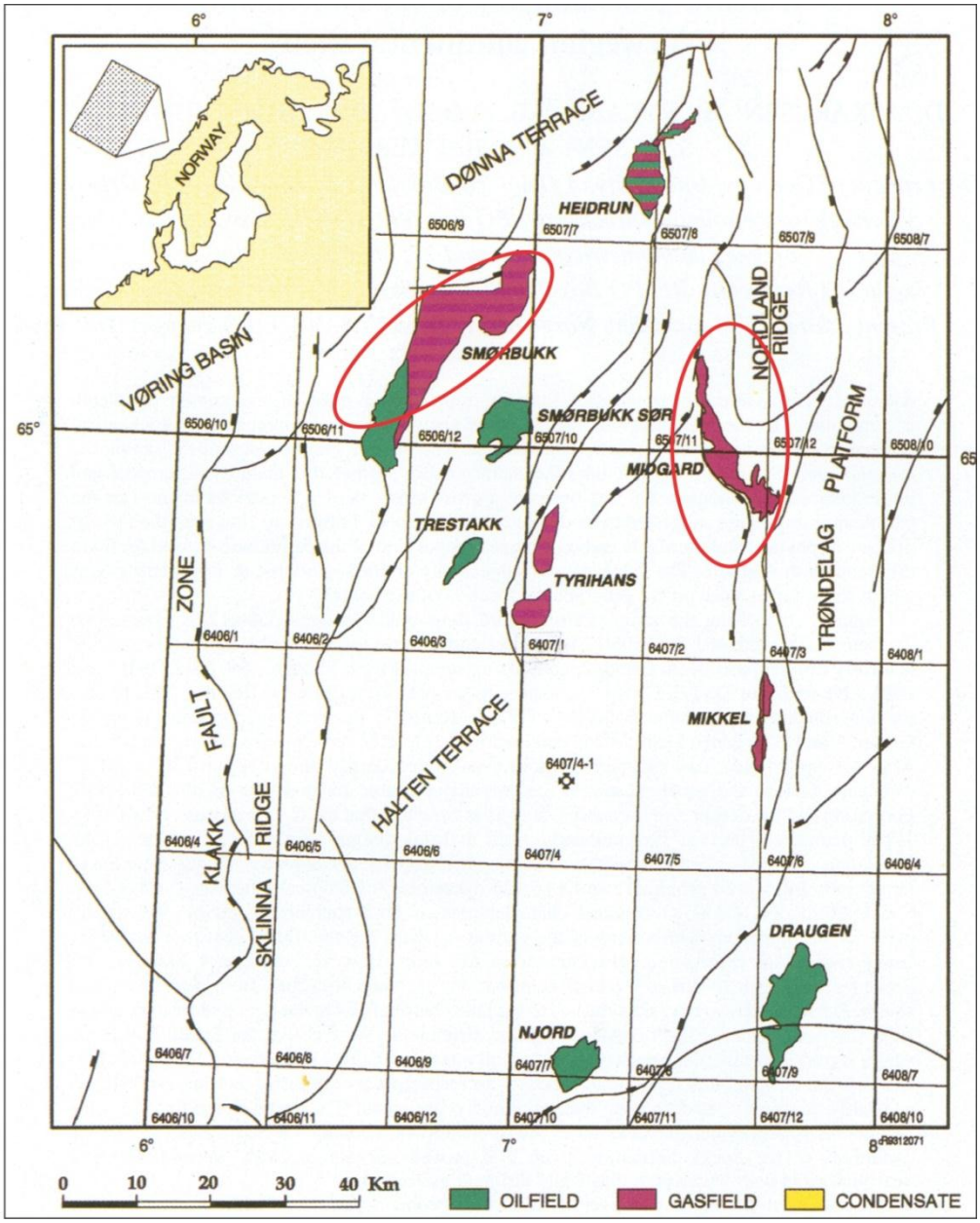

Figure 2.1: Structural elements map of the Haltenbanken area showing some of the major HC accumulations. Red circles point to the location of the study area (modified from Karlsen et al., 1995).

According to Ehrenberg et al. (1992), major tectonic events of Haltenbanken area may be summarised in the following chronological order: First a crustal extension episode experienced by this area belongs to the early Permian, recorded by N-NW trending basement that is onlapped by seismic reflections representing the Triassic succession. Continental strata were deposited on both the Haltenbanken and the Trøndelag Platform during the middle Triassic to the earliest Jurassic (Figure 2.2). The second rifting phase is observed throughout the Halten terrace during the early Jurassic that resulted in down-to-the-west growth faulting, oriented in NNE direction. This area experienced regression during the middle Jurassic, which is also considered as a tectonically dormant period. Since the middle Jurassic to the early Cretaceous, a major transgression started which resulted in the deposition of marine shales with lean organic content (the Melke Formation) followed by deposition of an organic rich source rock (the Spekk Formation). A regional rift-related extension occurred during this period resulting in the formation of tilted fault blocks and horsts that contain most of the HC accumulation of this area. The Haltenbanken and the Trøndelag Platform underwent rapid subsidence from late Pliocene while during the same time, mainland Norway experienced uplift and erosion due to the isostatic adjustment (Ehrenberg et al., 1992). However, deposition during the Pliocene-Quaternary resulted in further deepening and higher temperatures of the strata over the entire Haltenbanken area. This further enhanced the thermal cracking of the kerogens and subsequent expulsion and migration from the source rocks (Ehrenberg et al., 1992).

2.3 Stratigraphy

Sedimentary succession ranging from the Triassic to the Quaternary has been deposited and preserved in the Haltenbanken Petroleum Province (Figure 2.3), which is briefly discussed below:

2.3.1 Triassic

Continental strata were deposited over the Halten Terrace and the Trøndelag Platform during the middle Triassic to the early Jurassic period. This sedimentary package includes two evaporite formations, Red Beds overlain by coal bearing delta-plain clastic deposits of the Åre Formation (Ehrenberg et al., 1992, Whitley, 1992).

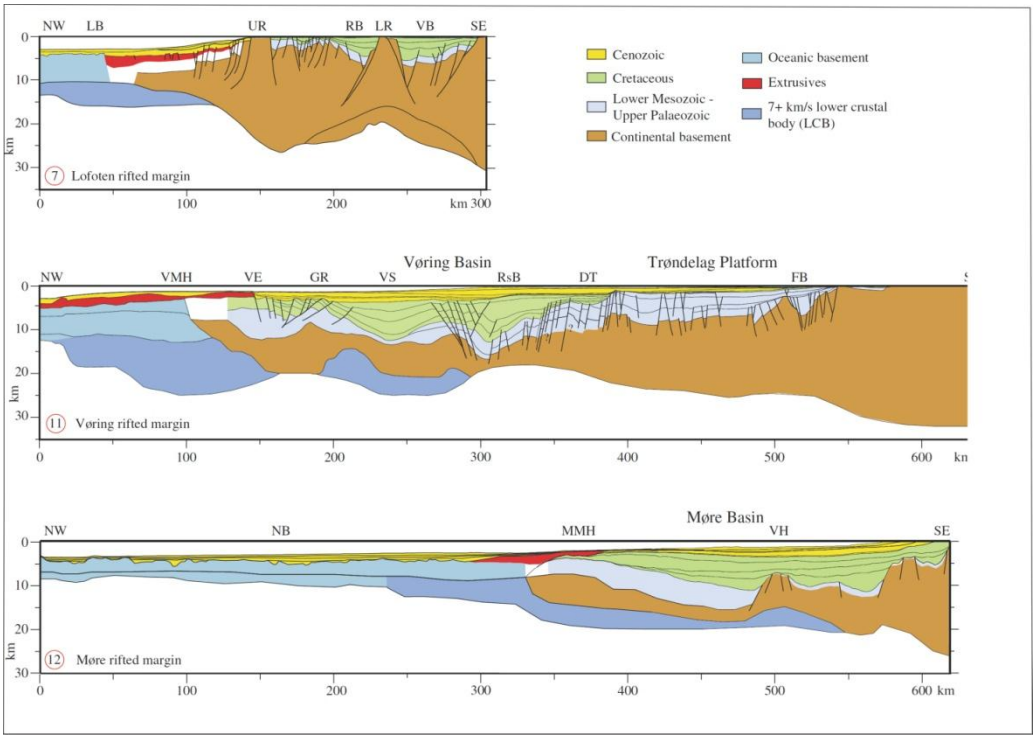

Figure 2.2: Regional transect across mid Norwegian Continental Margin (adapted from Faleide et al., 2008).

2.3.2 Lower Jurassic

Lower Jurassic is represented by Båt Group which is comprised of following three formations:

1) Åre Formation
2) Tilje Formation
3) Ror Formation

The Åre Formation constitutes shales, coals and sandstone units and represents a fluvio-deltaic depositional environment. This formation also represents two hiati; however, the Triassic sequence of this formation is believed to be in conformable contact with the overlying Jurassic strata. Similarly, some marine input is documented in the upper part of this formation. Coaliferous part of Åre Formation is believed to have huge hydrocarbon source potential (Heum et al., 1986; Forbes et al., 1991). However, it is assumed to be a gas-prone source rock due to the coaly kerogen but a little oil generating potential cannot be ruled out (Whitley, 1992). According to Karlson (1984), the reservoir quality of this formation is stated as poor due to extremely low sand content.

The Tilje Formation overlies the Åre Formation and consists of cyclic shale/mudstone and sand units; however, sand content considerably improves upward from the bottom (Heum et al., 1986). The Ror Formation overlies the Tilje Formation and consists of an upward coarsening sequence. Marine shales/mudstone and sand units are predominant lithologies within this formation and storm-generated laterally extensive sedimentary structures are also present (Ehrenberg et al., 1992; Provan, 1992).

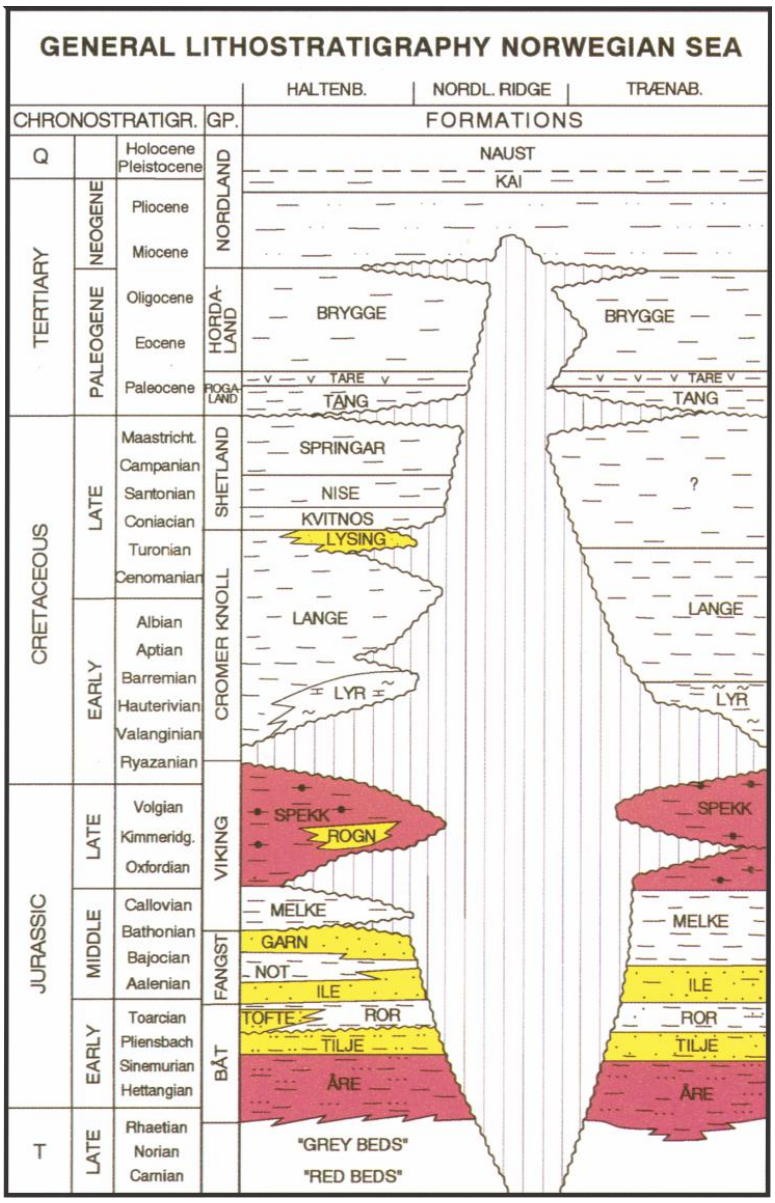

Figure 2.3: Generalized stratigraphy and terminology of the Haltenbanken region. Proposed source rocks and the main reservoir formations are indicated (modified from Karlsen et al., 1995).

2.3.3 Middle Jurassic

Fangst Group represents the middle Jurassic sedimentary succession and consists of the following formations:

1) Ile Formation
2) Not Formation
3) Garn Formation

The Ile Formation is dominated by stacked bar sand deposits which are separated by thin marine shale intervals which reduce in thickness towards NE. This formation is believed to be deposited in the shallow marine offshore to coastal environment in wave and tide dominated areas. This formation represents good quality reservoir rock (Provan, 1992).

The Not Formation consists of shales at the base that grades upward into bioturbated siltstones (Ehrenberg et al., 1992). Sandstones at the top of this formation becomes progressively micaceous and the depositional environment is interpreted to be lagoon or sheltered bays for the basal part and deltaic to coastal environment for the upper part (Dalland et al., 1988).

The Garn Formation is represented by thick, uniform sandstone interval which becomes thinner towards the central and the northern part of the Halten Terrace. This formation is considered as an important reservoir rock with good to excellent reservoir rock properties (Heum et al., 1986).

2.3.4 Upper Jurassic

This age is represented by the Viking Group which consists of following formations:

1) Melke Formation
2) Spekk Formation
3) Rogn Formation

The Melke Formation is comprised predominantly of the shales with intercalated silt and / claystone while some sporadic sandstone layers and carbonate cemented horizons are also found. An open marine below wave-base, depositional environment is assigned to this formation. The Melke Formation is reasonably organic rich (ca. 1-4% TOC), but it is not considered as a source rock in the Haltenbanken Area (Heum et al., 1986). Still, TOC values in this range are worldwide considered as “good to very good” (Peters and Cassa, 1994) and it is quite possible that the significance of this formation as a source rock is overlooked due to

the existence of the very prolific Spekk Formation in this region. This is in part why this study also focused to model the hydrocarbon generation from the Melke Formation.

The Spekk Formation unconformably overlies the Melke Formation and is bounded by the unconformities (Figure 2.3). This formation is chronostratigraphical equivalent of the Draupne Formation and the Kimmeridge Clay of the North Sea. This is considered as an important source rock bearing oil generation potential (Hollander et al., 1984; Heum et al., 1986; Karlson et al., 1984), with the TOC values ranging between 6-8% (Karlsen et al., 1995). Depositional environment is interpreted as stagnant bottom water conditions (Provan, 1992).

The Rogn Formation consists of coarsening upward sequence from shales, siltstones to the sandstones towards the top. Upward decrease in clay and mica content contributes toward the good reservoir quality. Depositional environment is interpreted to be shallow marine sand bar deposits (Ellenor & Mozetic, 1986; Dalland et al., 1988).

2.3.5 Cretaceous

During the Cretaceous, thick marine shales with thin carbonate and sandy intervals were deposited throughout the Haltenbanken Area under rapid subsidence (Ehrenberg et al., 1992; Whitley, 1992). The Cretaceous period at the Haltenbanken is represented by two major groups:

1) The Cromer Knoll Group.
2) The Shetland Group.

These groups are further subdivided into various formations. Depositional environment assigned to all the formations belonging to this period is transgressional marine. Shales and mudstones onlapping against the Cimmerian structures are common (Whitley, 1992).

2.3.6 Tertiary

Tertiary period is represented by two main groups which are:

1) The Rogaland Group.
2) The Hordaland Group.

Lithologically, these groups comprises of thick marine shales which are separated from the shales of upper Cretaceous by a regional unconformity (Heum et al., 1986).

2.3.7 Quaternary

Rapid subsidence occurred through the late Pliocene to the Quaternary period which resulted in the formation of poorly sorted, glacio-marine clastic sedimentation of Naust Formation. This formation consists of alternating layers of gray shales and poorly sorted sands (Ehrenberg et al., 1992).

Chapter 3

Petroleum System

A "Petroleum system" is a geologic system that encompasses the HC source rocks and all related oil and gas and which includes all of the geologic elements and processes that are essential if a HC accumulation is to exist (Magoon & Dow, 1994). In order to have a vivid understanding of the origin and environment of hydrocarbons, the essential components such as investigation of sedimentary basins, petroleum systems, play and prospects are required (Figure 3.1). These can be viewed as separate levels of investigation (Magoon and Dow, 1994). The stratigraphic sequence and structural style of sedimentary strata is defined by the sedimentary basin investigation. A petroleum system consists of a natural system that incorporates a pod of source rock (active or depleted) and all the related oil and gas (Magoon and Dow, 1994) and the relevant geologic elements and processes which are vital for hydrocarbon accumulation to exist (Magoon, 1988; Magoon and Dow, 1994). These two levels of investigation are independent of the economic considerations as compared to the play and the prospect evaluations (Figure 3.1) (Magoon and Dow, 1994). The term *Petroleum* constitutes either (1) thermal or biogenic gas found in conventional reservoirs or gas hydrate, tight reservoirs, fractured shale and coal; or (2) naturally occurring crude oil, condensates and asphalts. The term *system* depicts the elements (source rock, reservoir rock, seal rock and overburden rock) which are independent and processes (trap formation and generation-migration-accumulation of petroleum) that form the practical unit which creates the hydrocarbon accumulations (Magoon and Dow, 1994).

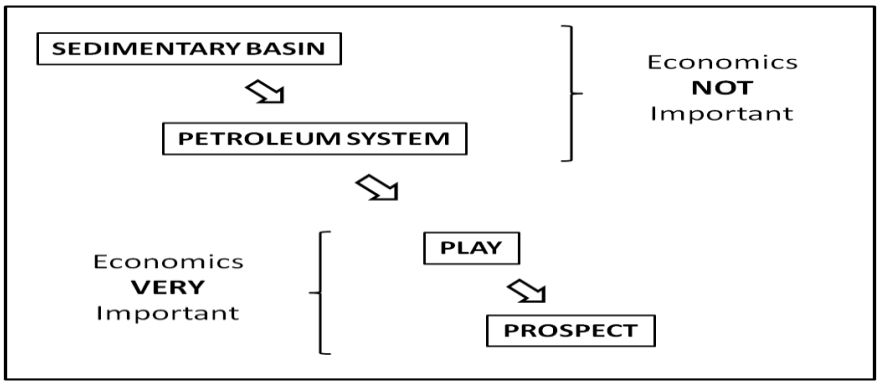

Figure 3.1: Different levels of hydrocarbon investigation (modified from Magoon and Dow, 1994).

2.1 History of the Petroleum System

The habitat of HCs has been explained through early research in organic geochemistry by Trask and Wu (1930), Triebs (1936), Hunt and Jamieson (1956) and Phillipi (1957), in which they identified ways to map and measure the source rock and associated products (Magoon and Dow, 1994). Dow (1974) separated a play from the oil system as a distinguished unit based on the geochemistry. Ulmishek (1986) distinguished the (independent) petroliferous system from a play and the sedimentary basin. Magoon (1989b) postulated different levels of petroleum investigation as sedimentary basin investigation, petroleum system, play and prospect (Table 3.1) (Magoon and Dow, 1994).

Table 3.1: Factors' comparison in the four levels of petroleum system investigation (modified from Magoon and Dow, 1994).

Factor	Sedimentary Basins	Petroleum System	Play	Prospect
Investigation	Sedimentary rocks	Petroleum	Traps	Trap
Econimics	None	None	Essential	Essential
Geologic time	Time of deposition	Critical moment	Present-day	Present-day
Existence	Absolute	Absolute	Conditional	Conditional
Cost	Very low	Low	High	Very high
Analysis and modeling	Basin	System	Play	Prospect

The term "Petroleum System" is used following Dow (1974) and its inimitability comes from the petroleum-source rock correlation. Since "Petroleum" refers to all forms of hydrocarbons (solid, liquid or gas) (Levorsen, 1967) and the term "System" explains the mutual relationship between the essential elements (source rock, reservoir rock, seal rock and overburden rock) and the processes (generation-migration-accumulation of petroleum and trap formation), therefore the term *petroleum system* has been devised. Previously, the name "petroleum system" has been used by Perrodon (1980, 1983 a,b) and Perrodon and Masse (1984) and the term "*essential elements"* was put forward by Meissner et al. (1984) and Ulmishek (1986). These researchers also formalized the term "*processes"*.

2.2 Components of a Complete Petroleum System Study

Magoon and Valin (1994) have summarized the components of a complete petroleum system study in the form of a table (Table 2). However, it is not essential to follow all these components in every study (Magoon & Valin , 1994).

Table 3.2: Components of a complete petroleum system study (modified from Magoon & Valin, 1994)

Figure or table	Information required	Purpose
Map	Locate Petroleum fields included in system. Indicate whether oil or gas. Indicate surface and subsurface oil or gas shows included in system. Indicate direction of Petroleum migration and indicate distribution of POD of active source rock.	Geographic extent of a petroleum system at critical moment shown by circumscribing the pod of active source rock and the outer limit of migrated hydrocarbons. Source rock name from pod of active source rock and Petroleum system burial history chart location
Table	List all oil or gas fields by petroleum system indicate discovered reserves and in-place petroleum by stratigraphic unit trap type reservoir rock name, age, and lithology and seal rock name, age, and lithology For oil field indicate GOR, API gravity, sulphur content, and Pr/Ph ratio and For gas field indicate GOR, $\delta^{13}C$, and $C_1/C_2+ C_3$ ratio.	In-place petroleum for mass balance calculations reservoir rock name from that reservoir with the heights percentage of in-place petroleum. Seal rock most common occurring in trap and oil or gas province from average GOR.
Cross section	Structural stratigrahic information such deformation style and rock units indicate oil window and gas window indicate petroleum shows and accumulations draw at critical moment and indicate direction and conduits for petroleum migration	Stratigraphic extent of petroleum system at the critical moment by identifying the base of the pod of active source rock or base of hydrocarbon column, whichever is deeper Geographic extent of petroleum system pod of active source rock shown overburden rock shown and petroleum system burial history chart location
Burial history chart	Stratigrahic units penetrated in well time rock – units work deposited thickness of rock units Names of rock unit Lithology of rock units Present day thermal maturity profile Present day Geothermal gradient Computer programme to determine time and depth for oil window and gas window and indicate essential elements of petroleum system	Petroleum system events chart information determine from chart, such as onset and end (at uplift) of petroleum generation , and critical moment Essential elements of petroleum system shown oil window depth for cross section at critical moment and Gas Window depth for cross section at critical moment
Events Chart	Age of essential elements of petroleum system Onset and end of trap formation Onset at end of petroleum generation, migration, accumulation Preservation time of petroleum system and critical moment	Petroleum system events chart summarizes in one diagram the essential elements and processes of the system, as well as the preservation time and critical moment.
Petroleum-petroleum correlation	Geochemical evidence, such as bulk properties, biological markers, and isotopic data to show that more than one petroleum accumulation came from the same source rock (but not necessarily the pod of active source rock)	Geographic and stratigraphic extent of a petroleum system is established with this geochemical correlation in concert with the structure and stratigraphy of the pod of active source rock and the adjacent traps
Petroleum- source rock correlation	Geochemical evidence such as biological marker and isotopic data, to indicate a certain petroleum originated from a specific source rock	Level of certainty is established using geological and geochemical evidence and indicates the confidence that a specific source rock expelled a given petroleum
Mass balance calculation	TOC and rock-Eval pyrolysis source rock density and volume of pod of active source rock	Mass of petroleum generated to determine petroleum system generation-accumulation efficiency (GAE).

2.3 Petroleum System of the Haltenbanken Area

2.3.1 Source Rocks

Three main organic-rich source rocks have been identified in this region which are Spekk, Melke and Åre formations of the Jurassic period (Karlsen et al., 2004; Karlsen & Skeie, 2006).

2.3.1.1 Åre Formation

The lower Jurrasic Åre Formation is considered over-mature in the western part of the Haltenbanken (Vøring Basin) and immature toward the East where the Trøndelag Platform is located (Figure 2.1). The Åre Formation reached peak oil generation during the early Tertiary in the Halten Terrace area (Campbell & Ormamassen, 1987; Karlesen et al., 1995). The coal and shales of this formation have produced around 135 kg of petroleum per tonne (gas≈30%, condensate≈50%, oil≈20%) of rock throughout it burial to ca. 4% vitrinite reflectance (Heum et al., 1986). The Åre Formation is considered as immature in the adjoining areas of the Midgard and Draugen fields (Karlsen et al., 1995). The Gas Oil Generation Index (GOGI) of this formation is around 0.33±0.06 (n=5) that gives rise to "mixed oil and gas" (Cohen and Dunn, 1987).

Some researchers consider the oil potential of the Åre formation to be of importance at least at the local level (Heum et al., 1986). According to Mo et al. (1989), the quantitative importance of Åre Formation is more than the Spekk Formation in terms of oil generated in the drainage area of the Midgard Field (about 6.5 times). They made an assumption that cracking to gas (condensate) in deeper parts, owing to rapid burial during the last 3.5 M.Y.b.p. is attributed to the slow pace of the generated oil. Mo et al. (1989) did the maturity modelling of this formation and proposed that the peak oil generation occurred in the deepest part of the basin during the late Cretaceous. There is a strong likelihood that the generation continues still today in the gradually subsiding basin flanks towards the Midgard Horst (laterally migrating oil kitchen) (Karlsen et al., 1995).

2.3.1.2 Melke Formation

Melke Formation comprises predominantly of the shale intervals with intercalated silt and claystone while some sporadic sandstone layers and carbonate cemented horizons are also found. Its thickness varies from 44 m to 116.5 m at the reference wells and this formation

belongs to the Bajocian to Oxfordian age (NPD data). Open marine below wave-base depositional environment is assigned to this formation. Melke Formation is reasonably organic rich (ca. 1-4% TOC) and it is considered as a good example of a lean source rock. Upon attaining approximately 1.7% VR, this formation expelled mainly gas (Heum et al., 1986; Karlsen et al., 1995).

The oil potential of the Melke formation is insignificant as compared to the Spekk Formation and the deeper Åre Formation (Heum et al., 1986; Cohen et al., 1987). It is believed to have expelled not more than 1.5 kg of petroleum per ton of rock (mainly gas C_{5-} and some condensate C_{6-}-C_{14}) as compared to the 30-35 kg of petroleum per ton of rock (gas≈15%, condensate≈45%, oil, i.e. C_{15+}≈40%) expelled by the Spekk Formation (Heum et al., 1986). However, there is still a strong possibility that the oil potential of the Melke Formation may show lateral variation towards the mid Norway Continental Margin and further systematic investigation on facies variation is required especially from deeper parts of the basins where the formation may have developed as "anoxic ponds" (Karlsen et al., 2004). Still, the TOC values in this range are globally considered as "good to very good" (Table 5.2) (Peters and Cassa, 1994) and it is quite possible that the previous workers have overlooked the significance of this formation due to the existence of the very prolific Spekk Formation. In the present study, an attempt to model the hydrocarbon generation of Melke Formation is carried out to understand its generation potential and contribution to the reservoired HCs if any.

2.3.1.3 Spekk Formation

The Spekk Formation belongs to the late Jurassic age and has an accumulated thickness of about 400 m in undrilled structural depressions. This formation has a mature rating in the areas of Haltenbanken where most of the hydrocarbon accumulation has occurred and is considered immature in the eastern platform area (the Trøndelag Platform). Towards the west (i.e. the Vøring Basin), this formation is rated as over-mature (Karlsen et al., 1995). Peak oil generation is considered to have reached during the late Tertiary in the Halten Terrace (Campbell and Ormaasen, 1987).

According to Leadholm et al., (1985), peak oil generation is estimated to have occurred at the 3400 m burial over large areas of Haltenbanken Province. Cohen and Dunn (1987) evaluated the initial oil expulsion to have occurred at ca. 120^{o}C, which corresponds to a burial depth of 3100 m in their data set. On the basis of vitrinite reflectance equivalence (VR), Heum et al., (1986) proposed the threshold for primary migration to a maturity value of 0.7%. This is

equivalent in their dataset to ca. 3900 m depth. Cohen and Dunn (1987) estimated this depth to be related with the initial oil to gas cracking (T≈150^{o}C) and a depth of ca. 4600 m is postulated as the initial refractory gas generation depth. Similar depth of approximately 4700 m has been inferred by Heum et al., (1986) for the deepest limit of oil generation at 1.0% VRE (Karlsen et al., 1995). Biomarker distributions from core sample of the Spekk Formation have been studied by Karlesn et al., (1995) and they suggest that substantial oil expulsion has occurred at a depth shallower than 3900 m.

2.3.2 Reservoir Rocks

Major reservoir rocks of the Haltenbanken region belong to the early and middle Jurassic age. These are the sands of Åre, Tilje, Tofte, Ile and Garn Formations that have alternating sandstones and shale layers (Bjørlykke, 2010). These formations belong to the Jurassic Fangst Group and the Båt Group e.g. the Smørbukk and the Heidrun fields' reservoir belong to the Fangst Group and the Njord field's reservoir belongs to the Båt Group. An exception to this trend is the late Jurassic sandstones of the Rogn Formation which is an important reservoir unit in Haltenbanken area e.g. Draugen Field (Karlsen et al., 1995).

2.3.3 Hydrocarbon Traps

In this region major HC traps are structural in origin and belong to the Jurassic age rotated fault blocks in horst and graben system of the Halten Terrace (Bjorlykke, 2010). These horst and graben structures are the result of extensional faulting during the Kimmerian phase. There are also salt induced structures that are believed to have formed over the Triassic salt upwelling during the late Jurassic (Jackson & Hastings, 1986; Karlsen et al., 1995) e.g. the Smørbukk Sør and the Tyrihans South fields. However, exception to this widely found trapping mechanism does exist towards the eastern platform (the Trøndelag Platform) within the Haltenbanken Petroleum Province where HCs are trapped in a gentle anticlinal structure e.g. Draugen field (Provan et al., 1992; Karlsen et al., 1995).

2.3.4 Seal Rocks

Thick sequences of fine-grained Tertiary sediments provide effective regional seals for major structures (Spencer et al., 1993).

2.4 Petroleum System Modelling

Petroleum system modelling is a tool to provide a comprehensive and unique record of petroleum generation, migration and accumulation and its loss in the petroleum system through geologic time. It represents a petroleum system in terms of a digital model which correlates the processes and their outputs can be simulated in order to provide a vivid understanding and prediction. It varies from a single charge or drainage area to an entire basin and it essentially is a 3D depiction of geological data in an area of interest (Hantschel & Kauerauf, 2009).

2.5 Petroleum System Event Chart

A petroleum system event chart represents a temporal relationship among the essential elements and processes for a system and its preservation time and critical moment (Magoon and Dow, 1994). Petroleum systems event chart for the two wells (the Midgard 6407/4-1 and the Smørbukk 6506/12-9S) located in the Haltenbanken area are constructed on the basis of the input data from maturity modelling results (Chapter 5) and the pre-published data (Figure 3.2 & Figure 3.3). Special attention is paid to the timing of petroleum generation from the source rocks Åre, Melke and Spekk Formations.

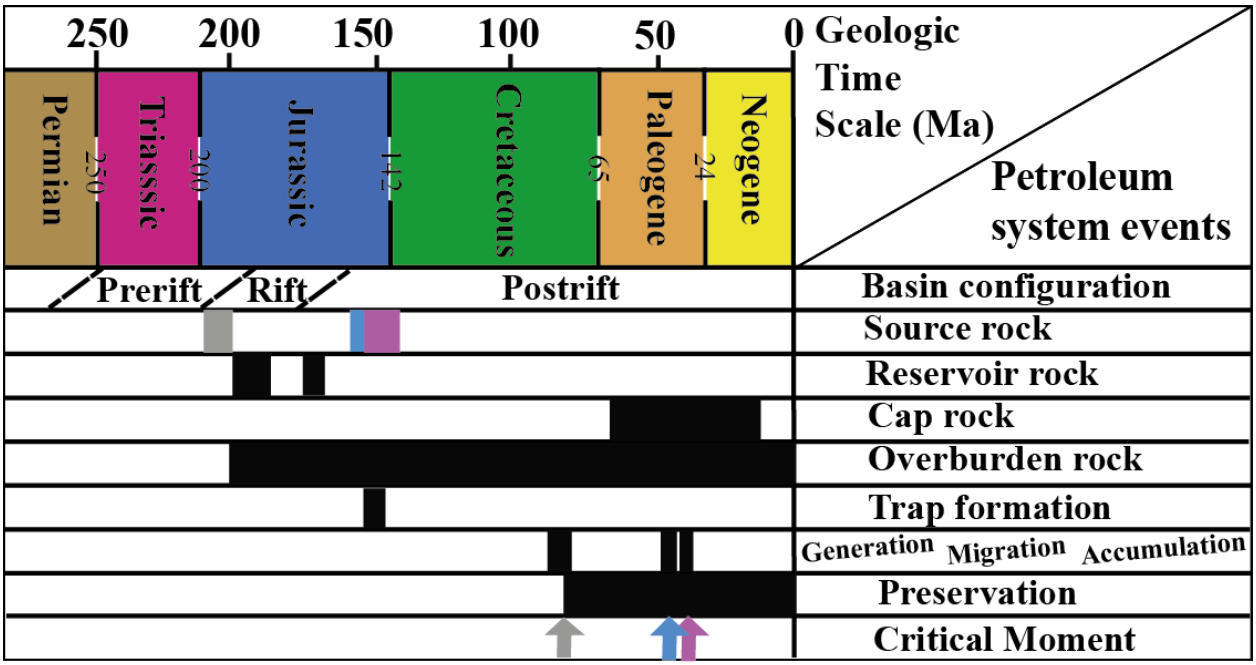

Figure 3.2: Petroleum system event chart for the Midgard well 6407/4-1 showing the relationship between the essential elements and processes as well as the preservation time and critical moment. The

colours grey, blue and pink (boxes and arrows) represent the Åre, Melke and Spekk Formations respectively.

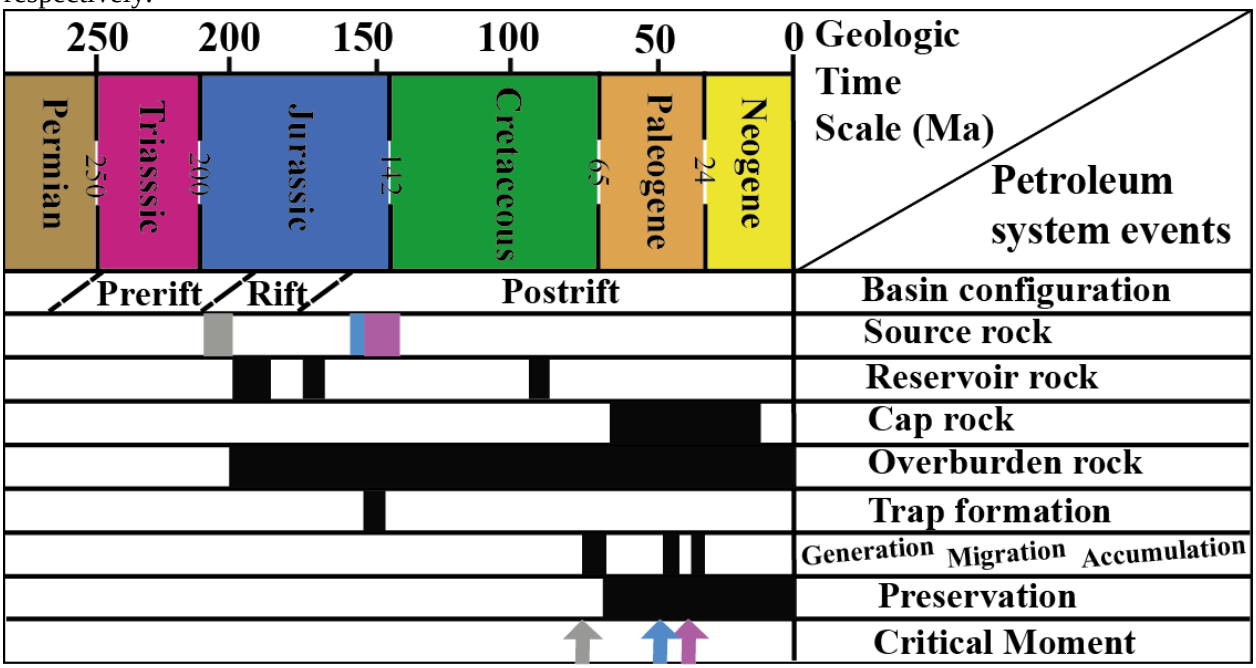

Figure 3.3: Petroleum system event chart for the Smørbukk well 6506/12-9S showing the relationship between the essential elements and processes as well as the preservation time and critical moment. The colours grey, blue and pink (boxes and arrows) represent the Åre, Melke and Spekk Formations respectively.

2.5.1 Critical Moment

A point in time that best illustrates the most generation-migration-accumulation of hydrocarbons in a petroleum system which is selected by the investigator, is termed as the critical moment (Magoon and Dow, 1994). In the petroleum system event charts for the two wells, three different critical moments have been identified for each of the three source rocks.

2.5.2 Preservation Time

The preservation time of a petroleum system begins after hydrocarbon generation-migration-accumulation processes are complete. Processes such as remigration, physical or biological degradation and complete destruction of HCs may occur during preservation time (Magoon and Dow, 1994).

2.5.3 Level of Certainty

Three levels of uncertainty i.e. known, hypothetical and speculative can be used to identify the level of uncertainty in a petroleum system (Magoon and Dow, 1994). For a *known* petroleum system a good geochemical match is required between the source rock and the

hydrocarbon accumulation. Also, a petroleum system is said to be *hypothetical* if it lacks a geochemical match and only the geochemical information identifies the source rock. Whereas, a *speculative* petroleum system is the one in which the geologic and geophysical evidence is employed entirely to postulate the evidence of either a source rock or petroleum (Magoon and Dow, 1994).

A "known" level of uncertainty is postulated for the petroleum system in this study since a good geochemical match exists between the source rock and the hydrocarbon accumulation for both wells.

Chapter 4

Burial and Thermal History Modelling

4.1 Introduction

In the basin modelling study, a conceptual model of regional geological history is developed which works as a framework for the reconstruction of the basin's depositional, erosional and thermal histories. Burial history reconstruction includes important events occurring during the geologic time represented by deposition and non-deposition / erosion (unconformities) while taking into account various rock's physical and thermal parameters. The input data for a basin modelling project is mostly obtained from the well samples, well logs, seismic data and the outcrops.

4.2 Burial History Modelling

It is the reconstruction of the burial history for the formations based on their thickness and age (derived for instance, from palynology). Decompaction is performed to compensate for the loss of water and porosity from formations during burial. When a burial history is combined with thermal data it is possible to model the conversion of kerogen to oil and gas as functions of increased burial depth and temperature. In this way may the time for oil and gas genesis can be predicted. Burial history modelling assists in calculating the rate with which kerogen breaks down under thermal stress to generate petroleum as a function of depth and time (Figure 4.3 & Figure 4.5).

4.3 Thermal History Modelling

Thermal history modelling is used to estimate the temperature history of stratigraphic layers in a sedimentary basin and is calibrated with thermal indicators such as vitrinite reflectance, measured biomarker maturity parameters or fission track analysis of the minerals apatite and zircon. Maturity modelling needs that the temperature must be assigned at all depths throughout the geological time. It is pertinent to note that the importance of complete thermal history reconstruction of a sedimentary basin is usually over-emphasized because most HC generation occurs around the maximum paleo-temperature (Hermanrud, 1993; Waples, 1994). Nevertheless, a complete thermal history reconstruction mitigates the issues of identifying the

maximum paleo-temperature together with the duration over which it remained prevalent in the sedimentary basin (Figure 4.4 & Figure 4.6) (Waples, 1994).

4.4 Surface Temperatures

Surface temperatures were generally given little importance while performing thermal maturity modelling. While computing the mean annual surface temperature for the areas above sea level, two factors are important to consider:

i) Latitudinal position through time

ii) Global climatic trends

Similarly, for the offshore areas temperature gradient of 4^0C/100m for the upper 200m water column and 2^0C/100m for the deeper water must be used. Additionally, variation in sea floor temperature due to change in global circulation pattern must also be taken into account (Waples, 1994).

4.5 Heat Flow

Heat in the sedimentary basins can be transferred by the processes of conduction, convection, and radiation (Beardsmore and Cull, 2001, Hantschel & Kauerauf, 2009). Most basin modelling softwares support heat flow in by means of geothermal gradient method and the conductivity method. A brief account on each method is presented to get an insight into these different techniques.

4.5.1 Heat flow - Geothermal Gradient Method

Subsurface temperatures can be specified into the heat flow models in two different ways:

i) These can be specified directly by making use of geothermal gradients or the corrected bottom hole temperatures derived from the boreholes.

ii) They can be specified indirectly by utilizing the heat flow – conductivity method.

When the geothermal gradient method is adopted, gradients are designed both for present and the past geologic times at each step forward in time. However, there are certain limitations to this methodology especially associated with the use of linear gradients due to lack of data even though the actively subsiding sedimentary sections always have non-linear geothermal

gradients. Additionally, geothermal gradients are effects of heat flow through the sedimentary basin therefore they do not offer a reasonable platform for the development of a conceptual model (Waples, 1994).

4.5.2 Heat flow – Conductivity Method

There is a rapid increase in application of heat flow-conductivity method while performing maturity modelling. This is largely due to the fact that this technique is based on the fundamental physical principles. The application of this sophisticated method allows the modeller to construct complex thermal histories which are probably more realistic than those derived from the geothermal gradient method (Waples, 1984)

Heat flow is the measure of the product of the thermal conductivity and the geothermal gradient across the given rock unit. There is a wide variation in the present day heat flow values obtained all across the sedimentary basins of the world (Gretener, 1981). Similarly, models of heat flow from the mantle to the crust cannot explain heat flow values precisely for the majority of cases (Leadholm et al., 1985). Moreover, heat flow models usually ignore the impact of radiogenic heating within the sedimentary basins. Many authors (e.g., Rybach, 1986) suggest that radiogenic contributions must be considered while modelling heat flows (Waples, 1994).

4.6 Thermal Conductivities

The values of thermal conductivities of sedimentary basin being modelled are generally assigned by the software itself based on the knowledge of the lithologies entered by the user. However, such values must be considered as the rough first estimates because they are prone to several misappropriations, such as:

i) Errors while specifying lithologies

ii) Undercompaction

iii) Anisotropy

iv) Errors in averaging procedure of the algorithms used by the software.

There are various problems associated with the precise estimation of thermal conductivities therefore; conductivities should be calibrated with measured temperature data to optimize the

heat flow values (Waples. 1994). Geological events and paleo-heat flow are adjusted for unconformity periods to attain an acceptable model. The goal of modifying paleo-heat flows is to optimize the model. The maturity modelling can also be optimized using known vitrinite reflectivity values or biomarker maturity ratios from real wells. For this optimization input burial, thermal and other relevant data should be corrected accordingly (Waples, 1994). By using this optimized burial and thermal history modelling, HC generation and expulsion timing is calculated which is dealt with in the next chapter (Chapter 5).

4.2 Input Data for Burial and Thermal History:

The workflow of the pertinent data which are necessary for reconstructing burial and thermal history through BAS (*Basin Simulator*) for the aforementioned the Smørbukk(6506/12-9s) and the Midgard(6407/4-1) wells are shown below. This data involves present day stratigraphic input (depth and thickness of formations along with their ages) and the calibrated thermal data (Figure 4.1 and Tables 4.1 & 4.2).

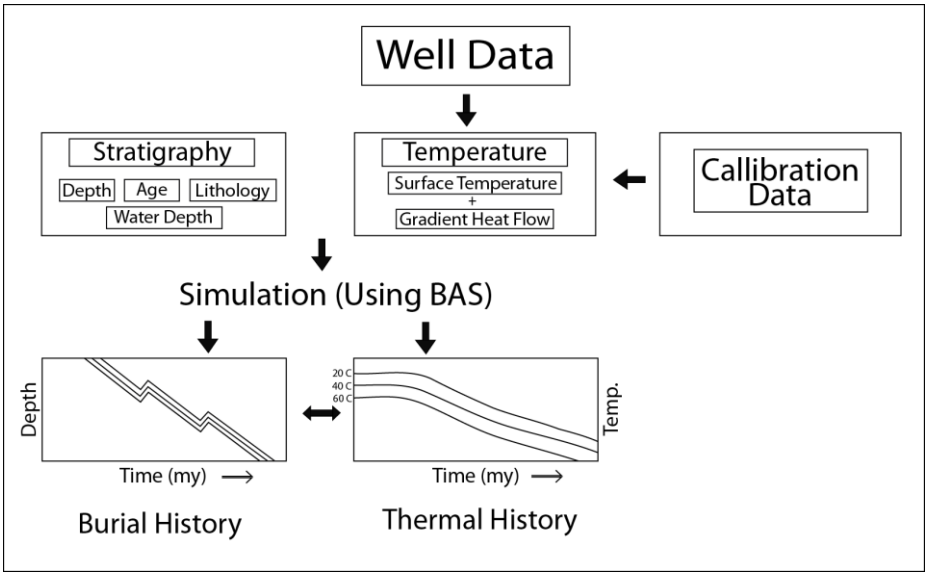

Figure 4.1: Schematic diagram for reconstruction of the burial and thermal histories of the Smørbukk (6506/12-9s) and the Midgard (6407/4-1) wells by using BAS software. Input parameters for 1D basin modelling include stratigraphic, thermal and calibration data. (modified from Matha, 2005).

Stratigraphic input data includes the age of formation (start time, end time), thickness of the formations which includes top and bottom depths, lithologies of the formations and finally the erosional thickness. The stratigraphic input data for the Smørbukk(6506/12-9s) and the Midgard(6407/4-1) wells are shown in the tables below (Tables 4.1 & 4.2)

4.2.1 Midgard Modelling Input Data

Table 4.1: Input data for burial and thermal histories reconstruction for the Midgard (6407/4-1) well. Sh= Shale, SSt= sandstone and F= Formation

Formation	Process	Time start	Time End	Depth Top-	Depth Bot.	Thickness	Lithology	Remarks
NAUST FM	F	3.4	0	247	1264.5	1017.5	Sh.	
KAI FM	F	20	3.4	1264.5	1430	165.5	Sh.	
BRYGGE FM	F	51.5	20	1430	2097.5	667.5	Sh.	
TARE FM	F	55.8	51.5	2097.5	2174	76.5	Sh.	
TANG FM	F	69.3	55.8	2174	2265	91	Sh.	
SPRINGAR FM	F	76.1	69.3	2265	2422	157	Sh.	
NISE FM	F	87.5	76.1	2422	2598	176	Sh.	
KVITNOS FM	F	89	87.5	2598	3010	412	Sh.	
LANGE FM	F	127	89	3010	3682	672	Sh.	
LYR FM	F	138	127	3682	3710	28	Sh.	
SPEKK FM	F	142	138	3710	3772	62	Sh.	Source rock
MELKE FM	F	161	142	3772	3889.5	117.5	Sh.	Source rock
GARN FM	F	173	161	3889.5	3969	79.5	SSt.	Reservoir rock
NOT FM	F	179	173	3969	4021	52	SSt.	
ILE FM	F	180	179	4021	4106	85	SSt.	Reservoir rock
ROR FM	F	185	180	4106	4150	44	SSt.-Sh.	
TOFTE FM	F	189	185	4150	4208.5	58.5	SSt.	Reservoir rock
ROR FM	F	190	189	4208.5	4272	63.5	SSt.-Sh.	
TILJE FM	F	198	190	4272	4500	228	SSt.-Sh.	Reservoir rock
ÅRE FM	F	210	198	4500	4835	335	SSt.-Sh.	Source rock

4.2.2 Smørbukk Modelling Input Data

Table 4.2: Input data for burial and thermal histories reconstruction for the Smørbukk well (6506/12-9s). Sh= Shale, SSt= Sandstone and F= Formation

Formation	Process	Time start	Time End	Depth TOP.	Depth BOT.	Thickness	Lithology	Remarks
NORDLAND FM	F	0	2.4	340	1458	1118	SH	
KAI FM	F	2.4	20	1458	1903	445	SH	
BRYGGE FM	F	20	51.1	1903	2218	315	SH	
TARE FM	F	51.1	55.8	2218	2307	89	SH	
TANG FM	F	55.8	69.3	2307	2370	63	SH	
SPRINGAR FM	F	69.3	76.1	2370	2530	160	SH	
NISE FM	F	76.1	87.5	2530	2780	250	SH	
KVITNOS FM	F	87.5	89	2780	3344	564	SH	
LYSING FM	F	89	90.5	3344	3383	39	SSt	Reservoir rock
LANGE FM	F	90.5	127	3383	4127.5	745	SH	
LYR FM	F	127	138	4127.5	4169	41	SH	
SPEKK FM	F	138	142	4169	4197	28	SH	Source rock
MELKE FM	F	142	161	4197	4379	182	SH	Source rock
GARN FM	F	161	173	4379	4436	57	SST	Reservoir rock
NOT FM	F	173	179	4436	4464	28	SH	
ILE FM	F	179	180	4464	4533	69	SST	Reservoir rock
ROR FM	F	180	183	4533	4601	68	SH	
TOFTE FM	F	183	184	4601	4660	59	SST	Reservoir rock
ROR FM	F	184	185	4660	4672	12	SH	
TILJE FM	F	185	198	4672	4836.5	165	SST	Reservoir rock
ÅRE FM	F	198	210	4836.5	4910	400	SH	Source rock

It is relevant to mention that the knowledge of hiati in sedimentary rock record is of particular significance because it may affect the timing of hydrocarbon generation. Comparison of the input data with adjacent stratigraphic sections is a useful method to reconstruct these events since no standard formula or method exists. This approach can yield information about the age and amount of rock deposited and successively removed (Waples, 1994). Quantitative analysis of erosion can be done through careful usage of several types of measured subsurface data (e.g. Theis et al., 1993).

Two methods have been discussed by Waples, 1994. Firstly, presence of an unconformity may be tentatively deduced from a change in interval transit time (Δt) between two adjacent shale layers (Magara, 1978). However, these Δt values are generally affected by time and reburial of the unconformity (Waples et al., 1992b). Secondly, several thermal indicators such as vitrinite reflectance also serve a similar purpose. In case of significant erosion, there will be a "break" in the vitrinite reflectivity profiles at the unconformity. This method has been employed in the present study; however, a smooth resultant curve is observed showing a gradual increase in VR with depth without an observable break in the linear trend (Figure 4.2). The data has been taken from the NPD website (vitrinite values chart attached as appendix). Importantly, on the basis of measured (NPD) vitrinite reflectance data an unconformity in mid Jurassic is observed however, no such evidence could be documented in the modelled results of vitrinite reflectance data. Therefore, the present study is advanced without taking into account any major break in sedimentation or if there is such a hiatus it has negligible impact on the maturation history of the source rocks of the study area (Figure 4.2).

1D modelling (burial and thermal history) of wells may be done without specifying the water depths. Some basin modelling software, however, needs to use water depth values because water depths effects temperatures at the sediment-water interface. These values are used as surface temperatures and utilized to create geo-history plots (Van Hinte, 1978). Micropaleontological data is usually the main indicator of paleo-water depths estimation. (Waples, 1994). Typical water depths in the study area are about 300 to 400m. A depth of 372 m was chosen for both wells the Smørbukk(6506/12-9s) and the Midgard (6407/4-1) in this study.

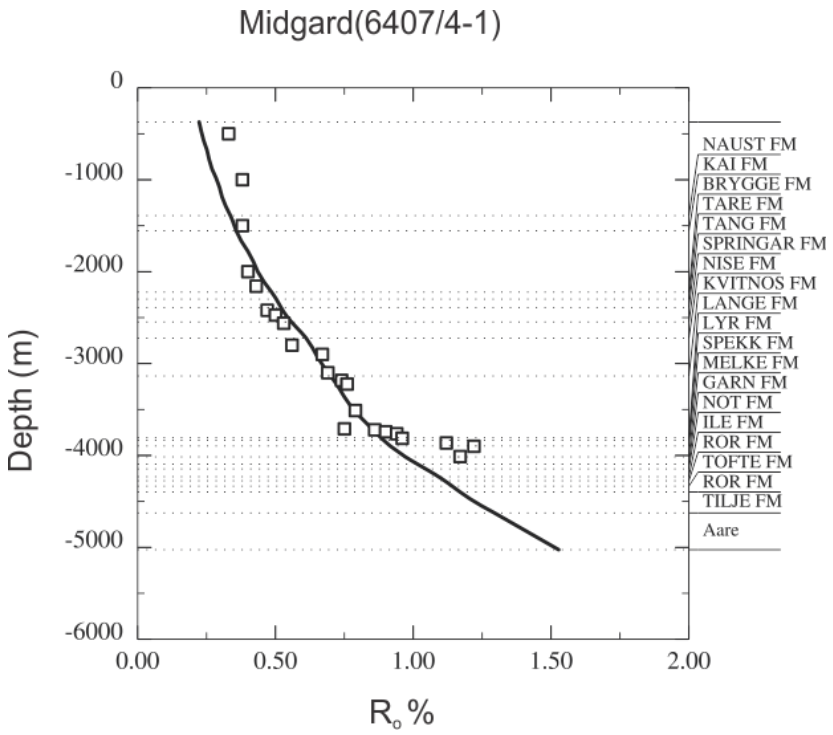

Figure 4.2: Plot of measured vitrinite reflectance against depth for the Midgard (6407/4-1) well (data sourced from NPD report), solid line shows vitrinite reflectance data sourced from the modelled results using BAS software while the small squares show plot of vitrinite reflectance data based on NPD report. A general good agreement exists between the two data sets except at approximately 4000 m depth where the two data do not coincide (see text for details).

Sediment surface temperatures in the region of the Norwegian Sea is about 4 ^{0}C which is used for the burial and thermal history reconstruction for both wells (personal communication with Magnus, 2011) .Values for heat fluxes for both wells were set at 0.0065 W/m^2 following Ritter et al. (2004) and this value has been used as typical for the Mid Norwegian Continental shelf. Published final well reports and vitrinite reflectance are used for the calibration of modelled results.

4.8 Results

The available data was used in the basin modelling software BAS in order to calculate the burial and thermal histories. The figures discussed in the following section belong to the case-1 of present study. The case-1 involves input data from NPD and the kinetic approach of Pepper & Corvi (1995) for kerogen transformation during maturity modelling. It is pertinent to note at this stage that maturity modelling results obtained from the case-2 & case-3 are placed in the Appendix-C and Appendix-D respectively.

4.8.1 Smørbukk (6506/12-9s) Well

4.8.1.1 Burial History Reconstruction

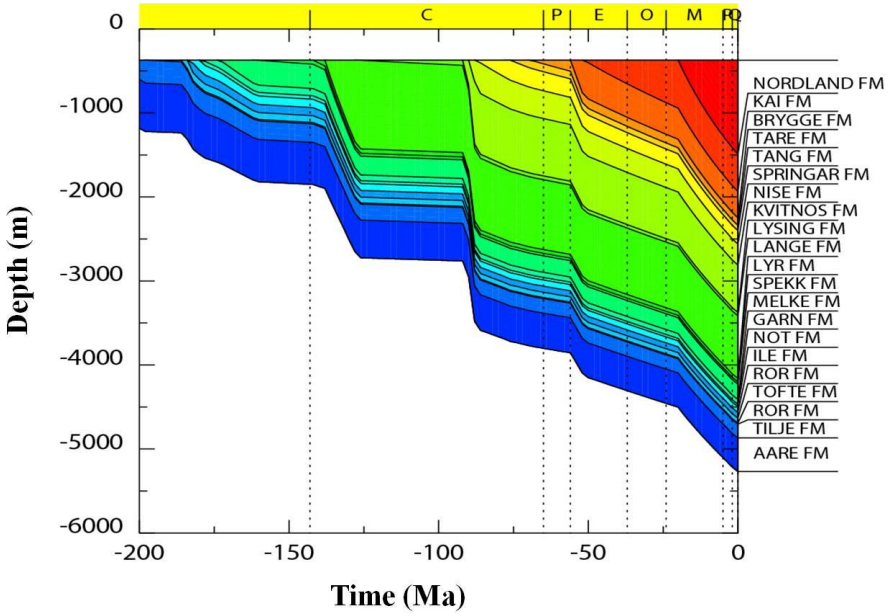

Figure 4.3: Burial history reconstruction for the Smørbukk (6506/12-9s) well which display a relatively gradual burial trend through time. The results are based on kinetic model of Pepper & Corvi (1995) and the input data is taken from the NPD geochemical data (Case-1).

4.8.1.2 Thermal History Reconstruction

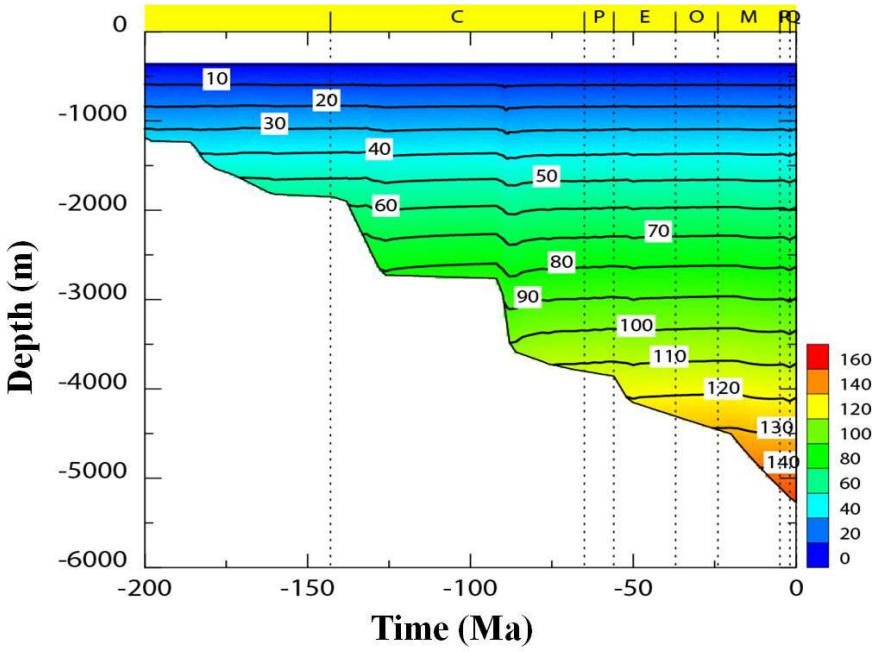

Figure 4.4: Thermal history reconstruction for the Smørbukk well (6506/12-9s) well. The results are based on kinetic model of Pepper & Corvi (1995) and the input data is taken from the NPD geochemical data (Case-1).

4.8.2 Midgard (6407/4-1) Well

4.8.2.1 Burial History Reconstruction

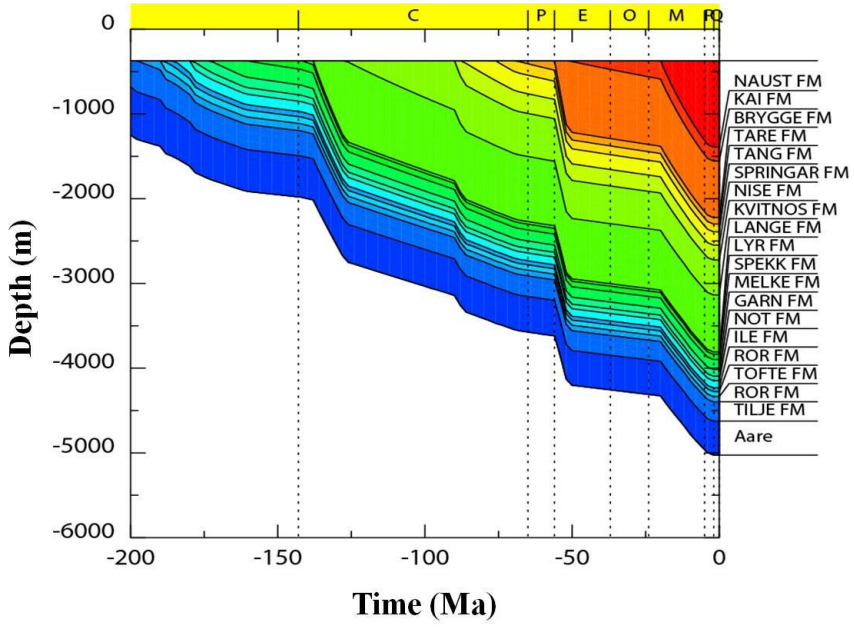

Figure 4.5: Burial reconstruction for the Midgard well (6407/4-1), also showing a gradual burial history trends through time. The results are based on kinetic model of Pepper & Corvi (1995) and the input data is taken from the NPD geochemical data (Case-1).

4.8.2.2 Thermal History Reconstruction

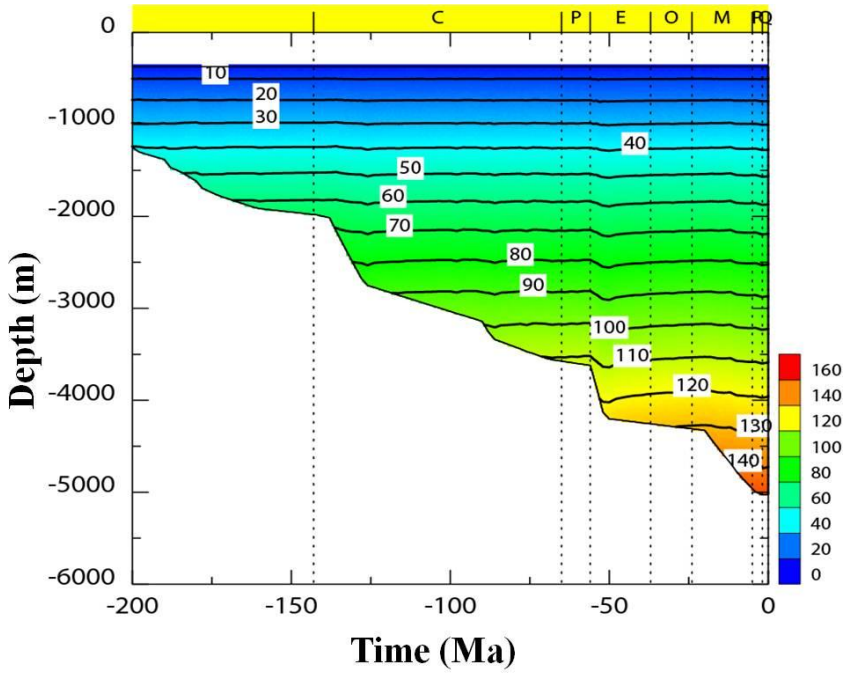

Figure 4.6: Thermal history reconstruction for the Midgard well (6407/4-1). The results are based on kinetic model of Pepper & Corvi (1995) and the input data is taken from the NPD geochemical data (Case-1)

.

Chapter 5

HC Generation Modelling

5.1 Introduction

This chapter covers aspects related to petroleum generation, its timing and quantity based on pre-exponential factors and distribution of activation energies. In petroleum exploration, first of all it is imperative to reconstruct the burial and thermal histories of the source rock and determine their kinetic parameters (activation energies E, Arrhenius constant A) before applying mathematical models of the oil and gas generation. The depths of oil and gas window, timing of HC generation and the reconstruction of pale-geothermal gradient in the sedimentary basins can be modelled by using these kinetic parameters (Espitalie, 1993). In chapter 4 , Burial and thermal histories have already been modelled for both wells (the Midgard 6407/4-1 and the Smørbukk 6506/12-9s) to estimate the petroleum generation, its timing and quantity by using kinetics data (activation energies E, pre-factor).

5.2 Petroleum Generation

Petroleum generation is the result of kerogen breakdown with rising temperature. Time and temperature are the key factors in the kerogen breakdown. The rate of kerogen breakdown can be calculated with the help of Arrhenius equation (Allen and Allen, 2005). The part of kerogen which is able to generate HCs is called reactive kerogen. The reactive kerogen is further divided in two parts as labile kerogen and refractory kerogen, both of which produce oil and gas as their major portion. The range for labile kerogen is approximately 100-150 ^{0}C and 150-220 ^{0}C for refractory kerogen. During current study, these terms are referred to as oil generative and gas generative kerogens respectively using the Pepper and Corvi kinetic model.

Modelling of geochemical processes include petroleum generation and its associated maturation parameters which are vitrinite reflectance, molecular biomarkers and mineral diagenesis. Tissot and Welte (1984) divided transformation and maturation of OM into three phases: diagenesis, catagenesis and metagenesis (Hantschel & Kauerauf, 2009). The formation of coal and petroleum with respect to depth and temperature is described vividly in Figure 5.1

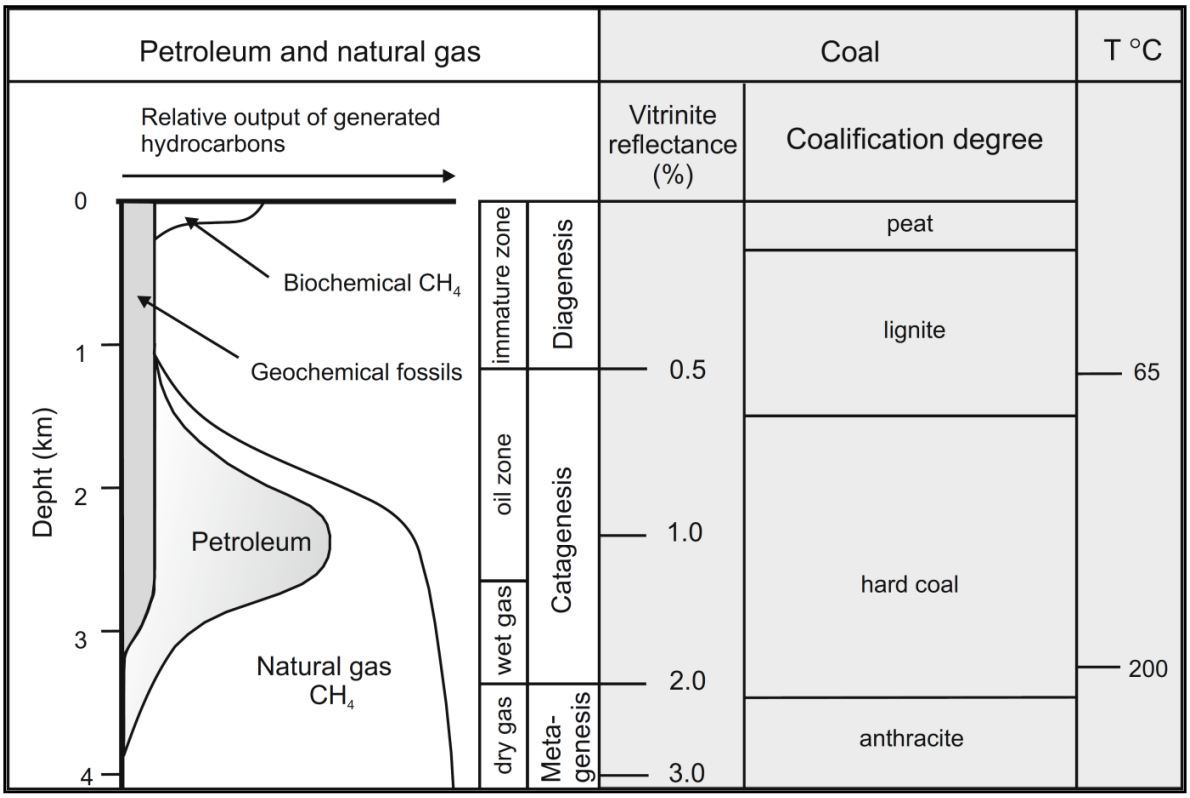

Figure 5.1: Evolution of organic matter: Diagenetic, catagenetic and metagenetic processes define the generation of oil, gas and coalification (modified from Bahlburg & Breitkreuz, 2004).

OM is transformed in volatiles such as CH_4, NH_3 and CO_2 during the process of diagenesis due to microbiological processes inside kerogen (Fig 5.1). During catagenesis, most of the HC is generated when kerogen is thermally cracked to heavier and lighter hydrocarbons and NSO (nitrogen, sulfur, oxygen) compounds. The rate of HCs transformation depends on the type of OM and the time–temperature history. Between 1 to 3 km depth, also referred as the so called "oil window", heavier petroleum components are generally generated first and then cracked into lighter components at higher temperature. Thermogenic hydrocarbon gas is generated at greater depths (Hantschel and Kauerauf, 2009)

Chemical kinetics is the best way to quantify the generation and maturation of HC-components, molecular biomarkers and coal macerals (Hantschel and Kauerauf, 2009). During the current study, a set of chemical kinetics is chosen to describe the generation, quality and quantity of HCs.

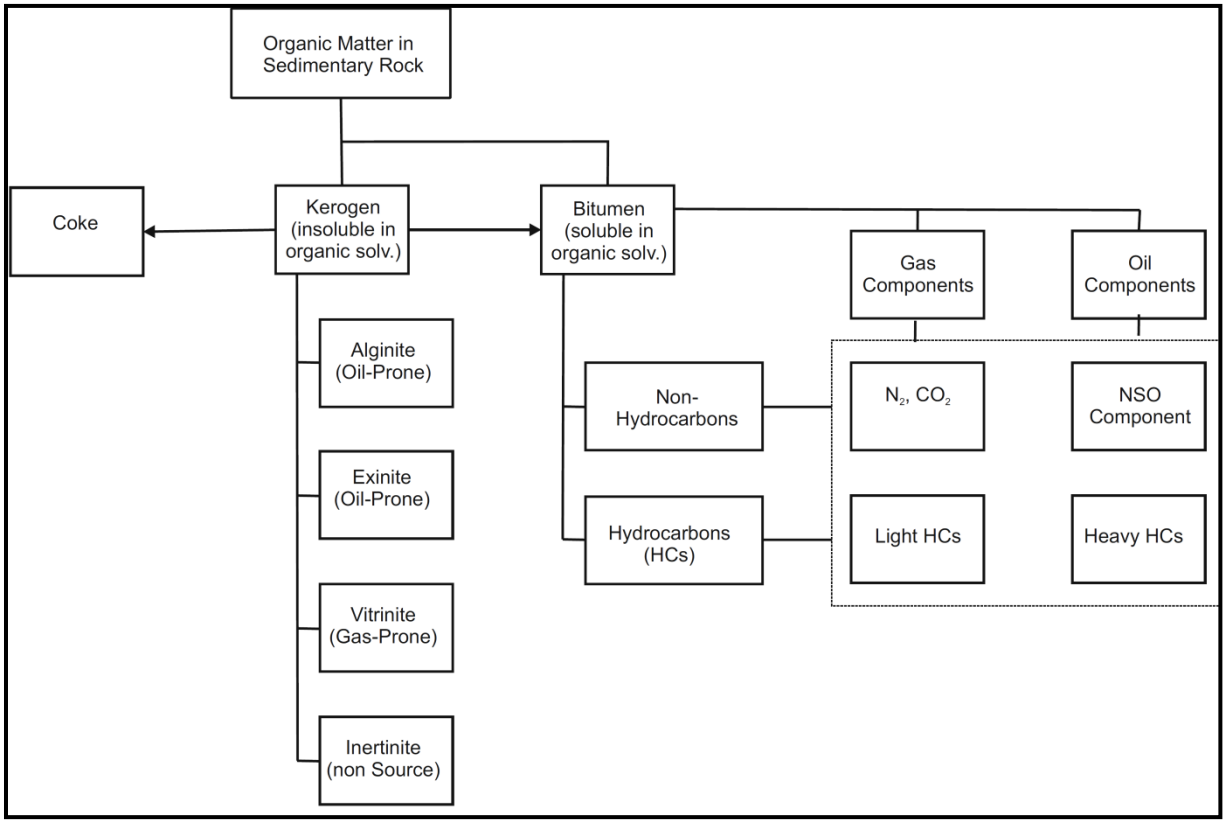

Figure 5.2: A simplified classification of organic matter in sedimentary rocks (Tissot and Welte, 1984)

Before stating the chemical kinetic data utilized during the present work, it is relevant to revisit some general terms which are used in through-out this chapter.

5.2.2. Kerogen

The part of OM which is insoluble in common organic solvents is termed as kerogen. It maintains its solubility due to its large molecular size. Kerogen may be divided in different types based on the concentration of five basic elements, carbon, hydrogen, oxygen, nitrogen and sulphur. Each type of kerogen has different potential for generating HC (Allen and Allen, 2005).

5.2.3. Bitumen

It is the part of OM which is extractable with organic solvents. It commonly forms a small portion of the total organic carbon in the rock (Allen and Allen, 2005).

5.2.4. Source Rock

Sedimentary organic matter which is capable of expelling petroleum is referred as source rock. These rocks are formed when organic carbon in Earth's carbon cycle is buried in sedimentary environments where oxidation is low or anoxic conditions prevail (Allen and Allen, 2005). To predict and understand the distribution and type of source rock in space and time (Modelling), the origin of HC is considered as biological. In the present study, there are three source rocks in the Haltenbanken area which are:

Spekk Formation (Oxfordian to Ryazanian)

Melke Formation (Bajocian to Oxfordian)

Åre Formation (Rhaetian to Pliensbachian)

5.2.5. Rock-Eval Analysis

Rock-Eval analysis is an open system pyrolysis technique which is used to identify the type, maturity and to detect the HC potential in sedimentary organic matter. The rock sample which contains OM is heated about 50K/min and the released masses of HCs and CO_2 are measured to interpret the results (Figure 5.3) (Hantschel and Kauerauf, 2009). Four basic parameters that are measured from Rock-Eval analysis are described;

S1: It represents the free HC in the rock sample. As shown in the figure it is measured in mg per g of the rock sample. It is indication of oil show.

S2: It shows the amount of HC generated through thermal cracking of non-volatile organic matter. S2 is the measure of quantity of HC in the rock sample.

S3: It represents the amount of CO_2 produced during the pyrolysis of OM. It is the indication of oxygen present in that rock sample.

Tmax= Temperature at which maximum release of HC occurs from the cracking of organic matter during pyrolysis. In the figure below, it is the top of S2 peak. Tmax is also a measure of the maturation of OM.

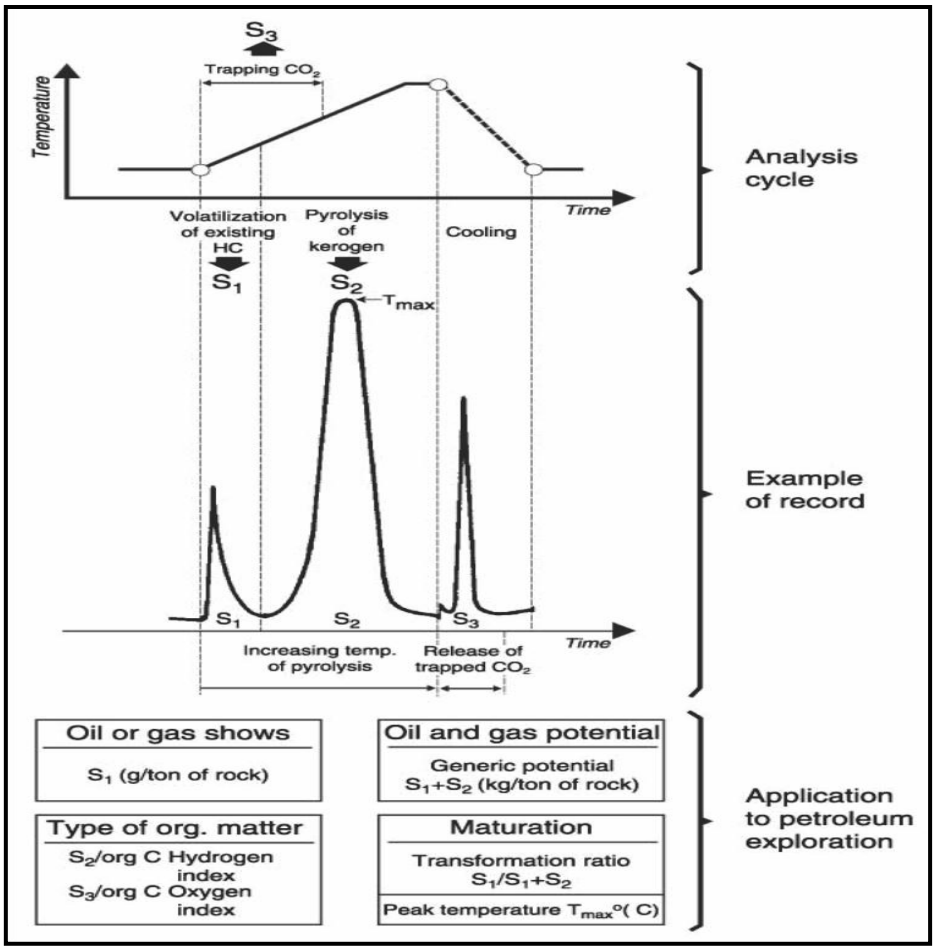

Figure 5.3: Figure showing the simplified procedure for Rock-Eval pyrolysis with all relevant peaks (Taken from Tissot and Welte, 1984)

Following parameters are used to identify the maturity and type of OM which are:

Hydrogen Index (HI)= 100 *S2/TOC

Oxygen Index (OI)= 100*S3/TOC

Production Index (PI)= S1/(S1+S2)

Pyrolyzable Carbon (PC)= 0.083*(S1+S2)

S2= HI* TOC/100 (which will be used for input data later)

5.3. Thermal Calibration Parameters:

There are numerous parameters which are used for thermal maturity and calibrations like vitrinire reflectnace, Tmax, molecular biomarkers and mineral diagenesis (Fission track analysis). During the current study, only Vitrinite Reflectance and Tmax values are considered as maturity parameters and calibration due to available data.

5.3.1 Vitrinite Reflectance (%Ro)

Vitrinite reflectance is the measurement of reflectance of vitrinite particles derived from the higher plants. It is the most widely used indicator for source rock maturity. Vitrinite particles are meaured from the sample under study. To ensure good results, multiple studies are carried out on the same sample. In basin analysis studies, it is used to calibrate the burial and thermal history models (Allen and Allen, 2005)

Table 5.1: Vitrinite reflectance and compensated kerogen types for HC generation (modified from Dembicki, 2009)

Oil-Prone Generation		Gas-Prone Generation	
Generation Stage	**R_o(%)**	**Generation Stage**	**R_o(%)**
Immature	<0.6	Immature	<0.8
Early Oil	0.6-0.8	Early Gas	0.8-1.2
Peak Oil	0.8-1.0	Peak Gas	1.2-2.0
Late Oil	1.0-1.35	Late Gas	>2.0
Wet Gas	1.35-2.0		
Dry Gas	>2.0		

Kerogen Type	R_o(%)
Type I	0.7
TypeII	0.4
TypeIII	0.45-0.5
TypeIV	0.8

5.3.2 Tmax

Tmax values are taken from Rock-Eval analysis. It is the temperature where maximum HC's are released during pyrolysis of rock sample through cracking of OM. In Rock-Eval pyrolysis program, it is recorded at the peak of S2 (Figure 5.3). T_{max} values increases with the thermal maturity of the rock sample (Hantschel & Kauerauf, 2009).

5.3.3 Relationship Between Vitrinite Reflectance and Tmax

According to Jarvie et al., (2001) values of vitrinire reflectance can be measured from T_{max} values by the relation: %Ro= 0.018*tmax-7.16

5.4. Total Organic Carbon (TOC)

TOC is an expression of the total amount of organic carbon present in the sediments (Ronov, 1958; Dembicki, 2009). If the value of TOC is less than 0.5%, it considered as a poor source rock for oil and gas generation (Table 5.2). Even rocks with more than 0.5% TOC can not be guaranted to generate HC because it may be inert organic carbon (Allen and Allen,2005). For OM to generate HCs, it must contain reduced carbon and hence it must contain hydrogen (H). If more hydrogen is associated with carbon, a larger part of the carbon, a larger part of the

carbon pool in the source rock is able to generate more hydrocarbon compounds and release oil and gas (Dembicki, 2009). For the current study, both wells contain source rocks and TOC values are shown in tables 5.8 & 5.9. TOC values are measued in weight percentage (w%) (Peter,1986; Jarvie,1991; Dembicki, 2009)

Table 5.2: Total Organic Carbon (TOC) with richness scale (modified from Dembicki, 2009)

Richness	TOC (wt %)
Poor	0.0-0.5
Fair	0.5-1.0
Good	1.0-2.0
Very good	>2.0

5.5. Kinetic Modelling

Kinetic modelling defines the chemical rates of product generation (oil and gas) from reactant (kerogen) which varies with time and temperature. All chemical reactions follow a specific rate dependence from reactants to products. Time and temperature are the most important factors which control the organic matter's maturation. Thermal cracking to model HCs for normal alkanes and their rate of degradation may be defined by the first order reaction (Voge and Good, 1949; Fabuss et al., 1962, 1964; Ungerer, 1990) as below:

$$dx/dt = -kx$$

Where,

x = the amount of the reactant
t = time
k = the reaction rate

k has units of reciprocal time for uni-molecular reactions and the negative sign reflects that x decreases with time.

The temperature dependence of the "k" which is the reaction rate is described by the Arrhenius law with two other parameters, the frequency factor A and the activation energy E as following (Ungerer, 1990):

$$k = Ae^{-E/RT}$$

Where,

K = the reaction rate constant
A = the pre-exponential factor or frequency factor
(Units are reciprocal time for uni-molecular reactions)
E = the activation energy
R = the universal gas constant (1.987 cal/mol•K)
T = the absolute temperature (Kelvins)

Activation energy (E) is the minimum energy required to start a chemical reaction. Its units are K Joule/mol. The frequency at which the molecules will be transformed is represented by the frequency factor "F" (amplitude or pre-exponential factor) and the required threshold energy to initiate the reaction is described by the activation energies "E". The Arrhenius law was established by transition theory with a temperature dependent frequency factor but it was initially developed as an empirical equation (Glasstone et al., 1941; Benson, 1968; Hantschel & Kauerauf, 2009).

Kinetic data for every kerogen type is considered to be consisting of varying molecular bond types which differ in activation energies by one or two kilocalories per mole. Mostly, the pre-exponential factor in the models is thought to be same for all bonds within the kerogen, usually in the order of 1013-1016/ sec. However, if pre-exponential factors are taken as same for all the bond types, small changes in activation energy such as a few kilocalories per mole can result in major differences in the temperature and timing of maturation of the Kerogen. Similarly, if pre-exponential factors change among the bond types then it becomes increasingly difficult to make generalization about the timing of HC generation and expulsion. Therefore, it is mandatory to consider the pre-exponential factors and the activation energies while computing kinetic parameters (Waples, 1994).

5.5.1. Petroleum Generation Kinetics

OM (organic matter in the form of kerogen and bitumen) is commonly reflected by the TOC (total organic carbon) in mass % (Figure 5.2). TOC is the ratio of the mass of all carbon atoms in the organic particles to the total mass of the rock matrix which is described in detail in section 5.4. The generation of petroleum is a breakdown reaction, from heterogeneous mixtures of kerogen macromolecules to lighter petroleum molecules. The kinetics of the petroleum is grouped with respect to:

(a) Kerogen type (I - IV).
(b) Cracking type (primary or secondary).

(c) Number and type of the generated petroleum components (bulk, oil/gas, compositional kinetics).

However, TOC does not take into consideration that only parts of the TOC may have oil or gas generative capabilities. This is better reflected by the hydrogen index (HI). An HI of 600 means that 60% of the kerogen is generative, while 40% is inert. Kerogen types are chemically classified on the basis of the elements, carbon (C), hydrogen (H) and oxygen (O) (Peters et al., 2005; Hantschel and Kauerauf, 2009). This is based on well-known coal maceral classifications by van Krevelen (1961) and it is based on the ratios of the H/C and O/C originally used. This has resulted in the definition of three main kerogen types I, II and III (Hantschel and Kauerauf, 2009).

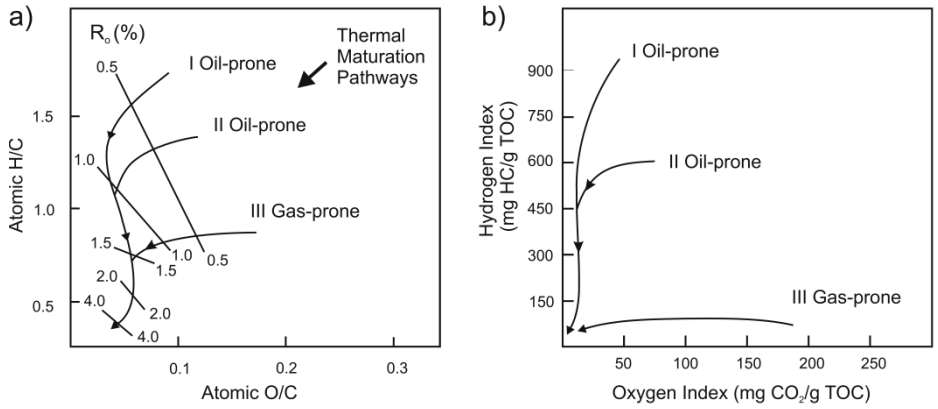

Figure 5.4: Classification of kerogen by van–Krevelen diagrams after Peters et al.,2005; Hantschel and Kauerauf, (2009), (a) van-Krevelen diagram based on the elemental analytical ratios of H/C and O/C, (b) van-Krevelen diagram based on HI (hydrogen index) and OI (oxygen index) ratios derived from Rock–Eval pyrolysis and vitrinite reflectance Ro, evolutionary pathways are idealized while real samples are usually different.

5.5.2. Derivation of Kinetic Parameters

Kinetic parameters for each individual reaction are imitated from laboratory experiments and empirical data from wells or both (Waples, 1994). Open system pyrolysis data (Rock Eval Analysis) is used for deriving kinetic parameters. It has more uncertainties than closed system pyrolysis. Thus, closed system pyrolysis is required for improved results. High quality pyrolysis data results from closed system pyrolysis can improve the quality and accuracy of the kinetic parameters and further investigating more organic types or sub types (Ungerer, 1993).

5.5.3. Selection of the Kinetic Model

Kinetic modelling of HC generation started as TTI modelling but these initial models (Tissot, 1969; Tissot and Espitalie, 1975) were not as precise nor as sophisticated as their modern counterparts (Waples, 1994). However, today numerous kinetic models are used for the maturity modelling of source rocks. The most widely used kinetic models are those by IFP (French Petroleum Institute) and LLNL (Lawrence Livermore National Laboratory). The major difference between these models is that the LLNL model allows generation of the gas directly from kerogen while the IFP model generates gas from the cracking of the oil (Waples, 1994).

Activation energies and pre-exponential factors are considered important for predicting HC generation. If Activation energies and pre-exponential factors are similar, different kinetic models can predict similar generation behaviour over a range of geological conditions (Waples, 1994). Pre-exponential factor "F" is mostly used to compensate the differences in the activation energies between two different kinetic models which give similar predictions about oil generation for the most geological histories (Waples, 1994).

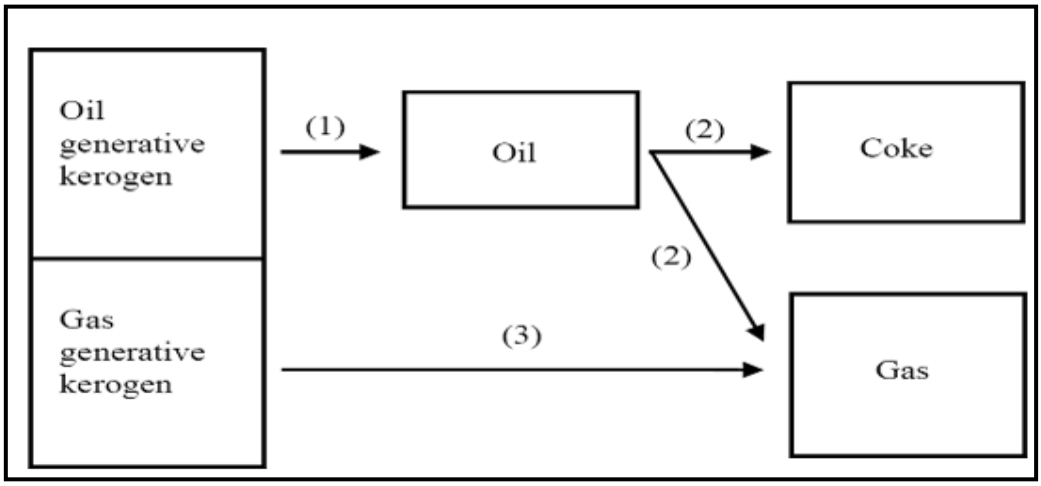

Figure 5.5: Two hydrocarbon groups, gas (C1−5) and oil (C6+) as per Pepper/Corvi model for hydrocarbon generation. Oil is generated from oil generative kerogen (arrow (1)), but it is a volatile group and upon further maturation it is cracked to gas and coke, (arrow (2)). Conversion of kerogen obeys 1st order Arrhenius kinetics, indicated by the arrows. Gas generative kerogen directly generates gas however, gas can also be formed as a product of oil-cracking, shown by the arrows (3) and (2) respectively.(adapted from Wangen, 2002)

For this study, Pepper and Corvi global kinetic model (1995) has been selected for the HC generation and quantification. This model is very similar to LLNL (Lawrence Livermore National Laboratory) kinetic model because it also allows generation of the gas directly from

the kerogen (Figure 5.5). Another reason for selecting this model is because it is a reasonable approach to predict the oil and gas generation from the basins where only limited knowledge or data is available (Pepper and Corvi, 1995). The same holds true for the study area (Haltenbanken) where no kinetic data is available.

5.6. Pepper and Corvi's Global kinetic Approach

According to the Pepper and Corvi model for hydrocarbon generation, the hydrocarbons can be divided into three groups;

Gas (C1−5)
Oil (C6+)
Coke (Inert Carbon)

Oil is generated only from oil generative Kerogen, whereas gas is produced from both gas generative kerogen and oil cracking. Oil is cracked into stable end products, i.e gas and coke (Figure 5.1). Kerogen can further be subdivided into two parts based on Pepper & Corvi (1995) kinetic model.

Reactive Kerogen (S2): is defined as the fraction of Kerogen which has the potential to generate hydrocarbons and is given in units of mg/g rock.

Inert Kerogen: is the remaining fraction of Kerogen which is not able to produce any Hydrocarbons.

Table 5.3: The different parts building up organic carbon in a source rock. The notation used is explained in table 5.4 (Wangen, 2002).

<table>
<tr><th colspan="4">TOC (Total Organic Carbon)</th></tr>
<tr><td rowspan="3">Intial Oil
Co= W S_1</td><td colspan="3">Kerogen
C_K = TOC − WS_1</td></tr>
<tr><td rowspan="2">Inert Kerogen
C_{KI} = TOC −WS_1 −WS_2</td><td colspan="2">Reactive Kerogen C_{KR} = WS_2</td></tr>
<tr><td>Gas Generative
C_{KG} = WS_2G</td><td>Oil Generative
CKG = WS2(1 − G)</td></tr>
</table>

Reactive Kerogen is sub divided into gas generative Kerogen and oil generative. 'G' denotes the fraction of gas generative Kerogen in reactive Kerogen. ***Gas Generative Kerogen*** which is able to produces gas .***Oil Generative Kerogen*** is the fraction of the reactive kerogen that produces oil in primary cracking and then gas from that oil during secondary cracking.

Table 5.4: Notation used to quantify the different parts of a source rock. These parts are illustrated in table 5.3 (Wangen, 2002).

SYMBOL	**EXPLANATION**	**UNITS** %
TOC	Total Organic Carbon	$\frac{\text{g carbon}}{\text{g sediment}}$
W	Carbon fraction of HC	$\frac{\text{g carbon}}{\text{g sediment}}$
S_1	Initial oil content	$\frac{\text{mg hc}}{\text{g sediment}}$
S_2	Reactive kerogen content	$\frac{\text{mg hc}}{\text{g sediment}}$
G	Relative portions of oil and gas reactive kerogen	

5.6.1. Pepper and Corvi Model for HC Generation from Kerogen

Use of kinetic models for predicting the amount of petroleum generation within the possible source rocks is most important technique in basin analysis. The Pepper and Corvi (1995) global kinetic model has distributed the kinetic parameters to the specific source rocks on the basis of depositional environment and stratigraphic age. This technique is very useful for exploration in frontier areas where very few geochemical data is available. This model has described five kerogen organofacies, separately considered by a specific organic matter input in addition to a depositional/early digenetic overprint (Pepper and Corvi, 1995). These organofacies are related to wide-ranging sedimentary facies like:

A =Aquatic, marine environment, siliceous or carbonate/ evaporate lithofacies, any age

B= Aquatic, marine environment, siliclastic lithofacies, any age

C= Aquatic, non-marine, lacustrine environment, Phanerozoic

D/E= Terrigenous, non-marine, ever-wet coastal environment, Mesozoic and younger

F= Terrigenous, non-marine, coastal environment, late Palaeozoic and younger

Further detail about these organofacies is described in the section (5.6.3).

5.6.2. Basis of the Pepper and Corvi Model

Most of the modern kinetic models of HC generation are based on the two principles which are:

1- First-order kinetics
2- Arrhenius law

Pepper and Corvi model also based on the same above mentioned principles. Kerogen degradation can be modelled as a first-order reaction, i.e. the rate of degradation dcldt is proportional to the concentration c of kerogen at any time dc/dt = *-kc (12).* This is an important simplification because it implies that the only quantity required in modelling kerogen breakdown is the initial concentration of the oil- or gas generating kerogen. (In this respect it is analogous to radioactive decay). The rate constant *k* of this first- order reaction is assumed to be governed by the Arrhenius law which relates the reaction rate to A, the frequency factor (in s-‘) and the activation energy “E” (in J mol). R is the universal gas constant (8.31441 J mol K-l); T is absolute temperature (K). A and E are properties of the reactant (i.e. oil- or gas-generating kerogen); they may be conceptualized as measures of the vibrational frequency and strength of a molecular bond, respectively. We discuss possible relationships between these mathematical constants and the known chemical properties of kerogens after the presentation of our results.

5.6.3 Kerogen kinetic classification: Organofacies

Organofacies: This term is referred to kerogen which is derived from the same source, deposited under similar environmental conditions and similar to early diagenetic histories (Pepper and Corvi, 1995). Pepper and Corvi global kinetic model is based on the organofacies concept (as described in table for organofacies below) which is the simple five-fold kerogen kinetic classification. This organofacies classification model is motivated and developed by Dr A. J. G. Barwise in the early 1980s (Pepper and Corvi, 1995).

The existing possibility offered by the organofacies approach lies in its potential to link global kinetic parameters to broad sedimentary facies. Given only a regional seismic survey, it is usually possible to construct a simple paleogeography (e.g. the cartoon in Figure 5) and arrive at some rudimentary understanding of gross depositional environment (GDE) or position within the systems tract (e.g. Vail, 1987; Van Wagoner et al., 1988) within which potential source rocks of organofacies A-F could be forecasted.

Table 5.5: Kerogen kinetic classification: definitions of five global organofacies (Pepper and Corvi, 2005).

Orgno-facies	Descriptor	Principal Biomass	Sulphur incorporator	Environmental/age association	Possible IFP classification
A	Aquatic marine siliceous or carbonate/evaporite	Marine algae, bacteria	High	Marine upwelling zones,clastic-starved zones basins (any age)	TypeII
B	Aquatic marine siliceous	Marine algae bacteria	Moderate	Marine, clastic basin (any age)	TypeII
C	Aquatic nonmarine, lacustrine	Freshwater algae bacteria	Low	'Tectonic' non marine basins; minor or coastal plains (Phanerozoic)	Type I
D E	Terrigenous non marine, waxy	Higher, Plant cuticle resin, lignin; Bacteria. Higher, Plant cuticle resin, lignin; Bacteria.	Low	Some (Mesozoic and younger) 'ever-wet' coastal plains	TypeIII 'H'
F	Terrigenous non marine, wax-poor	Lignin	Low	Coastal plains (late Palaeozoic and younger)	TypeIII\IV

5.6.4. Depositional, Environmental and Stratigraphic Framework of the Organofacies

According to Pepper and Corvi, 1995, organofacies approach has gained much importance over the years due to the fact that it has the potential to establish link between global kinetic parameters and broad sedimentary facies. Even with sparse data such as a regional seismic survey, it usually provides the possibility to achieve some elementary understanding of gross depositional environment (GDE) or location within the system tract (e.g. Vail, 1987; Van Wagoner et al., 1988) so that potential source rocks of organofacies A-F could be predicted. This can be done because the organofacies approach usually makes it possible to construct a simple paleogeography.

A : Transgressive to maximum flooding systems on carbonate platforms (Can be directly detected due to abnormally low acoustic impedence provided that the thickness is sufficient); lagoonal and intra-shelf topographic depressions.

B: Transgressive to maximum flooding systems on elastic depositional margins. These are also directly detectable (as in organofacies A), and probably one of the most protruding seismic reflectors in a sedimentary basin, e.g. the "Base Cretaceous" reflector of the North Sea. It might be difficult to distinguish between the flooding system and the distal toe set of the overlying highstand progradational system on seismic data, which results in recurrent fallacy of "prodelta" source rocks.

C: Relative lake highstands within major lacustrine depositional systems; principally common features in organofacies C. (e.g. Pematan Brown Shale, Central Sumatra, Indonesia; Longley et al., 1990. Lacustrine source rock development has more complex control system than for marine systems (Powell, 1986; Katz, 1990).

D/E : These organofacies is deposited either behind the shoreline of the transgressive systems tract or during aggradation of the topsets in response to the highstand system. In a depositional sequence small proportion of low velocity, low density coal may be directly detectable based on low acoustic impedance (e.g. Eocene coal measures of the East Java Sea; Barley et al., 1992).

F: It belongs to the same systems tracts as organofacies D/E, but identified on interpreted age (if Palaeozoic) climate/palaeolatitude or position relative to the seismically defined shoreline. Apart from geological age, there will be a high probability of passing through the upper delta plain to a relatively elevated and oxidizing alluvial plain environment with increasing in landward distance from the shoreline (definitions Sense Galloway and Hobday, 1983; Fielding, 1985). Detection on seismic follows the same principles as D/E (e.g. Westphalian coals of the southern North Sea Basin; Evans et al., 1992)

5.6.5 Optimization of the Pepper and Corvi Model

The kinetic parameter for each organofacies eminently characterizing degradation of oil and gas generative kerogen is given in table 5.6 and 5.7. The confidence level has been maintained and checked for each parameter set before applying the results (Pepper and Corvi, 1995). For current study, organofacies B has been selected for Åre Formation and D/E

organofacies for Melke and Spekk Formations based on the kerogen type, age and environment of deposition (figures 5.7 & 5.8) respectively.

5.6.6 Oil Generation Parameters

The oil-generative kerogen results (Table 5.6) typically appear robust. At first the small σE value for organofacies C kerogen might basically reflect a relatively small number of samples with less geological scatter. However, as organofacies D/E and F data sets had fewer data suites, but produced a larger optimized on, it believed that the relatively tight activation energy distribution of organofacies C is not an artifact of this sort (Pepper and Corvi, 1995)

Table 5.6: Result of optimization of kinetic parameters for gas generation from the five kerogen organofacies (Pepper and Corvi, 2005).

Organofacies	A(S^{-1})	E_{mean} (KJ mol^{-1})	σ_E (KJ mol^{-1})
A	$3.93e^{12}$	206.7	10.7
B	$2.17e^{18}$	278.7	18.4
C	$2.29e^{16}$	250.4	10.1
D E*	$1.88e^{11}$	206.4	7.7
F	$1.93e^{16}$	275.0	9.9

5.6.7 Gas Generation Parameters

The results for the gas-generative kerogen (Table 5.7) are not as certain as for oil-generative kerogen, because of their relative concentrations. Therefore, gas-generation data are more 'noisy', being more susceptible to measurement errors as a result of natural scatter. Particularly low confidence in the organofacies D/E gas-generative parameters and in this case very low A and E_{mean} values give spurious result based on a poor data set; therefore, it is recommend that the kinetic data for gas-generative organofacies F is used in its place. There is a reasonably wide variation within the remaining gas-generation parameters, being organofacies F the most reliable, which typically have comparatively gas-rich reactive kerogens (Pepper and Corvi, 1995)

The organofacies A, B, C and, to a lesser extent, D/E, normally have gas-poor reactive kerogens. The overall effect of any errors in the kinetic description of gas generation will cause a minute effect on the bulk generation profile (Pepper and Corvi, 1995)

Table 5.7: Result of optimization of kinetic parameters for gas generation from the five kerogen organofacies. (Pepper and Corvi, 2005).

Organofacies	A(S^{-1})	E_{mean} (KJ mol^{-1})	σ_E (KJ mol^{-1})
A	$2.13e^{13}$	206.4	8.2
B	$8.14e^{13}$	215.2	8.3
C	$2.44e^{14}$	221.4	3.9
D E	$4.97e^{14}$	228.2	7.9
F	$1.23e^{17}$	259.1	6.6

5.7 Software Working

In the following section, a brief review of the "BAS" software which handles and works with the kinetics and kerogen parameters is presented.

Reactive kerogen is sub-divided into gas generative and oil generative kerogen. 'G' denotes the fraction of gas generative part of reactive Kerogen. The different parts of Kerogen are given by a block delimited for all schemes of hydrocarbon generation, like the Pepper/Corvi model or the Tissot/ ´ Espetaliet model. For instance,

```
begin_init_kerogen
     TOC_total_organic_carbon     1.0000       #[gCarbon/gSed]#
     S1_initial_oil               0.30000      #[mgHC/gSed]#
     S2_inital_kerogen            20.0000      #[mgHC/gSed]#
     W_carbon_content             0.8300       #[gCarbon/gHC]#
     G_gas_oil_kerogen            0.5000       #[-]#
     F_gas_coke_ratio             0.50000      #[-]#
     expulsion_limit_gas          1.0000       #[gCgas/gCkerogen]#
     expulsion_limit_oil          1.10000      #[gCoil/gCkerogen]#
end_init_kerogen
```

During oil cracking, the relative portion of the (stable) reaction products gas and coke is given by the parameter `F_gas_coke_ratio`. For example, if this factor is '1' oil cracking leads to gas, and if this factor is 0.5, then the oil will be cracked by an equal amount of gas and coke (Wangen, 2002).

Table 5.6: The expulsion limits for gas and oil out of a source rock. (Wangen, 2002)

SYMBOL	EXPLANATION	UNITS
L_G	Expulsion limit gas	$\frac{\text{g C gas}}{\text{g C kerogen}}$
L_O	Expulsion limit oil	$\frac{\text{g C oil}}{\text{g C kerogen}}$

During expulsion, the amount of oil and gas lost in a source rock is controlled by `expulsion_limit_gas` and `expulsion_limit_oil` parameters. These losses are in proportion with the mass of TOC in the cell, and the factors of proportionality represent precisely these parameters (sum of masses of inert Kerogen, reactive Kerogen and coke refer to as the mass of TOC). For example, no oil will migrate unless the amount of oil generated exceeds the mass given by the expulsion limit for oil and the same implies for gas as well. The expulsion limits are applied independently for both gas and oil. A source rock can expel oil but not gas, if the amount of gas generated is not sufficient compared to the expulsion threshold. Both expulsion limits are shown in the table 5.6. The same control variables have been applied to all kerogen definitions in a simulation (Wangen, 2002). For instance,

```
begin_pc_kerogen
      name "ExPepperCorviKerogen"


begin_init_kerogen
     TOC_total_organic_carbon  0.010      #[gCarbon/gSed]#
     S1_initial_oil            0.150      #[mgHC/gSed]#
     S2_inital_kerogen         1.500      #[mgHC/gSed]#
     W_carbon_content          0.850      #[gCarbon/gHC]#
     G_gas_oil_kerogen         0.900      #[-]#
     F_gas_coke_ratio          0.500      #[-]#
     expulsion_limit_gas       0.020      #[gCgas/gCkerogen]#
     expulsion_limit_oil       0.020      #[gCoil/gCkerogen]#
end_init_kerogen


begin_gas_kerogen
     # [-]          [1/s]        [kJ/mole] #
       0.010        3.16e+13     184.1
       0.030        3.16e+13     196.6
       0.080        3.16e+13     205.0
       0.451        3.16e+13     213.4
```

```
        0.146        3.16e+13   221.8
        0.098        3.16e+13   230.1
        0.070        3.16e+13   238.5
        0.073        3.16e+13   251.0
        0.030        3.16e+13   267.8
        0.012        3.16e+13   284.5
end_gas_kerogen


begin_oil_kerogen
      # [-]          [1/s]      [kJ/mole] #
        0.015        3.16e+13   184.1
        0.033        3.16e+13   196.6
        0.092        3.16e+13   205.0
        0.556        3.16e+13   213.4
        0.148        3.16e+13   221.8
        0.085        3.16e+13   230.1
        0.043        3.16e+13   238.5
        0.028        3.16e+13   251.0
end_oil_kerogen


begin_unstable_hc
        # [-]                    [1/s]              [kJ/mole] #
        1.000                  5.00e+13           246.9
       end_unstable_hc
end_pc_Kerogen
```

A kerogen definition for the Pepper/Corvi type is given as block delimited by `begin_pc_kerogen` and `end_pc_kerogen`. The first part of the block contain kerogen name, for example "`ExPepperCorviKerogen`" in this case Kerogen name as a string. The different parts of TOC are specified in the next part of the block. There are three blocks by setting the Arrhenius parameters for the three reactions in the model. These reactions are shown in Figure 5.5. Each block is representing a reaction, contains data for series of parallel Arrhenius laws. The last block shows one Arrhenius law (for oil cracking). This reaction can be modeled by number of parallel Arrhenius law (Wangen, 2002).

The blocks of Arrhenius parameters have the same format. The only difference is in the keyword which delimits the blocks for example begin_oil_kerogen and end_oil_kerogen. The Arrhenius parameters are given in three columns which are the weight fraction of a reaction, the Arrhenious perfactor and the activation energy. Unit for the prefactor is s^{-1} whereas unit

for the activation energy is kJmole^{-1}. In a row of parallel reactions one reaction is given by each line with Arrhenius parameters and weight is given by mass fraction. The sum of the weights in the column represented by the mass fraction, must add up to 1. The Normal distributed activation energy also gives the Arrhenius parameters. However, the Arrhenius prefactor has been kept same for the entire distribution (Wangen, 2002). The normal distribution energy with respect to activation energy is given below, for the kinetics of gas generative kerogen:

```
begin_gas_kerogen
A 3.0e+12       meanE 205.0     sigmaE 10.0     steps 10
end_gas_kerogen
```

The common Arrhenius perfactor is written after the keyword `A` with units s^{-1}. This was followed by the normal distribution of the activation energies, where the mean activation energy is given after the keyword mean E. The standard deviation is written after the keyword sigma E, and the number of steps of the required distribution divided into is written after keyword steps. The activation energy is given in unit kJmole^{-1} (Wangen, 2002).
Kerogen definitions for different sources rocks have been collected in a kerogen library. These kerogen definitions are placed between the keywords `begin_kerogen_library` and `end_kerogen_library`, for example below and as shown in appendix A.

```
begin_kerogen_library
     begin_pc_kerogen
           name "KerogenTypeI"
           .....
     end_pc_kerogen

     begin_pc_kerogen
           name "KerogenTypeII"
           .....
     end_pc_kerogen

     begin_pc_kerogen
           name "KerogenTypeIII"
           .....
     end_pc_kerogen

     .....

end_kerogen_library
```

During the present study, a separate library for the source rock parameters has been maintained which later was utilized in different case runs as Case1 andCase-2. BAS (Basin Simulator) does not allow having kerogens of Pepper/Corvi and Tissot / ´ Espetaliet, in the same library. These different models work with different hydrocarbon groups. The following elements variables are produced by a Pepper/Corvi source rock

`mass_coke`	(mass coke in an element, [kg])
`Dens_coke`	(mass coke per element volume, [kg m^{-3}])
`mass_C1_C5`	(mass C_{1-5} in an element, [kg])
`dens_C1_C5`	(mass C_{1-5} per element volume, [kg m^{-3}])
`Mass_C6_PLUS`	(mass C_{6+} in an element, [kg])
`Dens_C6_PLUS`	(mass C_{6+} per element volume, [kg m^{-3}])
`Mass_expelled_C1_C5`	(mass expelled C_{1-5} from an element, [kg])
`dens_expelled _C1_C5`	(mass expelled C_{1-5} per elem. vol., [kg m^{-3}])
`Mass_expelled_C6_PLUS`	(mass expelled C_{6+} from an element, [kg])
`dens_expelled_C6_PLUS`	(mass expelled C_{6+} per elem. vol., [kg m^{-3}])

The masses of kerogen and the different hydrocarbons groups are given in Kg's of pure carbon. So, it is useful to express the amount of hydrocarbons generated and expelled as mass carbon per volume of rock. The volumes of generated and expelled HCs are estimated by multiplying these quantities with the area and thickness of a source rock (Wangen, 2002)

5.8. Input Data

This part discusses the input data that have been used for maturity modelling (1D modelling) for two wells the Midgard (6407/4-1) and the Smørbukk (6407/4-1). Three cases have been modelled by using two different geochemical input data sets with the two different kinetic modelling approaches. Case1 is discussed in detail within this chapter while the results of other two cases (Case-2 and Case-3) are attached as appendices. However differences found in the consequent modelling results based on different geochemical data input (S_2, HI and TOC) and kinetic modelling approaches is briefly addressed in Chapter 8 (Conclusion). The Haltenbanken is defined as a mature exploration area. However, no data is available for the source rock kinetics.

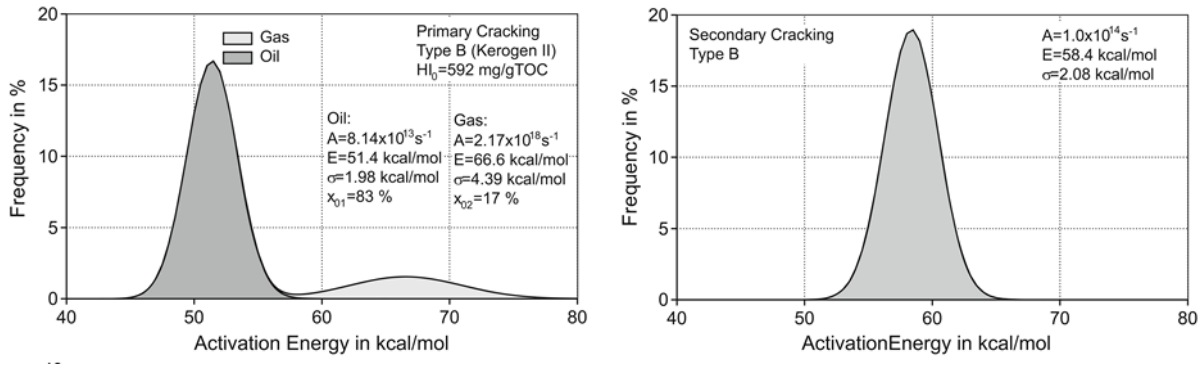

Figure 5.7: Typical HCs kinetics for type III kerogen, after Pepper and Corvi (1995a); Pepper and Dodd (1995); Hantschel and Kauerauf, (2009).

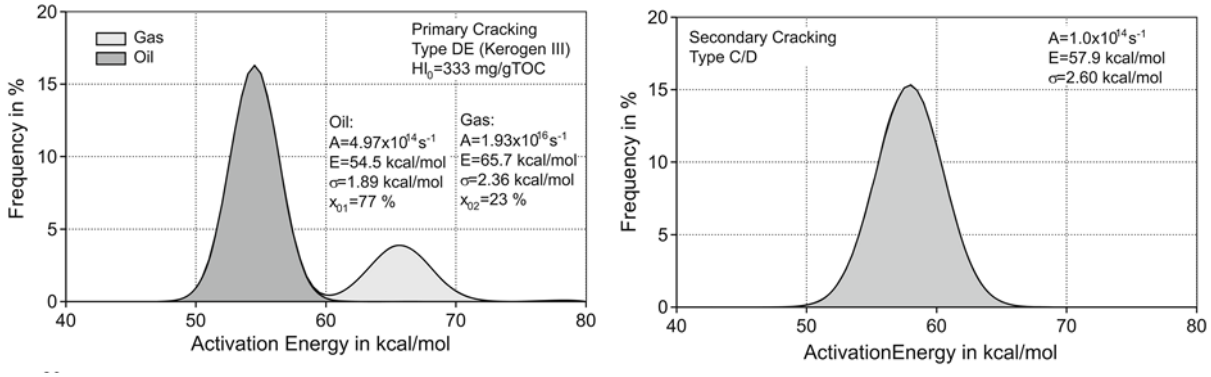

Figure 5.8: Typical HCs kinetics for type II after Pepper and Corvi (1995a); Pepper and Dodd (1995); Hantschel and Kauerauf, (2009).

As already discussed, Pepper and Corvi global kinetic model has been used for source rock kinetics for Case-1 and Case-2 while Tissot kinetic modelling approach has been used for Case-3. Detail of these cases with input data is described below:

5.8.1 CASE-1

In the Case-1 for 1D maturity modelling, Pepper and Corvi global kinetic modelling approach has been selected and used to find the timing of HC generation and its quantity (Pepper and Corvi, 1995). Geochemical data (S2, HI and TOC) has been taken from NPD (detail is in the appendix) as shown in the Tables 5.8 & 5.9 for both wells respectively;

Table 5.8: Input data which has been used for the modelling of the Midgard well (6407/4-1), Values for TOC, HI and S2 has been taken from the NPD data except for the Åre Formation which has been assumed to check its potential as coal beds. Values for kinetic parameter has been selected from pepper and corvi(1995) as figures 5.7 and 5.8. Remaining data as kerogen type, EOD (environment of deposition), lithology and age are taken from Karlsen et al., 1995.

Formation	**TOC (%)**	**HI (mg HC/g TOC)**	**S2**	**A (S^{-1})**		**E mean (KJ mol^{-1})**		**σE (KJ mol^{-1})**		**Kerogen Type**	**EOD**	**Lithology**	**Age (Ma)**	**Thickness (m)**	**North sea Equivalents**
				G.G.K	O.G.K	G.G.K	O.G.K	G.G.K	O.G.K						
Spekk	4.9	145.51	7.13	$2.17e^{18}$	$8.14e^{13}$	278.7	215.2	18.4	8.3	I	Marine Anoxic	Hot Black Shales	Oxfordian-Ryazanian (155.6-140)	117	Draupne Fm.
Melke	1.24	69.25	0.891	$2.17e^{18}$	$8.14e^{13}$	278.7	215.2	18.4	8.3	II/III	Open Marin	Clay, Siltstone, L.st.	Bajocian - Oxfordian (164.7-155.6)	62	Heather Fm
Åre	50	350	175	$1.88e^{11}$	$4.97e^{14}$	206.4	228.2	7.7	7.9	III	Coastal Plain to Deltaic Plain	Shale, Sst, Clay	Rhaetian - Pliensbachian (199.6-183.0)	400	Brent Fm.

Table 5.9: Input data which has been used for the modelling of the Smørbukk (6407/4-1) Values for TOC, HI and S2 has been taken from the NPD data except for the Åre Formation which has been taken from Mo et al., 1989. Values for kinetic parameter have been selected from Pepper and Corvi (1995) as figures 5.7 & 5.8. Remaining data as kerogen type, EOD (environment of deposition), Lithology and age are taken from Karlsen et al. (1995).

Formation	TOC (%)	HI (Mg HC/g TOC)	S2	A (S^{-1})		Emean (KJ mol^{-1})		σE (KJ mol^{-1})		Kerogen Type	EOD	Lithology	Age (Ma)	Thickness (m)	North sea Equivalents
				G.G.K	O.G.K	G.G.K	O.G.K	G.G.K	O.G.K						
Spekk	6	219	13.14	$2.17e^{18}$	$8.14e_{13}$	278.7	215.2	18.4	8.3	II	Marine Anoxic	Hot Black shales	Oxfordian - Ryazanian (155.6-140)	28	Draupne Fm.
Melke	1.97	91.37	1.8	$2.17e^{18}$	$8.14e_{13}$	278.7	215.2	18.4	8.3	II/III	Open Marin	Clay, Siltstone, L.st	Bajocian - Oxfordian (164.7-155.6)	182	Heather Fm
Åre	8	200	16	$1.88e^{11}$	$4.97e_{14}$	206.4	228.2	7.7	7.9	III	Coastal Plain to Deltaic Plain	Clay Shale, Sst,	Rhaetian - Pliensbachian (199.6-183.0)	400	Brent Fm.

5.8.2 CASE-2

In the Case-2, the same set of kinetics (Pepper and Corvi, 1995) has been used except for a different set of geochemical data which is taken from the already published data from previous workers i.e., Mo et al. (1989) and Forbes et al. (1991). Geochemical data for the Midgard (6407/4-1) well has been taken from Mo et al., 1989 and for the Smørbukk well (6407/4-1) is taken from Forbes et al. (1991) due to their close vicinity. Results obtained from modelling of Case-2 are attached at the end of this report as Appendix-C.

5.8.3 CASE-3

In the Case-3, same set of geochemical data has been used as in Case-1 (NPD data) but with different kinetic modelling approach (Tissot &´ Espetaliet, 1969 & 1975) as already have been used by Forbes et al., 1991. Results obtained from modelling of Case-2 are attached at the end of this report as Appendix-D.

Kinetic Data used for the Spekk & Melke formations:

A= 1.5 $10e^{14}$ S^{-1}

MeanE= 226 KJ/mole

SigmaE= 8.37 KJ/mole

Kinetic Data used for the Åre Formation:

A= 0.55 $10e^{15}$ S^{-1}

MeanE= 251 KJ/mole

SigmaE= 20.93 KJ/mole

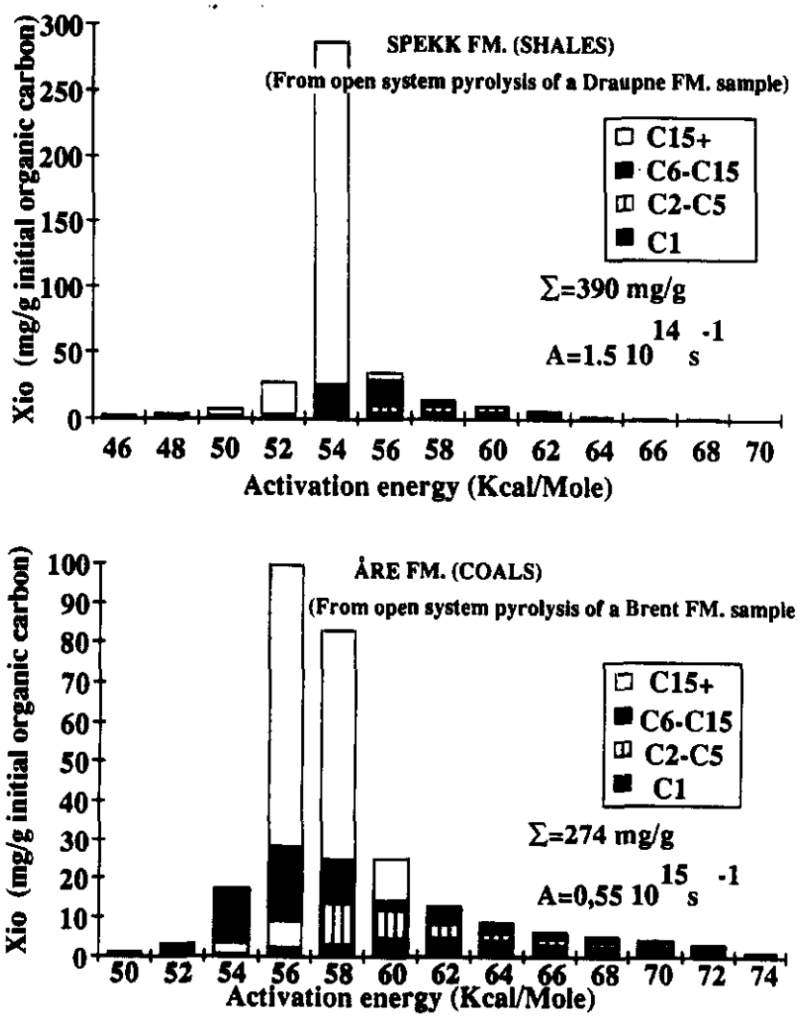

Figure 5.9: Distribution of activation energies used for the maturity modelling of the Åre, Spekk and the Melke formations. These have been modified from the data of equivalent North Sea formations (Espitalie' et al., 1988). Xio is part of the initial Kerogen that modifies to generate petroleum products with the activation energy Ei (adapted from Forbes et al., 1991).

5.9 1-D Modelling Results (Maturity Modelling)

5.9.1 Case-1: Midgard Well (6407/4-1)

Generalized temperature-to-depth cross-plot for the Midgard well (6407/4-1) shows a linear relationship between these values (Figure 5.10a). Similarly, porosity to depth cross-plot shows decrease in porosity values with depth. However, it is pertinent to note that decrease in porosity is a function of compaction, also above 80 ^{0}C chemical compaction starts which disturbs the linear relationship of porosity loss with depth and it is well documented in the Midgard well (Figure 5.10b). A comparison of modelled and observed vitrinite reflectance

versus depth cross-plot for the Midgard well (6407/4-1), shows general concordance, however, some minor differences have also been observed at approximately the depth of 4000m (Figure 5.10c).

The Åre Formation in the time-depth cross-plot shows some sudden drops in the burial curve (shown in circles) at ca. -150 M.Y., -90 M.Y., -55 M.Y. and -20 M.Y. representing major tectonic subsidence at these time intervals (Figure 5.11a). Its time-temperature cross-plot shows a general increase in temperature with time. However some abrupt rises at ca. -150 M.Y., -90 M.Y., -55 M.Y. and -20 M.Y. are also apparent. Therefore, following Hunt (1996), the Åre Formation on the basis of present study, remained in oil window between at ca. -170 M.Y. & -10 M.Y. while it is currently in gas window (5.11b). This formation in the time-mass reactive kerogen cross-plot shows decrease in mass reactive kerogen with time at ca. -125 M.Y. transformation of reactive kerogen is evident while peak transformation can be placed at ca. -50 M.Y. Presently however, less than 10% of the reactive kerogen is shown to be left within the Åre Formation as per present modelling results (Figure 5.11c).Åre Formation in the time-kerogen transformation cross-plot represents the start of bulk kerogen transformation at ca. -120 M.Y. while peak transformation can be placed at ca. -50 M.Y. Presently modelling results suggest that less than 5% of the bulk kerogen is left within the Åre Formation (Figure 5.11d). Similarly, the time-light HCs (gas) cross-plot shows start of HCs generation at ca. -110 M.Y. Similarly, timing of peak generation can be placed at ca. -50 M.Y., shown by the steep curve at this time after which a decline is recorded (Figure 5.11e). Additionally, the time- HCs (oil) cross-plot shows start of generation at ca. -125 M.Y. Similarly, timing of peak generation can be placed at ca. -50 M.Y., shown by the steep curve at this time after which curve flattens at the top between ca. -40 M.Y. and -20 M.Y. after which a clear decline in oil generation is observed (Figure 5.11f). Time- Mass coke cross-plot shows start of coke generation at ca. -50 and increases forward in time. An abrupt increase in the coke formation between -20 M.Y. 0 M.Y. is also observed (Figure 5.11 g). Vitrinite reflectance cross-plot for the Åre Formation shows start of early oil generation at ca. -105 and peak oil generation is observed at -75 M.Y. that increases forward in time (Figure 5.11h).

The Melke Formation in the time-depth cross-plot shows sudden drops in the burial curve (shown in circles) at ca. -135 M.Y., -85 M.Y., -55 M.Y. and -20 M.Y. representing major tectonic subsidence at these times (Figure 5.12a). Its time-temperature cross-plot shows a general increase in temperature with time that is evident with abrupt rises at ca. -135 M.Y., -

85 M.Y., -55 M.Y. and -20 M.Y. Modelling results from the present study are in good agreement with the findings of Hunt (1996) and this formation is placed in oil window from ca. -135 M.Y. to recent (Figure 5.12b). Similarly, the kerogen transformation cross-plot shows start of bulk kerogen transformation at ca. -125 M.Y. while, peak transformation is placed at ca. -50 M.Y. Presently, however, less than 10% of the bulk kerogen is left within the Spekk Formation as per modelling results (Figure 5.12c). The time to mass reactive kerogen cross-plot shows decrease in mass reactive kerogen with time. At ca. -75 M.Y. transformation of reactive kerogen is evident while peak transformation can be placed at ca. -50 M.Y. Presently however, about 50% of the reactive kerogen is still left within the Melke Formation as per modelling results (Figure 5.12 d). The time to light HCs (gas) cross-plot shows start of generation at ca. -50 M.Y. for the Melke Formation. Similarly, timing of peak generation can be placed at ca. -20 M.Y., shown by the steep curve at this time after which the a general decrease is observed (Figure 5.12e). The time-HCs (oil) cross-plot shows start of generation at ca. -50 M.Y. Similarly, timing of the peak generation is placed at ca. -50 M.Y. (Figure 5.12f). The time-mass coke cross-plot for the Melke Formation shows start of coke generation at ca. -25 that increases with time. An abrupt increase in the coke formation between -10 M.Y. and 0 M.Y. is also observed (Figure 5.12g). The time-vitrinite reflectance cross-plot shows start of early oil generation at ca. -60 while the peak oil generation is observed at -20 M.Y. that increases with time (Figure 5.12h).

Spekk Formation in the time-depth cross-plot shows sudden drops in the burial curve (shown in circles) at c. -140 M.Y., -85 M.Y., -55 M.Y. and -20 M.Y. representing major tectonic subsidence at these times (Figure 5.13 a). The time-temperature cross-plot for the Spekk Formation shows a general increase in temperature with time however abrupt rises at c. -140 M.Y., -85 M.Y., -50 M.Y. and -20 M.Y. are also observed. The present study shows concordance with Hunt (1996) and predicts that this formation is still in oil window from ca. -120 M.Y. to recent (Figure 5.13b). The time-mass reactive kerogen cross-plot shows decrease in mass reactive kerogen with time. At c. -70 M.Y. transformation of reactive kerogen is evident while peak transformation is placed at ca. -50 M.Y. Presently however, about 50% of the reactive kerogen is left within the Spekk Formation as per modelling results (Figure 5.13c). The time-kerogen transformation cross-plot shows start of bulk kerogen transformation at ca. -75 M.Y. while peak transformation is placed at ca. -55 M.Y. Presently however, less than 5% of the bulk kerogen is left within the Spekk Formation as per

modelling results (Figure 5.13d). The time-Light HCs (gas) cross-plot shows start of generation at ca. -50 M.Y. Similarly, timing of peak generation is placed at c. -20 M.Y., shown by the steep curve at this time after which it gradually decreases (Figure 5.13e). The time- HCs (oil) cross-plot shows start of generation at ca. -50 M.Y. Similarly, timing of peak generation is placed at ca. -50 M.Y. (Figure 5.13f). The time- Mass coke cross-plot for the Spekk Formation shows start of coke generation at ca. -20 that increases with time. An abrupt increase in the coke formation between -10 Ma 0 M.Y. is also observed (Figure 5.13g). The time-vitrinite reflectance cross-plot shows start of early oil generation at ca. -55 and peak oil generation is observed at -15 M.Y. and increases forward in time (Figure 5.13h).

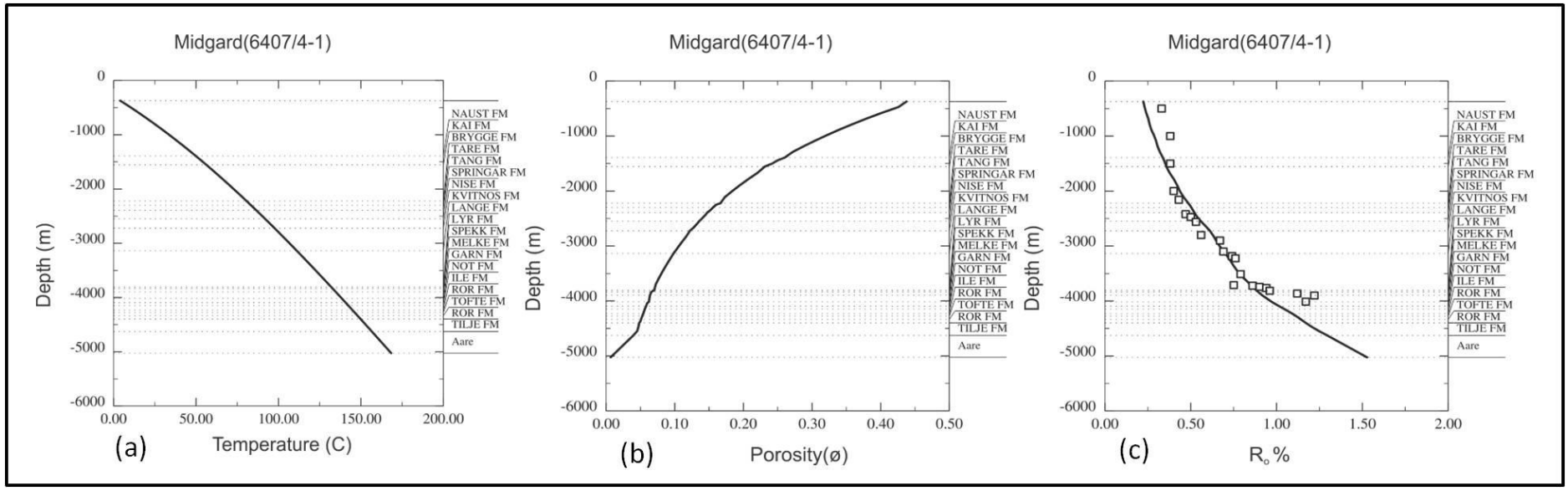

Figure 5.10: (a) Temperature to depth cross-plot for the Midgard well (6407/4-1). (b) Porosity to depth cross-plot shows decrease in porosity values with depth (c) A comparison of modelled and observed vitrinite reflectance versus depth cross-plot for the Midgard well (6407/4-1). For details refer to text in section 5.9.1 Case-1-1: The Midgard well (6407/4-1).

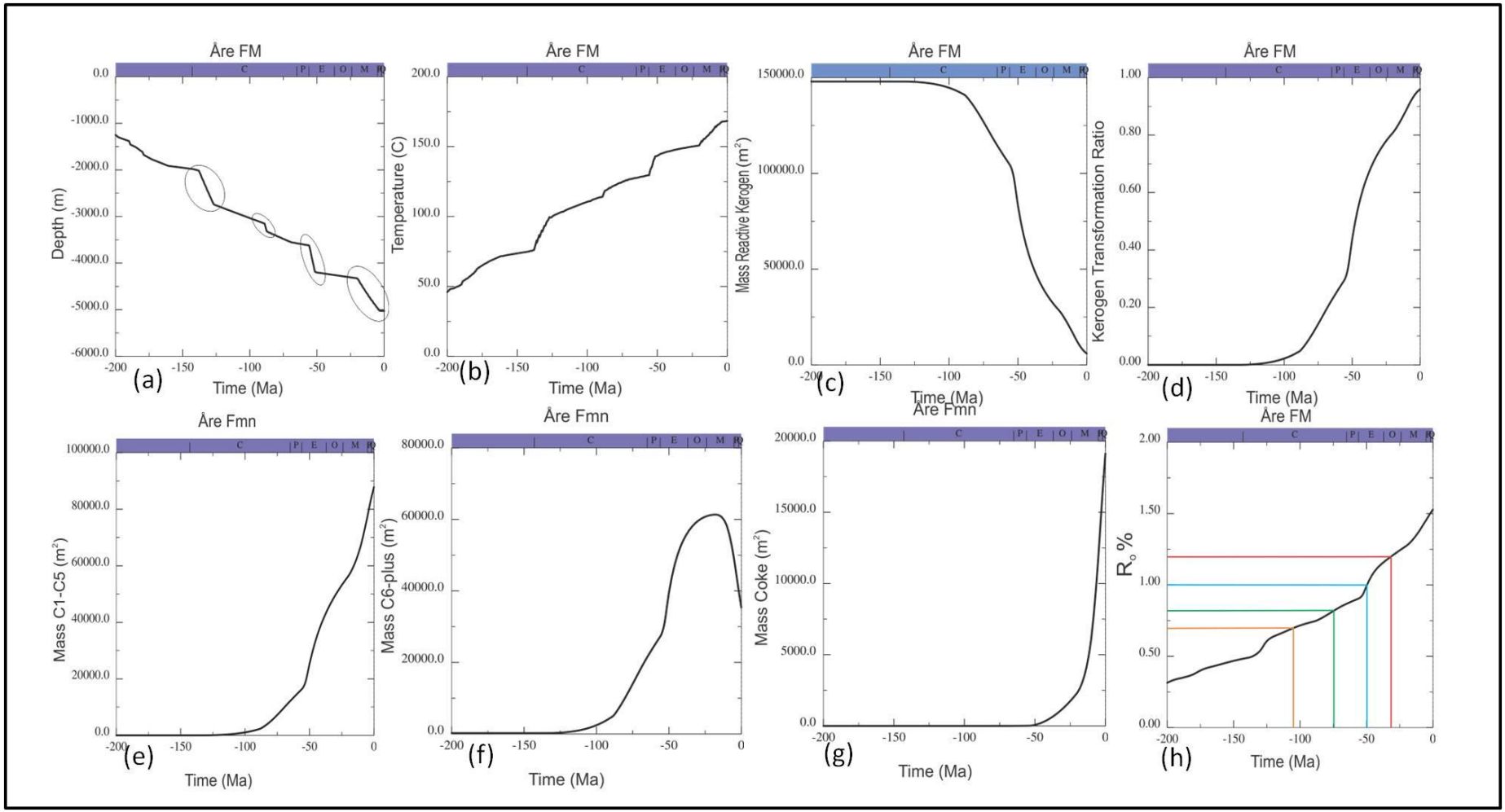

Figure 5.11: (a) Time-Depth cross-plot of the Åre Formation. (b) Time-Temperature cross-plot of the Åre Formation. (c) Kerogen transformation cross-plot. (d) Åre Formation in the time-kerogen transformation cross-plot (e) Time-mass (C1-C5) cross plot (f) Time-Mass (C6 plus) cross plot (g) Time-Mass coke cross-plot (h) Time-VR (%) cross plot. For details refer to the text in section 5.9.1 Case-1: The Midgard well (6407/4-1).

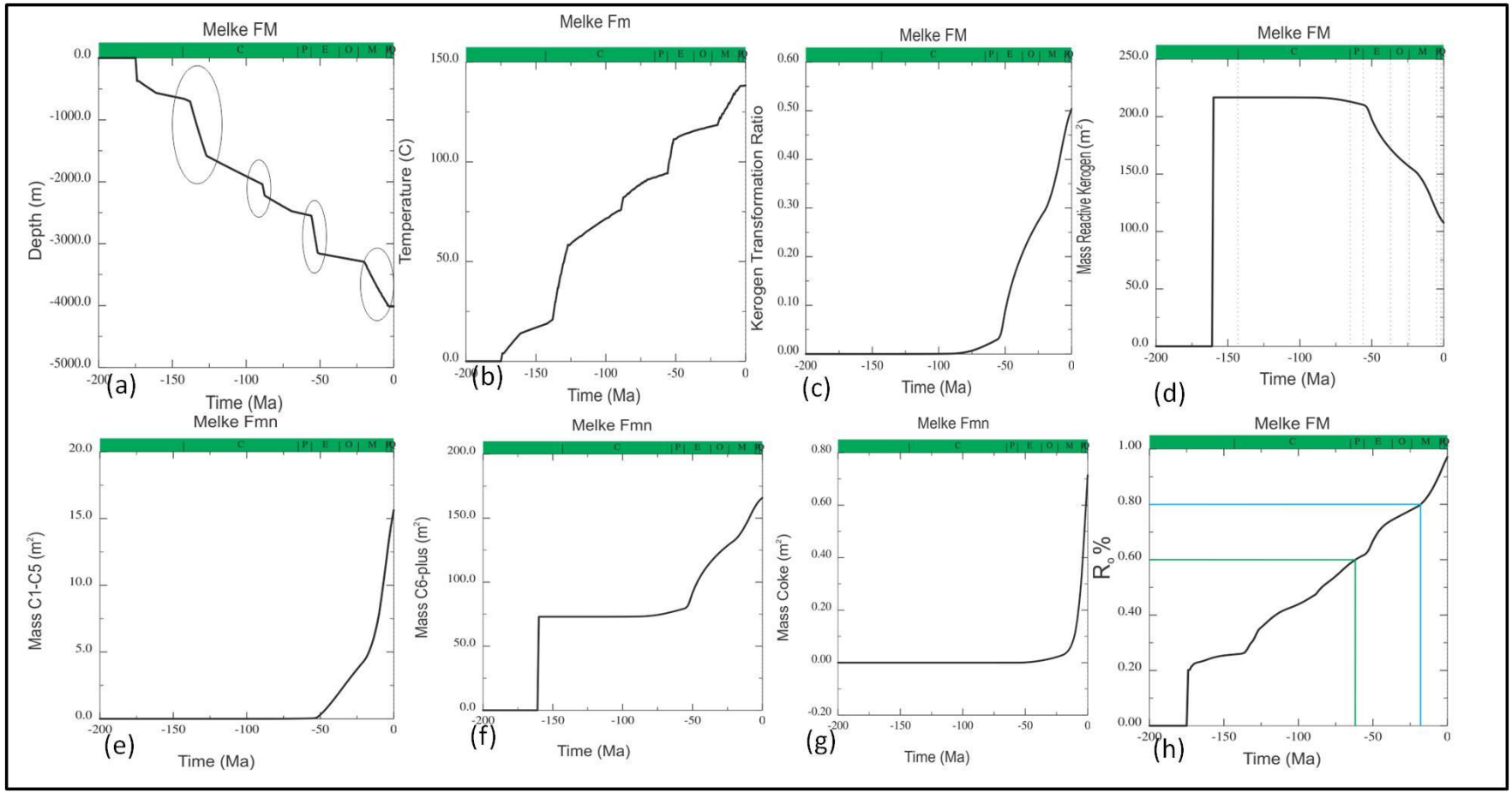

Figure 5.12: (a) Time-Depth cross-plot of the Melke Formation. (b) Time-Temperature cross-plot of the Melke Formation. (c) Kerogen transformation-Time cross-plot. (d) Melke Formation in the time-kerogen transformation cross-plot (e) Time-mass (C1-C5) cross plot (f) Time-Mass (C6 plus) cross plot (g) Time-Mass coke cross plot (h) Time- VR (%) cross plot. For details refer to the text in section 5.9.1 Case-1: The Midgard well (6407/4-1).

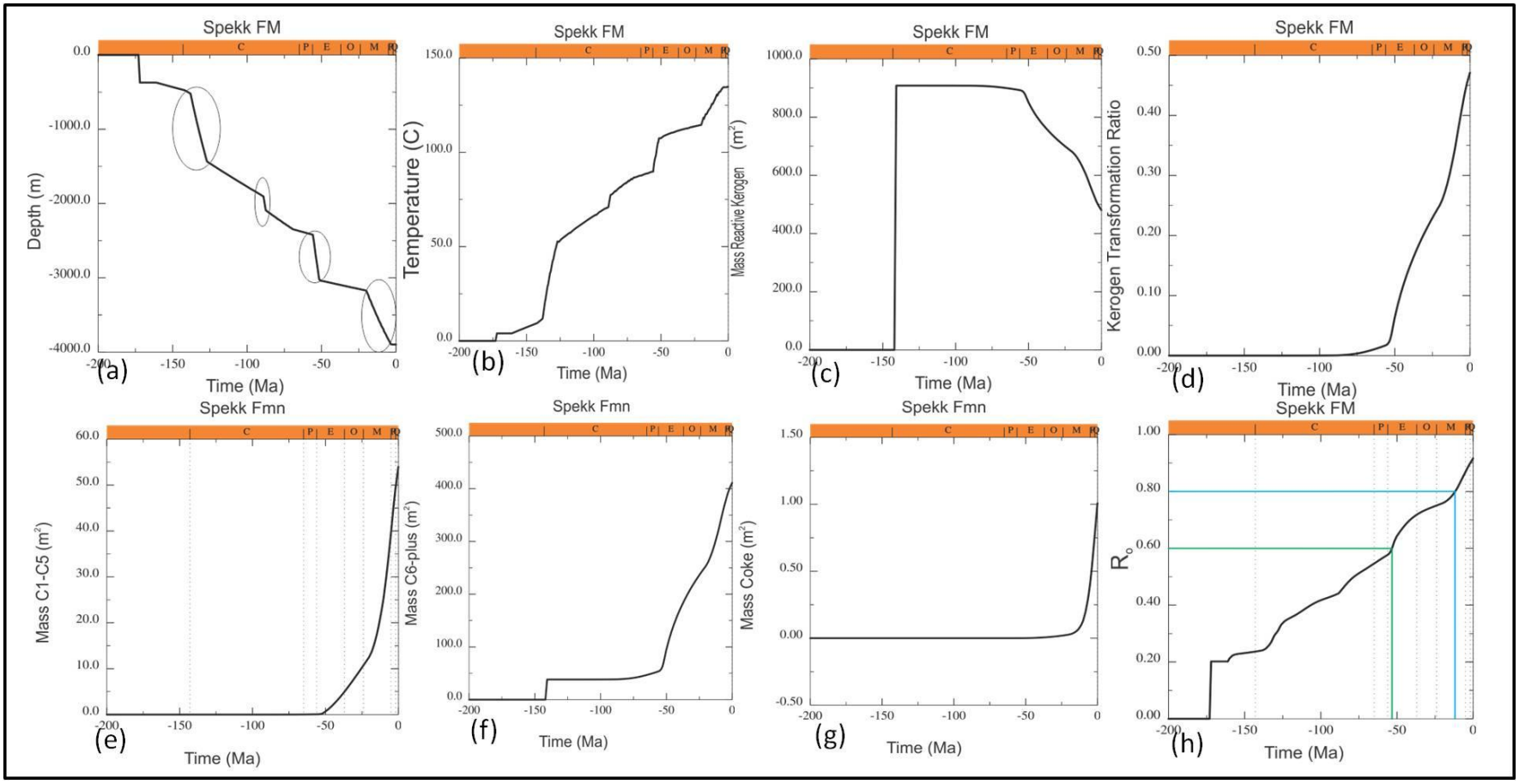

Figure 5.13: (a) Time-Depth cross-plot of the Spekk Formation. (b) Time-Temperature cross-plot of the Spekk Formation. (c) Time-Kerogen transformation cross-plot. (d) Spekk Formation in the time-kerogen transformation cross-plot (e) Time-mass (C1-C5) cross plot (f) Time-Mass (C6 plus) cross plot (g) Time-Mass coke cross plot (h) Time-VR (%) cross plot. For details referred to section 5.9.1 Case-1: The Midgard well (6407/4-1).

5.9.2 Case-1: Smørbukk Well (6506/12-9S)

A generalized temperature to depth cross-plot for the Smørbukk well (6506/12-9S) shows a linear relationship of these parameters (Figure 5.14a). Porosity versus depth cross-plot for Smørbukk well (6506/12-9S) shows decrease in porosity with depth. However, it is pertinent to note that decrease in porosity is a function of compaction, also above 80 ^{0}C chemical compaction starts which disturbs the linear relationship of porosity loss with depth (Figure 5.14b). The modelled and observed vitrinite reflectance versus depth cross-plot for this well is compared, which shows a good agreement in results (Figure 5.14c). Observed VR values have been taken from the NPD database (Data sheet is attached in the appendix).

The Åre Formation in the time-depth cross-plot shows sudden drops in the burial curve (shown in circles) at ca. -130 M.Y., -90 M.Y., -55 M.Y. and -20 M.Y. representing major tectonic subsidence at these times (Figure 5.15a). The time-temperature cross-plot for the Åre Formation shows general increase in temperature with time while with abrupt rises at c. -130 M.Y., -90 M.Y., -55 M.Y. and -20 M.Y. are also observed. Following Hunt (1996) the Åre Formation remained in oil window between at ca. -170 M.Y. & -10 M.Y. and is currently in gas window (Figure 5.15 b). The time-kerogen transformation cross-plot shows start of bulk kerogen transformation at ca. -105 M.Y. while peak transformation is placed at ca. -90 M.Y. Presently however, less than 3% of the bulk kerogen is shown to be left within the Åre Formation as per modelling results (Figure 5.15c). The time-mass reactive kerogen cross-plot shows decrease in mass reactive kerogen with time. Starting at ca. -80 M.Y. transformation of reactive kerogen is evident while peak transformation is placed at ca. -80 M.Y. Presently however, less than 3% of the reactive kerogen is left within the Åre Formation as per modelling results (Figure 5.15d). The time-light HCs (gas) cross-plot shows start of generation at ca. -90 M.Y. Similarly, timing of peak generation is placed at ca. -50 M.Y., shown by the steep curve at this time after which it gradually decreases (Figure 5.15e). The time-HCs (oil) cross-plot shows start of generation at ca. -90 M.Y. Similarly, timing of peak generation is placed at ca. -40 M.Y., shown by the steep curve at this time after which there is a clear decline (Figure 5.15f). The time-mass coke cross-plot shows start of coke generation at c. -50 and an abrupt increase in the coke formation between -25 M.Y. -0 M.Y. is also observed (Figure 5.15g). The time- vitrinite reflectance cross-plot shows start of early oil

generation at ca. -90 M.Y. and peak oil generation is observed at -72 M.Y. Formation is recently in Gas window as per modelling results (Figure 5.15h).

The Melke Formation in the time-depth cross-plot shows sudden drops in the burial curve (shown in circles) at ca.-170, -140 M.Y., -90 M.Y., -55 M.Y. and -20 M.Y. representing major tectonic subsidence at these times (Figure 5.16a). The time-temperature cross-plot for the Melke Formation shows a general increase in temperature with time that is evident with abrupt rises at ca.-170 M.Y., -140 M.Y., -90 M.Y., -55 M.Y. and -20 M.Y. Following Hunt (1996) Melke Formation is in oil window from ca. -125 M.Y. to recent (Figure 5.16b). The time-kerogen transformation cross-plot shows start of bulk kerogen transformation at ca. -85 M.Y. while peak transformation is placed at ca. -85 M.Y. Presently however, less than 10% of the bulk kerogen is left within the Melke Formation as per modelling results (Figure 5.16c). The time-mass reactive kerogen cross-plot shows that at ca. -90 M.Y. transformation of reactive kerogen started for the Melke Formation while peak transformation is placed at ca. -90 M.Y. Presently however, more than 40% of the reactive kerogen is shown to be left within the Melke Formation as per modelling results (Figure 5.16 d). The time-light HCs (gas) cross-plot shows start of generation at ca. -55 M.Y. Similarly, timing of peak generation can be placed at ca. -20 M.Y., shown by the steep curve at this time after which the slope gradually decreases (Figure 5.16 e). The time-HCs (oil) cross-plot shows start of generation at ca. -90 M.Y. Similarly, timing of peak generation can be placed at ca. -90 M.Y. (Figure 5.16 f). The time-mass coke cross-plot shows start of coke generation at ca. -20 that increases forward in time. An abrupt increase in the coke formation between -10 M.Y. -0 M.Y. is also quite apparent (Figure 5.16g). The time-vitrinite reflectance cross-plot shows start of early oil generation at ca. -72 M.Y. and the peak oil generation is observed at -25 M.Y. that increases forward in time (Figure 5.16h).

The time-depth cross-plot for the Spekk Formation shows sudden drops in the burial curve (shown in circles) at ca. -135 M.Y., -90 M.Y., -55 M.Y. and -20 M.Y. representing major tectonic subsidence at these times intervals (Figure 5.17a). The time-temperature cross-plot for this formation shows a general increase in temperature with time along with abrupt rises at ca. -135 M.Y., -90 M.Y., -55 M.Y. and -20 M.Y. Following Hunt (1996) Spekk Formation is still in the oil window since ca. -125 M.Y. to the recent (Figure 5.17b). The time-kerogen transformation cross-plot represents start of the bulk kerogen transformation at ca. -85 M.Y. while the peak transformation can be placed at c. -85 M.Y. Presently however, less than 10%

of the bulk kerogen is left within the Spekk Formation as per modelling results (Figure 5.17c). The time-mass reactive kerogen cross-plot shows a general decrease in mass reactive kerogen with time. Nevertheless, at ca. -80 Ma transformation of reactive kerogen is evident while the peak transformation is placed at ca. -50 M.Y. Presently however, more than 40% of the reactive kerogen is left within the Spekk Formation as per the current modelling results (Figure 5.17d). The time-light HCs (gas) cross-plot shows start of generation at ca. -70 M.Y. Similarly, timing of peak generation is placed at ca. -20 M.Y., shown by the steep curve at this time after which a gradual decrease is observed (Figure 5.17e). The time-HCs (oil) cross-plot represents the start of generation at ca. -90 M.Y. Similarly, timing of peak generation can be placed at c. -50 M.Y. The time-mass coke cross-plot shows start of coke generation at ca. -15 M.Y. An abrupt increase in the coke formation between -10 M.Y. -0 M.Y. can also be observed (Figure 5.17g). The time-vitrinite reflectance cross-plot shows start of early oil generation at ca. -80 M.Y. and peak oil generation is observed at ca. -35 M.Y. (Figure 5.17h).

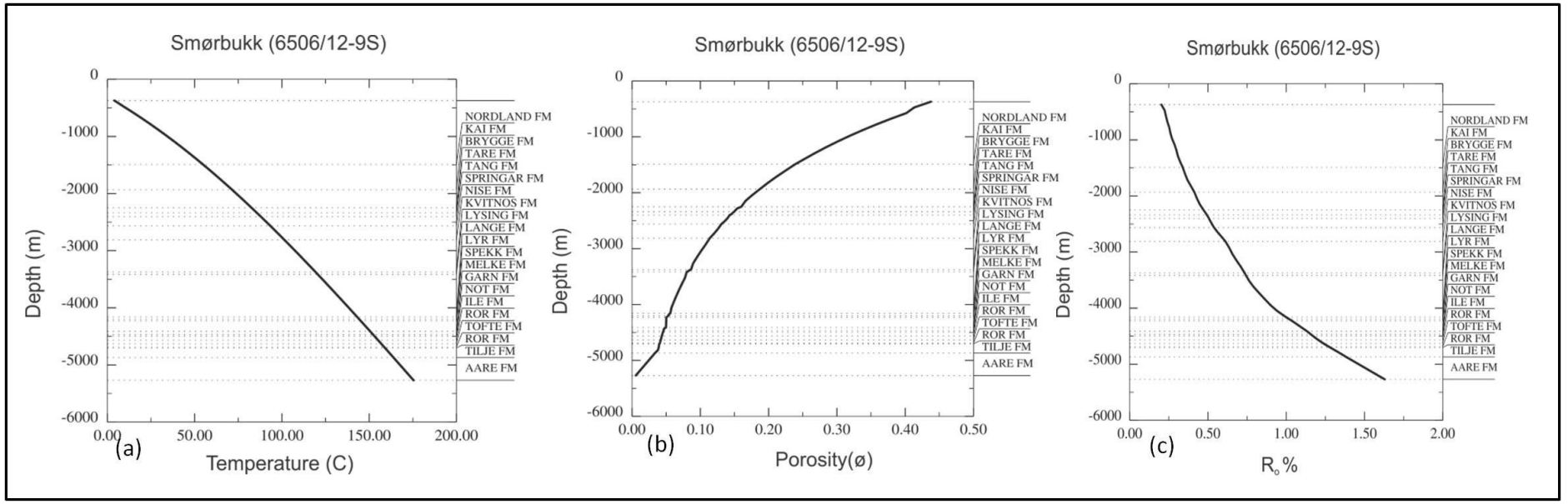

Figure 5.14: Temperature to depth cross-plot for the Smørbukk Well (6506/12-9S) (b) Porosity to depth cross-plot shows decrease in porosity values with depth (c) A comparison of modelled and observed Vitrinite reflectance versus depth cross-plot for the Smørbukk Well (6506/12-9S). For details referer to section 5.9.2 Case-1: The Smørbukk Well (6506/12-9S)

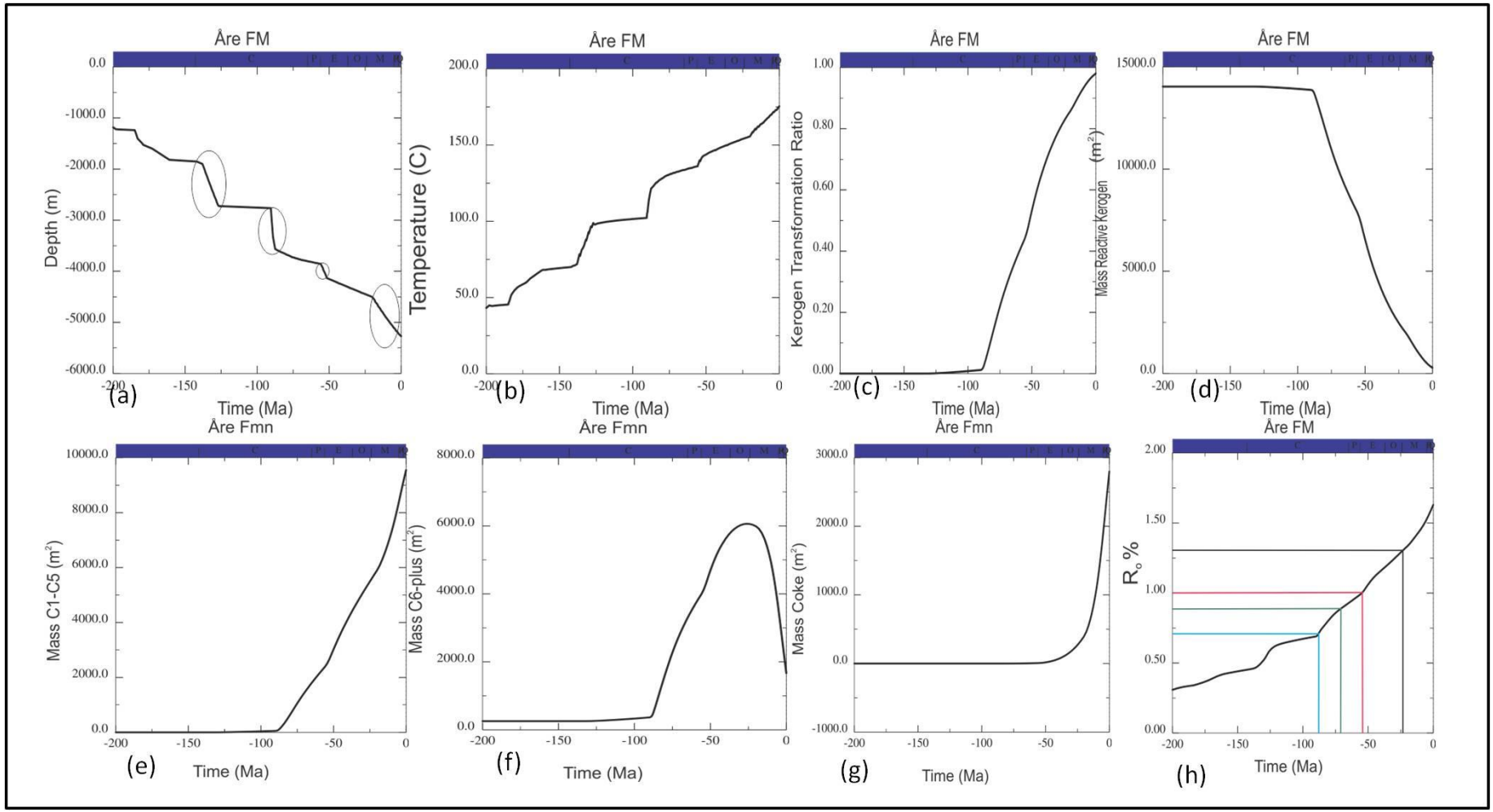

Figure 5.15: (a) Time-Depth cross-plot of the Åre Formation. (b) Time-Temperature cross-plot of the Åre Formation. (c) Kerogen transformation cross-plot. (d) Åre Formation in the time-kerogen transformation cross-plot (e) Time-mass (C1-C5) cross plot (f) Time-Mass (C6 plus) cross plot (g) Time-Mass coke cross plot (h) Time- VR (%) cross plot. For details refer to section 5.9.2. Case-1: The Smørbukk Well (6506/12-9S)

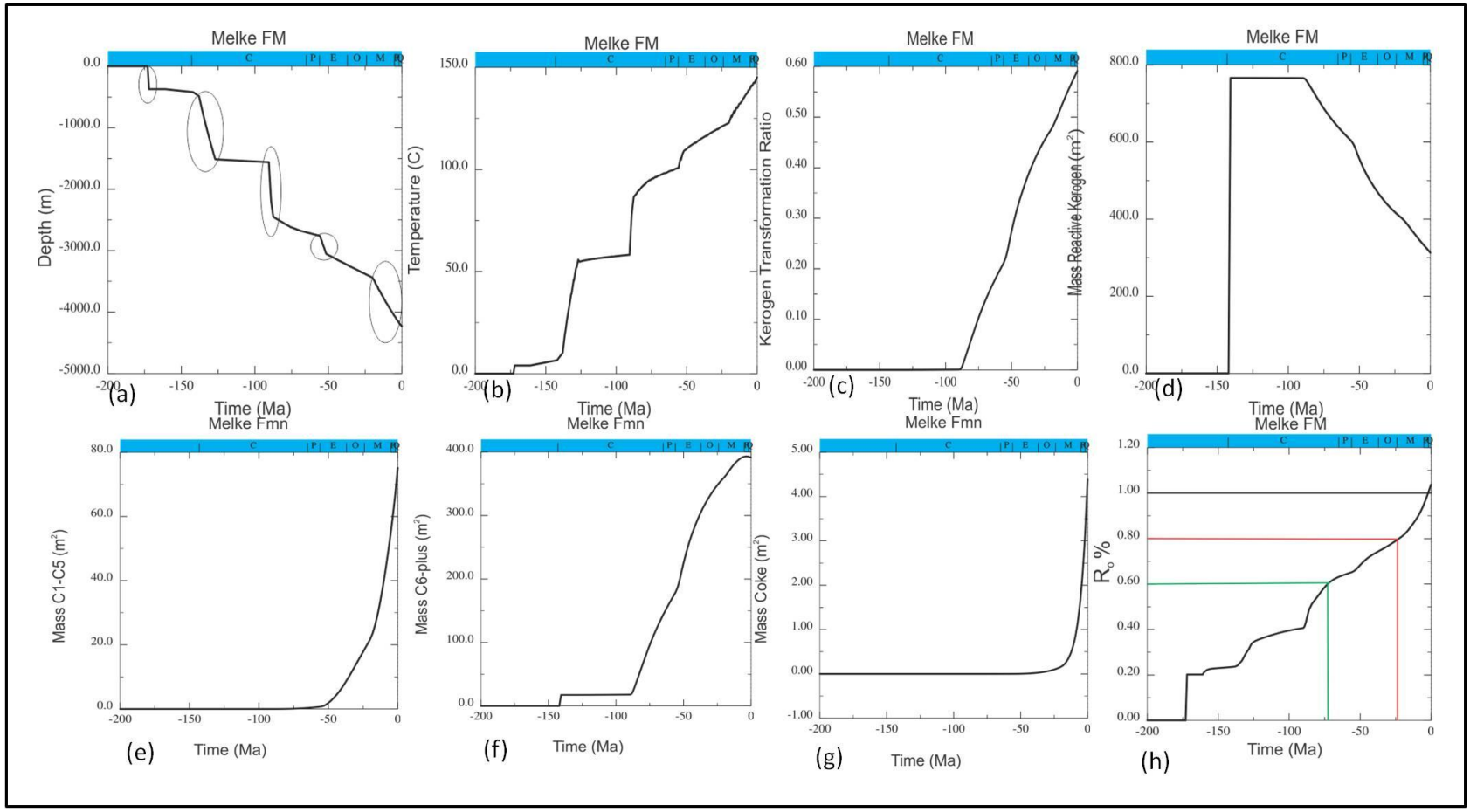

Figure 5.16: (a) Time-Depth cross-plot of the Melke Formation. (b) Time-Temperature cross-plot of the Melke Formation. (c) Kerogen transformation cross-plot. (d) Melke Formation in the time-kerogen transformation cross-plot (e) Time-mass (C1-C5) cross plot (f) Time-Mass (C6 plus) cross plot (g) Time-Mass coke cross plot (h) Time- VR (%) cross plot. For details refer to section 5.9.2 Case-1: The Smørbukk Well (6506/12-9S

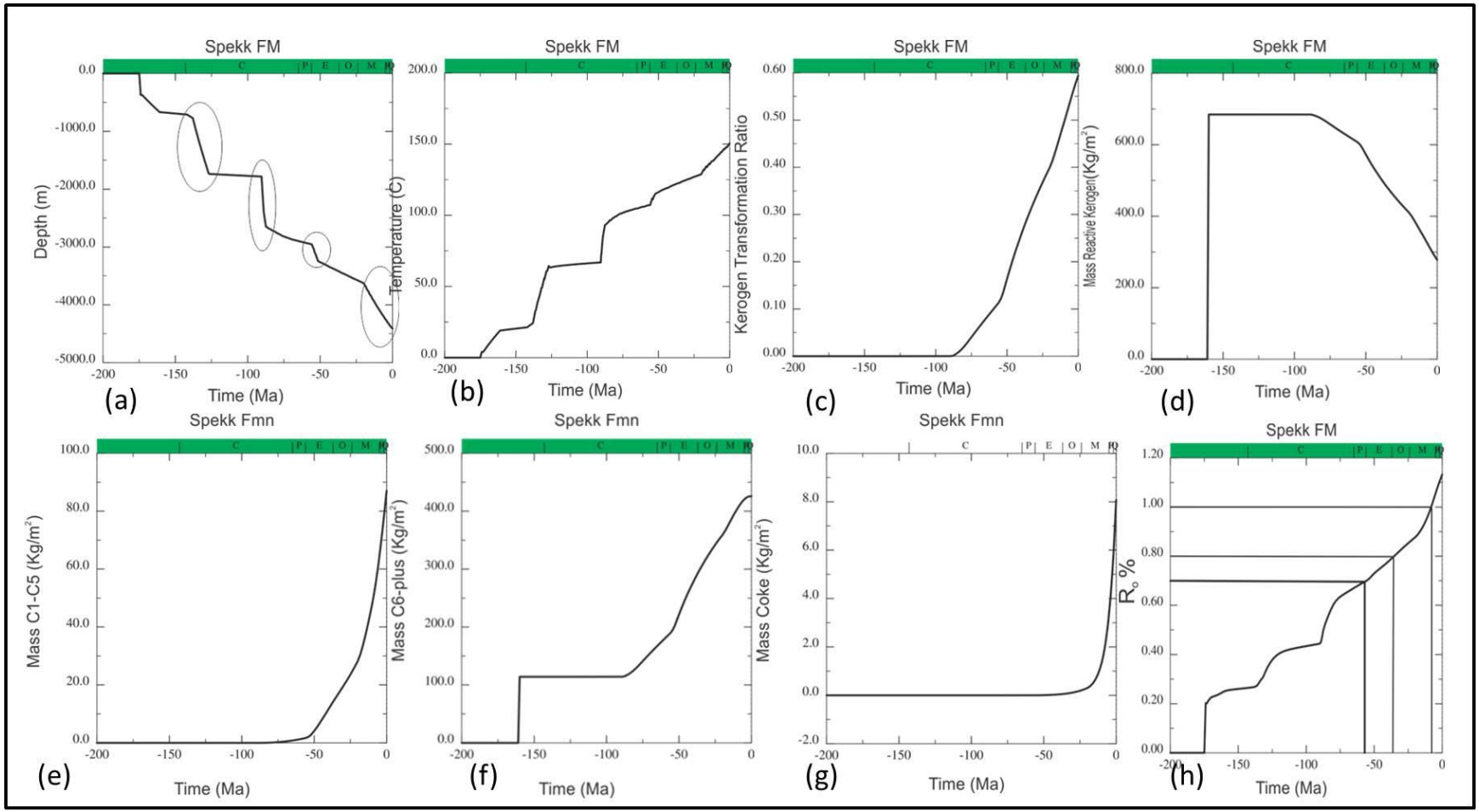

Figure 5.17: (a) Time-Depth cross-plot of the Spekk Formation. (b) Time-Temperature cross-plot of the Spekk Formation. (c) Kerogen transformation cross-plot. (d) Spekk Formation in the time-kerogen transformation cross-plot (e) Time-mass (C1-C5) cross plot (f) Time-Mass (C6 plus) cross plot (g) Time-Mass coke cross plot (h) Time- VR (%) cross plot. For details refer to section 5.9.2. Case-1: The Smørbukk Well (6506/12-9S

5.10 GOR Plots for Midagrd Well (6407/4-1)

GOR plots for each source rock which might have contributed to the reservoir HC charges have been plotted separately, but not the accumulated mixture of HCs that ends up in a trap.

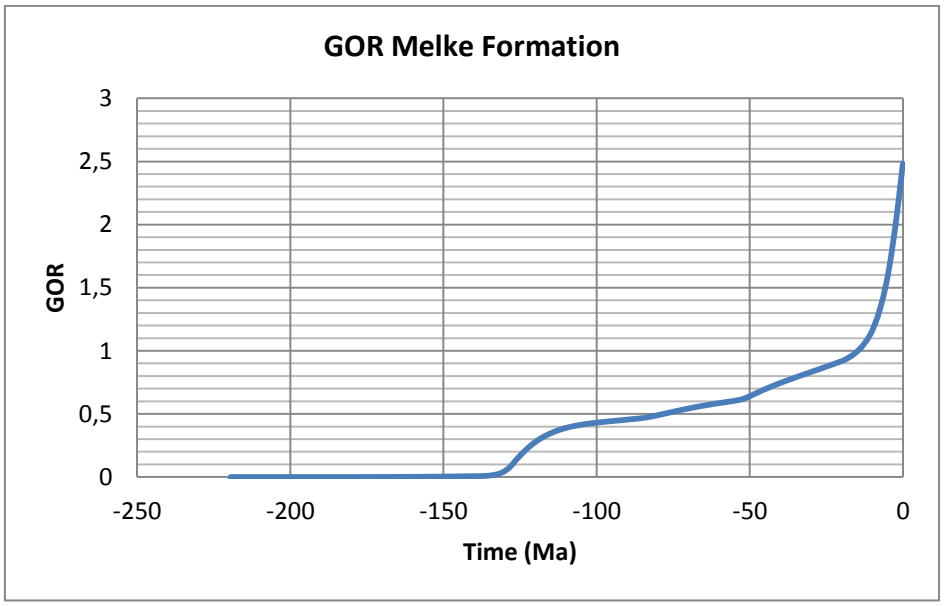

Figure 5.18: Computed GOR for Melke Formation based on borehole data from the Midgard field, a steep curve near -10 M.Y. occurs representing increased amount of cracking of oil to gas.

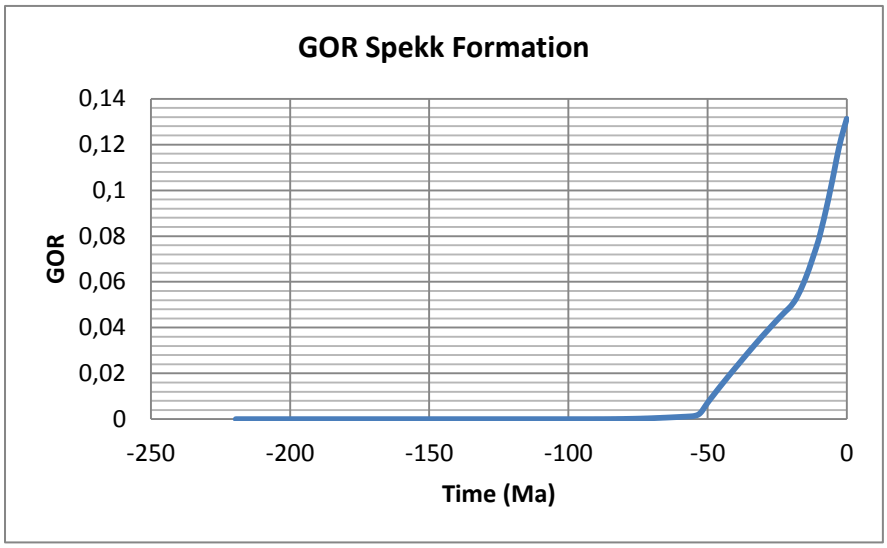

Figure 5.19: Computed GOR for the Spekk Formation based on borehole data from the Midgard field. Start of oil cracking to gas can be observed at ca. -55 M.Y. and peak GOR is observed at c. -20 M.Y.

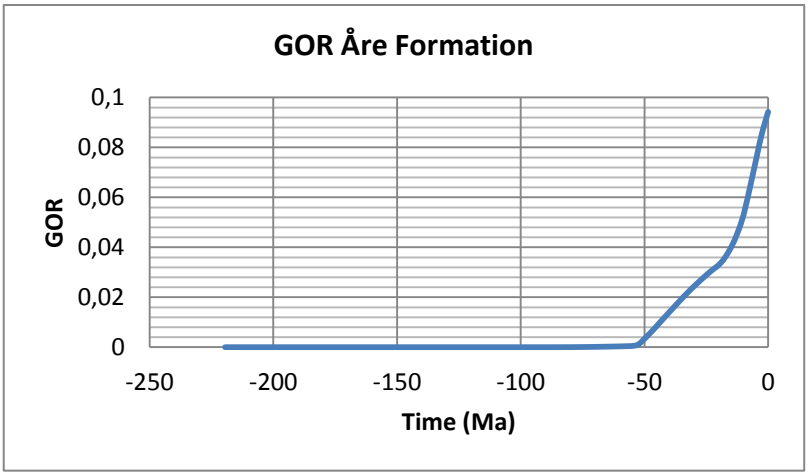

Figure 5.20: Computed GOR for the Åre Formation based on borehole data from the Midgard field, start of oil cracking to gas can be observed at ca. -55 M.Y. and peak GOR is observed at ca. -20 M.Y.

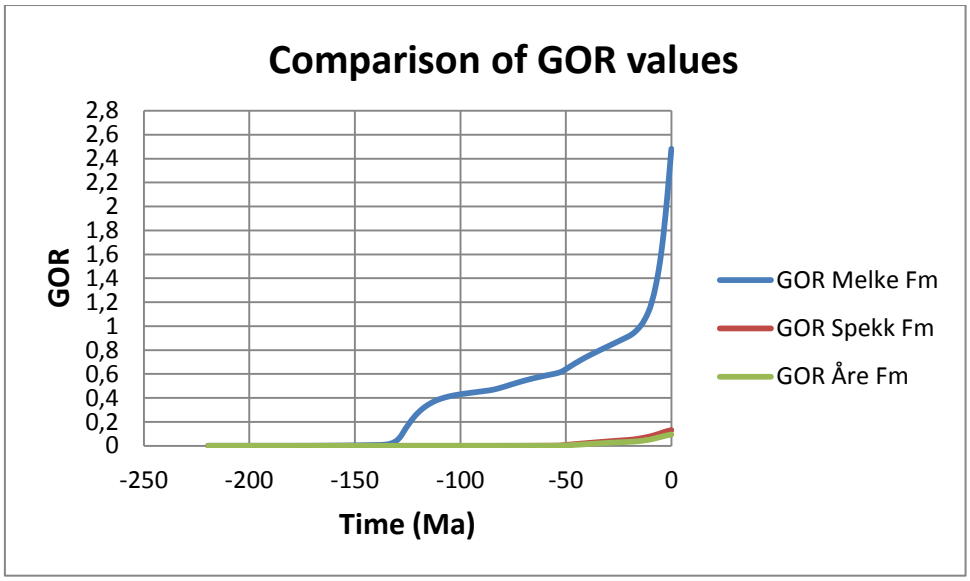

Figure 5.21: Comparison of GOR values based on the modelled results of the three formations for the Midgard well data.

5.11 GOR Plots for Smørbukk Well (6505/12-9S)

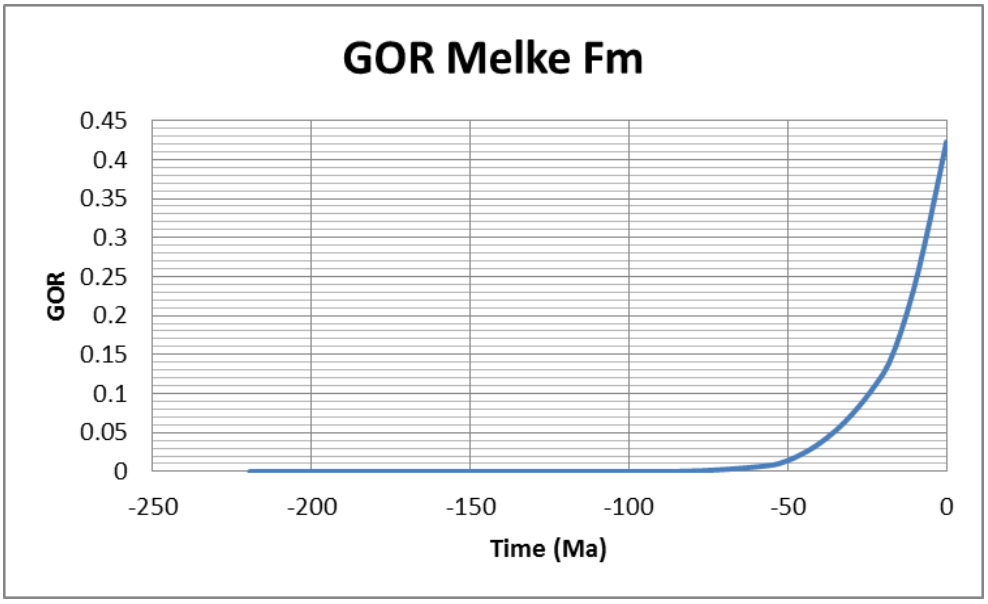

Figure 5.22: Computed GOR for the Melke Formation based on borehole data from the Smørbukk well.

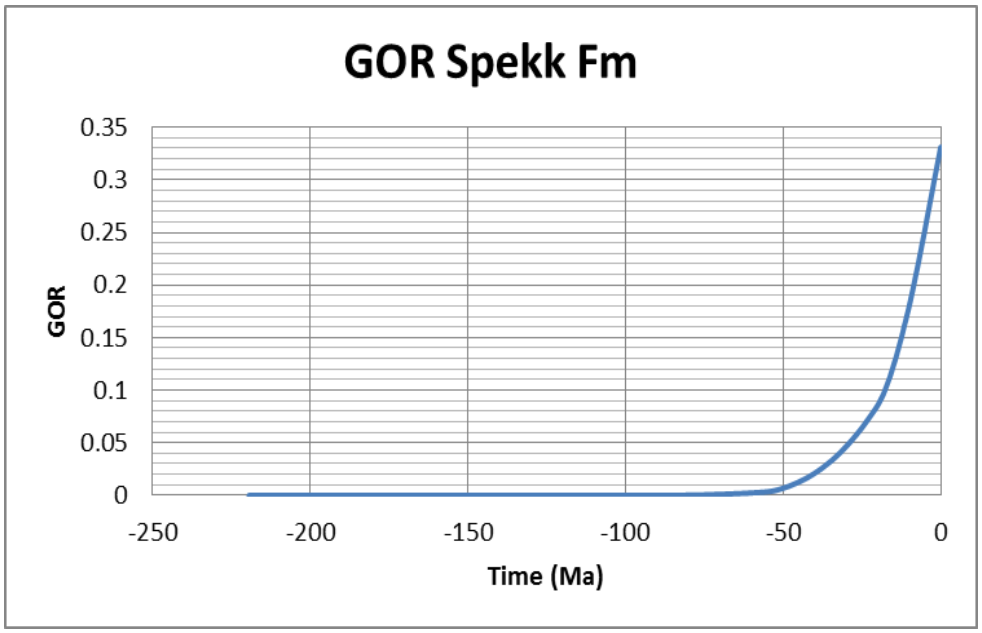

Figure 5.23: Computed GOR for the Spekk Formation based on borehole data from the Smørbukk field, start of oil cracking to gas can be observed at ca. -55 M.Y. and peak GOR is observed at ca. -20 M.Y.

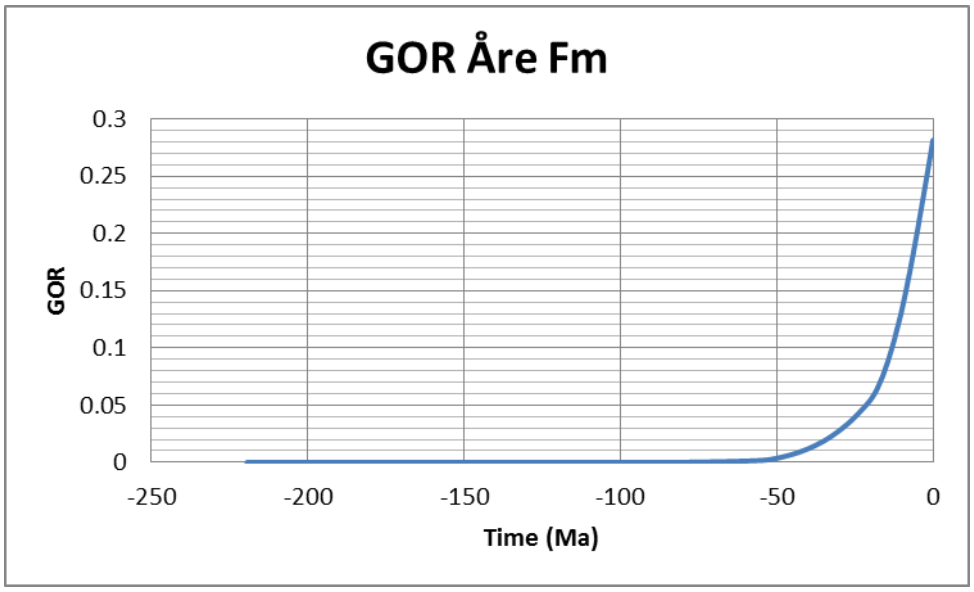

Figure 5.24: Computed GOR for the Åre Formation based on borehole data from the Smørbukk field, start of oil cracking to gas can be observed at ca. -55 M.Y. and peak GOR is observed at ca. -20 M.Y.

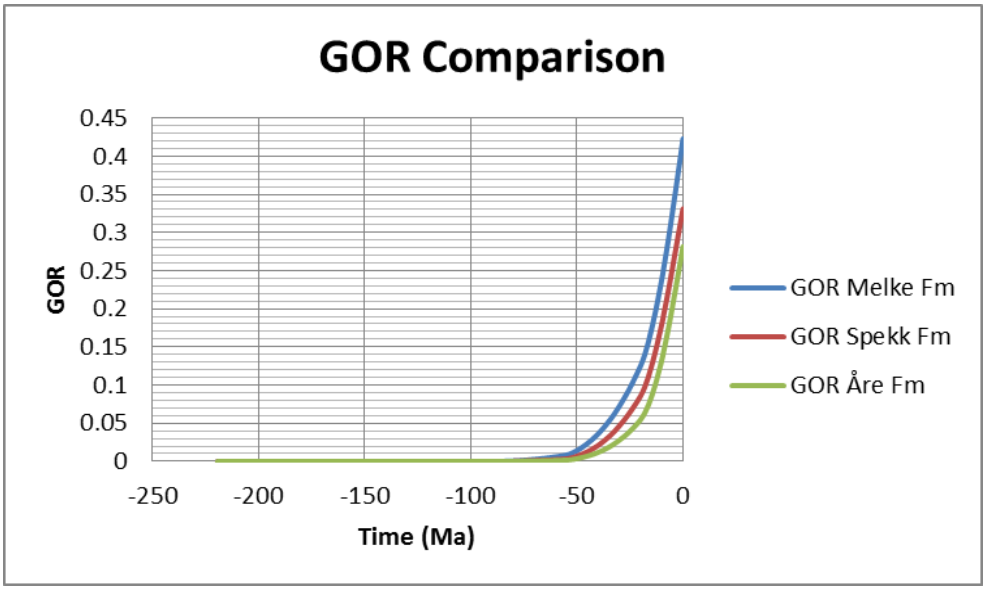

Figure 5.25: Comparison of GOR values based on the modelled results of the three formations in the Smørbukk well data.

Chapter 6

Uncertainties in the Input Data

In this chapter, possible errors and uncertainties in the input data are briefly discussed. The geological model, its assumptions and input parameter carries uncertainties (Figure 6.1). Therefore, it is necessary to quantify the value of data or reliability of the model in the basin modelling. The aim of modelling exercise is to construct an optimized model that is closest with the one in reality (Wenderbourg and Trabelsi, 2003).

Generally, models are constructed on the basis of uncertain data. As a result of uncertainties additional tasks are incorporated within a comprehensive model analysis. These tasks are classified as "risking", "understanding", and "calibration". These three tasks can be treated simultaneously by an effective method of Monte Carlo simulations (Hantschel and Kauerauf, 2009). Uncertainty and risk analysis has not been carried out in this study however, different errors and uncertainty of input data has been explained to comprehend the resulted model.

Maturity modelling is constrained by computer limitations, lack of data control and imperfect Knowledge of history and nature of rocks. Therefore, it is a best crude approximation of the general characteristics of reality; however it always contains intrinsic uncertainties and errors that limit the accuracy of its prediction (Waples, 1994).

Stratigraphic information is the primary parameter that has been used in maturity modelling (Table 4.1 and 4.2). Stratigraphy input data is based on previously published data (taken from the NPD). During the present study, there is greater confidence about the stratigraphy input data because the studied wells belong to one of the most mature areas of the Norwegian continental shelf, and therefore it is the most reliable parameter with insignificant effect of uncertainties.

A kinetic model encompasses certain limitations and therefore inherits number of flaws. Predominantly, kinetic parameters are derived from laboratory measurements which always contain some uncertainties such as temperature control (Espitallie et al., 1993; Waples, 1994). Data developed from high-temperature laboratory experiments are used to calibrate the kinetic models which surely do not reflect the true subsurface conditions.

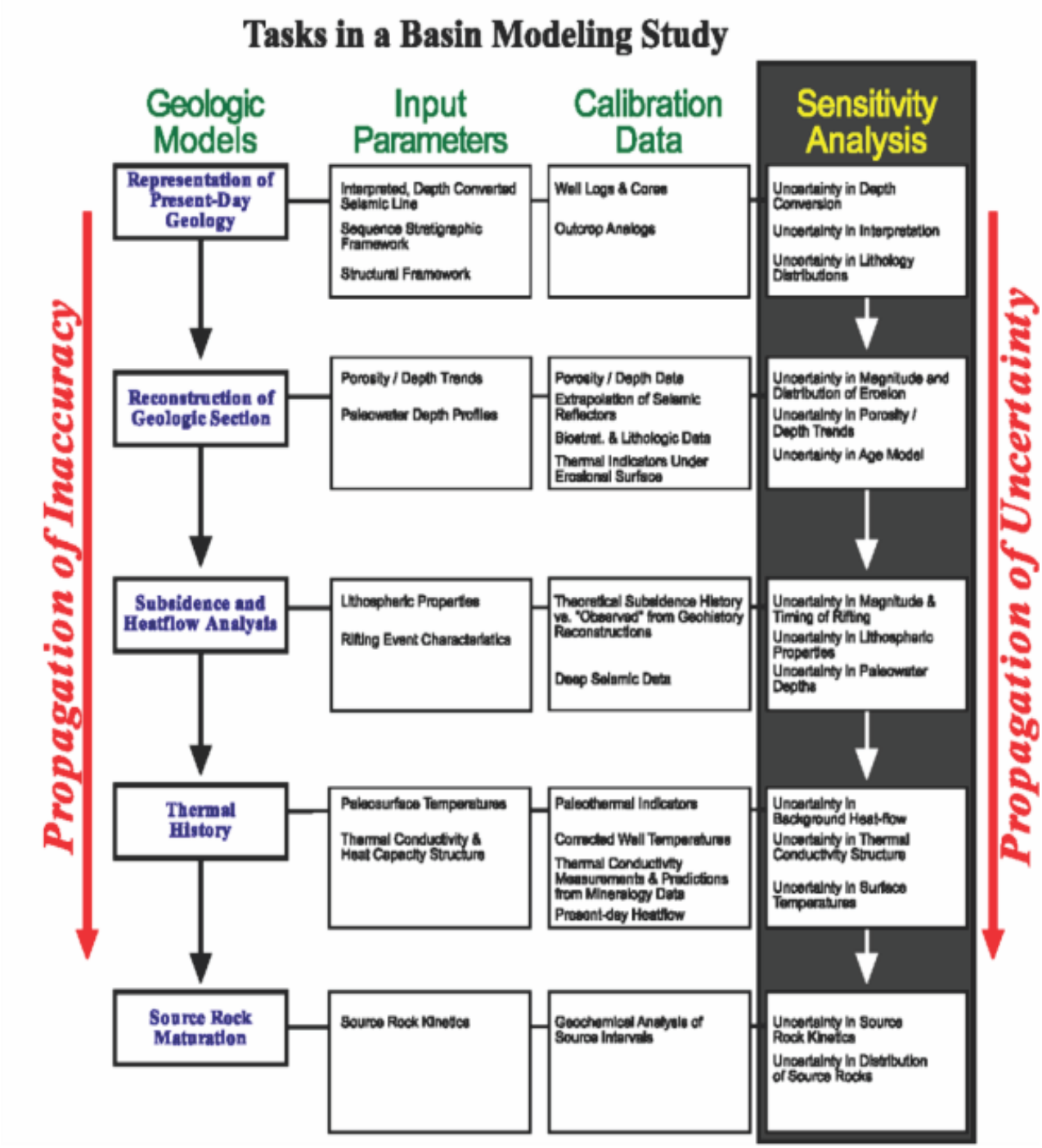

Figure 6.1: Basic tasks that are performed within basin modelling studies for uncertainty evaluation (class lecture Geo-4270).

The processes occurring in laboratory conditions are good analogs but are certainly different from those occurring in nature. Even if the laboratory experiments are consistent with nature there will be statistical errors in extrapolating from laboratory conditions to natural situations. Over the years, published kinetic parameters for number of kerogen are obtained from source

rock by different laboratories using a variety of techniques and equipment. As a result of this some discrepancies have been reported. (Waples, 1994). In most cases, these discrepancies are insignificant for exploration purposes; however they might occasionally lead to different exploration decisions. (Waples, 1994).

In the upper part of the well, modelled vitrinite reflectance is reasonably consistent with the observed vitrinite reflectance measured in laboratory, however it does not follow the same trend in the deeper part of the well (Figure 4.2). This error in the modelled vitrinite reflectance is the result of insufficient data input because hiatus is not defined in the input parameters properly.

The accuracy of the modelled results depends upon the input data i.e., how well the thermal history is constrained by thermal maturity and paleo-temperature indicators and how well the kerogen type and its kinetic parameters are known (Waples, 1994).

Chapter 7

Discussion

One of the core objectives of the present study is to model the "Critical Momemt" for the Åre, Melke and Spekk formations in the Midgard (6407/4-1) and the Smørbukk (6506/12-9S) wells of the Haltenbanken Petroleum Province. The Smørbukk field lies toward the East of the Vøring basin, where the basin becomes comparatively deeper than the Midgard field which lies to the West of the Trøndelog Platform (Figure 2.1). The Haltenbanken is a highly faulted, tectonically induced basin with major faults showing oblique–slip (Figure 2.2) (Gabrielsen et al., 1984; Bøen et al., 1984; Bugge et al., 1984; Buckovics & Ziegler 1985; Karlsen et al., 1995). The high prospectivity of the Halten Terrace is attributed to its structural configuration. The abundance of fault-blocks and the intermediate structural position between the deep Møre and Vøring basins and the shallower Trøndelog Platform provides an ideal mix of maturity and structuring at the Jurassic level where the main source and reservoir rocks are present (Heum et al., 1986).

Relatively simple subsidence history and geological setting makes the Haltenbanken an ideal area for advanced basin modelling studies (Heum et al., 1986). During the present study, three cases (Case 1, 2, 3) have been adopted to model the burial and thermal histories of source rocks for the Midgard (6407/4-1) and the Smørbukk (6506/12-9S) wells. As discussed earlier,Case-1 involves NPD derived geochemical input data (TOC %, HI) and utilises first order kinetic modelling approach following Pepper and Corvi (1995).Case-2 entails geochemical input data derived from the work of previous authors (Mo et al., 1989; Forbes et al., 1991) and uses the same first order kinetic modelling approach following Pepper and Corvi (1995). Finally, Case-3 includes geochemical input data derived from the NPD database (same as Case-1) and applies an alternative first order kinetic modelling approach following Tissot and ´Espitalie (1975, as cited in Forbes et al. (1991).

7.1 Analysis of the Two Kinetic Modelling Approaches

Use of the kinetic models for predicting the amount of petroleum generation within the possible source rocks is the most common technique in sedimentary basin analysis (Pepper and Corvi., 1995). During this study, no direct kinetic parameters of the source rocks were available for the source rocks in the study regions of the Midgard and the Smørbukk fields

albeit it is assumed as low risk to utilize standard parameters for the kerogen known for these formations in the general study regions. Furthermore, to measure the sensitivity, two different kinetic modelling approaches have been worked with, in order to determine the activation energies and pre-exponential factors etc. The underlying purpose of using different kinetic modelling approaches is to analyse their influence on modelling results of different source rocks and to compare the differences if any. These modelling approaches include:

i) Pepper and Corvi global kinetic model (Pepper and Corvi., 1995)
ii) Tissot / ´Espetaliet kinetic model (after Forbes et al., 1991)

For the Case-1 and Case-2 in the current study, kinetic parameters have been derived from Pepper and Corvi global kinetic model (1995). Forbes (1991) used North Sea equivalent formations' kinetic data for Åre and Spekk Formations (discussed by Espitalie et al., 1975), which also have been utilized during the present work forCase-3.

The Pepper and Corvi (1995) global kinetic model relates the kinetic parameters to the specific source rocks on the basis of depositional environments and stratigraphic ages. This model described five kerogen organofacies, defined by a specific organic matter input in addition to a depositional / early digenetic overprint (Pepper and Corvi, 1995). The Pepper / Corvi model divides the hydrocarbons into three groups, gas (C1−5), oil (C6+) and coke. Oil is generated only from the oil generative kerogen while gas could be generated from both gas generative kerogen and oil cracking (Figure 5.5).

The Tissot / ´Espetaliet (Tissot, 1969; Tissot and ´Espitalie, 1975) model is similar to the Pepper/Corvi model, except for two elements. Firstly, this model cannot generate gas directly from kerogen (Figure 5.6). Secondly, the generated gas does not come under one group rather it could be divided into several smaller groups (BAS user manual) (for detail discussion on both the models, refer to chapter 5).

During the present study however, no significant differences were found in the obtained results by the application of both these kinetic modelling techniques (Case-2 and Case-3 in Appendix C & D respectively).

7.2 Comments on the Burial and Thermal History Modelling

Burial and thermal histories are reconstructed and modelled for the three cases (case1, 2, 3) of the Midgard (6407/4-1) and the Smørbukk (6506/12-9S) wells. Flow-chart diagram has

already been discussed with important input data which is necessary for any burial and thermal history modelling exercise (Figure 4.1). Key input data includes present day stratigraphy and the rock's thermal parameters. Stratigraphic input data includes, age of the formation (start and end time for deposition of a stratal unit), thickness, lithology and erosional thickness (if any). However, it is pertinent to note that during current modelling exercise, impact of any erosional thicknesses is ignored. Thermal input data includes heat flux, surface temperature and other parameters. Value of heat flux used during modelling for both wells is 0.065 W/m2, which is typical for Mid Norwegian Continental shelf (Ritter et al., 2004).

7.3 Critical Times for Hydrocarbon Generation

As discussed earlier, establishing the "Critical Moment" of HC generation is one of the prime objectives of the current study. A comparison of already published data on timing of HC generation for the three source rocks with the present study is carried out. HC generation modelling has been conducted for both wells (the Midgard & the Smørbukk) separately with all three cases (Case1, Case2 and Case3).

Trapped petroleum could decipher the information about hydrocarbon generation, expulsion, migration and accumulation (Karlsen and Skeie, 2006). Knowledge of the timing of HC generation is of fundamental significance for two reasons. Firstly, migration conduits can vary with time owing to compaction, diagenesis, cementation, fracturing and later structural configuration. In order to understand the HC migration pathways and their ultimate accumulations that may result from migration, it is imperative to know when petroleum charges were on the move. Secondly, if generation occurs in geologically late periods, there would be less time for biodegradation, cracking, seal rupture and other destructive processes that destroy or modify HC accumulations (Waples, 1994). Basin modelling is better at estimating source rock maturity than hydrocarbon expulsion or the volumes of migrated petroleum (cf. Larter, 1988; Waples, 1994; Karlsen and Skeie, 2006).

Reservoir oil in the discovered fields of the Haltenbanken Petroleum Province has maturity value of about 0.7-0.8 VR (%) (Karlsen et al., 1995; Karlsen and Skeie, 2006) therefore, during the present study, the maturity value of 0.7-0.8 VR (%) has been used as the benchmark for the interpretation of results obtained from modelling study.

The Åre Formation reached peak oil generation during the Early Tertiary in Halten Terrace area (Campbell & Ormamassen, 1987; Karlsen et al., 1995). The Åre Formation is deemed as immature in the adjoining areas of the Midgard and Draugen fields (Karlsen et al., 1995). Mo et al. (1989) did the maturity modelling of this formation and proposed that the peak oil generation occurred in the deepest part of the basin during the Late Cretaceous. There is a strong likelihood that the generation continues still today in the slowly subsiding basin flanks towards the Midgard Horst (Karlsen et al., 1995). According to the present modelling for Case-1, the Åre Formation started HC generation during the Late Cretaceous at depth ca. 3300 m (absolute time; Turonian 92 Ma) which is quite consistent with the modelling results of Mo et al (1989) in the Midgard field (Figure 5.11h). The Åre Formation is currently at the depth of ca. 5000 m and its recent temperature in the Midgard well is 160 ^{0}C (Figure 7.1) . It is pertinent to mention that Case-2 & Case-3 modelling results on timing of HC generation are consistent with the results of Case-1 in the Midgard well.

Table 7.1: Critical Moments for the Midgard well derived from the modelling results.

Critical Moments for the Midgard (6407/4-1) well			
Formations	Case 1 (Abs. age Ma)	Case 2 (Abs. age Ma)	Case 3 (Abs. age Ma)
Åre	92	94	89
Melke	47	45	44
Spekk	40	40	40

There is no significant difference in timing of HC generation for the Åre Formation in the Smørbukk well. Its absolute HC generation timing is 90 Ma and it achieved maturity at the depth of ca. 3200m (Figure 7.2). However, there is a slight difference between the recent temperatures for the Smørbukk well which is 175 ^{o}C and the Midgard well (Figure 5.13 & 5.40). Similar to the Midgard well, Case-2 &Case-3 modelling results on HC generation are consistent with the results of Case-1 in the Smørbukk well (Table 7.2).

Modelling results of the present study demonstrate good agreement with the study of Mo et al (1989) for the Midgard field. However, considerable difference exists between the present study and the regional study of Forbes et al (1991), as cited in Karlsen et al. (1995), who have

placed the timing of HC generation for the Åre Formation in the Early Tertiary while on the contrary this study considers it to be an event 92 Ma b.p. (Midgard) and 87 Ma b.p. (Smørbukk), a Turonian – Late Cretaceous event.

Table 7.2: Critical Moments for the Smørbukk well derived from the modelling results.

Critical Moments for the Smørbukk well (6506/12-9S)			
Formations	Case1(Abs. age Ma)	Case 2 (Abs. age Ma)	Case 3 (Abs. age Ma)
Åre	90	90	90
Melke	48	48	47
Spekk	55	55	55

The Melke Formation is reasonably organic rich (ca. 1-4% TOC) and it is considered as a good example of a lean source rock. This formation expelled mainly gas upon attaining approximately 1.7 (%) VR (Heum et al., 1986; Karlsen et al., 1995).

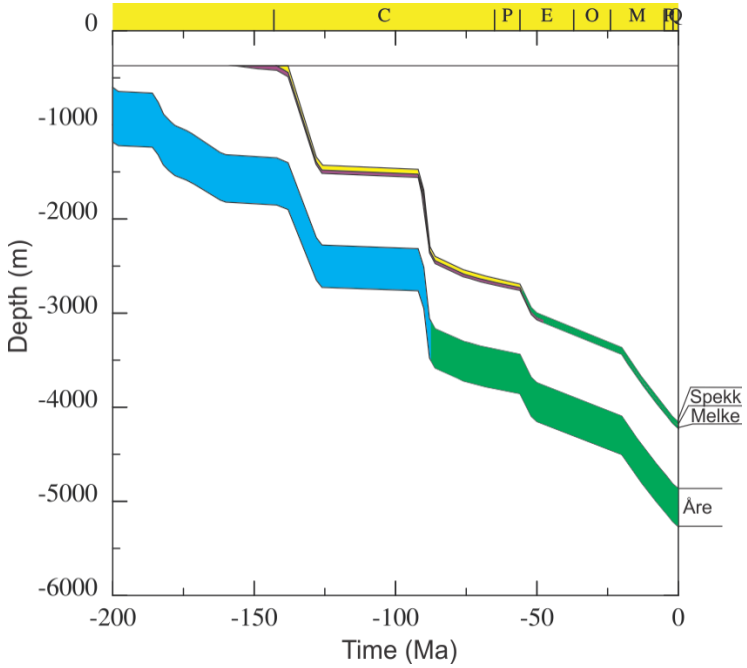

Figure 7.1: Time-depth cross plot for the Åre, the Melke and the Spekk formations for the Midgard well. The green colour represents mature part of the source rocks, the information on maturity is derived from the already presented VR (%)-Time cross-plots for the respective formations (figure 5.11h, figure 5.12h and figure 5.13h). Refer to Table 7.1. for the exact timing of modelled HC generation from the three source rocks.

Oil potential of the Melke Formation is considered insignificant as compared to Spekk Formation and the deeper Åre Formation (Heum et al., 1986; Cohen et al., 1987). However, there is a strong tendency that the oil potential of the Melke Formation may show lateral variation towards off Mid-Norway, and further systematic facies analyis is required especially from deeper parts of the basins where the formations may have developed as "anoxic ponds" (Karlsen et al., 2004). Still, the TOC values in this range are globally considered as "good to very good" (Table TOC chapter 5) cf. Peters and Cassa, (1994) and it is quite possible that the previous workers have overlooked the significance of this formation due to the existence of the very prolific Spekk Formation. In the present study, an attempt to model the hydrocarbon generation of Melke Formation is carried out to understand its generation potential and contribution to the reservoired hydrocarbons.
According to present modelling forCase-1, the Melke Formation started HC generation during Middle Eocene at depth ca. 3200m (Absolute time: 47 Ma, Lutetian) in the Midgard well (Table 7.1). The Melke Formation is currently at the depth of ca. 4200m and its recent temperature in the Midgard well is 140 ^{o}C.

There is no significant difference concerning the time for the HC generation from the Melke Formation for the Smørbukk well. Its absolute HC generation time is 48 Ma and started generation at the depth of ca. 3200m (Table 7.2). However, the two wells show small variation between the recent temperatures for Melke Formation i.e., 140 ^{o}C for the Midgard & 145 ^{o}C for the Smørbukk well.

Similar to the Case-1, Case-2 & Case-3 modelling results on HC generation for the Midgard and the Smørbukk wells are generally similar.

The Spekk Formation belongs to the upper Jurassic and has an accumulated thickness of about 400 m in undrilled structural depressions. This formation has a mature rating in the areas of the Haltenbanken where most of the hydrocarbon accumulation has occurred and is considered immature in the eastern platform area. Towards the west (i.e. the Vøring Basin), this formation is rated as over-mature (Karlsen et al., 1995). Peak oil generation is considered to be reached during the Late Tertiary in Halten Terrace (Campbell and Ormaasen, 1987). According to Leadholm et al., (1985), peak oil generation is estimated to have occurred at the 3400m burial over large areas of Haltenbanken area. Cohen and Dunn (1987) evaluated the initial oil expulsion to have occurred at ca. 120^{o}C, which corresponds to a burial depth of

3100m in their data. Whereas, Heum et al., (1986) deduced the threshold for primary migration from these formations on the basis of vitrinite reflectance equivalence (VR) to a value of 0.7%.

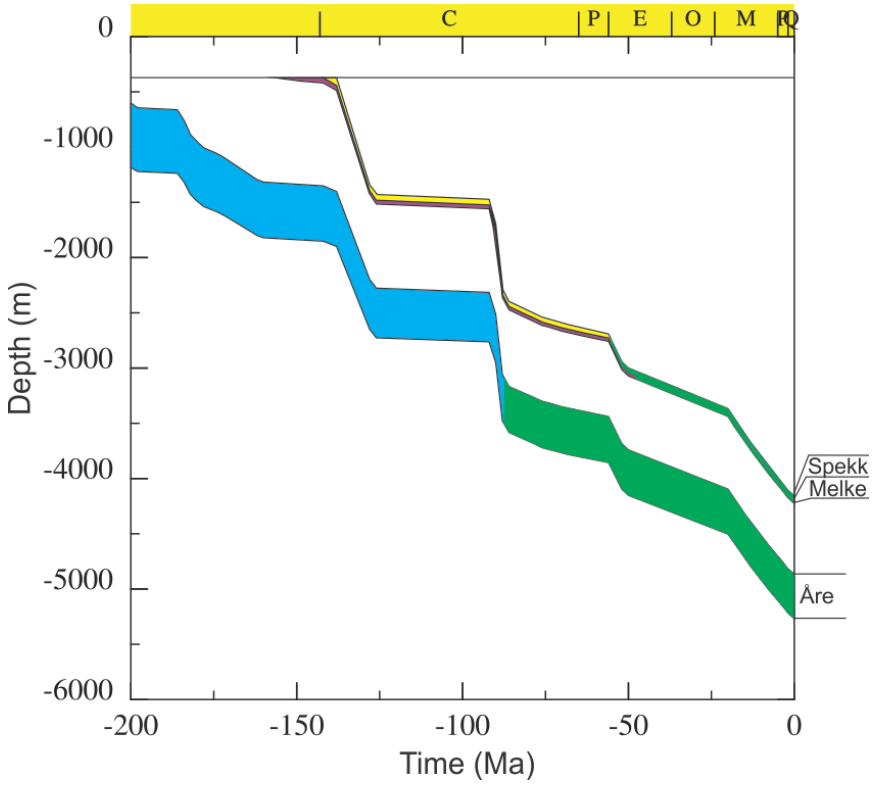

Figure 7.2: Time-depth cross plot for the Åre, Melke and Spekk formations for the Smørbukk (6506/12-9S) well. Green colour represents mature part of the source rocks, the information on maturity is derived from the already presented VR (%)-time cross plots for the respective formations (Figure 5.15h, Figure 5.16h and Figure 5.17h). Refer to Table 7.2 for the exact timing of modelled HC generation from the three source rocks.

This is equivalent in their dataset to ca. 3900m depth. Cohen and Dunn (1987) estimate this depth to be the related with the initial oil to gas cracking (T≈150^{o}C) therefore; a depth of ca. 4600 m is postulated as the initial refractory gas generation depth. Similar depth of approximately 4700 m has been inferred by Heum et al., (1986) for the deepest limit of oil generation at 1.0% VR (Karlsen et al., 1995). Biomarker distributions from core sample of Spekk Formation have been studied by Karlesn et al., (1995) and they suggest that substantial oil expulsion has occurred at a depth shallower than 3900m.

According to present modelling forCase-1, the Spekk Formation started HC generation during Middle Eocene at depth ca. 2900m (Absolute time; Bartonian 40 Ma) in the Midgard well (Table 7.1). The Spekk Formation is currently at the depth of ca. 4200m and its recent temperature in the Midgard well is 135 C^o. There is no significant difference in depth for the Smørbukk well. While its absolute HC generation time is Early Eocene (Absolute time 55 Ma; Ypresian) and it started generation at the depth of ca. 2800m (Table 7.2). There is however a slight difference of the recent temperatures for the Midgard and the Smørbukk wells where the temperature for the later well is 150 ^oC.

Likewise, modelling results of Case-2 and Case-3 on HC generation for the Midgard and the Smørbukk wells are generally similar (Table 7.1 & 7.2).

7.4 Remaining Potential of the Source Rocks

During the current study, an attempt was made to find out the remaining potential of the Åre, the Melke and the Spekk formations by the analysis of kerogen transformation ratios of respective formations. Modelled remaining potential for the three source rocks in all three cases (Case 1, 2, 3) have been compared in order to analyse the effects of using two different kinetic modelling approaches on the final results (Figure 7.3 – Figure 7.8).

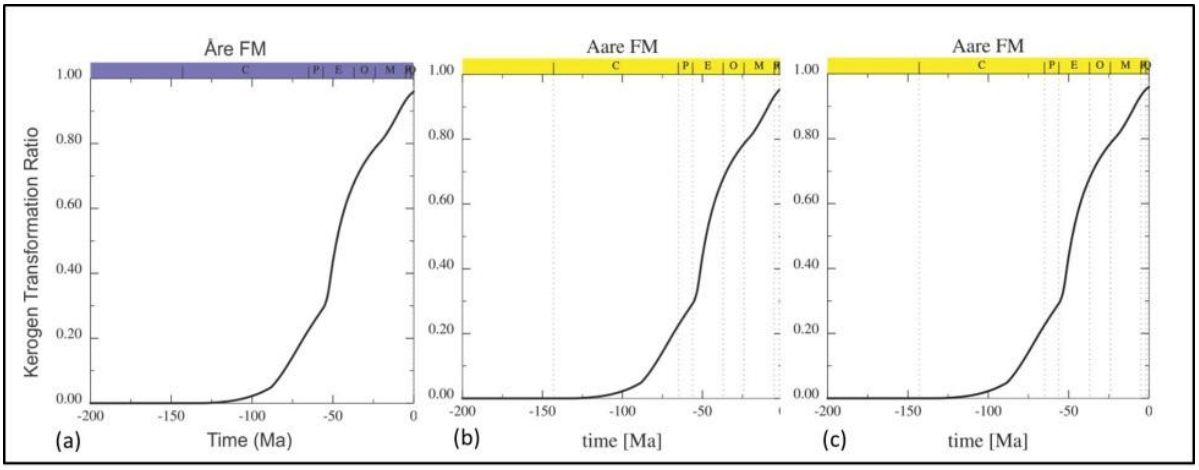

Figure 7.3: Modelling results of the transformation ratio of the Åre Formation for the Midgard (6407/4-1) well for case-1 (a), Case-2 (b) and Case-3 (c) are compared and they are exactly the same. Kerogen in the Åre formation has been transformed up to 95% and there is only 5% remaining potential for this formation.

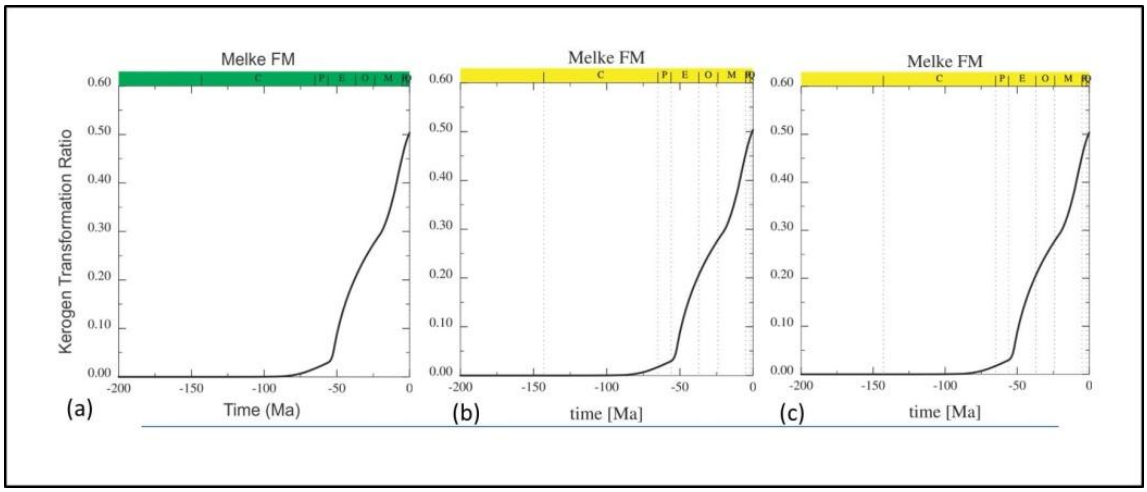

Figure 7.4: Modelling results of the transformation ratio of the Melke Formation for the Midgard (6407/4-1) well for case-1 (a), case-2 (b) and case-3 (c) are compared and they are largely the same. Kerogen in the Melke formation has been transformed upto 50% and there is only 50% remaining potential for this formation.

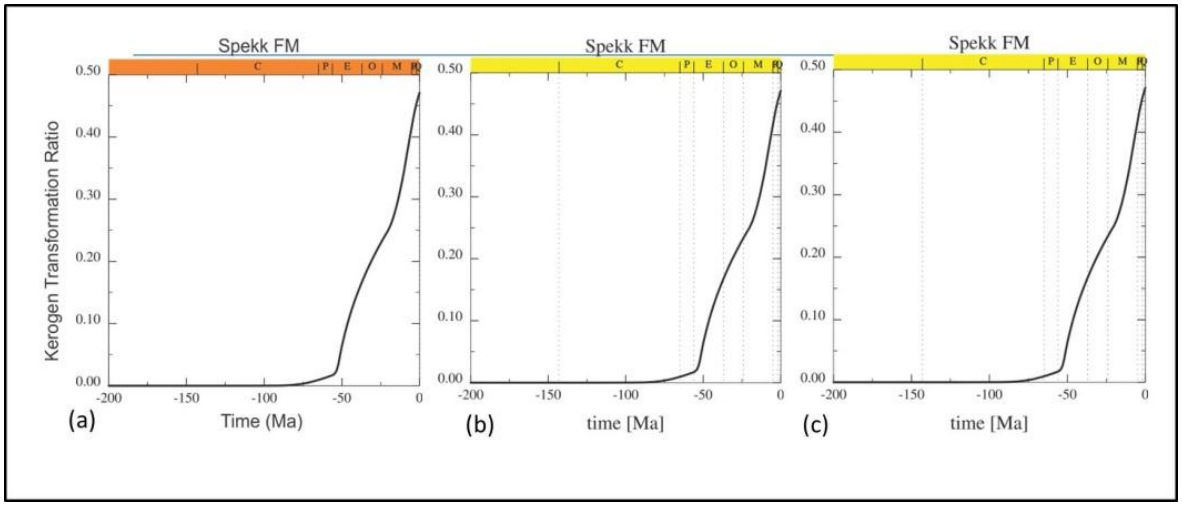

Figure 7.5: Modelling results of the transformation ratio of the Spekk Formation for the Midgard (6407/4-1) well for Case-1 (a), Case-2 (b) and Case-3 (c) are compared and there are essentially no differences. Kerogen in the Spekk formation has been transformed up to 47% and there is only 5% remaining potential for this formation.

An analysis of figures 7.3 - 7.8 reveals no substantial difference of kerogen transformation ratios, which implies that application of two different kinetic modelling approaches (see Section 7.1) yields similar output data. It is further inferred from the already discussed figures that the influence of these kinetic modelling approaches is either negligible or simply it does not effect the kerogen transformation ratios (Figure 7.3 – Figure 7.8).

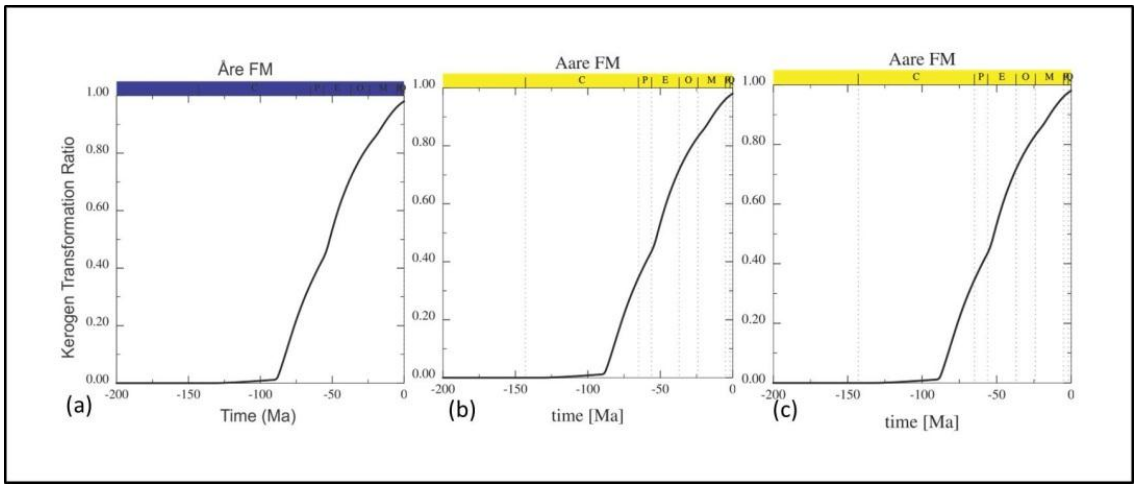

Figure 7.6: Modelling results of the transformation ratio of the Åre Formation for the Smørbukk (6506/12-9S) well for Case-1 (a), Case-2 (b) and Case-3 (c) are compared and they are exactly the same. Kerogen in the Åre formation has been transformed up to 98% and there is only 2% remaining potential for this formation.

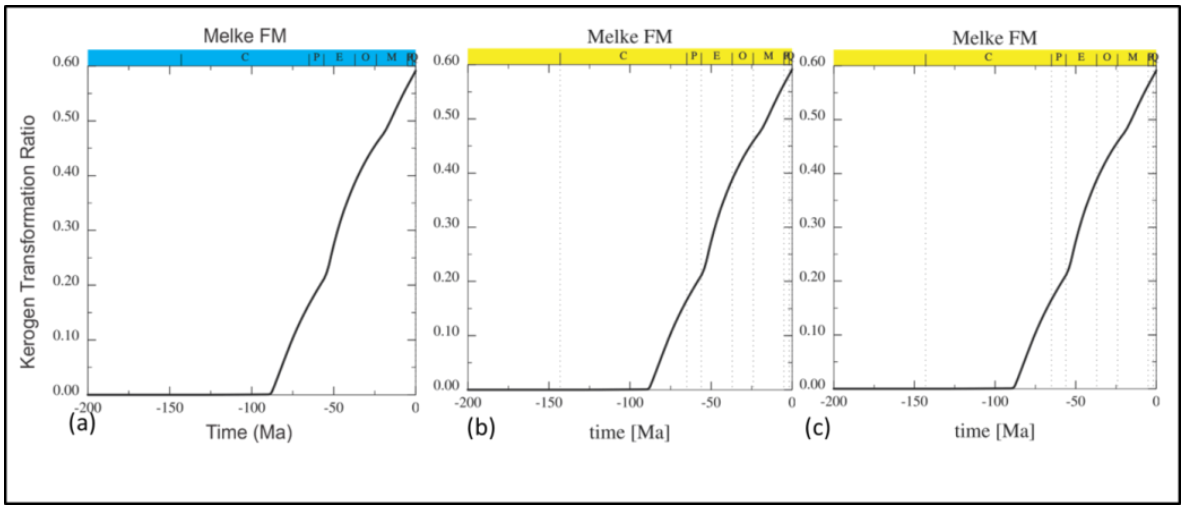

Figure 7.7: Modelling results of transformation ratio of the Spekk Formation for the Smørbukk (6506/12-9S) well for Case-1 (a), Case-2 (b) and Case-3 (c) are compared and are essentially the same. Kerogen in the Spekk formation has been transformed up to 60% and there is only 40% remaining potential for this formation.

During the present study, expulsion is zero because oil generation has not surpassed the expulsion limits. The kerogen definition on the input file has a very high expulsion limit, 1 gram per gram of rock. However, this is not important at this stage because the current study does not intend to model expulsion.

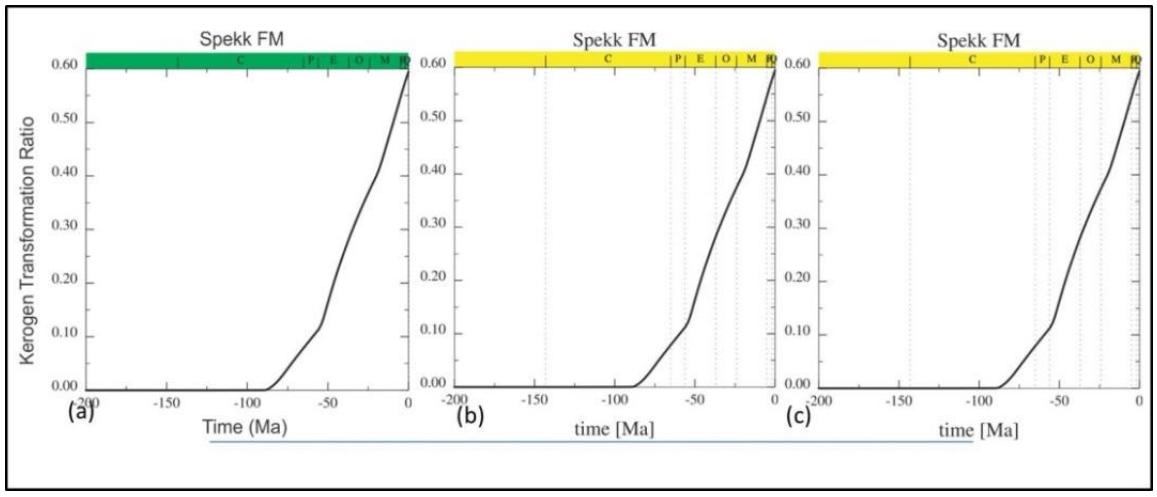

Figure 7.8: Modelling results of transformation ratio of the Spekk Formation for the Smørbukk (6506/12-9S) well for Case-1 (a), Case-2 (b) and Case-3 (c) are compared and are found exactly the same. Kerogen in the Spekk formation has been transformed up to 60% and there is only 40% remaining potential for the Spekk formation.

Therefore, it demonstrates that what has generated is reflection of what could have been expelled and the values are plotted only of what has been generated. Expulsion of HC is a process that is poorly understood and there are no state-of-art models of expulsion and expulsion varies from source rock to source rock. It is quite possible that some source rock expels all generated HC, while nothing is expelled in another source rock.

7.5 Critical Moments - A comparison Between the Two Wells

A Comparison of critical moments of HC generation between the studied the Midgard (6407/4-1) and the Smørbukk (6506/12-9S) wells has been undertaken. The Åre Formation yields the HC generation age of 89 to 92 Ma for the three modelled cases of the Midagrd well. Similarly, the critical moments of HC generation of the Åre Formation for the Smørbukk field is about 90 Ma (Tables 7.1 & 7.2). In the Midgard well the critical moments for the Melke Formation is ca. 44-47 Ma while the Smørbukk well predicts the HC generation age of about 47-48 M.Y. Modelling results of the Spekk Formation reveals the age of 40 Ma for HC generation in the Midgard well whereas, the Smørbukk modelling results assign an age of 55 Ma to this formation.

Briefly, it is summarized that the Åre and Melke formations do not show a considerable difference on timing of HC generation in the two wells while the Spekk Formation reveals substantial difference on the critical moments of HC generation between the two wells.

It is tempting to underline the importance of having a Critical Moment for a prospect or trap which is closer in time to the present. It is this fact which is the most likely explanation that Karlsen et al. (1995; 2004) concluded that all producing oil fields at the Haltenbanken produce Spekk derived oil. Little if any evidence was found for, what must have been huge contributions from the Åre Fm. This suggests that this gas or condensate was effectively lost from the traps long before onset of oil genesis from the Spekk Formation (cf. Karlsen et al., 1995; 2004) and this modelling gives us here estimates for the absolute time involved.

7.6 Predicting the GOR of Nearby traps from Present Modelling

The amount and composition of generated HCs can be estimated by maturity modelling. Most models predict gas-oil ratios but their precision largely depends on excellent characterization of the kerogen. When kerogen type and its kinetic parameters are well understood, such estimates are quite dependable (Waples, 1994). During the present study, GOR for the Åre, the Melke and the Spekk formations of both the Midgard (6407/4-1) and the Smørbukk (6506/12-9S) wells has been undertaken (Figures 5.63 - 5.70).

Initial propositions included to model the GOR for the source rocks (Åre, Melke and Spekk) so as to predict the gas to oil ratios in the adjacent traps of the area and to compare this with the present situation, based on the results obtained from the studied wells. After modelling GOR for the studied source rocks, it has been observed that prediction of GOR for the nearby traps, on the basis of present results could not give a meaningful solution. This is largely because of various constraints that impede a direct correlation of the modelled GOR with that of the nearby traps. These constraints include the following:

i) HCs migrate from the kitchen area to the traps and during migration, there are effects of volume change due to varying PT (Pressure-Temperature) conditions i.e., gas expansion and oil shrinkage, that alters the GOR values (Karlsen and Skeie, 2006).

ii) In the reservoired HCs there may be secondary alteration processes (biodegradation, water washing, deasphalting, thermal alteration, gravity segregation and dysmigration) on the trapped petroleum due to physical, chemical

and biological processes that lead to change the petroleum composition (Allen and Allen, 2005). These processes are capable of changing the GOR values of the reservoired HCs.

Therefore, in order to predict the GOR for the adjacent traps based on modelling results of the current study, it is important to address the constraints described above. However, this is not a trivial matter as it requires great amount of time to focus on these issues, while during the present study a limited time does not warrant exploring the effects of these mechanisms any further. Nevertheless, one possible method is to do oil characterization for both the wells which will define the contribution from each source rock and oil-source correlation will yield further information on the GOR of each source rock. Once the information on contribution from each source rock and its GOR becomes available then it would relatively be easy to predict change in behaviour of GOR up-dip from the studied wells, following the model of Sales (1997).

Chapter 8

Conclusion

1-D basin modelling of two (2) wells from the Haltenbanken Area (the Midgard well 6407/4-1; the Smørbukk well 6506/12-9S) was carried out using BAS software.

One of the core objectives was to estimate the critical moments (timing of HC generation and expulsion) for the Åre, Melke and Spekk formations. This was achieved by reconstructing the burial and thermal histories of these formations in space and time by employing their physical and thermal properties such as lithologies, age of horizons, geothermal gradients and other relevant parameters.

This study utilized two different kinetic modelling approaches i.e. the Pepper & Corvi (1995) model, and the Tissot & Espitalie (1969 & 1975) model to handle the kerogen transformation mechanism. Part of the focus of this work was to evaluate if results would differ according to which model was used.

These modelling approaches are based on the realistic source rocks' pre-exponential factors and distribution of activation energies. It was found that both kinetic modelling techniques yielded similar results for the critical moments and the remaining potentials for the source rocks but give different results for the expelled quantities of oil versus gas.

According to present study for the Case-1 (Pepper & Corvi, 1995 model), the Åre Formation started oil/condensate generation at ca. 92 Ma b.p. in the the Midgard region and at 87 Ma b.p in the Smørbukk region which corresponds to Turonian time (Late Cretaceous).

Modelling results suggest that gas generation from this formation started at ca.30 Ma (Rupelian – Early Oligocene) in the Midgard field and at ca. 50 Ma (Ypresian – Early Eocene) for the Smørbukk field for all the cases (Case-1, Case-2 and Case-3).

The Åre Formation started HC generation at the depth of 3200 m while at present this formation is at the depth of 5000 m. This formation has generated up to the 95 % out of its total potential thus with only ca. 5% potential is remaining for the Midgard (6406/4-1) and the Smørbukk (6506/12-9S) wells. Thus, the formation is "burnt out" at both locations which imply that today it has no generative potential in the deeper "kitchens" of both the Midgard and the Smørbukk traps.

Similar to the Case-1, Case-2 & Case-3 modelling results on HC generation for the Midgard and the Smørbukk wells show a general concordance.

Present modelling for the Case-1 reveals that oil generation from the Melke Formation took place at the depth of ca. 3200m (absolute time: 47 Ma b.p, Lutetian) in the Midgard region. At present this formation is at the depth of ca. 4200 m and its recent temperature is 140 ^{0}C. There is no significant difference in oil generation age of the Melke Formation for the Smørbukk field where it started to generate at ca. 48 Ma b.p. (Lutetian – Middle Eocene) corresponding to depth of ca. 3200 m. However, the two wells show small variations of the recent temperatures for the Melke Formation i.e., 140 ^{0}C for the Midgard & 145 ^{0}C for the Smørbukk well.

Gas generation of the Melke Formation in the Midgard field was initiated at ca.13 Ma (Serravallian – Middle Miocene) while for the Smørbukk field, gas generation is modelled to have started at ca. 20 Ma b.p. (Burdigalian – Early Miocene).

Similar to the Case-1, Case-2 & Case-3, modelling results on HC generation for the Midgard and the Smørbukk wells are in accordance with each other. The Melke Formation has generated up to 50 % from its total potential. However, it still has remaining potential of up to 50% in the Midgard (6406/4-1) well. Similarly, it has generated upto 60% in the Smørbukk field and has remaining potential of up to 40 %. This could mean that the Melke Formation has some real generative potential in the actual deeper “kitchen” areas of both the Smørbukk and the Midgard Fields.

According to present modelling for the Case-1, the Spekk Formation started oil generation during Middle Eocene at depth of ca. 2900m (absolute time; Bartonian 40 Ma) in the the Midgard well. The Spekk Formation is currently at the depth of ca. 4200 m in this well while its recent temperature is 135 ^{0}C. There is no significant difference in the current depth of the Melke Formation in the Smørbukk well. However, it’s absolute oil generation time is Early Eocene (Absolute time 55 Ma; Ypresian) and it started generating oil at the depth of ca. 2800m. There is however a slight difference of the recent temperatures for the Midgard and the Smørbukk wells where temperature for the later well is 150 ^{0}C.

Gas generation for the Midgard field was initiated at ca.10 Ma b.p. (Tortonian – Late Miocene) while for the Smørbukk field the modelled timing of gas generation is ca. 25 Ma b.p. (Chattian – Late Oligocene). Similarly, modelling results of Case-2 and Case-3 for HC

generation in the Midgard and the Smørbukk wells are in agreement. The Spekk Formation has generated up to 45 % of its total potential and has therefore 55% remaining potential in the Midgard (6406/4-1) region. Similarly, this formation has generated up to 60 % of its total potential in the Smørbukk field and therefore it has approximately 40% remaining potential.

It is clear that the relatively much more recent "Critical Moment" for the Spekk Formation compared to the Åre Formation at both locations and the continued source rock potential of the Spekk Formation means that the Spekk Formation has recently continued to feed oil and gas into the Midgard and Smørbukk structures.

It is possible that contributions of condensate or gas from the Åre Formation could have reached into the Midgard and Smørbukk traps, but at such an early time (early Critical Moment) that these charges were lost from the traps meaning that the cap rocks could not hold on to these charges during the ca. 80-90 Ma b.p.

Suggestions

This study has been accomplished during a limited time of 17 weeks. Therefore, a number of issues remained unaddressed which are deemed relevant to understand the maturation histories of the studied source rocks. These include:

- For better understanding the Haltenbanken petroleum system modelling, there is need to incorporate more geochemical data so that one could compare the relative amounts of reservoired oil to gas - to that modelled.
- Proper uncertainty and risk analysis should be performed for the construction of more realistic models.
- 2D and 3D basin modelling studies will be helpful for identification of the basin-scale migration pattern of the HCs.
- The information on contribution from each source rock and its GOR could be compared to changes in behaviour of GOR during up-dip migration, following the model of Sales (1997).
- Differences in modelled GOR versus that found today in traps could also be interpreted in terms of cap rock properties

References

Allen, P. A., & Allen, J. R. , 2005, The petroleum play. Basin Analysis, Blackwell Publishing, second edition, p. 405-474.

Bahlburg, H., & Breitkreuz, C., 2004, Grundlagen der Geology: Elsevier GmbH, Muenchen, second edition.

Barley, B. J., Chergotis, D., Wilson, M. & Young, S., 1992, Lithology prediction by extrapolating well data. In: Proceedin, Indonesian Petroleum Association 21st Annual Convention, p. 287-308.

Beardsmore, G. R., & Cull, P. J., 2001, Crustal Heat Flow: a guide to measurement and modelling: Cambridge University Press, p. 1-301.

Benson, S. W., 1968, Thermodynamical Kinetics: Wiley.

Bjørlykke, K., 2010, Petroleum Geoscience: From Sedimentary Environments to Rock Physics: springer, p. 1-501.

Bugge, T., Knarud, R., & Mørk, A, 1984, Bedrock geology on the Mid-Norwegian continental shelf. In: A. M. Spencer et al., (eds.) Petroleum Geology of the North European Margin. Norwegian Petroleum Society, Graham & Trotman, London, p. 271-284.

Bukovics, C., & Ziegler P. A. , 1985, Tectonic development of the Mid-Norway continental margin: Marine and Petroleum Geology, p. 2-22.

Bøen, F. S., Eggen, S. & Vollset, J, 1984, Structures and basins of the margin from 62° to 69°N and their development: A. M. Spencer, et al., (eds.) Petroleum Geology of the North European Margin. Norwegian Petroleum Society, Graham & Trotman, London, p. 253-270.

Campbell, C. J., & Ormaasen, E., 1987, The discovery of oil and gas in Norway: a historical synopsis. In: A. M. Spencer, et al., (eds.) Geology of the Norwegian Oil and Gas fields. Graham & Trotman, London, p. 1-37.

Cohen, M. J., & Dunn, M. E., 1987, The hydrocarbon habitat of the Haltenbanken-Trænabankken area offshore Mid Norway. In: J. Brooks, & K. Glennie (eds.), petroleum geology of North West Europe. Graham and Trotman, p. 1051-1104.

Dalland, A., Woersley, D., & Ofstad, K, 1988, A lithostratigraphic scheme for the Mesozoic succession offshore mid-and northern Norway: Norwegian Petroleum Directorate Bulletin, 4, p. 1-65.

Dembicki Jr, H., 2009, Three common source rock evaluation errors made by geologist during prospect or play appraisals: AAPG Bulletin, v. 93, p. 341-356.

Dow, W. G., 1974, Application of oil correlation and source rock data to exploration in williston basin: AAPG Bulletin, v. 58, n. 7, p. 1253-1262.

Dutranois, A., Li, W. C., Dulac, J. C., Lecomte, J. F., Callot, J. P., & Rudkiewicz, J. L., 2010, Breakthrough in basin modeling using time/space frame: Offshore Magazine p. 1-5.

Ehrenberg, S. N., Gjerstad, H. M., & Hadler-Jacobsen, E, 1992, Smcrbukk Field - a gas condensate fault trap in the Haltenbanken Province, offshore Mid-Norway. In: M. Z. Halbouty, (ed.) Giant Oil and Gas Fields of the Decade 1978-1988. American Association of Petroleum Geologists, Memoir, v. 54, p. 323-348.

Ellenor, D. W., & Mozetic, A, 1986, The Draugen oil discovery. In A. M. Spencer, et al., (eds.) Habitat of Hydrocarbons on the Norwegian Continental Shelf. Norwegian Petroleum Society, Graham & Trotman, London, p. 313-316.

Espitalie, J., Marquis. F., & Drouet, S., 1993, Critical study of Kinetic modelling parameters. In: A. G. Dore et al., (eds.), Basin Modelling: Advances and Application, Amesterdam, Esevier, p. 233-242.

Espitalie, J., Ungerer, P., Irvin, I., & Marquis, E., 1988, Primary cracking of kerogens: experiments and modeling C1, C2-C5, C6-C15 classes of hydrocarbon formed: Organic Geochemistry, v. 13, 4-6, p. 893-899

Evans, D. J., Menelly, A., & Brown, G., 1992, Seismic facies analysis of Westphalian sequences of the southern North Sea Marine and Petroleum Geology, v. 9, p. 578-589.

Fabuss, B. M., Smith, J. O., & Sattered field, C. N. , 1964, Thermal cracking of pure saturated hydrocarbons: Advance Petroleum Chemistry v. 7, p. 157-201.

Fabuss, B. M., Smith, J. O., Lait, R. I., Borsanyl, A. S., & Satterfield, C. N., 1962, Rapid thermal cracking of n-hexadecane at elevated pressures: Ind. Eng. Chem. Process Des. Dev. , v. 1, p. 293-299.

Faleide, J. I., 2010, Class Lecture – Geo 4270. Basin Modelling, Introduction, University of Oslo, Norway

Faleide, J. I., Bjørlykke, K., & Gabrielsen, R.H, 2010, Geology of the Norwegian Continental Shelf. In: K. Bjørlykke (ed.) Petroleum Geoscience: From Sedimentary Environment to Rock Physics. Springer, p. 467-501.

Faleide, J. I., Tsikalas, F., Breivik, A. J, Mjelde, R., Ritzmann, O., Engen, Ø., Wilson, J., & Eldholm, O, 2008, Structure and evolution of the continental margin off Norway and the Barents Sea: Episodes v. 31, p. 82–91.

Fielding, C. R., 1985, Coal depositional models and the distinction between alluvial and delta plain environments: Sedim. Geol., v. 42, p. 41-48.

Forbes, P. L., Ungerer, P. M., Kuhfuss, g. B., Riis, F., & Eggen, S., 1991, Compositional modelling of petroleum generation and expulsion: trial application to local mass balance in the Smørbukk Sør Field, Haltenbanken Area, Norway: AAPG, Bulletin, , v. 75, p. 873-893.

Gabrielsen, R. H., Faerseth, R., Hamar, G., & Ronnevik, H., 1984, Nomenclature of the main structural features of the Norwegian Continental Shelf north of the 62nd parallel. In: A. M. Spencer, (ed.) Petroleum Geology of the North European Margin: Norwegian Petroleum Society, Graham & Trotman, London, p. 41-60.

Galloway, W. E., & Hobday, D. K. , 1983, Terrigenous Clastic Depositional Systems: Springer Verlag, Berlin.

Glasstone, S., Laidler, K.J., & Eyring, H., 1941, The theory of rate processes.: McGraw-Hill.

Gretener, P. E., 1981, Geothermics: using temperature in hydrocarbon exploration: AAPG Education Course Notes Series v. 17, p. 1-156.

Hantschel, T., & Kauerauf, A. I., 2009, Introduction to Basin modelling. In: T. Hantschel & A. I. Kauerauf, (eds) Introduction to Basin and Petroleum System Modelling, Springer, p. 1-30

Hermanrud, C., 1993, Modelling technique - an overview. Basin Modelling. In Dore, A. G., et al., (eds.), Basin Modelling: Advances and Applications: NPF Special Publication v. 3, p. 1-34.

Hermanrud, C., Lerche, I., & Meislngset, K. K., 1991, Determination of virgin rock temperature from drillstem tests.: Journal of Petroleum Technology, v. 43, p. 1126-1131.

Heum, O.R., Dalland, A., & Meisingset, K. K., 1986, Habitat of hydrocarbons at Haltenbanken (PVTmodelling as predictive tool in hydrocarbon exploration). In: A. M.Spencer, et al., (eds.) Habitat of Hydrocarbons in the Norwegian Continental Shelf. Norwegian Petroleum Society, Graham & Trotman, London, p. 259-274.

Hollander, N. B., 1984, Geohistory and hydrocarbon evolution of the Haltenbanken Area: A. M. Spencer, (ed.) Petroleum Geology of the North European Margin. Norwegian Petroleum Society, Graham & Trotman, London, p. 383-388.

Hunt, J. M., 1996, Petroleum Geochemistry and Geology: W. H Freeman and Company, p. 743.

Hunt, J. M., & Jamieson, G. W., 1956, Oil and organic matter in source rock of petroleum: AAPG Bulletin, v. 40, n. 3, p. 477-488.

Jackson, J. S., & Hastings, D. S, 1986, The role of salt movement in the tectonic history of Haltenbanken and Tramabanken and its relationship to structural style. In: A. M. Spencer, et al., (eds) Habitat of Hydrocarbons in the Norwegian Continental Shelf: Norwegian Petroleum Society, Graham & Trotman, London, p. 241-257.

Jarvie, D. M., 1991, Factors affecting Rock-Eval derived kinetic parameters: Chemical Geology, v. 93, p. 79-99.

Karlsen, D. A., & Skeie, J. E. , 2006, Petroleum Migration, Faults and Overpressure, Part I: Calibrating basin modelling using petroleum in traps-A Review: Journal of petroleum geology, v. 29, p. 227-256.

Karlsen, D. A., Backer-Owe, K., Skeie, J. S., Bjørlykke, K., Olstad, R., Berge, K., Cecchi, M., Vik, E., & Schaefer, R. G., 2004, Petroleum migration faults and overpressure, Part II. Case history. The Haltenbanken Petroleum Province, offshore Norway, In: J. M. Cubitt, W. A. England, and S. R. Larter, (eds.), Understanding Petroleum Reservoirs : towards an Intergrated Reservior Engineering and Geochemical Approach: Geological Society, London, Special Publication v. 237, p. 305-372.

Karlsen, D. A., Nyland, B., Flood, B., Ohm, S. E., Brekke, T., Olsen, S., & Backer-Owe, K., 1995, Petroleum geochemistry of the Haltenbanken, Norwegian continental shelf. In: J. M. Cubitt & W. A. England (eds.) The Geochemistry of Reservoirs: Geological Society, London, Special Publications, 86, p. 203- 256.

Karlson, W., 1984, Sedimentology and diagenesis of Jurassic sediments offshore Mid-Norway. In: A. M. Spencer, (ed.) Petroleum Geology of the North European Margin: Norwegian Petroleum Directorate Society, Graham & Trotman, London, p. 389-396.

Katz, B. J., 1990, Controls on the distribution of lacustrine source rocks through time and space. In: B. J. Katz (ed.), Lacustrine Basin Exploration: AAPG Memoir Nci, v. 50, p. 132-139.

Larter, S., 1988, Some pragmatic perspectives in source rock geochemistry: Marine and Petroleum Geology, v. 5, p. 194-204

Leadholm, R. H., Ho, T. T. Y., & Sahai, S. K., 1985, Heat flow, geothermal gradients and maturations modelling on the Norwegian continental shelf using computer methods. In: B. M. Thomas et al., (eds.), Petroleum Geochemistry in Exploratoin of the Norwegian Shelf: Graham and Trotman, London, p. 131-143.

Levorsen, A. I., 1967, Geology of Petroleum, 2nd.: San Francisco, Freeman, p. 1-724.

Longley, I. M., Barraclough, R., Bridden, M. A., & Brown, S. , 1990, Pematang lacustrine petroleum source rocks from the Malacca Strait PSC, Central Sumatra, Indonesia. In: Proceedings, Indonesian Petroleum Association, 19th Annual Convention, p. 279-297.

Magara, K., 1978, Compection and Fluid Migration Amesterdam, Elsevier, v. 319.

Magoon, L. B., 1988, The Petroleum system - a classification scheme for research, exploration, and resource assesment In: L. B. Magoon, (ed.), Petroleum System of the United States: USGS Bulletin, v. 1912, p. 1-88.

Magoon, L. B., 1989b, Identified petroleum system within the United States - 1990. In: L. B. Magoon, (ed.), The petroleum system - status of research and methods,1990: USGS Bulletin, v. 1912, p. 2-9.

Magoon, L. B., & Dow, W. G., 1994a, The petroleum system from source to trap: American Association of Petroleum Geologists, Memoir, 60.

Magoon, L. B., & Valin, Z C., 1994b, Overview of Petroleum System Case Studies. In: L. B. Magoon, & W. G. Dow, (eds.), The petroleum system— From source to trap: AAPG Memoir., v. 60, p. 329-338.

Makhous, M., & Galushkin, Y. I., 2004, Basin analysis and modeling of the burial, thermal and maturation histories in sedimentary basins: Paris, France, E ´ ditions Technip, p. 400.

Matha, S., 2005, Chumphon Basin Modelling, Using Data from Nang Nuan Oil Field,Chumphon Basin, Gulf of Thailand, M.Sc. Thesis, Chulalongkorn University.

Meissner, F. F., Woodward, J., & Clayton, J. L., 1984, Stratigraphic relationships and distribution of source rock in the greater Rocky Mountain region. In: J. Woodward, F. F. Meissner, and J. L. Clayton, (eds.), Hydrocarbon source rock in the greater Rocky Mountain region: Dever, CO, Rocky Mountain Association of Geologists, p. 1-34.

Mo, E. S., Throndsen, T., Andresen, P., Backstrøm, A., Forsberg, A., Haug, S., & Tørudbakken, B. , 1989, A dynamic deterministic model of hydrocarbon generation in the Midgard Field drainage area offshore Mid-Norway: Geologische Runbschau v. 78, p. 305-317.

Pepper, A. S., & Corvi, P. J., 1995a, Simple kinetic models of petroleum formation: Part I— Oil and gas generation from kerogen: Marine and Petroleum Geology, v. 12, p. 291-319.

Pepper, A. S., & Dodd, T. A. , 1995b, Simple kinetic models of petroleum formation. Part II: oil-gas cracking: Marine and Petroleum Geology, v. 11, p. 321-340.

Pepper, A. S & Corvi., P. J. , 1995c, Simple Kinetic models for petroleum formation: Marine and Petroleum Geology, v. 12, p. 417-452.

Perrodon, A., 1980, Geodynamique petroliere. Geneses et repartition des gisements d hyrocarbures: Paris, Masson-Elf Aquitaine, p. 1-381.

Perrodon, A., 1983a, Dynamic of oil and gas accumulations: Pau, Elf Aquitaine p. 187-210.

Perrodon, A., 1983b, Geodynamique des bassins sedimentaires et systemes petroliers: Bulletin des Centres de Recherches Exploration- Production Elf Aquitaine v. 7, p. 645-676.

Perrodon, A., & Masse, P., 1984 Subsidence, sedimentation and petroleum systems Journal of Petroleum Geology, v. 7, n. 1, p. 5-26.

Peters, K. E., 1986, Guidelines for evaluating petroleum source rock using programmed pyrolysis: AAPGBulletin, v. 70, p. 318-329.

Peters, K. E., & Cassa, M. R., 1994, Applied source rock geochemistry. In: L. B. Magoon, & W. G. Dow, (eds.), The petroleum system— From source to trap: AAPG Memoir., v. 60, p. 93-117.

Peters, K. E., Walters, C. C., & Moldowan, J. M. , 2005, The Biomarker Guide, volume 1 and 2. : Cambridge University Press, second edition.

Philippi, G. T., 1957, Identification of oil - source beds by chemical means: Mexico City, Proceedings, 20th international Geologic Congress, 1956, sec. 3, p. 25-38.

Powell, T. G., 1986, Petroleum geochemistry and depositional setting of lacustrine source rocks: Marine and Petroleum Geology, v. 3, p. 200-219

Provan, D. M. J., 1992, Draugen Oil Field, Haltenbanken Province, Offshore Norway. In: M. T. HALBOUTY, (ed.) Giant Oil and Gas Fields of the Decade 1978-1988. American Association of Petroleum Geologists, Memoir, 54, p. 371-382.

Ritter, U., Zielinski, G. W., Weiss, H.M., Zielinski, R. L. B., and Sættem, J., 2004, Heat flow in the Vøring Basin, Mid-Norwegian Shelf: Petroleum Geoscience, v. 10, p. 353-365.

Ronovo, A. B., 1958, Organic carbon in sedimentary rocks (in relation to the presence of petroleum): Geochemistry, v. 5, p. 497-509.

Rybach, L., 1986, Amount and significace of radioactive heat source in sediments. In: J. Burrus, (ed.), Thermal Modeling in Sedimentary Basins: Paris, Editions Technip, p. 311-322.

Sales, J. K., 1997, Seal Strength vs Trap Closure - A Fundamental Control on the Distribution of Oil and Gas. In: R. C Surdam (ed.), Sales, traps and the petroleum system AAPG Memoir, 67, p. 57-83.

Spencer, A. M., Birkeland, O., & Koch, J. O.,, 1993, Petroleum geology of the proven hydrocarbon basins, offshore Norway: First Break, v. 11, no. 5, p. 161-176.

Theis, N. J., Nielsen, H. H., Sales, J. K., & Gail, G. J., 1993, Impact of data integration on basin modelling in the Barent Sea. In: A. G. Dore et al., (eds.), Basin Modelling: Advances and Application, Amesterdam, Esevier, p. 433-444.

Throndsen, T., & Wangen, M., 1998, A comparison between 1-D, 2-D and 3-D basin simulation of compaction, water flow and temperature evolution: Geological Society, London, Special Publications, v. 141, p. 109-116.

Tissot, B. P., 1969, Premieres donnees sur les mecanismes et la cinetique de la formation du petrole dans les sediments: simulation d un schema rectionnel sur ordinateur: Revue de I Institut Francais du petrole, v. 24, p. 470-501.

Tissot, B. P., & Espitalie, J. , 1975, L evolution thermique de Ia matiere organique des sediments: applications d une simulation mathematique: Revue de I Institut Francais du petrole, v. 30, p. 743-777.

Tissot, B.P.W., D. H. , 1984, Petroleum Formation and Occurance. 2nd ed., Berlin, Springer Verlag, p. 699.

Trask, P. D., & Wu, C. C., 1930, Does petroleum form in sediments at time of depositon?: AAPG Bulletin, v. 14, p. 1451-1463.

Triebs, A., 1936, Chlorophyll and Haminderviate in organischen Mineralstoffen Angew. Chemie v. 49, p. 682-686.

Ulmishek, G., 1986, Stratigraphic aspects of petroleum resource assessment. In D. D. Rice, (ed.), Oil and gas assessment-methods and application: AAPG Studies in Geology v. 21, p. 59-68.

Ungerer, P., 1993, Modelling of Petroleum generation and expulsion-an update to recent reviews. In: A. G. Dore et al., (eds.), Basin Modelling: Advances and Application, Amesterdam, Esevier.

Ungerer, P., Burrus, J., Doligez, B., Chenet, P. Y., & Bessis, F. , 1990, Basin evaluation by integrated two dimensional modelling of heat transfer, fluid flow, hydrocarbon generation and migration: AAPG Bulletin, v. 74, p. 309-335.

Vail, P. R., 1987, Seismic stratigraphy interpretation using sequence stratigraphy. In: A. W. Ballv (ed.), Atlas-of Seismic Stratigraphy, Vol. 1, AAPG Stud. GeoL No. 7, p. 1-10.

Van Hinte, J. E., 1978, Geohistory analysis; application of micropaleontology in exploration geology: AAPG Bulletin, v. 62, p. 201-222.

Van Waaoner, J. C., Posamentier, H. W., Mitchum, R. M., Vail, P. R., Sarg, J. F., Loutit, T. S., & Hardenbol, J. , 1988, An overview of sequence stratigraphy and key definitions. In: : C. W. Wilgus, B. J. Hastings, H. Posamentier, J. C. Van Wagoner, C. A. Ross & C. G. St.C. Kendall (eds.), Sea-level Changes: an Integrated Approach, v. Spec. Pub/. Sot. Econ. Palaeontol. Mineral. No. 42, p. 39-45.

Voge, H. H. G., C. M. , 1949, Thermal cracking of higher parafins: Journal of American Chemical Society, v. 71, p. 593-597.

Wangen, M., 2002, Basin simulator, User Guide IFE , Kjeller, Norway, Institute for Energy Technology, p. 1-132.

Wangen, M., & Throndsen, T., 2003, Simple 3-D modeling of hydrocarbon migration. In: S. Du¨ppenbecker and R. Marzi, (eds.), Multidimensional basin modeling: AAPG/Datapages Discovery Series No. 7, p. 243– 253.

Waples, D. W., 1994, Maturity Modelling: Thermal Indicator, Hydrocarbon generation and Oil Cracking. In: J. B. Magoon, W. G. Dow (eds.), The petroleum system - from source to trap. APPG Memoir 60, p. 285-306.

Waples, D. W., 1998, Basin modelling: how well have we done?: Geological Society, London, Special Publications, v. 141, p. 1-14.

Waples, D. W., Suizu, M., & Kamata, H., 1992b, The art of maturity modelling, part 2: alternative models and sensitivity analysis: AAPG Bulletin, v. 76, p. 47-66.

Welte, D. H., Horsfield, B., & Baker, D. R. , 1997, Petroleum and basin evolution: springer-Verlag, p. 1-536.

Welte, D. H., Yükler, M. A., Radke, M., Leythaeuser, D., Mann, U., & Ritter, U., 1983, Organic Geochemistry and Basin Modelling — Important Tools in Petroleum Exploration: Geological Society, London, Special Publications, v. 12, p. 237-252.

Wendebourg, J., & Trabelsi 2003, Uncertainty of petroleum generation using methods of experimental design and response surface modeling: Application to the Gippsland Basin, Australia. In: S. Du¨ ppenbecker & R. Marzi, (eds.), Multidimensional basin modeling: AAPG/Datapages Discovery Series no. 7, p. 295– 307.

Whitley, P. K., 1992, The geology of the Heidrun, a giant oil and gas field on the Mid-Norwegian Shelf. In: M. T. Halbouty, (ed.) Giant Oil and Gas Fields of the Decade 1978-1988. American Association of Petroleum Geologists, Memoir, 54, p. 383-406.

Yukler, A., Cornford, C., & Welte, D. H., 1978, One-dimensional model to simulate geologic, hydrodynamic and thermodynamic development of a sedimentary basin.: Geol. Rundschau, v. 67, p. 960-979.

http://factpages.npd.no/factpages/Default.aspx?culture=en. Last accessed 25th February, 2012.

APPENDICES

Appendix A: Input Case Files (the Midgard 6407/4-1 and Smørbukk 6506/12-9S wells)

Input Case File of the Midgard (6407/4-1) Well for the Basin Simulator.

```
begin_input

   define START 0 {-220}

   begin_parameters
      min_allowed_permeability = 0
      max_simulations = 7
      epsilon_pressure = 0.05
      epsilon_cell_row = 0.001
      dt_min = 0.001
      dt_max = 2.5
   end_parameters

   begin_control_vars
      use_easy_ro yes
      write_zeta_file yes
      reproduce_input_depths yes
      do_range_checking yes
   end_control_vars

   size_of_horizontal_basis 1 x 1
      horizontal_node_pos
      1/0.0
      1/0.0

 #( ====================
   Kerogen definitions
   ==================== )#

   begin_kerogen_library
   begin_pc_kerogen
      name "MelkeKerogen"
      begin_init_kerogen
         TOC_total_organic_carbon     1.0000  #[gCarbon/gSed]#
         S1_initial_oil             0.3000  #[mgHC/gSed]#
         S2_inital_kerogen          0.8910  #[mgHC/gSed]#
         W_carbon_content           0.8300  #[gCarbon/gHC]#
         G_gas_oil_kerogen_ratio     0.5000  #[-]#
         F_gas_coke_ratio           0.5000  #[-]#
         expulsion_limit_gas         1.0000  #[gCgas/gCkerogen]#
         expulsion_limit_oil        1.0000  #[gCoil/gCkerogen]#
      end_init_kerogen

      begin_gas_kerogen
         #( [1/s]     [kJ/mole]    [kJ/mole] )#
         A 2.17e+18   meanE 278.7   sigmaE 18.4   steps 10
      end_gas_kerogen

      begin_oil_kerogen
         #( [1/s]     [kJ/mole]    [kJ/mole] )#
         A 8.14e+13   meanE 215.2   sigmaE 8.3    steps 10
      end_oil_kerogen

      begin_unstable_hc
         #( [1/s]     [kJ/mole]    [kJ/mole] )#
         A 1.0e+15   meanE 250.0   sigmaE 5.0   steps 10
      end_unstable_hc
   end_pc_kerogen
```

```
  begin_pc_kerogen
     name "SpekkKerogen"
     begin_init_kerogen
        TOC_total_organic_carbon     1.0000  #[gCarbon/gSed]#
        S1_initial_oil             0.3000  #[mgHC/gSed]#
        S2_inital_kerogen          7.1300  #[mgHC/gSed]#
        W_carbon_content             0.8300  #[gCarbon/gHC]#
        G_gas_oil_kerogen_ratio      0.5000  #[-]#
        F_gas_coke_ratio           0.5000  #[-]#
        expulsion_limit_gas         1.0000  #[gCgas/gCkerogen]#
        expulsion_limit_oil        1.0000  #[gCoil/gCkerogen]#
     end_init_kerogen

     begin_gas_kerogen
        #( [1/s]     [kJ/mole]    [kJ/mole] )#
        A 2.17e+18   meanE 278.7   sigmaE 18.4   steps 10
     end_gas_kerogen

     begin_oil_kerogen
        #( [1/s]     [kJ/mole]    [kJ/mole] )#
        A 8.14e+13   meanE 215.2   sigmaE 8.3    steps 10
     end_oil_kerogen

     begin_unstable_hc
        #( [1/s]     [kJ/mole]    [kJ/mole] )#
        A 1.0e+15   meanE 250.0   sigmaE 5.0   steps 10
     end_unstable_hc
  end_pc_kerogen

  begin_pc_kerogen
     name "AareKerogen"
     begin_init_kerogen
        TOC_total_organic_carbon     1.0000  #[gCarbon/gSed]#
        S1_initial_oil             0.3000  #[mgHC/gSed]#
        S2_inital_kerogen          175.0000  #[mgHC/gSed]#
        W_carbon_content             0.8300  #[gCarbon/gHC]#
        G_gas_oil_kerogen_ratio      0.5000  #[-]#
        F_gas_coke_ratio           0.5000  #[-]#
        expulsion_limit_gas         1.0000  #[gCgas/gCkerogen]#
        expulsion_limit_oil        1.0000  #[gCoil/gCkerogen]#
     end_init_kerogen

     begin_gas_kerogen
        #( [1/s]     [kJ/mole]    [kJ/mole] )#
        A 1.88e+11   meanE 206.0   sigmaE 7.7   steps 10
     end_gas_kerogen

     begin_oil_kerogen
        #( [1/s]     [kJ/mole]    [kJ/mole] )#
        A 4.9e+14   meanE 228.2   sigmaE 7.9    steps 10
     end_oil_kerogen

     begin_unstable_hc
        #( [1/s]     [kJ/mole]    [kJ/mole] )#
        A 1.0e+15   meanE 250.0   sigmaE 5.0   steps 10
     end_unstable_hc
  end_pc_kerogen
  end_kerogen_library

#( =====================
```

```
Lithology definitions
====================== )#

begin_lithology_def
    name Basement
    density = 2800     #[kg/m3]#
    heat_cap = 1000    #[J/kgK]#
    expansibility = 3.0e-5 #[1/K]#
    heat_cond horizontal standard
        lambda = 2.5  #[W/mK]#
    heat_cond vertical standard
        lambda = 2.5  #[W/mK]#
    permeability horizontal zero
    permeability vertical zero
    porosity zero
    no_fracture_function
    no_radioactive_isotopes
    no_hc_parameters
end_lithology_def

begin_lithology_def
    name Sediments
    density = 2650.0  #[kg/m3]#
    heat_cap = 1000.00  #[J/kgK]#
    heat_cond horizontal standard
        lambda = 2.50  #[W/mK]#
    heat_cond vertical standard
        lambda = 2.50  #[W/mK]#
    permeability horizontal modified_standard
        k0 = 1.49e-07  #[mD]#
        k1 = 1000  #[mD]#
        c0 = 25.00  #[-]#
    permeability vertical modified_standard
        k0 = 1.49e-07  #[mD]#
        k1 = 1000  #[mD]#
        c0 = 25.00  #[-]#
    porosity standard
        func_of_z
        phi0 = 0.450  #[-]#
        alpha = 5.50e-04  #[1/m]#
    no_fracture_function
    no_radioactive_isotopes
    no_hc_parameters
end_lithology_def

begin_lithology_def
    name Spekk
    density = 2650.0  #[kg/m3]#
    heat_cap = 1000.00  #[J/kgK]#
    heat_cond horizontal standard
        lambda = 2.50  #[W/mK]#
    heat_cond vertical standard
        lambda = 2.50  #[W/mK]#
    permeability horizontal modified_standard
        k0 = 1.49e-07  #[mD]#
        k1 = 1000  #[mD]#
        c0 = 25.00  #[-]#
    permeability vertical modified_standard
        k0 = 1.49e-07  #[mD]#
        k1 = 1000  #[mD]#
        c0 = 25.00  #[-]#
```

```
    porosity standard
        func_of_z
        phi0 = 0.450  #[-]#
        alpha = 5.50e-04  #[1/m]#
    no_fracture_function
    no_radioactive_isotopes
    source_rock
        name "SpekkKerogen"
        density_kerogen = 1000.0
        density_onephase_hc = 750.0
        density_coke = 1200.0
end_lithology_def

begin_lithology_def
    name Melke
    density = 2650.0  #[kg/m3]#
    heat_cap = 1000.00  #[J/kgK]#
    heat_cond horizontal standard
        lambda = 2.50  #[W/mK]#
    heat_cond vertical standard
        lambda = 2.50  #[W/mK]#
    permeability horizontal modified_standard
        k0 = 1.49e-07  #[mD]#
        k1 = 1000  #[mD]#
        c0 = 25.00  #[-]#
    permeability vertical modified_standard
        k0 = 1.49e-07  #[mD]#
        k1 = 1000  #[mD]#
        c0 = 25.00  #[-]#
    porosity standard
        func_of_z
        phi0 = 0.450  #[-]#
        alpha = 5.50e-04  #[1/m]#
    no_fracture_function
    no_radioactive_isotopes
    source_rock
        name "MelkeKerogen"
        density_kerogen = 1000.0
        density_onephase_hc = 750.0
        density_coke = 1200.0
end_lithology_def

begin_lithology_def
    name Aare
    density = 2650.00  #[kg/m3]#
    heat_cap = 1000.00  #[J/kgK]#
    heat_cond horizontal standard
        lambda = 2.50  #[W/mK]#
    heat_cond vertical standard
        lambda = 2.50  #[W/mK]#
    permeability horizontal modified_standard
        k0 = 1.49e-07  #[mD]#
        k1 = 1000  #[mD]#
        c0 = 25.00  #[-]#
    permeability vertical modified_standard
        k0 = 1.49e-07  #[mD]#
        k1 = 1000  #[mD]#
        c0 = 25.00  #[-]#
    porosity standard
        func_of_z
        phi0 = 0.450  #[-]#
```

```
        alpha = 5.50e-04  #[1/m]#
      no_fracture_function
      no_radioactive_isotopes
      source_rock
        name "AareKerogen"
        density_kerogen = 1000.0
        density_onephase_hc = 750.0
        density_coke = 1200.0
  end_lithology_def

#( ========
  Basement
  ======== )#

  begin_basement
    basement  1/Basement/100e+3
    with 50 rows
  end_basement

#( ==============
  Burial history
  ============== )#

  begin_history_at START

    formation "Aare"
    sedimentation 1/Aare/400
    with 1 rows until -210

    formation "TILJE FM"
    sedimentation 1/Sediments/228
    with 3 rows until -198

    formation "ROR FM"
    sedimentation 1/Sediments/63
    with 3 rows until -190

    formation "TOFTE FM"
    sedimentation 1/Sediments/59
    with 3 rows until -189

    formation "ROR FM"
    sedimentation 1/Sediments/44
    with 3 rows until -185

    formation "ILE FM"
    sedimentation 1/Sediments/85
    with 3 rows until -180

    formation "NOT FM"
    sedimentation 1/Sediments/52
    with 3 rows until -179

    formation "GARN FM"
    sedimentation 1/Sediments/79
    with 3 rows until -173

    formation "MELKE FM"
    sedimentation 1/Melke/118
    with 1 rows until -161
```

```
    formation "SPEKK FM"
    sedimentation 1/Spekk/62
    with 1 rows until -142

    formation "LYR FM"
    sedimentation 1/Sediments/28
    with 3 rows until -138

    formation "LANGE FM"
    sedimentation 1/Sediments/672
    with 6 rows until -127

    formation "KVITNOS FM"
    sedimentation 1/Sediments/412
    with 4 rows until -89

    formation "NISE FM"
    sedimentation 1/Sediments/176
    with 3 rows until -87.5

    formation "SPRINGAR FM"
    sedimentation 1/Sediments/157
    with 3 rows until -76.1

    formation "TANG FM"
    sedimentation 1/Sediments/91
    with 3 rows until -69.3

    formation "TARE FM"
    sedimentation 1/Sediments/76
    with 3 rows until -55.8

    formation "BRYGGE FM"
    sedimentation 1/Sediments/668
    with 6 rows until -51.5

    formation "KAI FM"
    sedimentation 1/Sediments/165
    with 3 rows until -20

    formation "NAUST FM"
    sedimentation 1/Sediments/1018
    with 10 rows until -3.4

    pause until 0
end_history

begin_dump_times
    from START to 0 step 2
    0
end_dump_times

begin_column_listing_times
    -3.4
    -20
    -51.5
    -55.8
    -69.3
    -76.1
    -87.5
    -89
```

```
   -127
   -138
   -142
   -161
   -173
   -179
   -180
   -185
   -189
   -185
   -198
end_column_listing_times
begin_dump_times
   from START to 0 step 2
   0
end_dump_times

begin_column_listing_times
   0
   -3.4
   -20
   -51.5
   -55.8
   -69.3
   -76.1
   -87.5
   -89
   -90.5
   -138
   -173
   -179
   -180
   -185
   -189
   -198
   -208
end_column_listing_times

begin_water_depths
   depths 1/372  at START
   depths 1/372  at -11.2
   depths 1/372  at 0.0
end_water_depths

begin_surface_temps
   temp 1/4  at START
   temp 1/4  at -11.2
   temp 1/4  at 0.0
end_surface_temps

begin_heat_fluxes
   flux 1/0.075  at START
   flux 1/0.075  at -65.0
   flux 1/0.065  at -11.2
   flux 1/0.065  at   0.0
end_heat_fluxes

#( =====
NOTE: There are 50 basement elements.
Aare center element is: 3 + 50 = 53;
Spekk center element is: 31 + 50 = 81;
```

```
    ===== )#

    begin_log_variables
        #( node/elem 50 is Aare FM )#
        log temp in_node  50
        log zcoord in_node  50
        log hc_tr in_elem 50
        log mass_coke in_elem  50
        log mass_C6_PLUS in_elem  50
        log mass_C1_C5 in_elem  50
        log mass_expelled_C6_PLUS in_elem  50
        log mass_expelled_C1_C5 in_elem  50
        log mass_reactive_kerogen in_elem 50
        log easy_ro in_node 50

        #( node/elem 73 is Spekk FM )#
        log temp in_node  73
        log zcoord in_node  73
        log hc_tr in_elem 73
        log mass_coke in_elem  73
        log mass_C6_PLUS in_elem  73
        log mass_C1_C5 in_elem  73
        log mass_expelled_C6_PLUS in_elem  73
        log mass_expelled_C1_C5 in_elem  73
        log mass_reactive_kerogen in_elem 73
        log easy_ro in_node 73

        #( node/elem 72 is Melke FM )#
        log temp in_node  72
        log zcoord in_node  72
        log hc_tr in_elem 72
        log mass_coke in_elem  72
        log mass_C6_PLUS in_elem  72
        log mass_C1_C5 in_elem  72
        log mass_expelled_C6_PLUS in_elem  72
        log mass_expelled_C1_C5 in_elem  72
        log mass_reactive_kerogen in_elem 72
        log easy_ro in_node 72
    end_log_variables
end_input
```

Input Case File of the Smørbukk (6506/12-9S) Well for Basin Simulator.

```
begin_input

   define START 0 {-220}

   begin_parameters
      min_allowed_permeability = 0.0
      max_simulations = 7
      epsilon_pressure = 0.05
      epsilon_cell_row = 0.001
      dt_min = 0.001
      dt_max = 2.5
   end_parameters

   begin_control_vars
      use_easy_ro yes
      write_zeta_file yes
      reproduce_input_depths yes
      do_range_checking yes
      do_hc_expulsion no
   end_control_vars

   size_of_horizontal_basis 1 x 1
      horizontal_node_pos
      1/0.0
      1/0.0

 #( ====================
   Kerogen definitions
   ==================== )#

   begin_kerogen_library
   begin_pc_kerogen
      name "MelkeKerogen"
      begin_init_kerogen
         TOC_total_organic_carbon     1.0000  #[gCarbon/gSed]#
         S1_initial_oil               0.3000  #[mgHC/gSed]#
         S2_inital_kerogen            1.8000  #[mgHC/gSed]#
         W_carbon_content             0.8300  #[gCarbon/gHC]#
         G_gas_oil_kerogen_ratio      0.5000  #[-]#
         F_gas_coke_ratio             0.5000  #[-]#
         expulsion_limit_gas          1.0000  #[gCgas/gCkerogen]#
```

```
      expulsion_limit_oil        1.0000  #[gCoil/gCkerogen]#
   end_init_kerogen

   begin_gas_kerogen
      #( [1/s]     [kJ/mole]    [kJ/mole] )#
      A 2.17e+18   meanE 278.0   sigmaE 18.4   steps 10
   end_gas_kerogen

   begin_oil_kerogen
      #( [1/s]     [kJ/mole]    [kJ/mole] )#
      A 8.14e+13   meanE 215.2   sigmaE 8.3    steps 10
   end_oil_kerogen

   begin_unstable_hc
      #( [1/s]     [kJ/mole]    [kJ/mole] )#
      A 1.0e+15   meanE 250.0   sigmaE 5.0   steps 10
   end_unstable_hc
end_pc_kerogen

begin_pc_kerogen
   name "SpekkKerogen"
   begin_init_kerogen
      TOC_total_organic_carbon    1.0000  #[gCarbon/gSed]#
      S1_initial_oil            0.3000  #[mgHC/gSed]#
      S2_inital_kerogen         13.14000  #[mgHC/gSed]#
      W_carbon_content           0.8300  #[gCarbon/gHC]#
      G_gas_oil_kerogen_ratio     0.5000  #[-]#
      F_gas_coke_ratio          0.5000  #[-]#
      expulsion_limit_gas        1.0000  #[gCgas/gCkerogen]#
      expulsion_limit_oil        1.0000  #[gCoil/gCkerogen]#
   end_init_kerogen

   begin_gas_kerogen
      #( [1/s]     [kJ/mole]    [kJ/mole] )#
      A 2.17e+18   meanE 278.7   sigmaE 18.4   steps 10
   end_gas_kerogen

   begin_oil_kerogen
      #( [1/s]     [kJ/mole]    [kJ/mole] )#
      A 8.14e+14   meanE 215.2  sigmaE 8.3   steps 10
   end_oil_kerogen

   begin_unstable_hc
      #( [1/s]     [kJ/mole]    [kJ/mole] )#
      A 1.0e+15   meanE 250.0   sigmaE 5.0   steps 10
   end_unstable_hc
end_pc_kerogen

begin_pc_kerogen
   name "AareKerogen"
   begin_init_kerogen
      TOC_total_organic_carbon    1.0000  #[gCarbon/gSed]#
      S1_initial_oil            0.3000  #[mgHC/gSed]#
      S2_inital_kerogen         16.5000  #[mgHC/gSed]#
      W_carbon_content           0.8300  #[gCarbon/gHC]#
      G_gas_oil_kerogen_ratio     0.5000  #[-]#
      F_gas_coke_ratio          0.5000  #[-]#
      expulsion_limit_gas        1.0000  #[gCgas/gCkerogen]#
      expulsion_limit_oil        1.0000  #[gCoil/gCkerogen]#
   end_init_kerogen
```

```
      begin_gas_kerogen
         #( [1/s]     [kJ/mole]    [kJ/mole] )#
         A 1.88e+11   meanE 206.0   sigmaE 7.7   steps 10
      end_gas_kerogen

      begin_oil_kerogen
         #( [1/s]     [kJ/mole]    [kJ/mole] )#
         A 4.97e+14   meanE 228.0   sigmaE 7.9    steps 10
      end_oil_kerogen

      begin_unstable_hc
         #( [1/s]     [kJ/mole]    [kJ/mole] )#
         A 1.0e+15   meanE 250.0   sigmaE 5.0   steps 10
      end_unstable_hc
   end_pc_kerogen
   end_kerogen_library

#( =====================
   Lithology definitions
   ===================== )#

   begin_lithology_def
      name Basement
      density = 2800     #[kg/m3]#
      heat_cap = 1000    #[J/kgK]#
      expansibility = 3.0e-5 #[1/K]#
      heat_cond horizontal standard
         lambda = 2.5  #[W/mK]#
      heat_cond vertical standard
         lambda = 2.5  #[W/mK]#
      permeability horizontal zero
      permeability vertical zero
      porosity zero
      no_fracture_function
      no_radioactive_isotopes
      no_hc_parameters
   end_lithology_def

   begin_lithology_def
      name Sediments
      density = 2650.0  #[kg/m3]#
      heat_cap = 1000.00  #[J/kgK]#
      heat_cond horizontal standard
         lambda = 2.50  #[W/mK]#
      heat_cond vertical standard
         lambda = 2.50  #[W/mK]#
      permeability horizontal modified_standard
         k0 = 1.49e-07  #[mD]#
         k1 = 1000  #[mD]#
         c0 = 25.00  #[-]#
      permeability vertical modified_standard
         k0 = 1.49e-07  #[mD]#
         k1 = 1000  #[mD]#
         c0 = 25.00  #[-]#
      porosity standard
         func_of_z
         phi0 = 0.450  #[-]#
         alpha = 5.50e-04  #[1/m]#
      no_fracture_function
      no_radioactive_isotopes
      no_hc_parameters
```

```
end_lithology_def

begin_lithology_def
    name Spekk
    density = 2650.0  #[kg/m3]#
    heat_cap = 1000.00  #[J/kgK]#
    heat_cond horizontal standard
        lambda = 2.50  #[W/mK]#
    heat_cond vertical standard
        lambda = 2.50  #[W/mK]#
    permeability horizontal modified_standard
        k0 = 1.49e-07  #[mD]#
        k1 = 1000  #[mD]#
        c0 = 25.00  #[-]#
    permeability vertical modified_standard
        k0 = 1.49e-07  #[mD]#
        k1 = 1000  #[mD]#
        c0 = 25.00  #[-]#
    porosity standard
        func_of_z
        phi0 = 0.450  #[-]#
        alpha = 5.50e-04  #[1/m]#
    no_fracture_function
    no_radioactive_isotopes
    source_rock
        name "SpekkKerogen"
        density_kerogen = 1000.0
        density_onephase_hc = 750.0
        density_coke = 1200.0
end_lithology_def

begin_lithology_def
    name Melke
    density = 2650.0  #[kg/m3]#
    heat_cap = 1000.00  #[J/kgK]#
    heat_cond horizontal standard
        lambda = 2.50  #[W/mK]#
    heat_cond vertical standard
        lambda = 2.50  #[W/mK]#
    permeability horizontal modified_standard
        k0 = 1.49e-07  #[mD]#
        k1 = 1000  #[mD]#
        c0 = 25.00  #[-]#
    permeability vertical modified_standard
        k0 = 1.49e-07  #[mD]#
        k1 = 1000  #[mD]#
        c0 = 25.00  #[-]#
    porosity standard
        func_of_z
        phi0 = 0.450  #[-]#
        alpha = 5.50e-04  #[1/m]#
    no_fracture_function
    no_radioactive_isotopes
    source_rock
        name "MelkeKerogen"
        density_kerogen = 1000.0
        density_onephase_hc = 750.0
        density_coke = 1200.0
end_lithology_def

begin_lithology_def
```

```
      name Aare
      density = 2650.0  #[kg/m3]#
      heat_cap = 1000.00  #[J/kgK]#
      heat_cond horizontal standard
         lambda = 2.50  #[W/mK]#
      heat_cond vertical standard
         lambda = 2.50  #[W/mK]#
      permeability horizontal modified_standard
         k0 = 1.49e-07  #[mD]#
         k1 = 1000  #[mD]#
         c0 = 25.00  #[-]#
      permeability vertical modified_standard
         k0 = 1.49e-07  #[mD]#
         k1 = 1000  #[mD]#
         c0 = 25.00  #[-]#
      porosity standard
         func_of_z
         phi0 = 0.450  #[-]#
         alpha = 5.50e-04  #[1/m]#
      no_fracture_function
      no_radioactive_isotopes
      source_rock
         name "AareKerogen"
         density_kerogen = 1000.0
         density_onephase_hc = 750.0
         density_coke = 1200.0
   end_lithology_def

#( ========
   Basement
   ======== )#

   begin_basement
      basement  1/Basement/100e+3
      with 50 rows
   end_basement

#( ==============
   Burial history
   ============== )#

   begin_history_at START

      formation "AARE FM"
      sedimentation 1/Aare/400
      with 1 rows until -210

      formation "TILJE FM"
      sedimentation 1/Sediments/165
      with 3 rows until -198

      formation "ROR FM"
      sedimentation 1/Sediments/12
      with 3 rows until -185

      formation "TOFTE FM"
      sedimentation 1/Sediments/59
      with 3 rows until -184

      formation "ROR FM"
      sedimentation 1/Sediments/68
```

with 3 rows until -183

formation "ILE FM"
sedimentation 1/Sediments/69
with 3 rows until -180

formation "NOT FM"
sedimentation 1/Sediments/28
with 3 rows until -179

formation "GARN FM"
sedimentation 1/Sediments/57
with 3 rows until -173

formation "MELKE FM"
sedimentation 1/Melke/182
with 1 rows until -161

formation "SPEKK FM"
sedimentation 1/Spekk/28
with 1 rows until -142

formation "LYR FM"
sedimentation 1/Sediments/41
with 3 rows until -138

formation "LANGE FM"
sedimentation 1/Sediments/745
with 7 rows until -127

formation "LYSING FM"
sedimentation 1/Sediments/39
with 3 rows until -90.5

formation "KVITNOS FM"
sedimentation 1/Sediments/564
with 5 rows until -89

formation "NISE FM"
sedimentation 1/Sediments/250
with 3 rows until -87.5

formation "SPRINGAR FM"
sedimentation 1/Sediments/160
with 3 rows until -76.1

formation "TANG FM"
sedimentation 1/Sediments/63
with 3 rows until -69.3

formation "TARE FM"
sedimentation 1/Sediments/89
with 3 rows until -55.8

formation "BRYGGE FM"
sedimentation 1/Sediments/315
with 3 rows until -51.5

formation "KAI FM"
sedimentation 1/Sediments/445
with 4 rows until -20

```
    formation "NORDLAND FM"
    sedimentation 1/Sediments/1118
    with 11 rows until 0
end_history

begin_dump_times
    from START to 0 step 2
    0
end_dump_times

begin_column_listing_times
    -2.4
    -20
    -51.5
    -55.8
    -69.3
    -76.1
    -87.5
    -89
    -90.5
    -127
    -138
    -142
    -161
    -173
    -179
    -180
    -185
    -189
    -185
    -198
end_column_listing_times

begin_dump_times
    from START to 0 step 2
    0
end_dump_times

begin_water_depths
    depths 1/372  at START
    depths 1/372  at -11.2
    depths 1/372  at 0.0
end_water_depths

begin_surface_temps
    temp 1/4  at START
    temp 1/4  at -11.2
    temp 1/4  at 0.0
end_surface_temps

begin_heat_fluxes
    flux 1/0.075  at START
    flux 1/0.075  at -65.0
    flux 1/0.065  at -11.2
    flux 1/0.065  at  0.0
end_heat_fluxes

#( =====
NOTE: There are 50 basement elements.
Aare center element is: 3 + 50 = 53;
```

```
    Spekk center element is: 31 + 50 = 81;
    ===== )#

    begin_log_variables
        #( node/elem 50 is Aare FM )#
        log temp in_node  50
        log zcoord in_node  50
        log hc_tr in_elem 50
        log mass_coke in_elem  50
        log mass_C6_PLUS in_elem  50
        log mass_C1_C5 in_elem  50
        log mass_expelled_C6_PLUS in_elem  50
        log mass_expelled_C1_C5 in_elem  50
        log mass_reactive_kerogen in_elem 50
        log easy_ro in_node 50

        #( node/elem 72 is Spekk FM )#
        log temp in_node  72
        log zcoord in_node  72
        log hc_tr in_elem 72
        log mass_coke in_elem  72
        log mass_C6_PLUS in_elem  72
        log mass_C1_C5 in_elem  72
        log mass_expelled_C6_PLUS in_elem  72
        log mass_expelled_C1_C5 in_elem  72
        log mass_reactive_kerogen in_elem 72
        log easy_ro in_node 72

        #( node/elem 73 is Spekk FM )#
        log temp in_node  73
        log zcoord in_node  73
        log hc_tr in_elem 73
        log mass_coke in_elem  73
        log mass_C6_PLUS in_elem  73
        log mass_C1_C5 in_elem  73
        log mass_expelled_C6_PLUS in_elem  73
        log mass_expelled_C1_C5 in_elem  73
        log mass_reactive_kerogen in_elem 73
        log easy_ro in_node 73
    end_log_variables
end_input
```

Appendix-B: Input Geochemical data

A

Midgard (6407 / 4-1) Well

Melke Formation Geochemical Data (Rock-Eval) (From NPD)

GEOCHEM SAMPLE NUMBER	DEPTH	ORGANIC CARBON	S1 (mg/g)	S2 (mg/g)	PRODUCTION INDEX	HYDROGEN INDEX	Tmax (%C)
1175-201A	3760-3770	4.34	2.29	4.59	0.33	105.8	442
1175-203A	3770-3780	3.64	0.87	1.84	0.32	50.5	441
1175-202A	3771	6.23	4.70	11.38	0.29	182.7	450
1175-204A	3780-3790	1.48	0.33	0.64	0.34	43.2	438
1175-205A	3790-3800	1.67	0.39	0.81	0.32	48.5	444
1175-206A	3800-3810	1.29	0.20	0.28	0.42	21.7	441
1175-208A	3810-3820	0.78	0.13	0.15	0.46	19.2	432
1175-207A	3813.5	1.09	0.37	0.79	0.32	72.5	439
1175-211A	3820-3830	0.82	0.12	0.38	0.24	46.3	441
1175-209A	3822.0	1.04	0.32	1.14	0.22	109.6	446
1175-210A	3825.5	1.08	0.15	0.48	0.24	44.4	471
1175-212A	3830-3840	1.07	0.36	1.37	0.21	128.0	449
1175-213A	3840-3850	1.11	0.28	0.88	0.24	79.3	442
1175-214A	3850-3860	1.09	0.35	0.79	0.31	72.5	438
1175-216A	3860-3870	1.38	0.39	0.85	0.31	61.6	446
1175-215A	3864	1.60	0.30	0.83	0.27	51.9	456
1175-217A	3870-3880	1.59	0.36	0.95	0.27	59.7	442
1175-219B	3880-3890	2.04	0.54	1.92	0.22	94.1	444
1175-218A	3888	1.10	0.16	0.48	0.25	43.6	469
1175-220B	3890-3900	1.33	0.70	2.41	0.23	181.2	445

Spekk Formation Geochemical Data (Rock-Eval) (From NPD)

1175-182A	3710-3720	5.69	8.35	14.03	0.37	246.6	435
1175-178A	3710.5	5.44	4.81	9.47	0.34	174.1	436
1175-179A	3712	5.57	5.65	12.34	0.31	221.5	440
1175-180A	3717.5	5.62	6.28	10.08	0.38	179.4	444
1175-181A	3719	5.44	5.79	8.71	0.40	160.1	442
1175-186A	3720-3730	5.20	4.69	7.56	0.38	145.4	432
1175-183A	3721	6.51	8.16	10.89	0.43	167.3	437
1175-184A	3724.9	6.30	4.68	6.38	0.42	101.3	437
1175-185A	3729	5.75	7.82	11.03	0.41	191.8	437
1175-189A	3730-3740	5.24	3.76	5.23	0.42	99.8	434
1175-187A	3733.5	4.58	2.97	6.80	0.30	148.5	443
1175-188A	3739	4.97	6.47	6.29	0.51	126.6	435
1175-193A	3740-3750	4.76	3.81	5.43	0.41	114.1	433
1175-190A	3742.5	6.57	5.46	7.87	0.41	119.8	438
1175-191A	3746	4.43	3.55	4.72	0.43	106.5	437
1175-192A	3749.5	0.75	0.14	0.17	0.45	22.7	447
1175-196B	3750-3760	1.57	0.62	0.32	0.66	20.4	440
1175-194A	3754	5.27	5.61	8.86	0.39	168.1	442
1175-195A	3757.5	5.19	5.28	6.69	0.44	128.9	448
1175-201A	3760-3770	4.34	2.29	4.59	0.33	105.8	442
1175-197A	3760.5	4.93	6.74	9.87	0.41	200.2	441
1175-198A	3763.8	7.80	4.45	7.46	0.37	95.6	450
1175-199A	3766	5.16	3.95	6.67	0.37	129.3	442
1175-200A	3768.5	6.73	4.44	12.64	0.26	187.8	453

Smørbukk (6506/ 12-9S) well

Melke and Spekk formations Geochemical Data (Rock-Eval) (From NPD)

Depth unit of measure: m

Depth	Typ	Lithology	S1	S2	S3	S2/S3	TOC	HI	OI	PP	PI	Tmax	Sample
4130.00	swc	Sh/Clst: brn blk	2.12	2.48	3.58	0.69	1.41	176	254	4.6	0.46	358	0002-1L
4137.50	swc	Sh/Clst: brn blk	1.09	1.35	2.19	0.62	0.45	300	487	2.4	0.45	352	0003-1L
4150.00	cut	Sh/Clst: gy blk	0.59	0.43	1.34	0.32	0.68	63	197	1.0	0.58	343	0047-1L
4160.00	cut	Sh/Clst: red brn	0.41	0.21	0.89	0.24	0.30	70	297	0.6	0.66	444	0048-2L
4171.00	swc	Sh/Clst: brn blk	8.60	16.71	0.73	22.89	3.00	557	24	25.3	0.34	440	0004-1L
4180.00	cut	Sh/Clst: brn blk	9.53	11.09	1.21	9.17	5.90	188	21	20.6	0.46	435	0050-4L
4193.00	swc	Sh/Clst: dsk y brn	7.68	11.64	0.74	15.73	9.10	128	8	19.3	0.40	442	0005-1L
4198.00	swc	Sh/Clst: dsk y brn	4.02	6.23	1.24	5.02	6.23	100	20	10.3	0.39	441	0006-1L
4207.50	swc	Sh/Clst: dsk y brn	1.69	2.23	2.06	1.08	2.00	112	103	3.9	0.43	339	0007-1L
4260.00	cut	Sh/Clst: brn blk	0.70	0.31	0.92	0.34	0.30	103	307	1.0	0.69	386	0054-2L
4300.00	cut	Sh/Clst: brn blk to gy blk	0.61	0.19	0.98	0.19	0.30	63	327	0.8	0.76	345	0055-2L
4350.00	cut	Sh/Clst: brn blk	0.91	0.25	1.00	0.25	1.02	25	98	1.2	0.78	334	0056-2L

Vitrinite Reflectance Data of Midagard (6407 / 4-1) well (from NPD) samples at the specific depths with their VR (%) values.

Depth	Vitrinite Reflectance
-500	0.33
-1000	0.38
-1500	0.38
-2000	0.4
-2159	0.43
-2420.5	0.47
-2473	0.5
-2561	0.53
-2800	0.56
-2900	0.67
-3100	0.69
-3182.9	0.74
-3223.4	0.76
-3511	0.79
-3710.5	0.75
-3721	0.86
-3742.5	0.9
-3763.8	0.94
-3813.5	0.96
-3864	1.12
-3900	1.22
-4012	1.17

Appendix-C: Results forCase-2

CASE-2

The Midgard Well (6407/4-1)

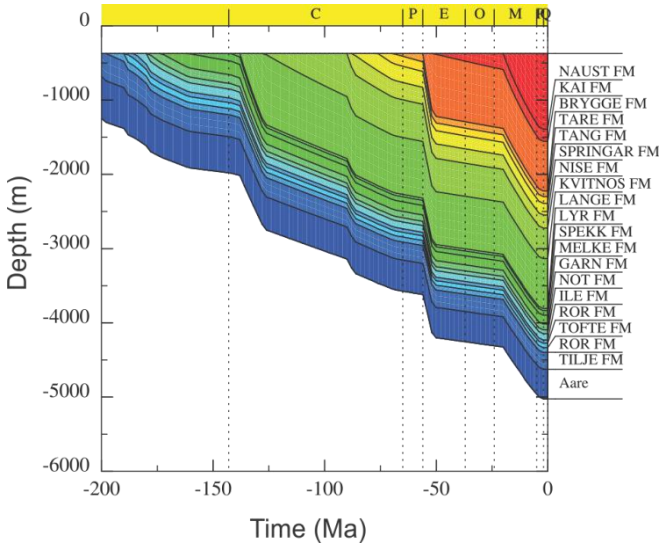

Figure 1: Burial reconstruction through time and depth for the Midgrad (6407/4-1) well which display a relatively gradual burial trend forCase-2.

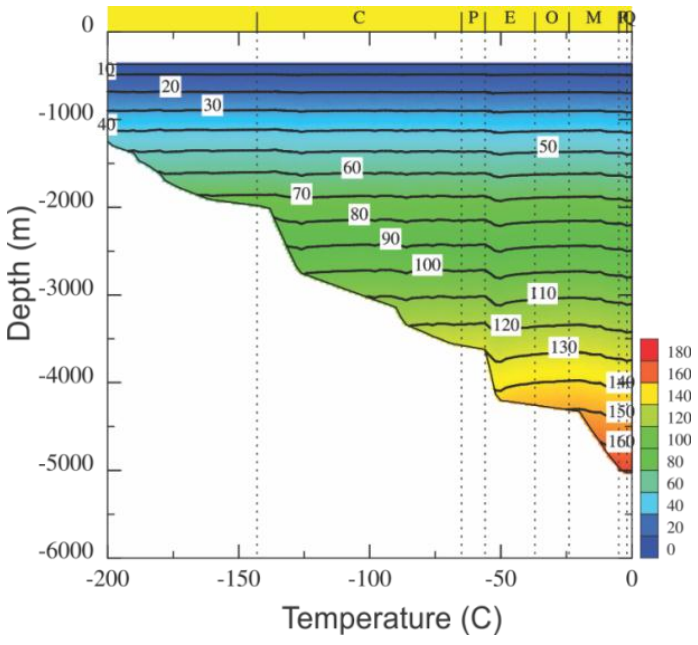

Figure 2: Thermal history reconstruction through time and depth for the Midgard well (6407/4-1) well forCase-2.

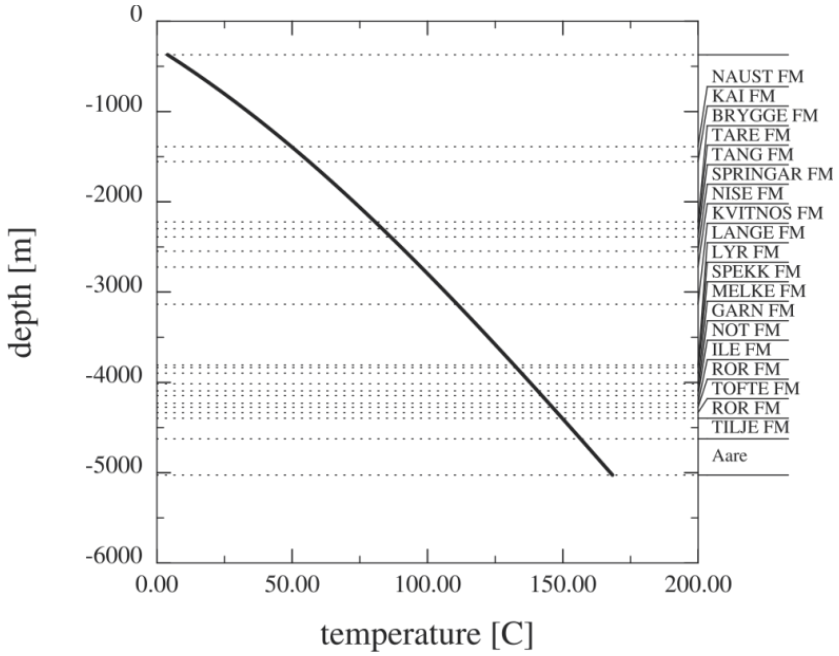

Figure 3: Temperature depth cross-plot for the Midgard well (6407/4-1) showing a linear relationship between the two values.

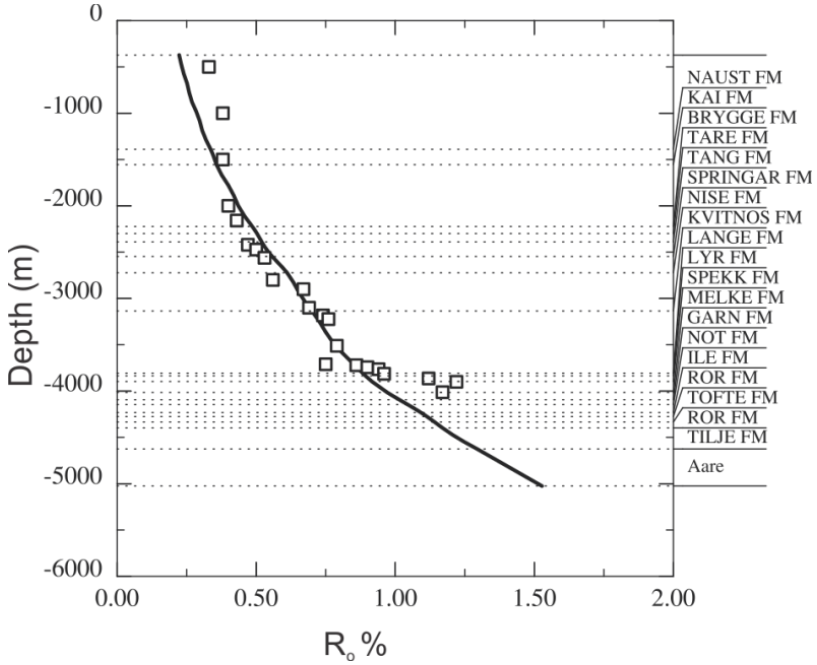

Figure 4: Plot of measured vitrinite reflectance (data source NPD as shown in the Appendix B) against depth for the Midgard (6407/4-1) well of modeled vitrinite reflectance against the depth for the same well (using BAS software).

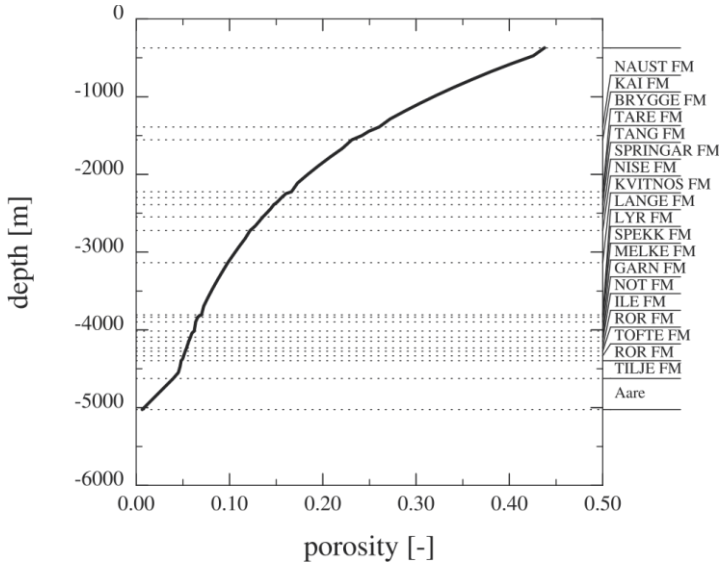

Figure 5: Porosity versus depth cross-plot for the Midgard well (6407/4-1) showing decrease in porosity with depth. However, it is pertinent to note that decrease in porosity is a function of compaction, also above 80 ^{o}C chemical compaction starts which disturbs the linear relationship of porosity lose with depth.

Åre Formation:

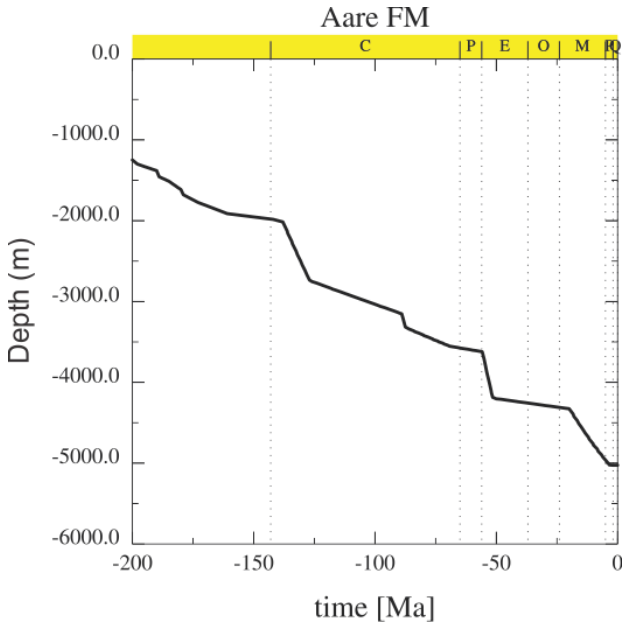

Figure 6: Time-Depth cross-plot for the Åre Formation showing burial depth of the formation at different time intervals. Note the sudden drops in the burial curve at ca. -150 Ma, -90 Ma, -55 Ma and -20 Ma representing major tectonic subsidence at these times.

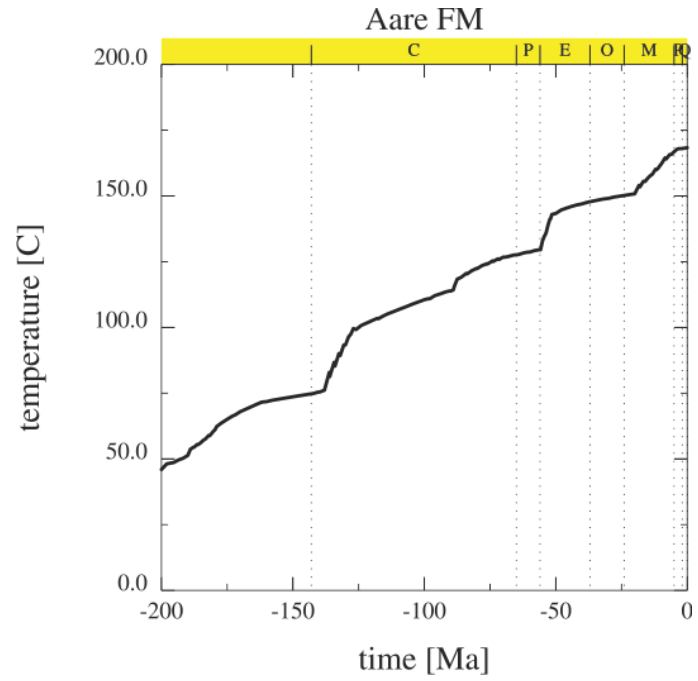

Figure 7: Time-Temperature cross-plot for the Åre Formation showing temperature of the formation at different time intervals. A general increase in temperature with time is evident with abrupt rises at ca. -150 Ma, -90 Ma, -55 Ma and -20 M.Y. Following classification by Hunt (1996), the Åre Formation remained in oil window between at ca. -170 Ma & -10 Ma and is currently in gas window.

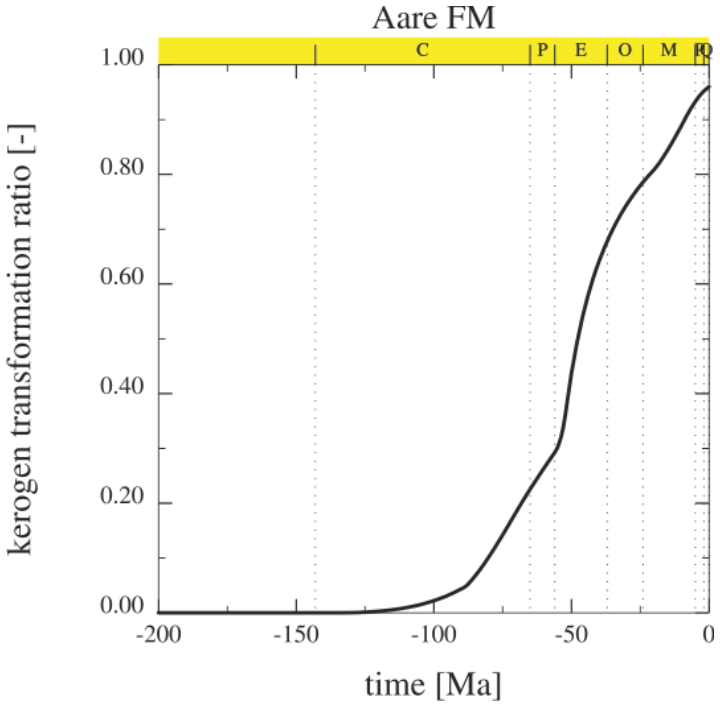

Figure 8: Time-Kerogen transformation cross-plot of the Åre Formation showing start of bulk kerogen transformation at ca. -120 M.Y. while peak transformation can be placed at ca. -50 M.Y. Presently however, less than 5% of the bulk kerogen is shown to be left within the Åre Formation as per modelling results.

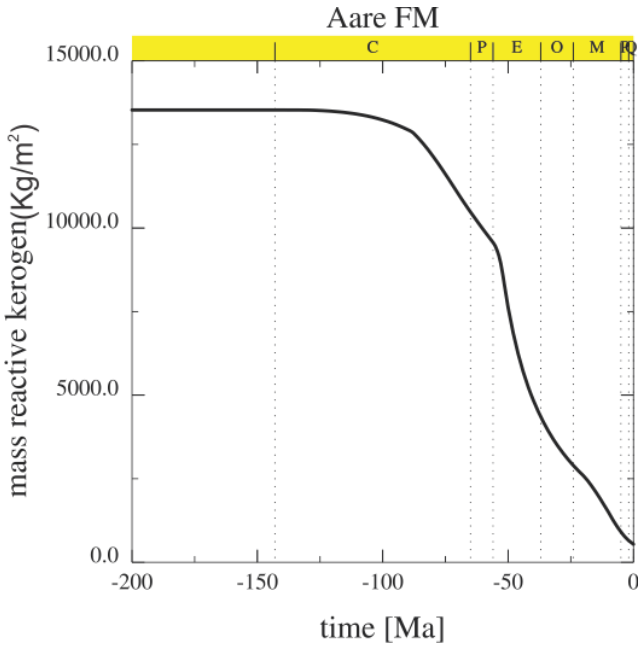

Figure 9: Time-Mass reactive kerogen cross-plot showing decrease in mass reactive kerogen with time at ca. -125 Ma transformation of reactive kerogen is evident while peak transformation can be placed at ca. -50 M.Y. Presently however, less than 10% of the reactive kerogen is shown to be left within the Åre Formation as per modelling results.

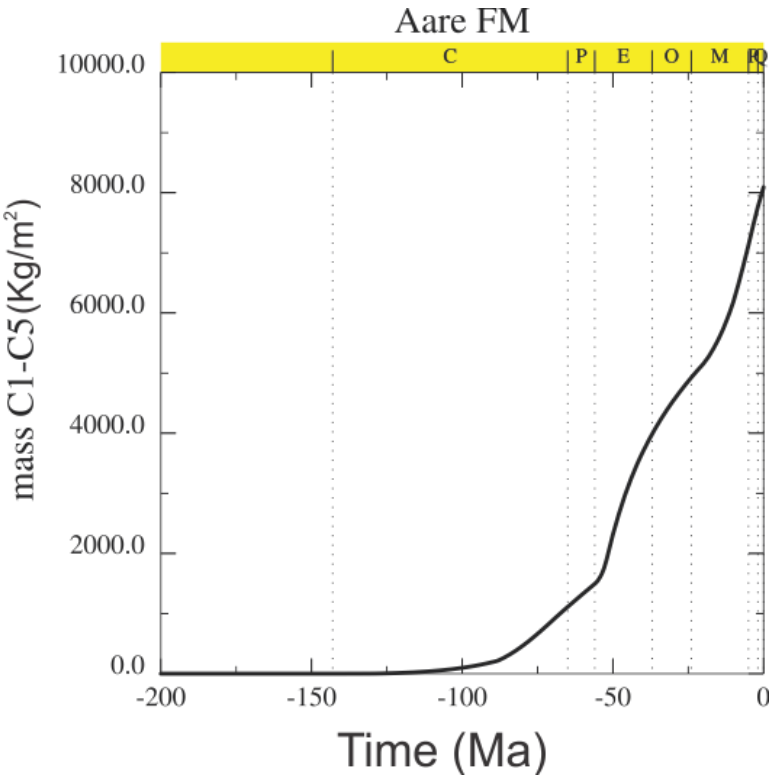

Figure 10: Time-Light HCs (gas) cross-plot showing start of generation at ca. -110 M.Y. Similarly, timing of peak generation can be placed at ca. -50 Ma, shown by the steep curve at this time after which the slope angle gradually decrease showing decline after the peak period.

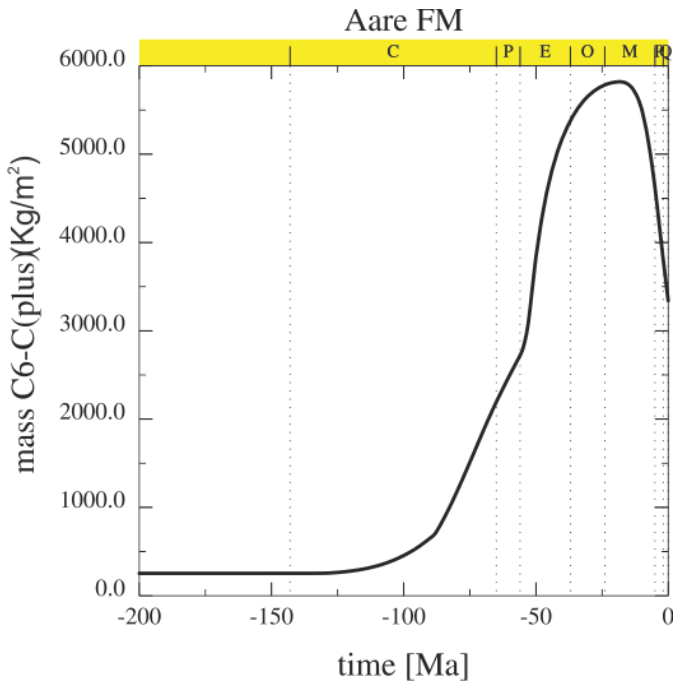

Figure 11: Time- HCs (oil) cross-plot showing start of generation at ca. -125 M.Y. Similarly, timing of peak generation can be placed at ca. -50 Ma, shown by the steep curve at this time after which curve flattens at the top between ca. -40 Ma and -20 Ma after which a clear decline in oil generation is observed

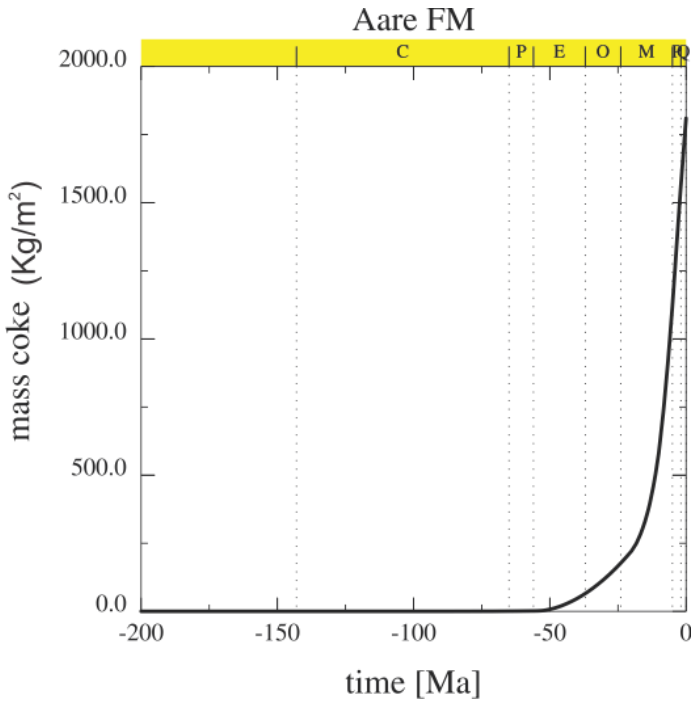

Figure 12: Time- Mass coke cross-plot showing start of coke generation at ca. -50 and increases forward in time. An abrupt increase in the coke formation between -20 Ma -0 Ma can be noticed period.

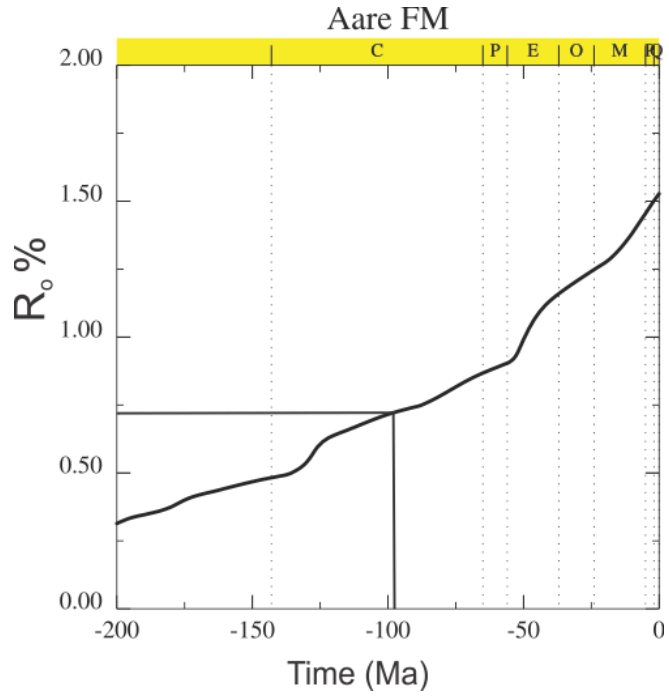

Figure 13: Time- Vitrinite reflectance cross-plot showing start of early oil generation at ca. -105 and peak oil generation is observed at -75 Ma and increases forward in time. An abrupt increase in the coke formation between -20 Ma -0 Ma can be noticed period. As mentioned in the table 5.1, peak oil generation is has been taken place ca. 50 Ma ago and Åre Formation is still in gas window.

Melke Formation:

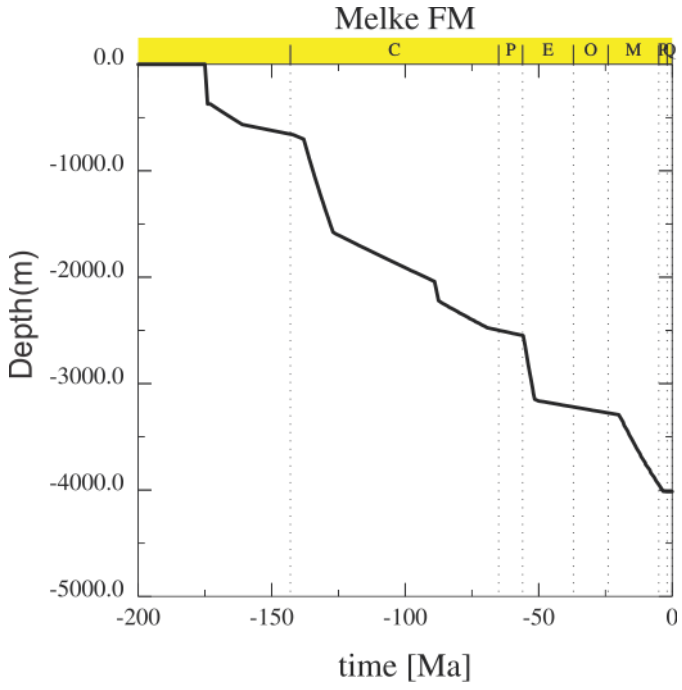

Figure 14: Time-Depth cross-plot for the Melke Formation showing burial depth of the formation at different time intervals. Note the sudden drops in the burial curve at ca. -150 Ma, -90 Ma, -55 Ma and -20 Ma representing major tectonic subsidence at these times.

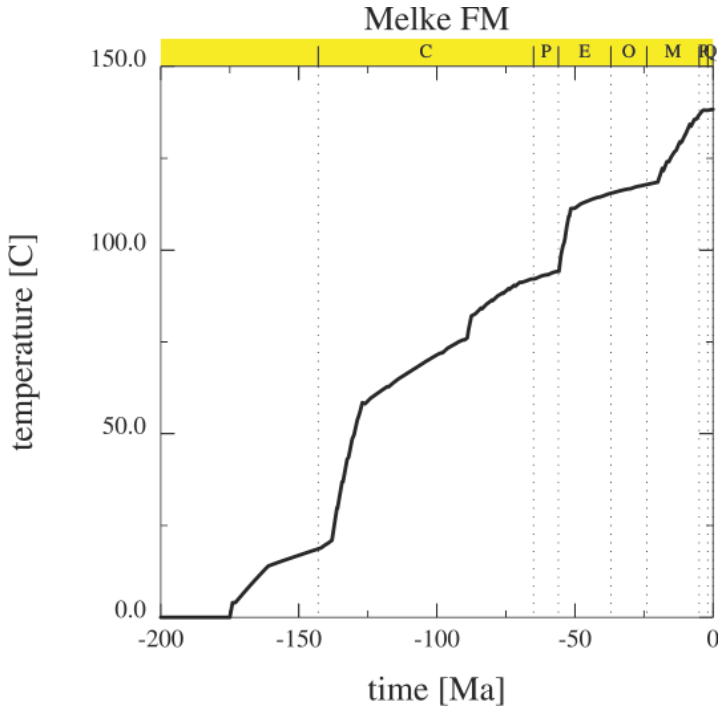

Figure 15: Time-Temperature cross-plot for the Melke Formation showing temperature of the formation at different time intervals. A general increase in temperature with time is evident with abrupt rises at ca. -150 Ma, -90 Ma, -55 Ma and -20 M.Y.

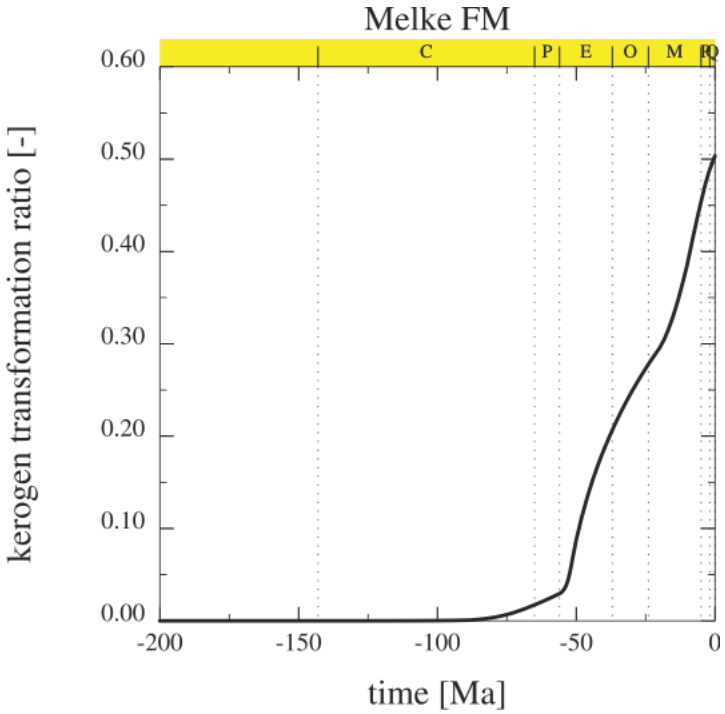

Figure 16: Time-Kerogen transformation cross-plot of the Melke Formation showing start of bulk kerogen transformation at ca. -110 M.Y. while peak transformation can be placed at ca. -50 M.Y. Presently however, less than 50% of the bulk kerogen is shown to be left within the Melke Formation as per modelling results.

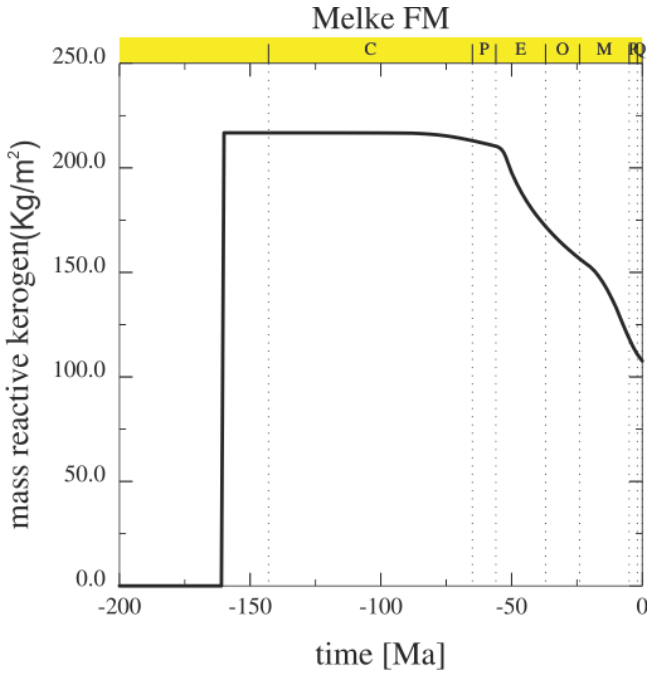

Figure 17: Time-Mass reactive kerogen cross-plot showing decrease in mass reactive kerogen with time at ca. -125 Ma transformation of reactive kerogen is evident while peak transformation can be placed at ca. -50 M.Y.

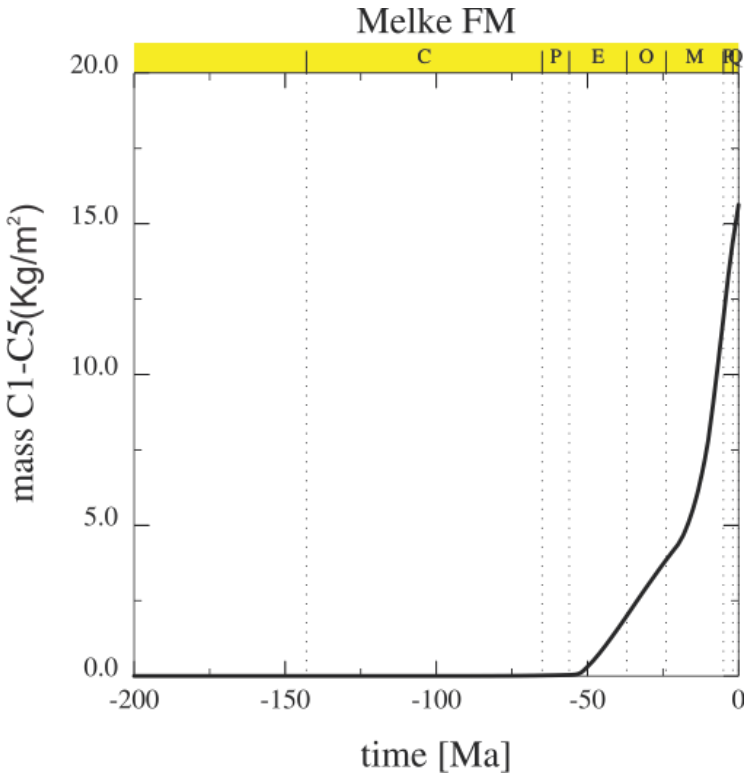

Figure 18: Time-Light HCs (gas) cross-plot showing start of generation at ca. -50 M.Y. Similarly, timing of peak generation can be placed at ca. -20 Ma, shown by the steep curve at this time after which the slope angle gradually decrease showing decline after the peak period.

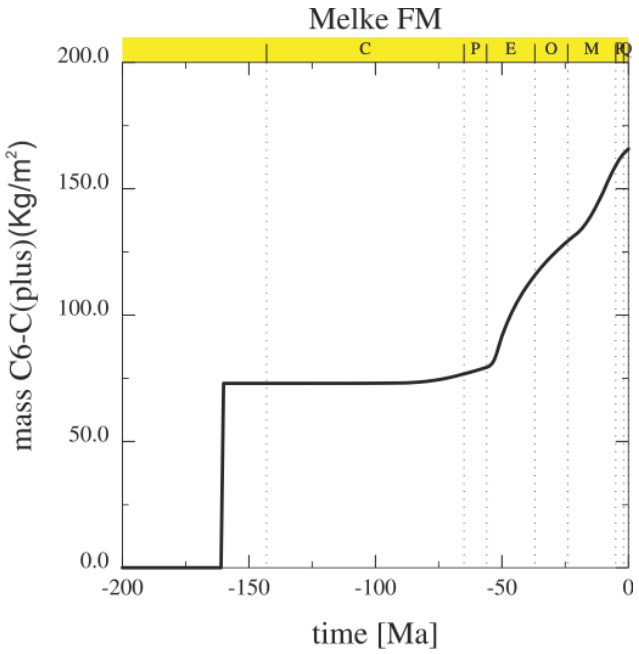

Figure 19: Time- HCs (oil) cross-plot showing start of generation at ca. -55 M.Y. Similarly, timing of peak generation can be placed at ca. -25 M.Y.

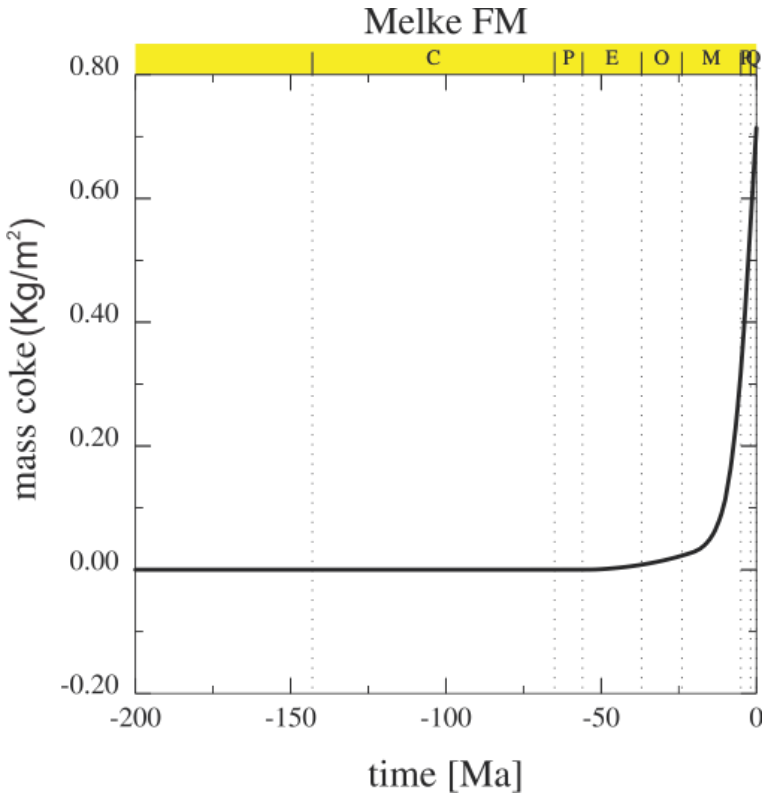

Figure 20: Time- Mass coke cross-plot showing start of coke generation at ca. -20 and increases forward in time. An abrupt increase in the coke formation between -20 Ma -0 Ma can be noticed period.

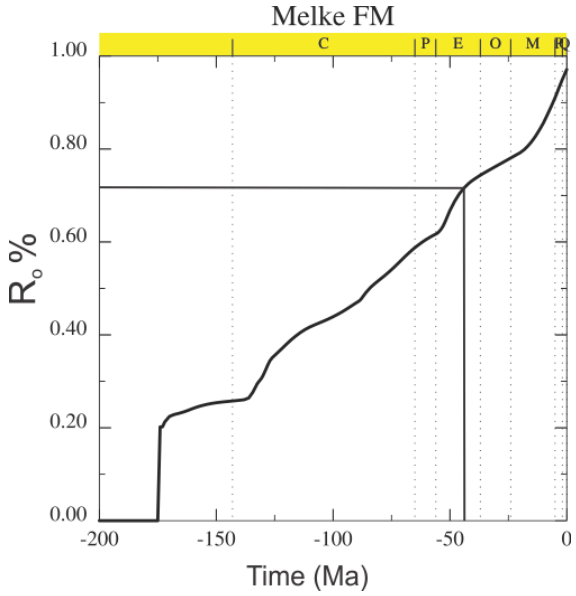

Figure 21: Time- Vitrinite reflectance cross-plot showing start of early oil generation at ca. -105 and peak oil generation is observed at -75 Ma and increases forward in time. An abrupt increase in the coke formation between -20 Ma -0 Ma can be noticed period. As mentioned in the table 5.1, peak oil generation is has been taken place recently and Melke Formation is still in oil window and generating HCs.

Spekk Formation:

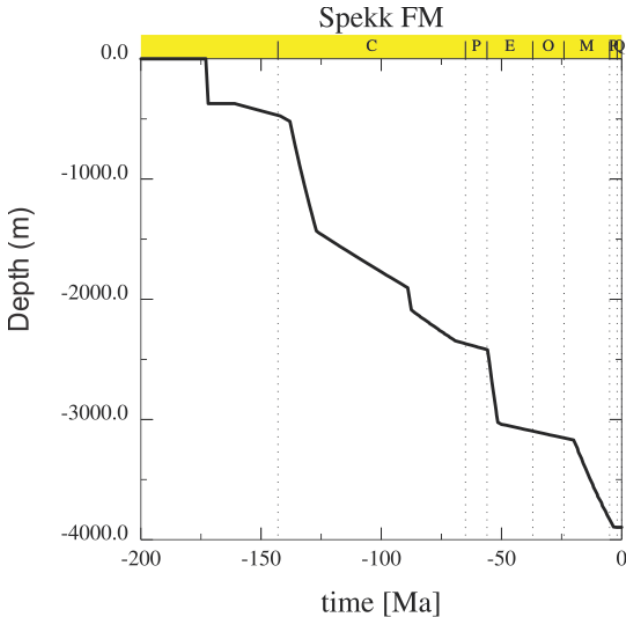

Figure 22: Time-Depth cross-plot for the Spekk Formation showing burial depth of the formation at different time intervals. Note the sudden drops in the burial curve at ca. -150 Ma, -90 Ma, -55 Ma and -20 Ma representing major tectonic subsidence at these times.

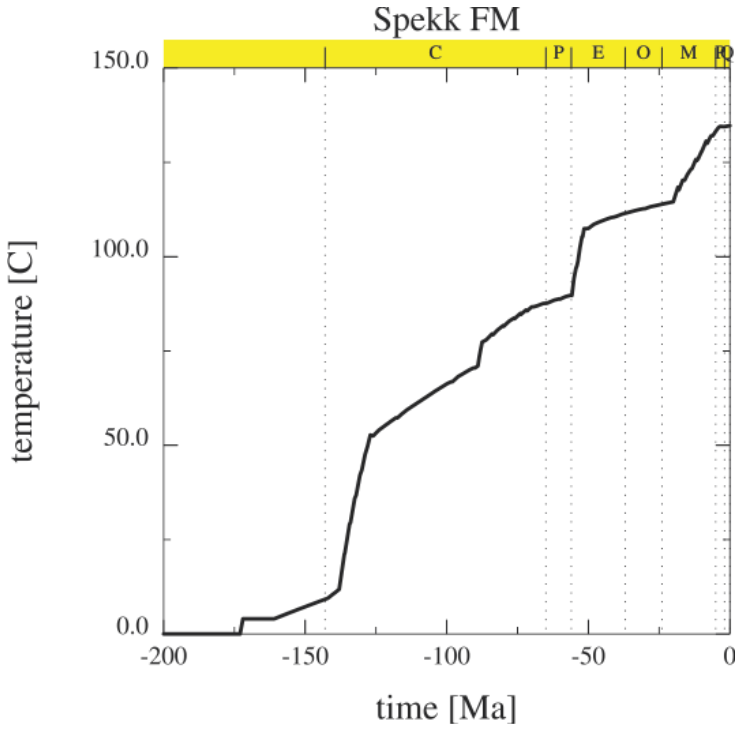

Figure 23: Time-Temperature cross-plot for the Spekk Formation showing temperature of the formation at different time intervals. A general increase in temperature with time is evident with abrupt rises at ca. -150 Ma, -90 Ma, -55 Ma and -20 M.Y.

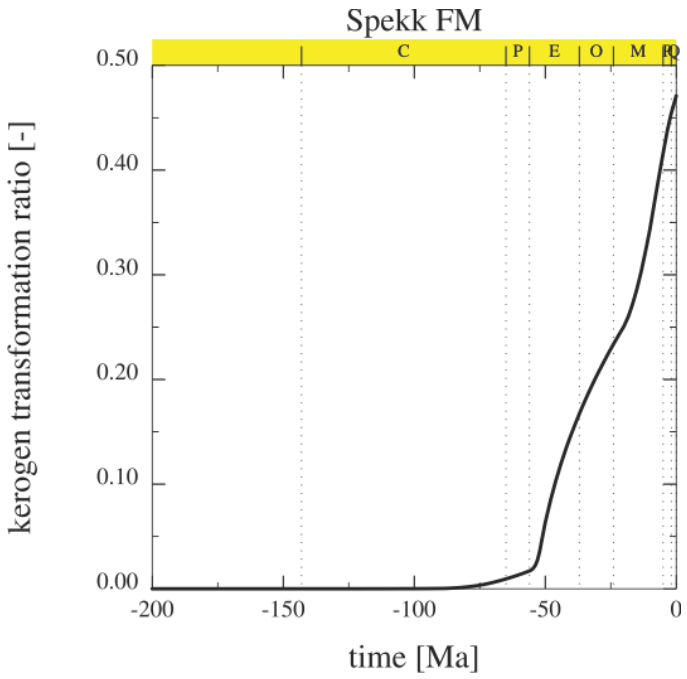

Figure 24: Time-Kerogen transformation cross-plot of the Spekk Formation showing start of bulk kerogen transformation at ca. -55 M.Y. while peak transformation can be placed at ca. -20 M.Y. Presently however, less than 5% of the bulk kerogen is shown to be left within the Spekk Formation as per modelling results.

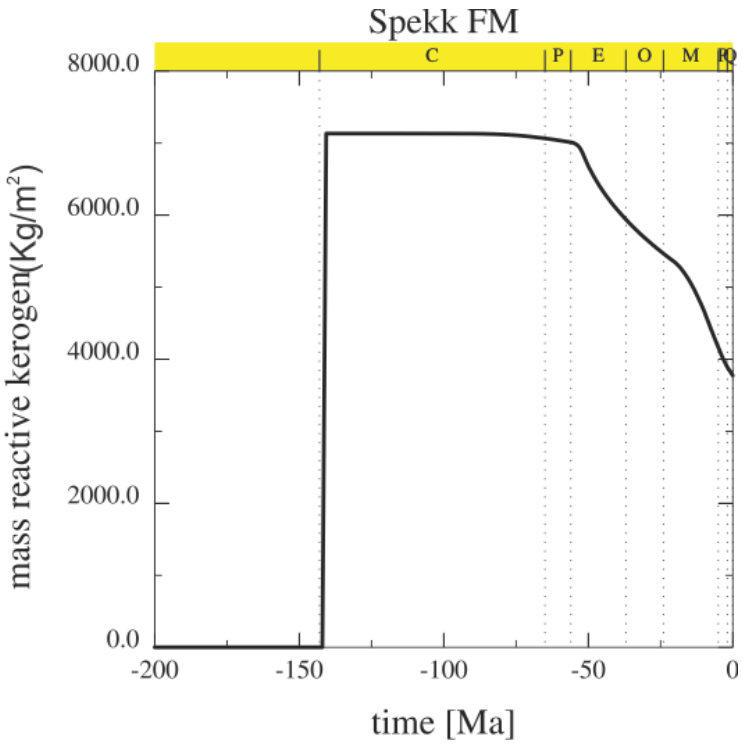

Figure 25: Time-Mass reactive kerogen cross-plot showing decrease in mass reactive kerogen with time at ca. -55 Ma transformation of reactive kerogen is evident while peak transformation can be placed at ca. -25 M.Y.

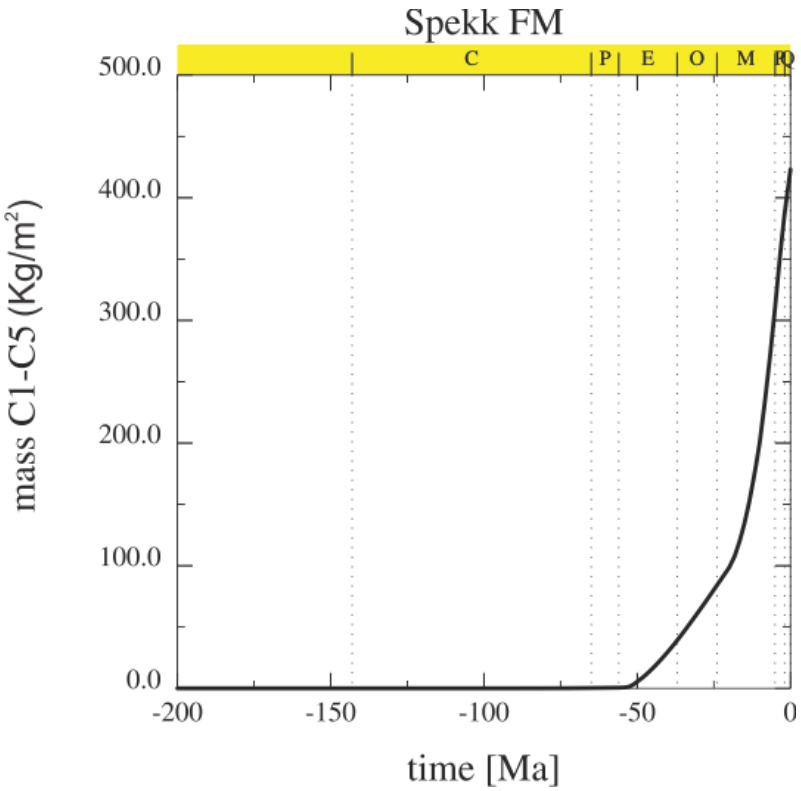

Figure 26: Time-Light HCs (gas) cross-plot showing start of generation at ca. -110 M.Y. Similarly, timing of peak generation can be placed at ca. -50 Ma, shown by the steep curve at this time after which the slope angle gradually decrease showing decline after the peak period.

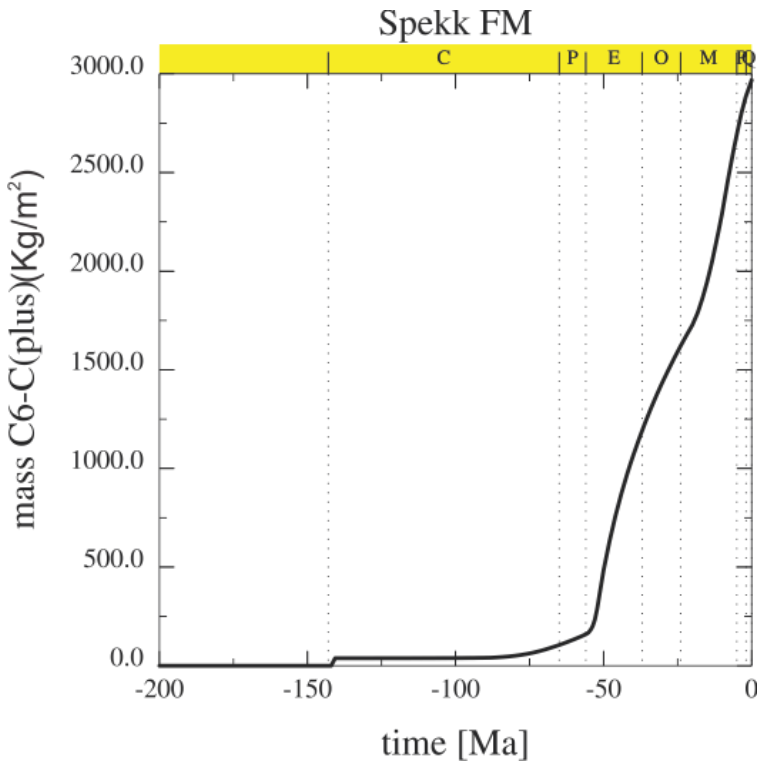

Figure 27: Time- HCs (oil) cross-plot showing start of generation at ca. -55 M.Y. Similarly, timing of peak generation can be placed at ca. -20 Ma, shown by the steep curve at this time.

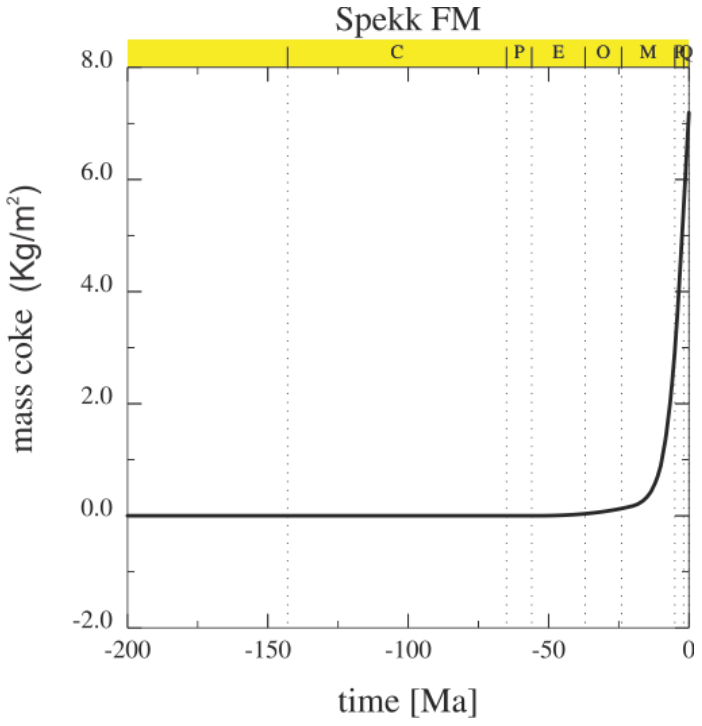

Figure 28: Time- Mass coke cross-plot showing start of coke generation at ca. -15 and increases forward in time. An abrupt increase in the coke formation between -10 Ma -0 Ma can be noticed period.

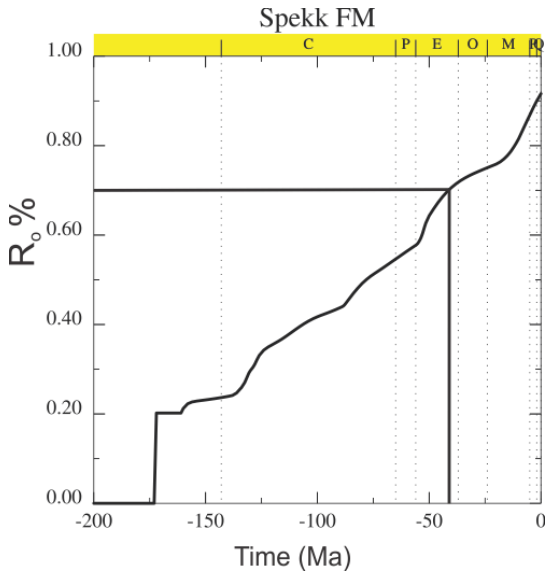

Figure 29: Time- Vitrinite reflectance cross-plot showing start of early oil generation at ca. -105 and peak oil generation is observed at -75 Ma and increases forward in time. An abrupt increase in the coke formation between -20 Ma -0 Ma can be noticed period. As mentioned in the table 5.1, Spekk Formation is still in oil window.

Smørbukk (6506/12-9s):

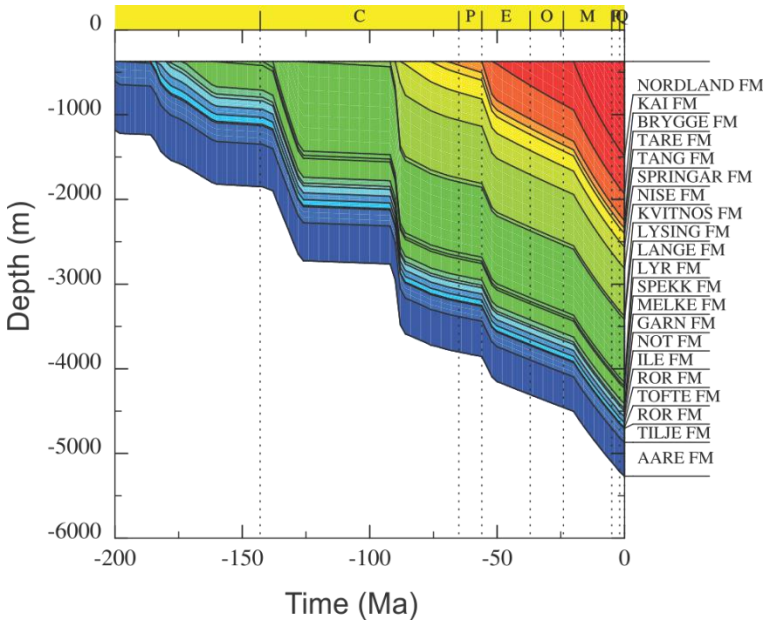

Figure 30: Burial reconstruction through time and depth for the Smørbukk (6506/12-9s) well which displays a relatively gradual burial trend, data used forCase-2.

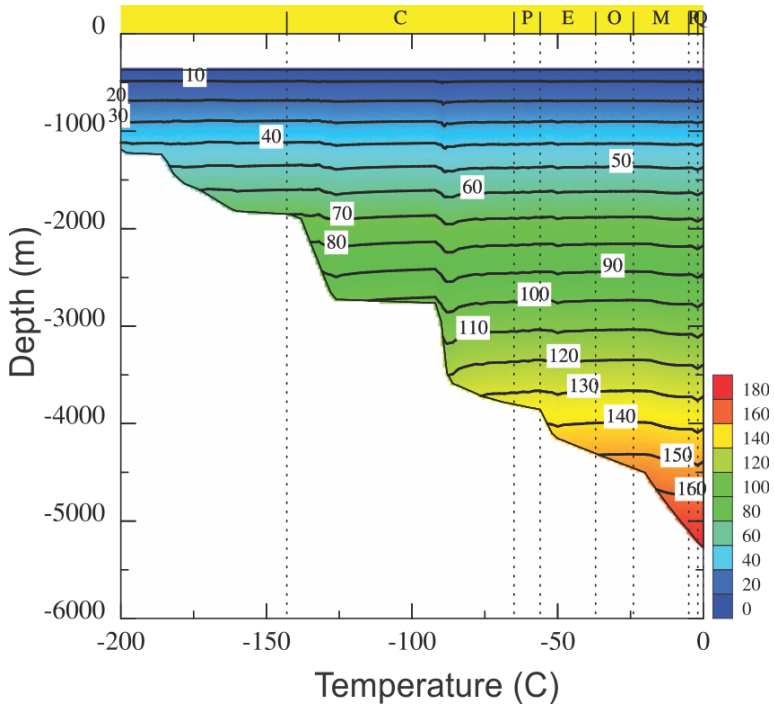

Figure 31: Temperature reconstruction through time and depth for the Smørbukk (6506/12-9s) well forCase-2.

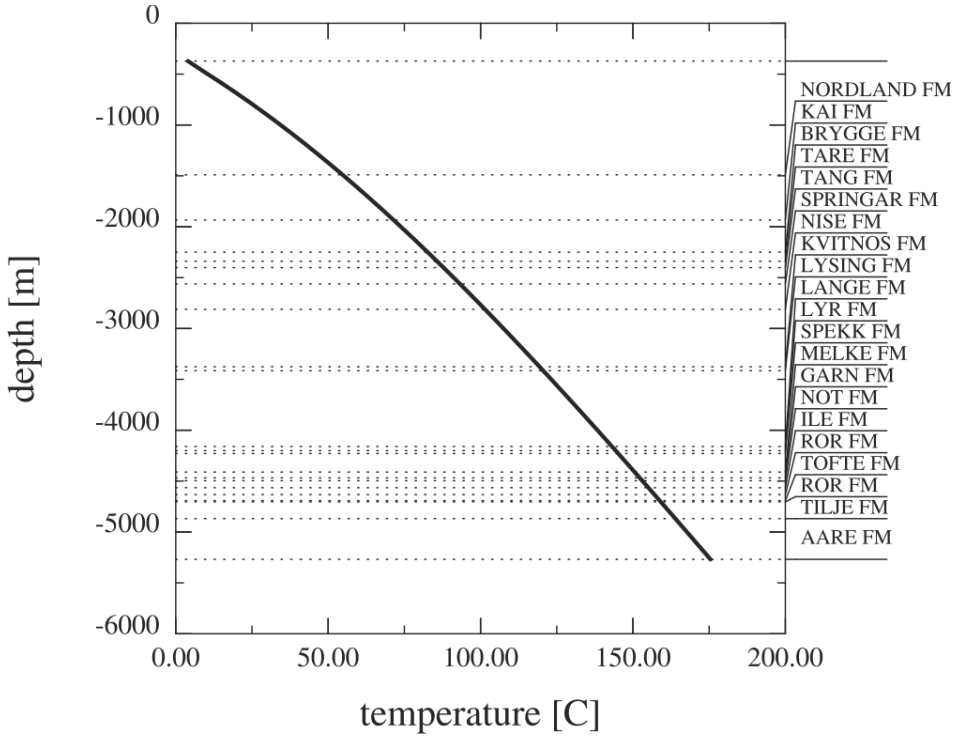

Figure 32: Temperature depth cross-plot for the Smørbukk (6506/12-9s) showing a linear relationship between the two values.

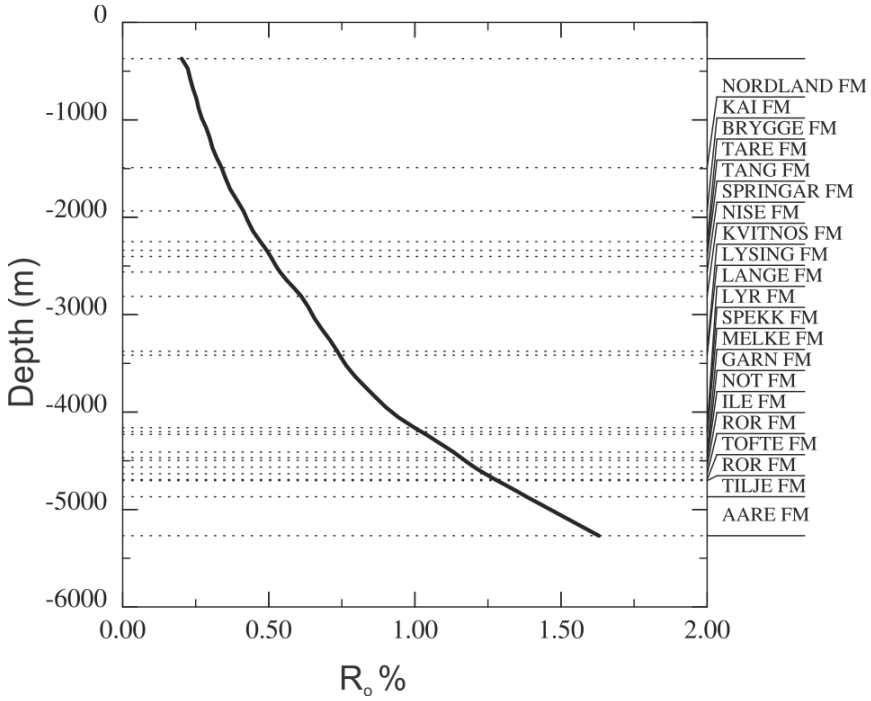

Figure 33: Plot of measured vitrinite reflectance against depth for the Smørbukk (6506/12-9s) well of modelled vitrinite reflectance against depth for the same well (using BAS software).

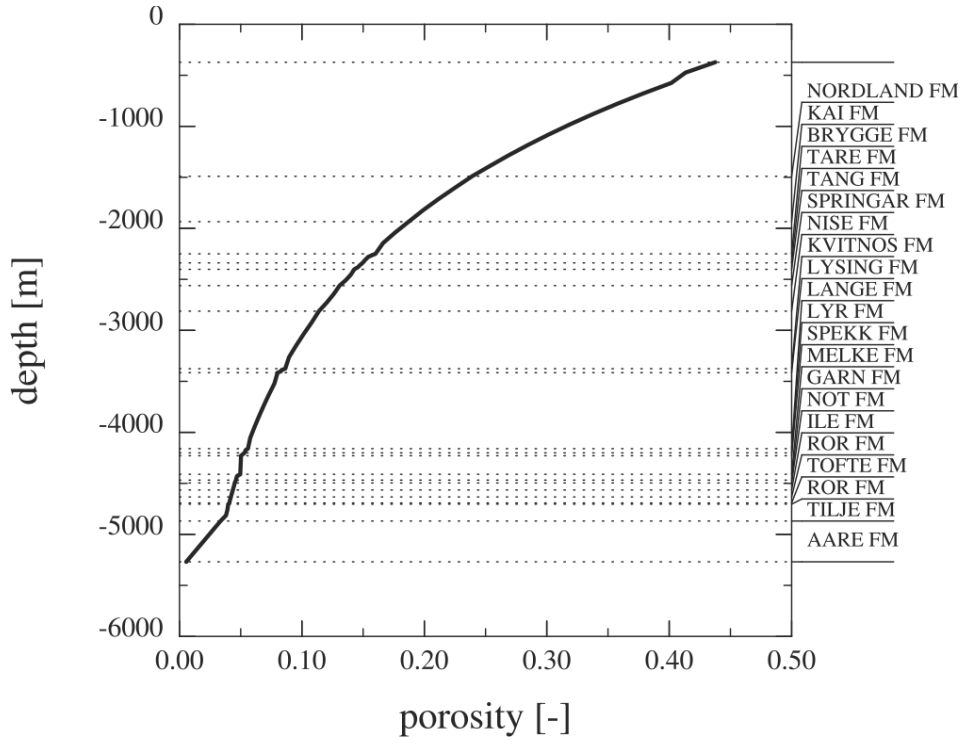

Figure 34: porosity versus depth cross-plot for the Smørbukk (6506/12-9s) showing decrease in porosity with depth. However, it is pertinent to note that decrease in porosity is a function of compaction, also above 80 C chemical compaction starts which disturbs the linear relationship of porosity lose with depth.

Åre Formation:

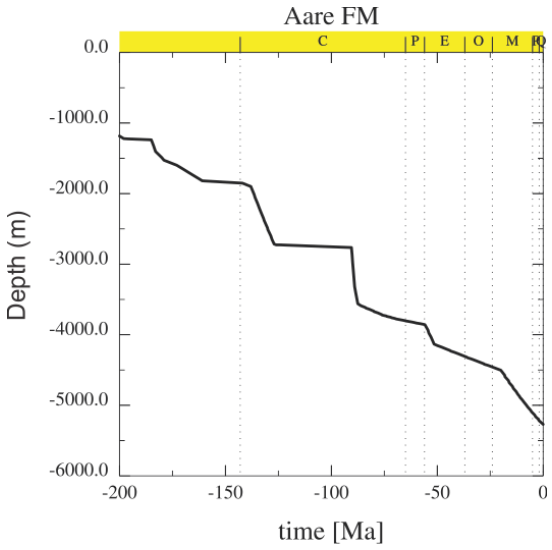

Figure 35: Time-Depth cross-plot for the Åre Formation showing burial depth of the formation at different time intervals. Note the sudden drops in the burial curve at ca. -140 Ma, -90 Ma, -55 Ma and -20 Ma representing major tectonic subsidence at these times.

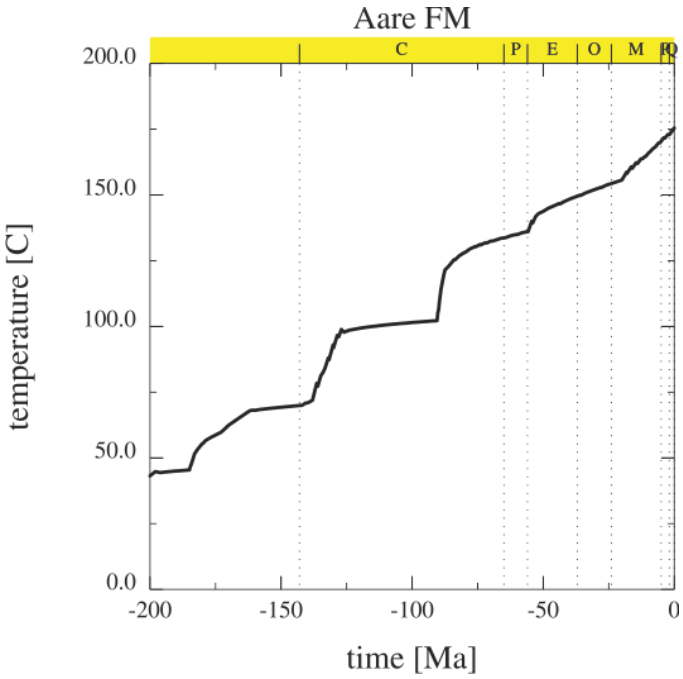

Figure 36: Time-Temperature cross-plot for the Åre Formation showing temperature of the formation at different time intervals. A general increase in temperature with time is evident with abrupt rises at ca. -140 Ma, -90 Ma, -55 Ma and -20 M.Y. Following Hunt (1996) Åre Formation remained in oil window between at ca. -170 Ma & -10 Ma and is currently in gas window.

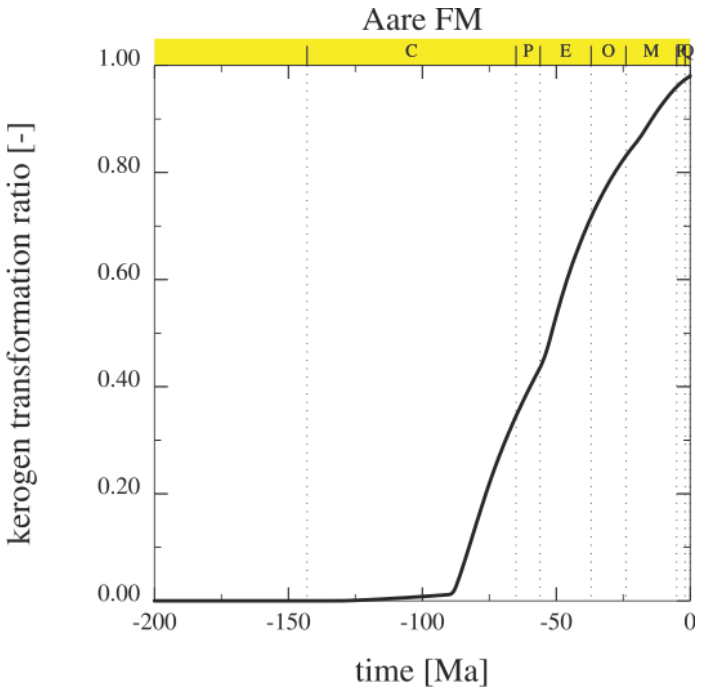

Figure 37: Time-Kerogen transformation cross-plot of the Åre Formation showing start of bulk kerogen transformation at ca. -110 M.Y. while peak transformation can be placed at ca. -80 M.Y. Presently however, less than 3% of the bulk kerogen is shown to be left within the Åre Formation as per modelling results.

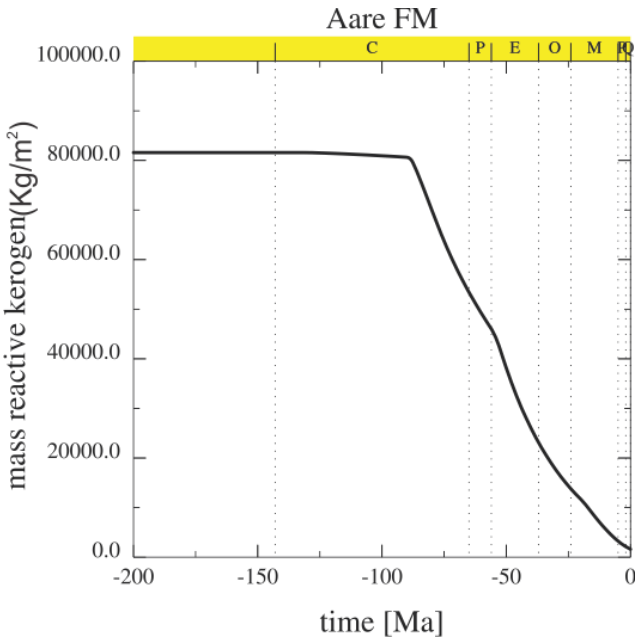

Figure 38: Time-Mass reactive kerogen cross-plot showing decrease in mass reactive kerogen with time at ca. -100 Ma transformation of reactive kerogen is evident while peak transformation can be placed at ca. -90 M.Y.

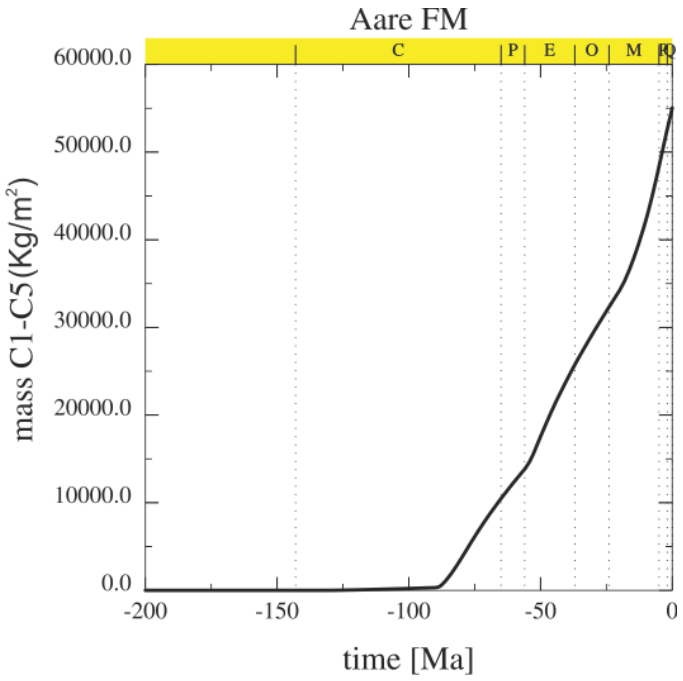

Figure 39: Time-Light HCs (gas) cross-plot showing start of generation at ca. -85 M.Y. Similarly, timing of peak generation can be placed at ca. -50 Ma, shown by the steep curve at this time after which the slope angle gradually decrease showing decline after the peak period.

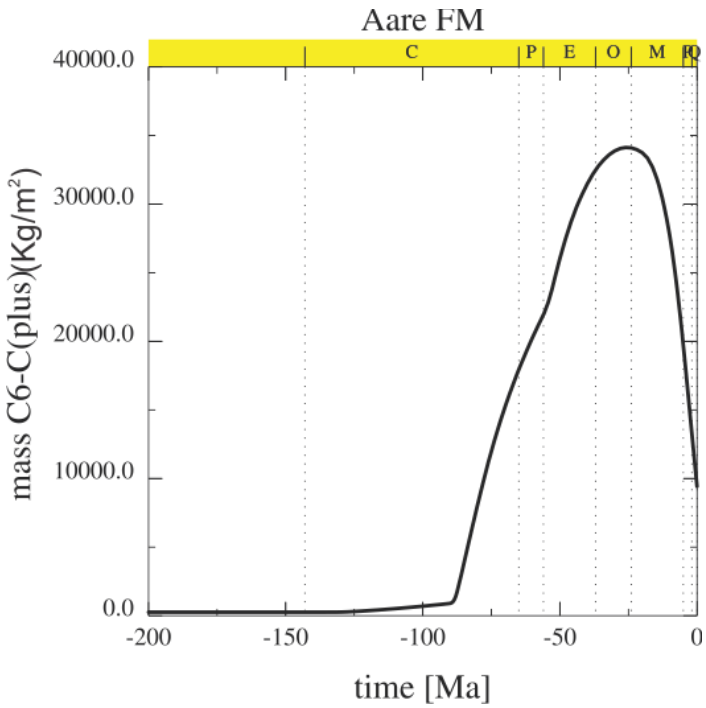

Figure 40: Time- HCs (oil) cross-plot showing start of generation at ca. -125 M.Y. Similarly, timing of peak generation can be placed at ca. -50 Ma, shown by the steep curve at this time after which curve flattens at the top between ca. -40 Ma and -20 Ma after which a clear decline in oil generation is observed.

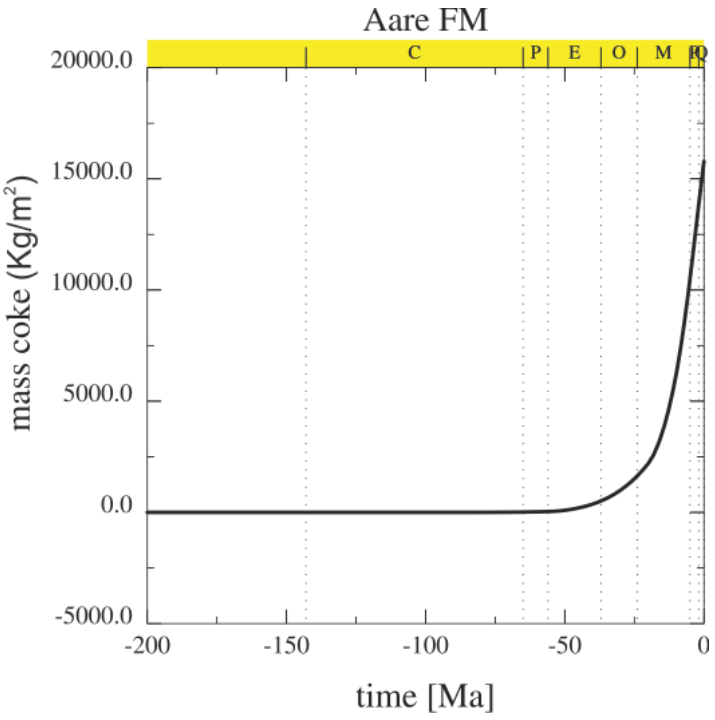

Figure 41: Time- Mass coke cross-plot showing start of coke generation at ca. -50 and increases forward in time. An abrupt increase in the coke formation between -20 Ma -0 Ma can be noticed period.

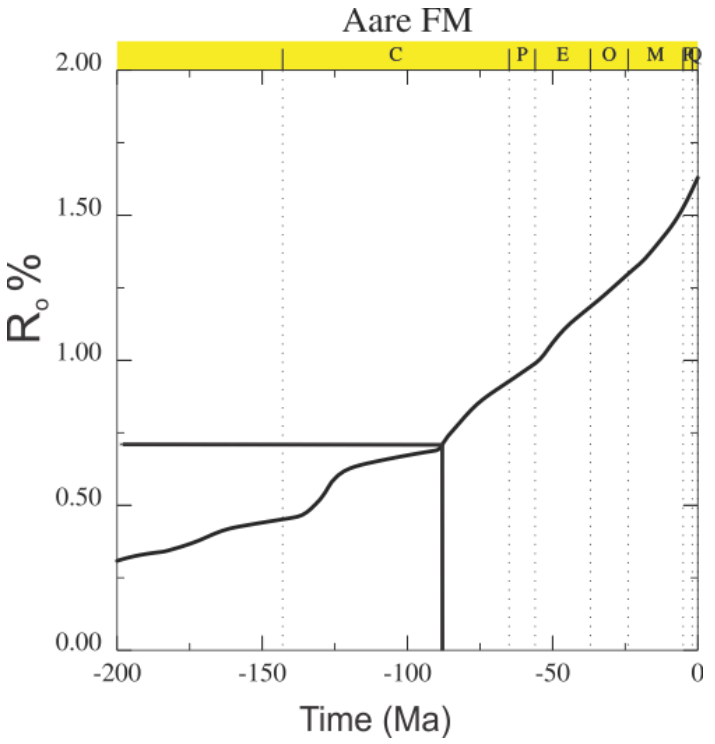

Figure 42: Time- Vitrinite reflectance cross-plot showing start of early oil generation at ca. -105 and peak oil generation is observed at -75 Ma and increases forward in time. An abrupt increase in the coke formation between -20 Ma -0 Ma can be noticed period. As mentioned in the table 5.1, peak oil generation has been taken place ca. 55 Ma ago and Åre Formation is still in gas window.

Melke Formation:

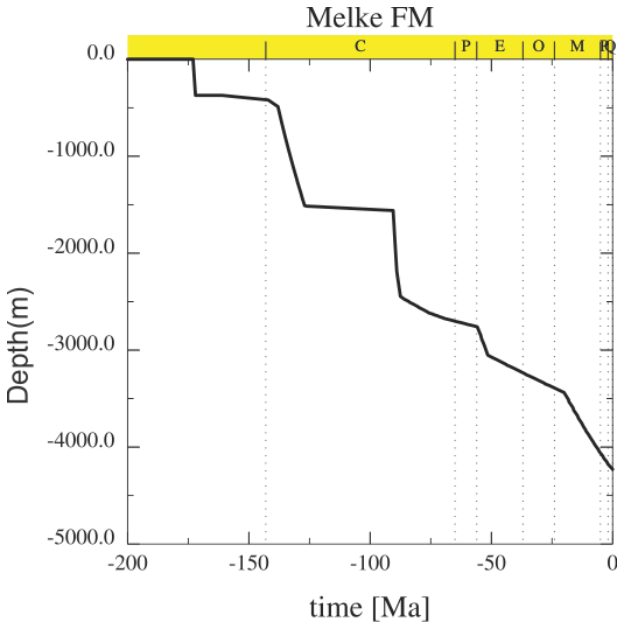

Figure 43: Time-Depth cross-plot for the Melke Formation showing burial depth of the formation at different time intervals. Note the sudden drops in the burial curve at ca. -140 Ma, -90 Ma, -55 Ma and -20 Ma representing major tectonic subsidence at these times.

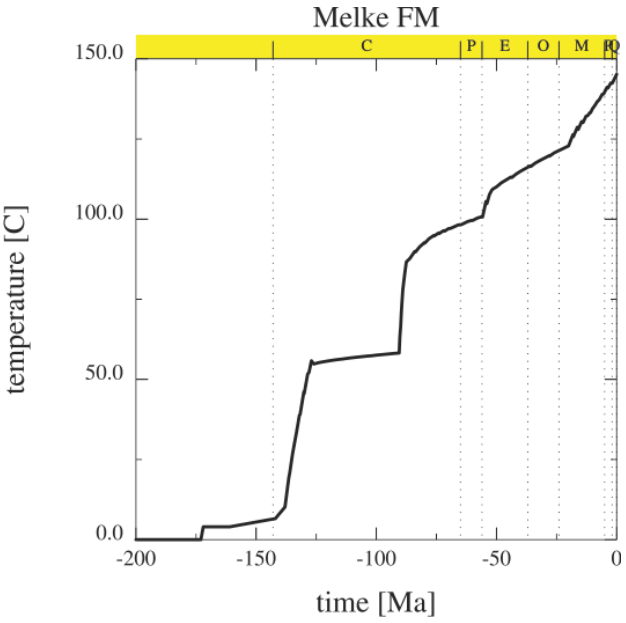

Figure 44: Time-Temperature cross-plot for the Melke Formation showing temperature of the formation at different time intervals. A general increase in temperature with time is evident with abrupt rises at ca. -150 Ma, -90 Ma, -55 Ma and -20 M.Y. Following Hunt (1996) Melke Formation remained in oil window between at ca. -170 Ma & -10 Ma and is currently in gas window.

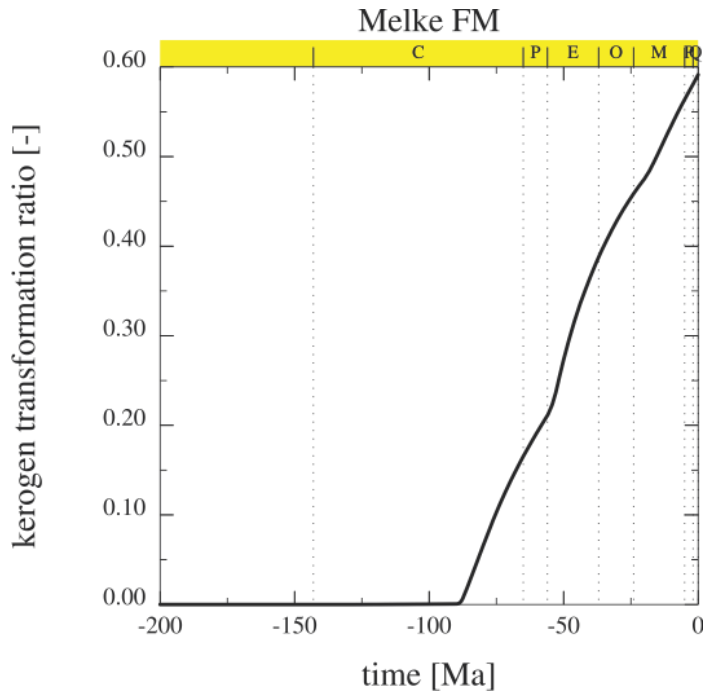

Figure 45: Time-Kerogen transformation cross-plot of the Melke Formation showing start of bulk kerogen transformation at ca. -120 M.Y. while peak transformation can be placed at ca. -50 M.Y. Presently however, less than 5% of the bulk kerogen is shown to be left within the Melke Formation as per modelling results.

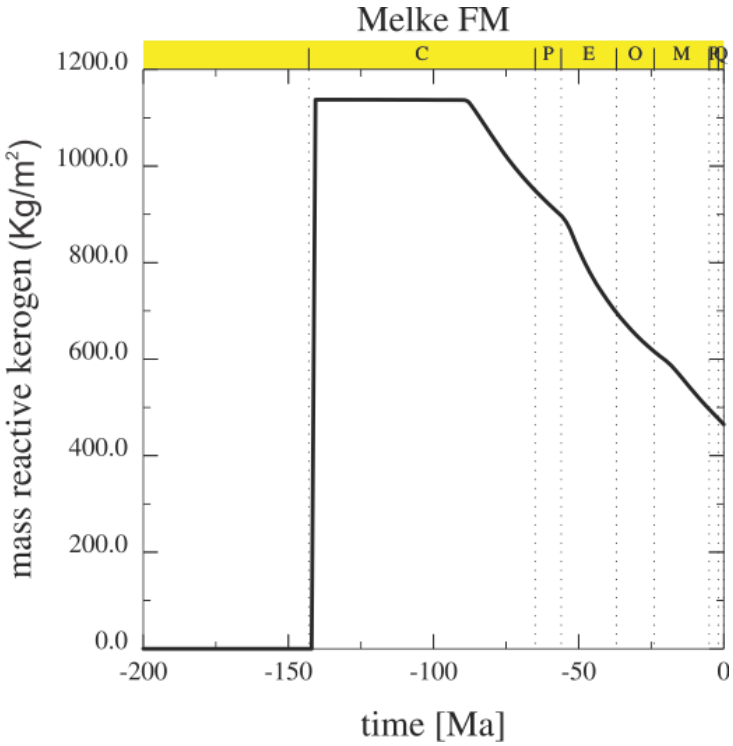

Figure 46: Time-Mass reactive kerogen cross-plot showing decrease in mass reactive kerogen with time at ca. -90 Ma transformation of reactive kerogen is evident while peak transformation can be placed at ca. -55 M.Y.

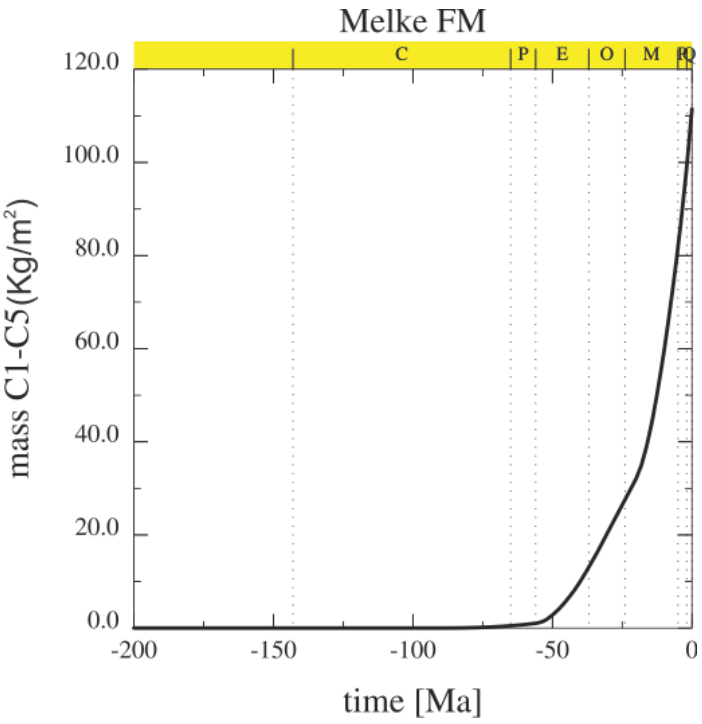

Figure 47: Time-Light HCs (gas) cross-plot showing start of generation at ca. -60 M.Y. Similarly, timing of peak generation can be placed at ca. -25 Ma, shown by the steep curve at this time after which the slope angle gradually decrease showing decline after the peak period.

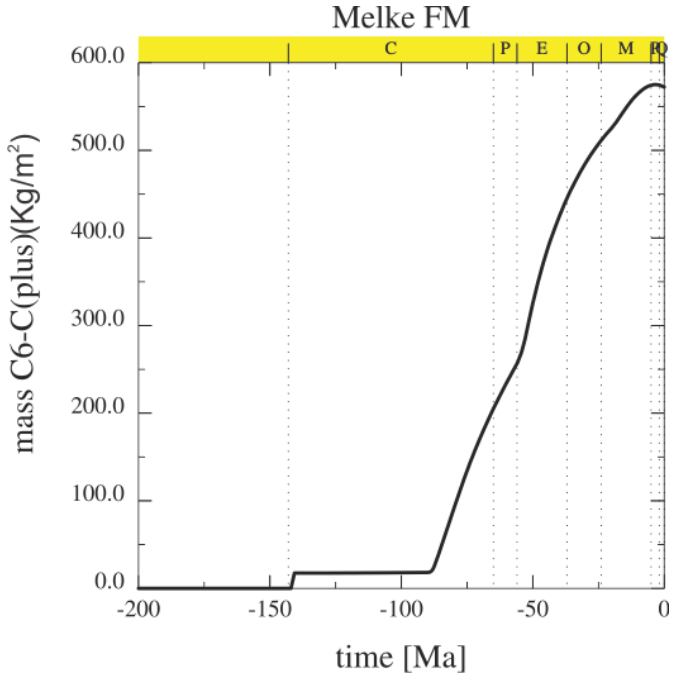

Figure 48: Time- HCs (oil) cross-plot showing start of generation at ca. -80 M.Y. Similarly, timing of peak generation can be placed at ca. -55 M.Y.

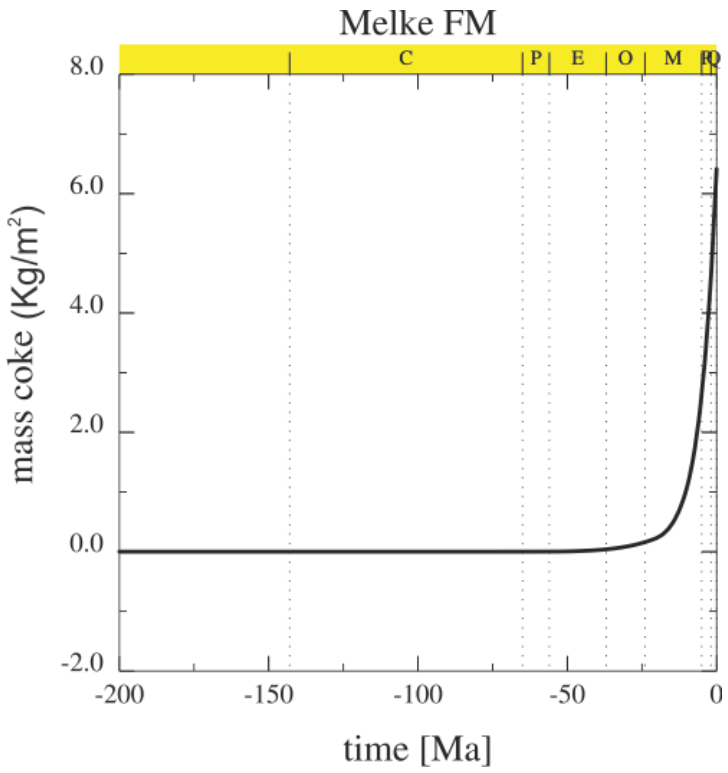

Figure 49: Time- Mass coke cross-plot showing start of coke generation at ca. -30 and increases forward in time. An abrupt increase in the coke formation between -20 Ma -0 Ma can be noticed period.

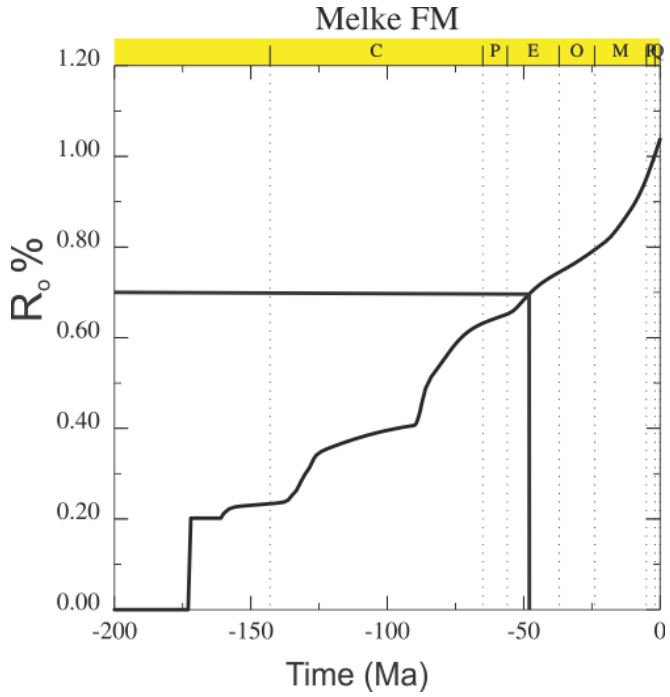

Figure 50: Time- Vitrinite reflectance cross-plot showing start of early oil generation at ca. -105 and peak oil generation is observed at -75 Ma and increases forward in time. An abrupt increase in the coke formation between -20 Ma -0 Ma can be noticed period. As mentioned in the table 5.1, peak oil generation has been taken place recently and the Melke Formation is still in oil window.

Spekk Formation:

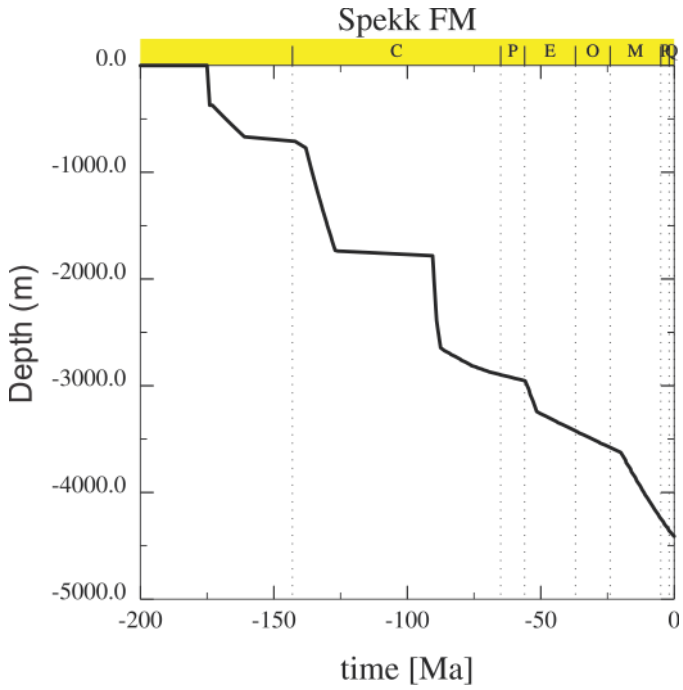

Figure 51: Time-Depth cross-plot for the Spekk Formation showing burial depth of the formation at different time intervals. Note the sudden drops in the burial curve at ca. -140 Ma, -90 Ma, -55 Ma and -20 Ma representing major tectonic subsidence at these times.

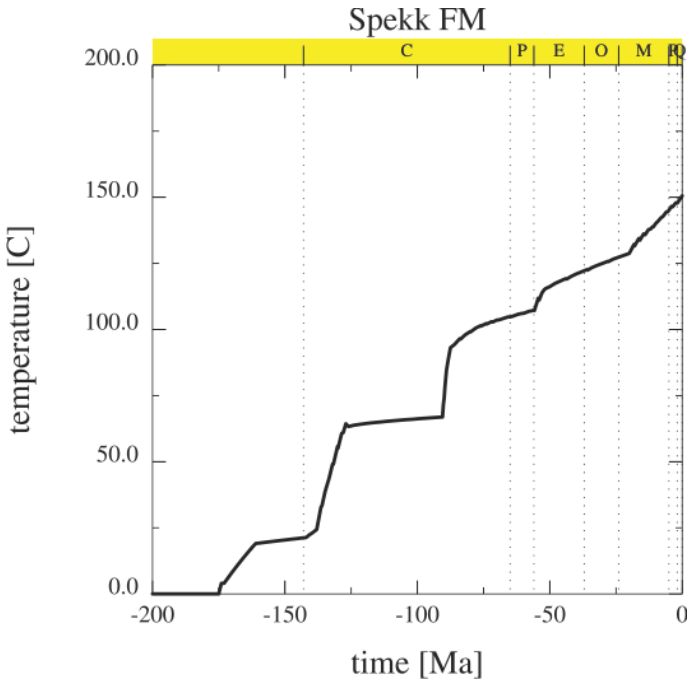

Figure 52: Time-Temperature cross-plot for the Spekk Formation showing temperature of the formation at different time intervals. A general increase in temperature with time is evident with abrupt rises at ca. -140 Ma, -90 Ma, -55 Ma and -20 M.Y.

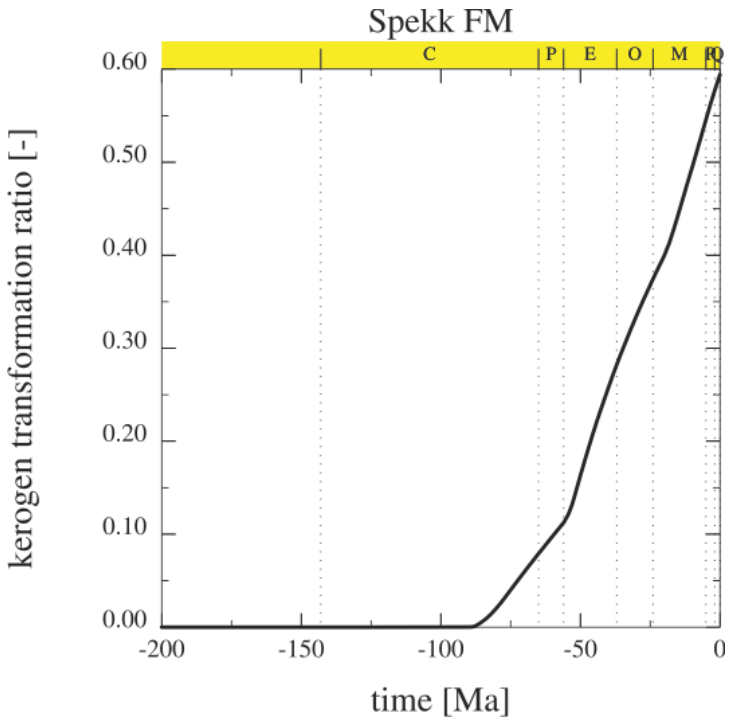

Figure 53: Time-Kerogen transformation cross-plot of the Spekk Formation showing start of bulk kerogen transformation at ca. -85 M.Y. while peak transformation can be placed at ca. -50 M.Y. Presently however, more than 5% of the bulk kerogen is shown to be left within the Spekk Formation as per modelling results.

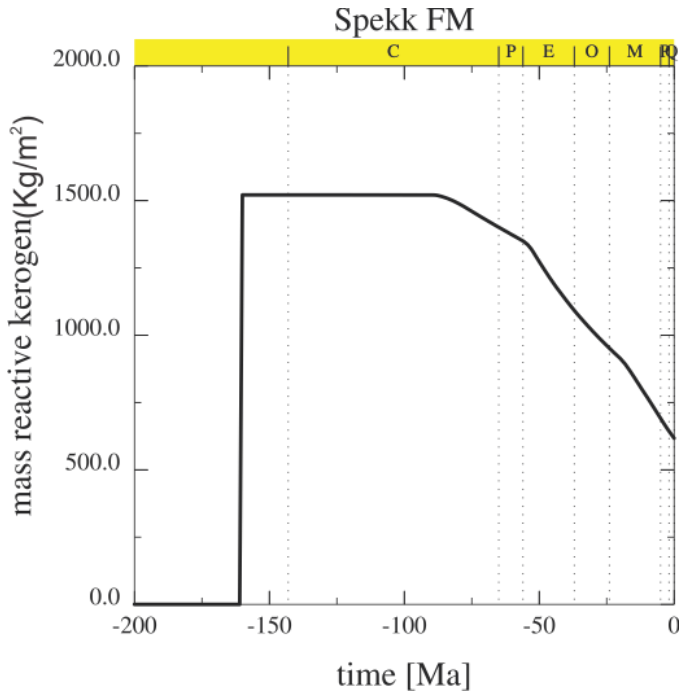

Figure 54: Time-Mass reactive kerogen cross-plot showing decrease in mass reactive kerogen with time at ca. -80 Ma transformation of reactive kerogen is evident while peak transformation can be placed at ca. -50 M.Y.

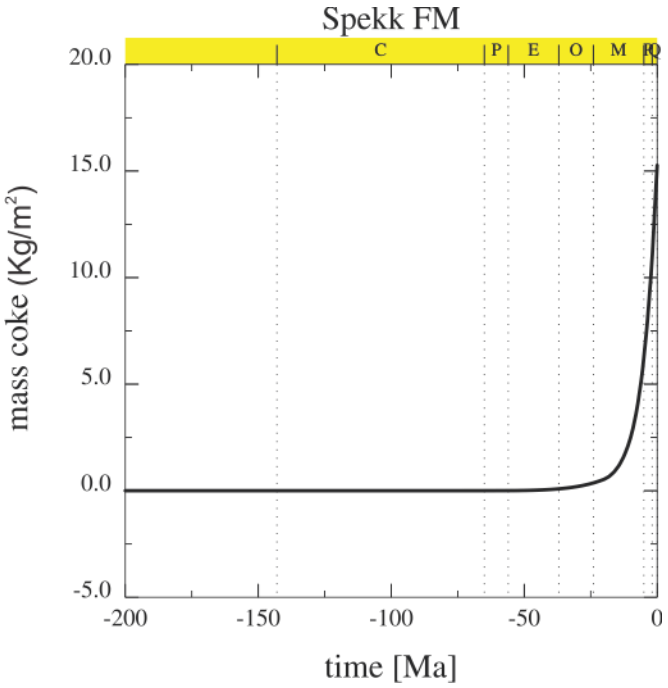

Figure 55: Time- Mass coke cross-plot showing start of coke generation at ca. -25 and increases forward in time. An abrupt increase in the coke formation between -20 Ma -0 Ma can be noticed period.

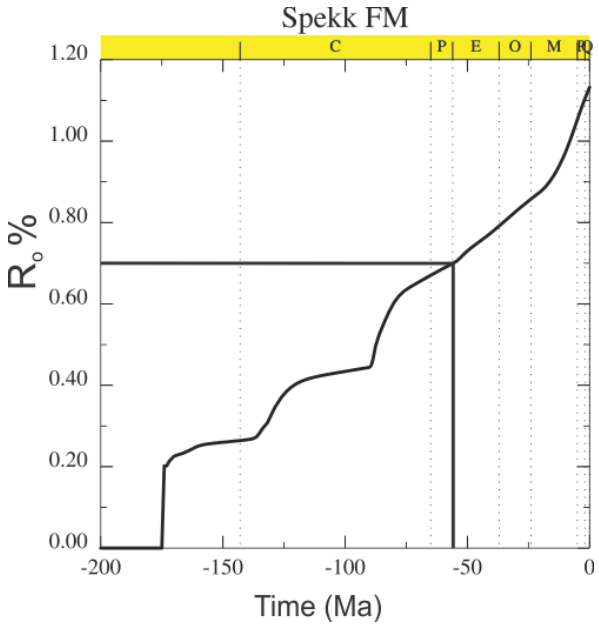

Figure 56: Time- Vitrinite reflectance cross-plot showing start of early oil generation at ca. -105 and peak oil generation is observed at -75 Ma and increases forward in time. An abrupt increase in the coke formation between -20 Ma -0 Ma can be noticed period. As mentioned in the table 5.1, peak oil generation has been taken place recently and the Spekk Formation is still generating HCs.

Appendix-D: Results forCase-3

CASE-3

The Midgard (6407/4-1) well:

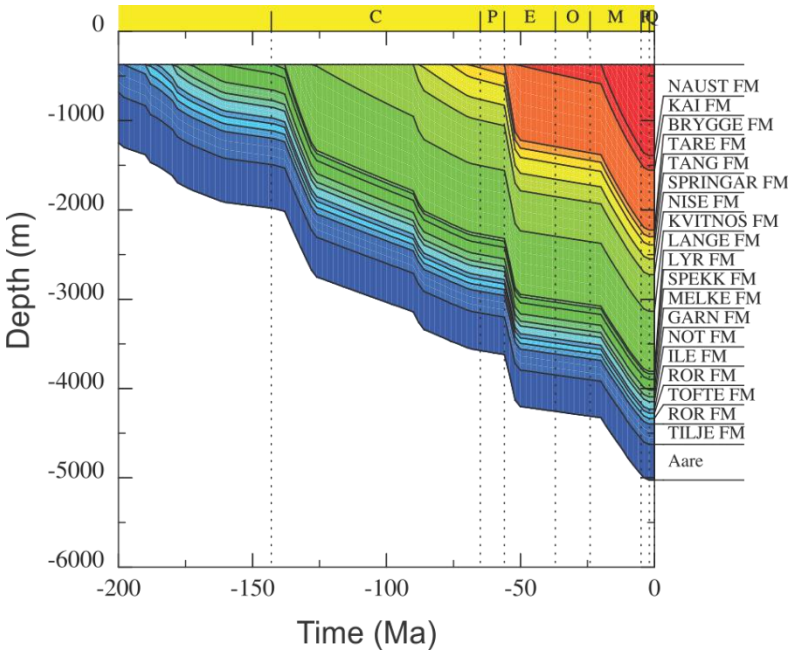

Figure 1: Burial reconstruction through time and depth for the Midgard (6407/4-1) well which displays a relatively gradual burial trend, data used forCase-3 (by using Tissot / Espitallie kinetic model).

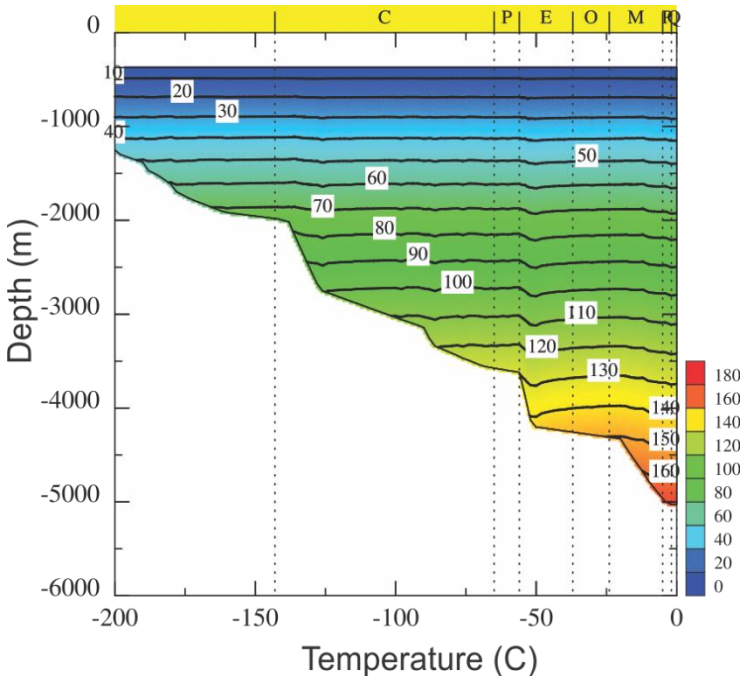

Figure 2: Thermal history reconstruction through time and depth for the Midgard (6407/4-1) well forCase-3 showing the deepest Formation is at 160 ^{o}C at present.

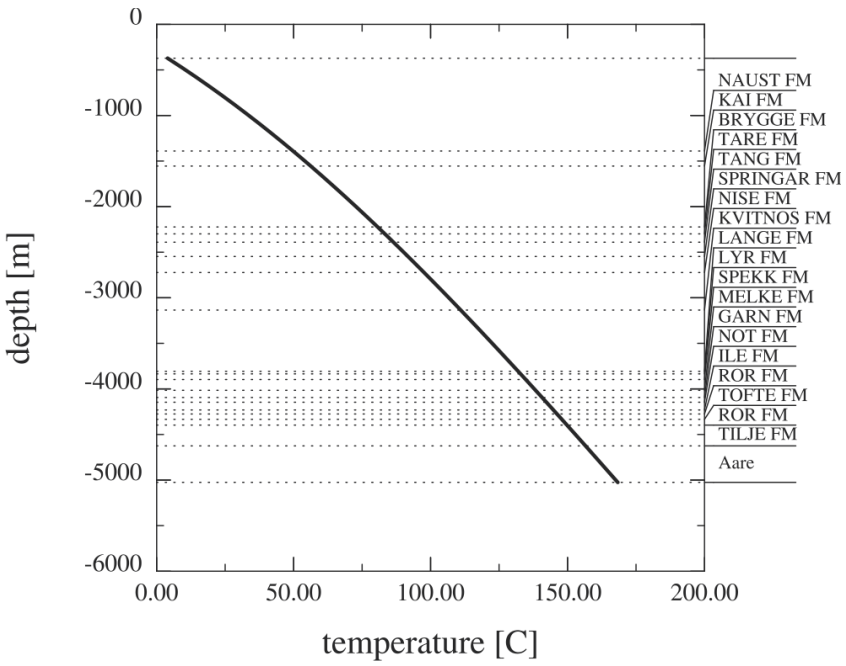

Figure 3: Temperature depth cross-plot for the Midgard well (6407/4-1) showing a linear relationship between the two values.

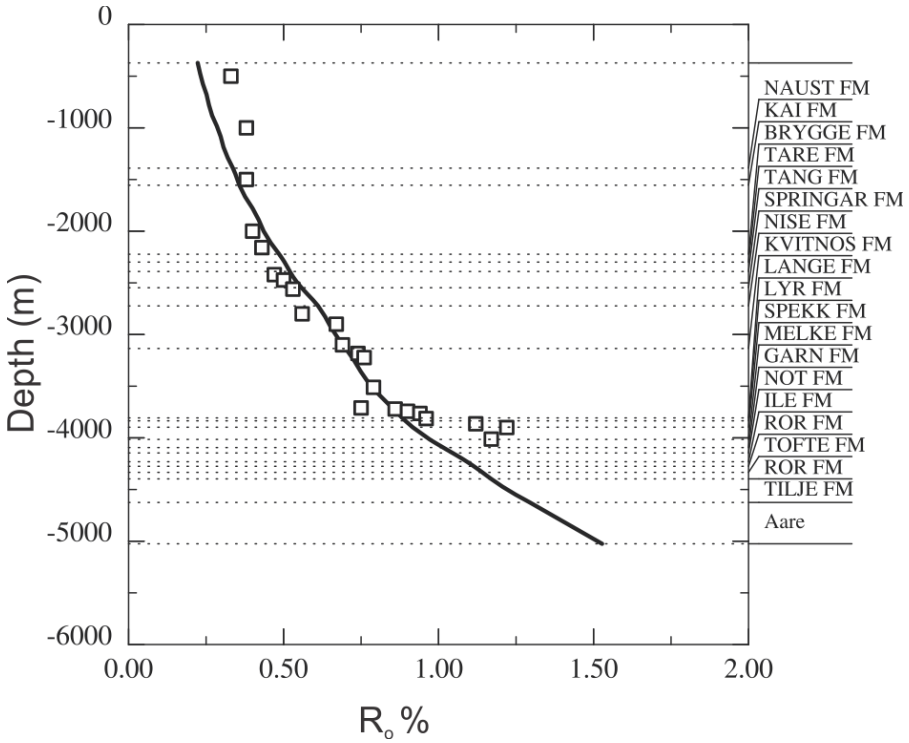

Figure 4: Cross-plot of the depth and Vitrinite reflectance (%) through the Midgard (6407/4-1) well, dots showing the measured VR (%) and line showing the modelled VR (%).

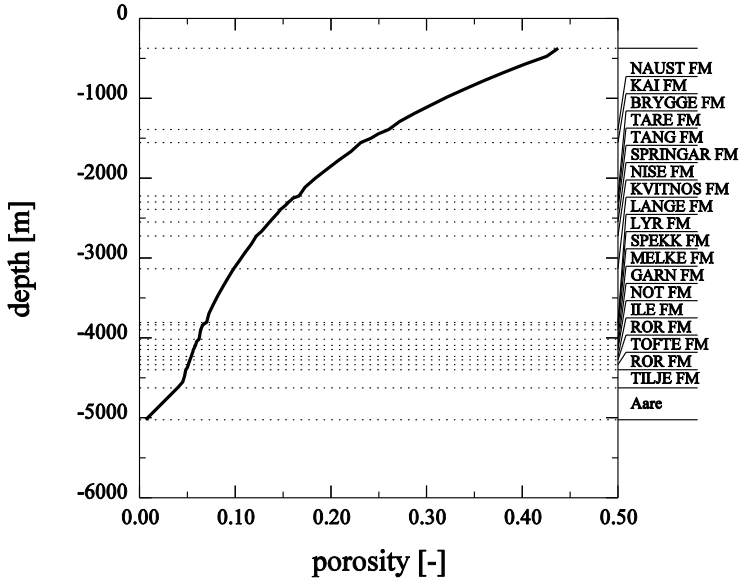

Figure 5: porosity versus depth cross-plot for the Midgard well (6407/4-1) showing decrease in porosity with depth. However, it is pertinent to note that decrease in porosity is a function of compaction, also above 80 C chemical compaction starts which disturbs the linear relationship of porosity lose with depth.

Åre Formation:

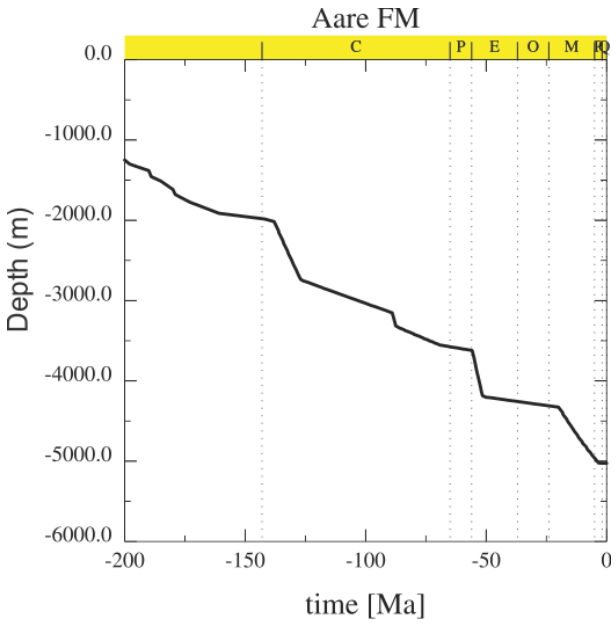

Figure 6: Time-Depth cross-plot for the Åre Formation showing burial depth of the formation at different time intervals. Note the sudden drops in the burial curve (shown in circles) at ca. -150 Ma, -90 Ma, -55 Ma and -20 Ma representing major tectonic subsidence at these times.

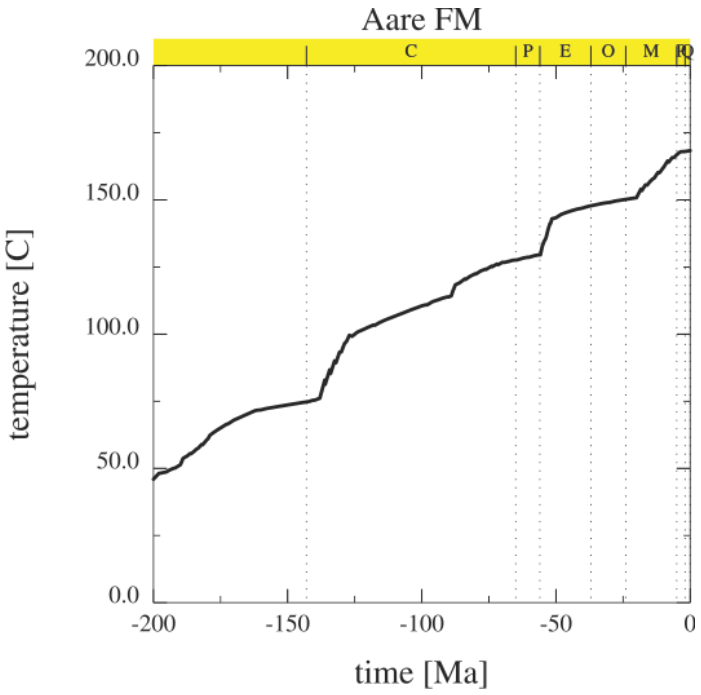

Figure 7: Time-Temperature cross-plot for the Åre Formation showing temperature of the formation at different time intervals. A general increase in temperature with time is evident with abrupt rises at ca. -145 Ma, -90 Ma, -55 Ma and -20 M.Y. Following Hunt (1996) Åre Formation remained in oil window between at ca. -170 Ma & -10 Ma and is currently in gas window.

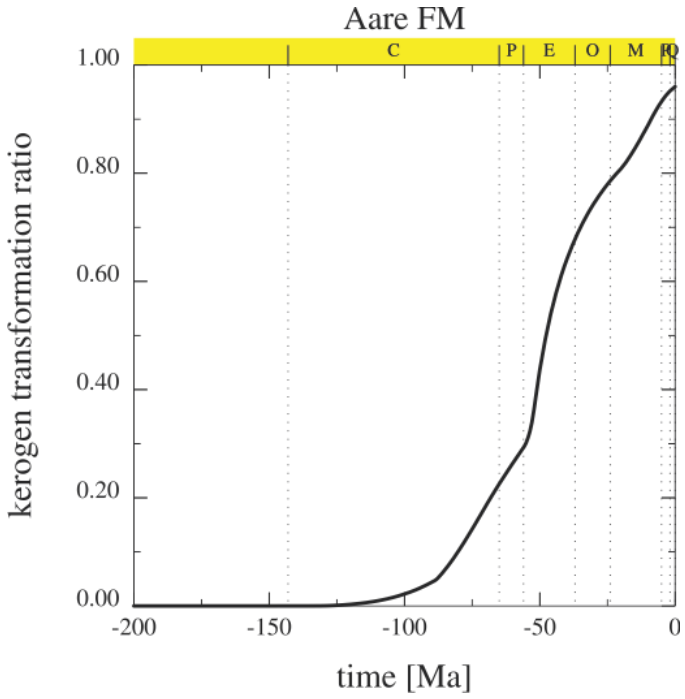

Figure 8: Time-Kerogen transformation cross-plot of the Åre Formation showing start of bulk kerogen transformation at ca. -120 M.Y. while peak transformation can be placed at ca. -50 M.Y. Presently however, less than 5% of the bulk kerogen is shown to be left within the Åre Formation as per modelling results.

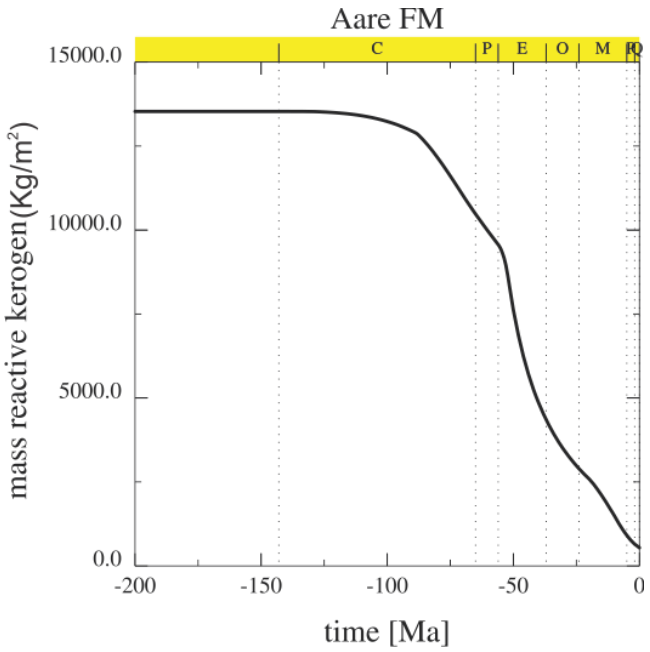

Figure 9: Time-Mass reactive kerogen cross-plot showing decrease in mass reactive kerogen with time at ca. -125 Ma transformation of reactive kerogen is evident while peak transformation can be placed at ca. -50 M.Y. Presently however, less than 10% of the reactive kerogen is shown to be left within the Åre Formation as per modelling results.

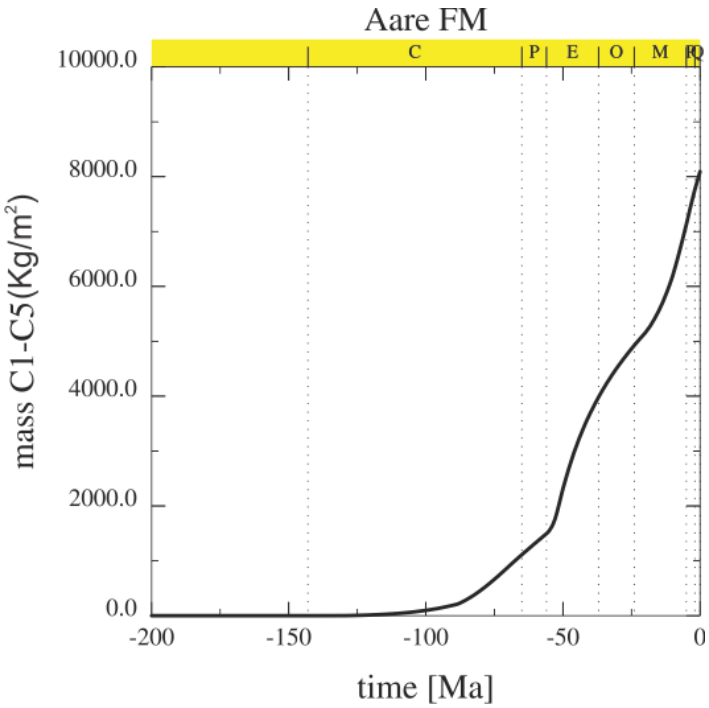

Figure 10: Time-Light HCs (gas) cross-plot showing start of generation at ca. -110 M.Y. Similarly, timing of peak generation can be placed at ca. -50 Ma, shown by the steep curve at this time after which the slope angle gradually decrease showing decline after the peak period.

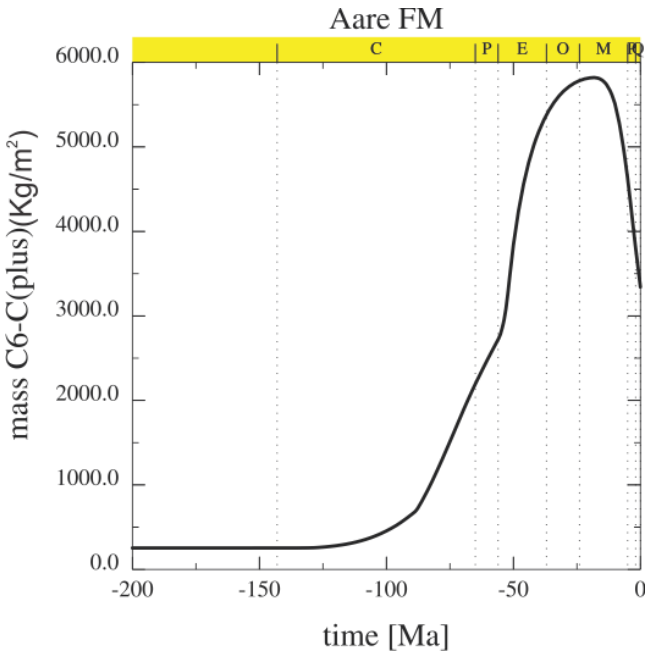

Figure 11: Time- HCs (oil) cross-plot showing start of generation at ca. -125 M.Y. Similarly, timing of peak generation can be placed at ca. -50 Ma, shown by the steep curve at this time after which curve flattens at the top between ca. -40 Ma and -20 Ma after which a clear decline in oil generation is observed.

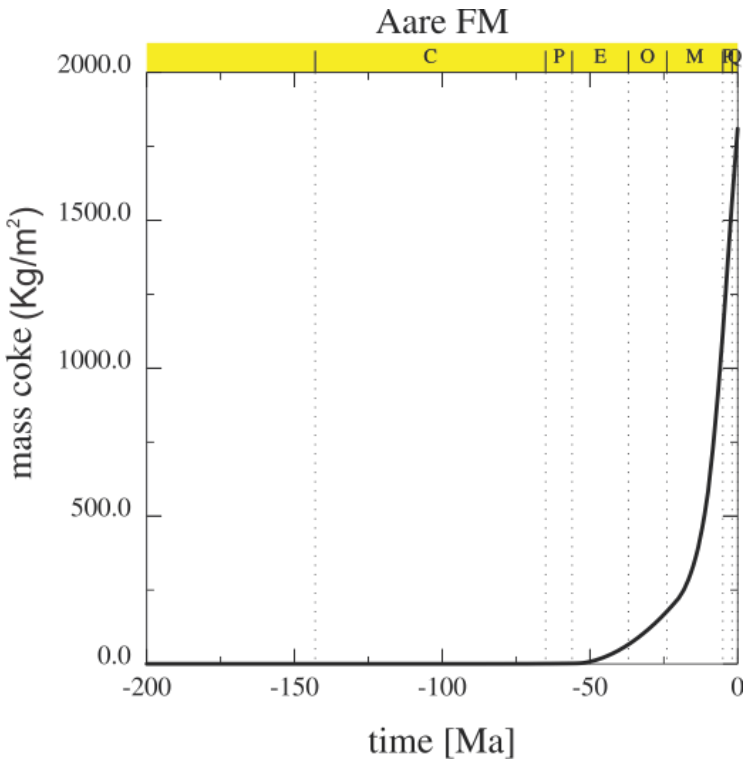

Figure 12: Time- Mass coke cross-plot showing start of coke generation at ca. -50 and increases forward in time. An abrupt increase in the coke formation between -20 Ma -0 Ma can be noticed period.

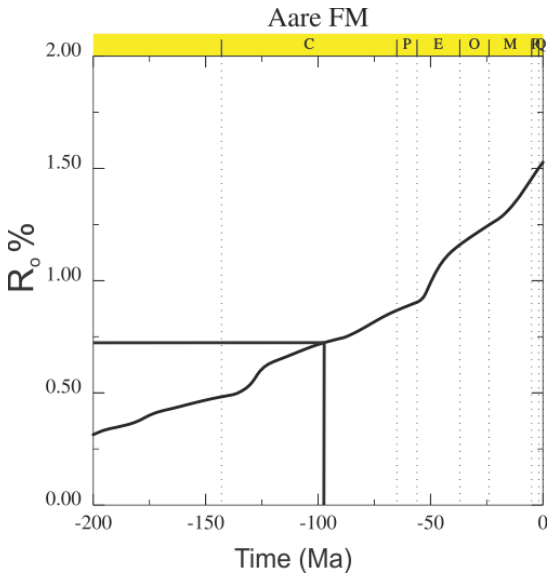

Figure 13: Time- Vitrinite reflectance cross-plot showing start of early oil generation at ca. -105 and peak oil generation is observed at -75 Ma and increases forward in time. An abrupt increase in the coke formation between -20 Ma -0 Ma can be noticed period. As mentioned in the table 5.1, peak oil generation has been taken place ca. 45 Ma ago and Åre Formation is still in gas window as maturity parameters discussed in Dembicki, 2009.

Melke Formation:

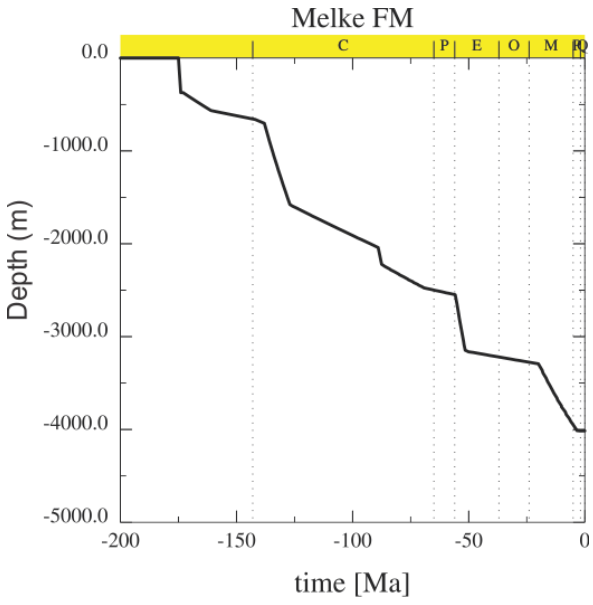

Figure 14: Time-Depth cross-plot for the Melke Formation showing burial depth of the formation at different time intervals. Note the sudden drops in the burial curve (shown in circles) at ca. -145 Ma, -90 Ma, -55 Ma and -20 Ma representing major tectonic subsidence at these times.

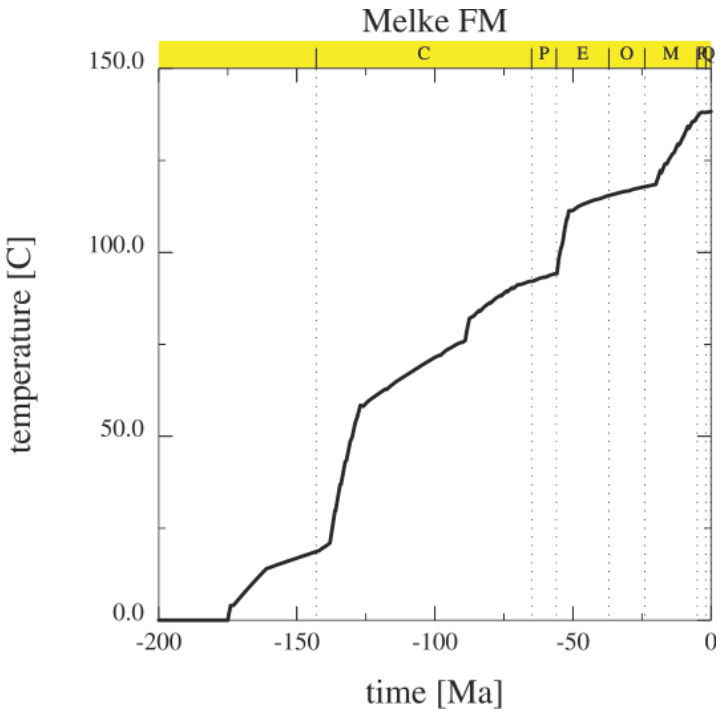

Figure 15: Time-Temperature cross-plot for the Melke Formation showing temperature of the formation at different time intervals. A general increase in temperature with time is evident with abrupt rises at ca. -145 Ma, -90 Ma, -55 Ma and -20 M.Y.

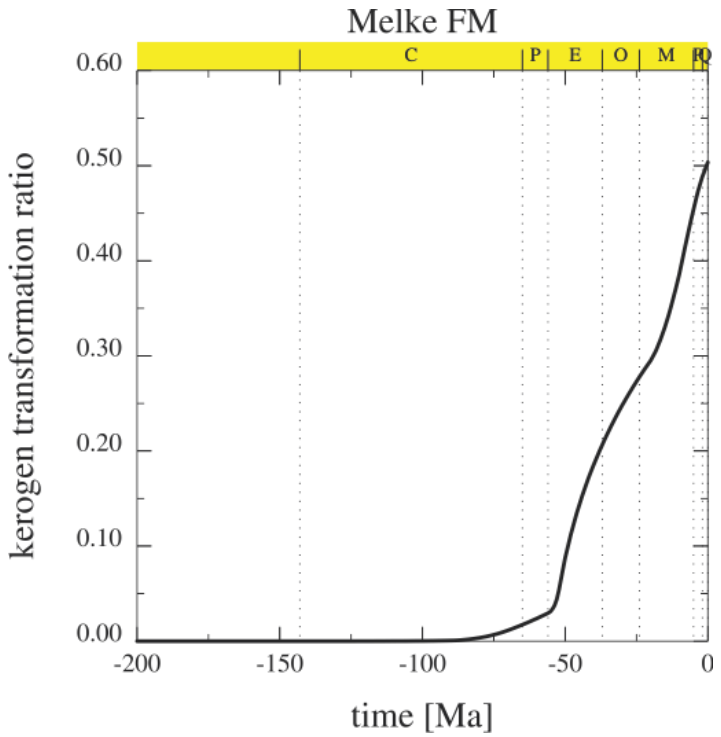

Figure 16: Time-Kerogen transformation cross-plot of the Melke Formation showing start of bulk kerogen transformation at ca. -120 M.Y. while peak transformation can be placed at ca. -50 M.Y.

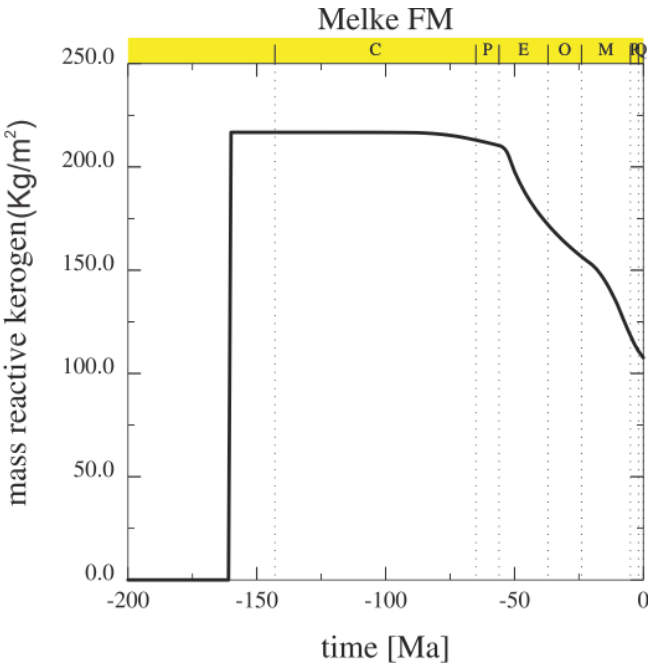

Figure 17: Time-Mass reactive kerogen cross-plot showing decrease in mass reactive kerogen with time at ca. -70 Ma transformation of reactive kerogen is evident while peak transformation can be placed at ca. -50 M.Y.

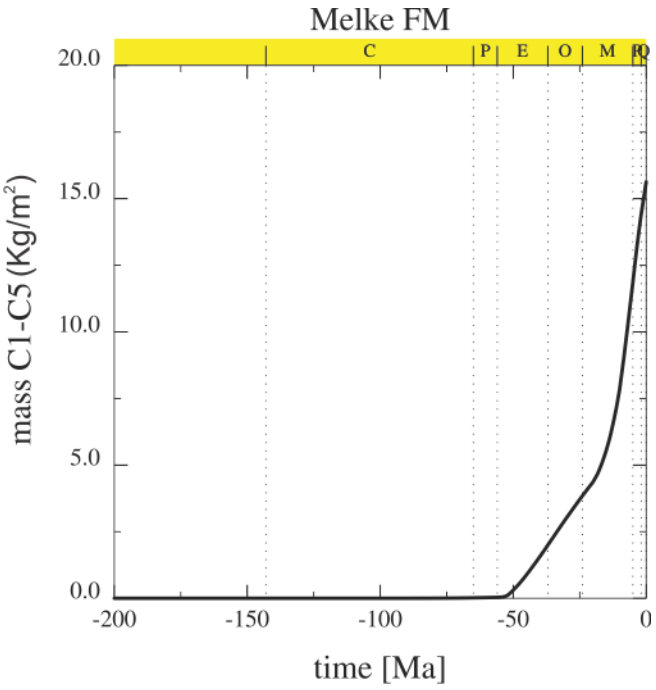

Figure 18: Time-Light HCs (gas) cross-plot showing start of generation at ca. -55 M.Y. Similarly, timing of peak generation can be placed at ca. -20 Ma, shown by the steep curve at this time after which the slope angle gradually decrease showing decline after the peak period.

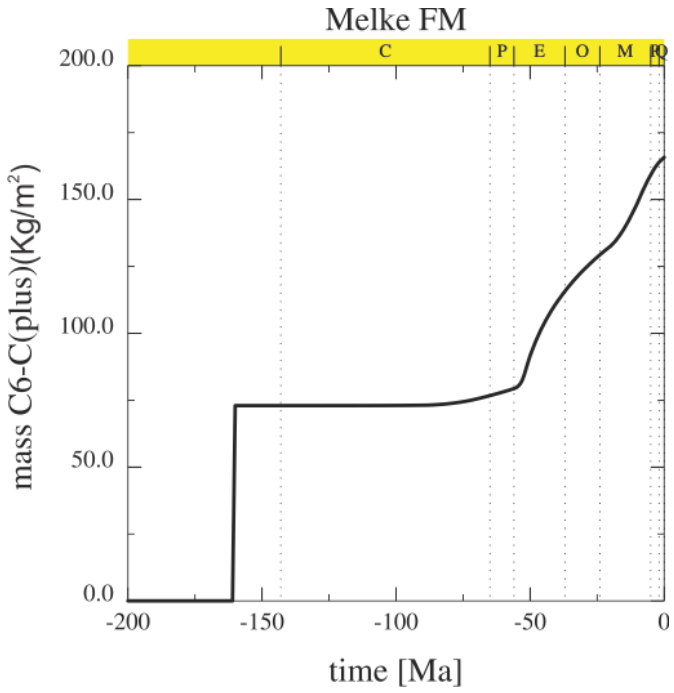

Figure 19: Time- HCs (oil) cross-plot showing start of generation at ca. -55 M.Y. Similarly, timing of peak generation can be placed at ca. -25 M.Y.

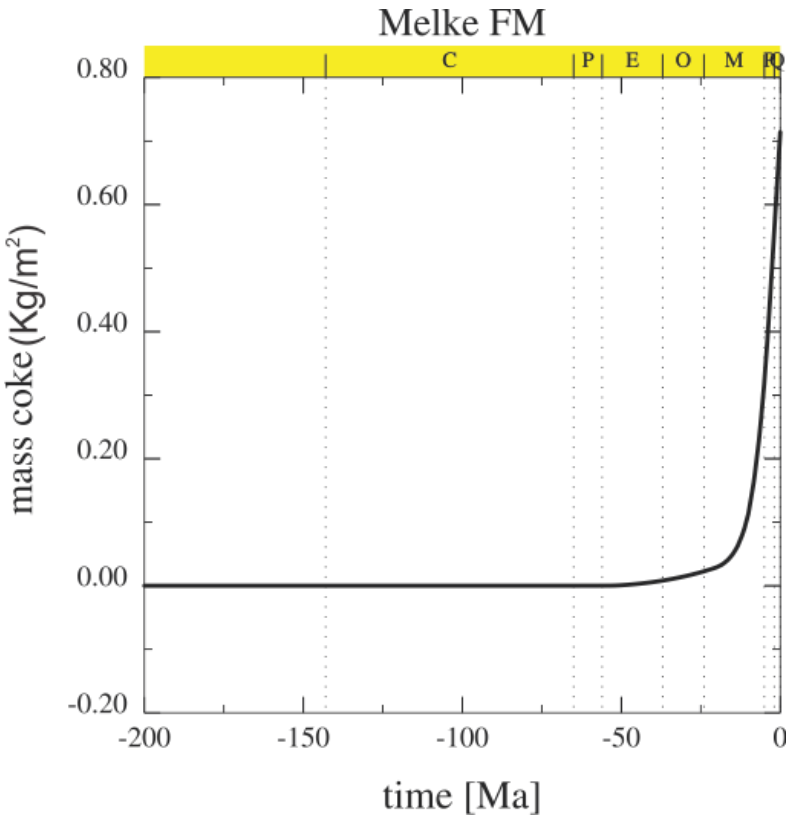

Figure 20: Time- Mass coke cross-plot showing start of coke generation at ca. -25 and increases forward in time. An abrupt increase in the coke formation between -20 Ma -0 Ma can be noticed period.

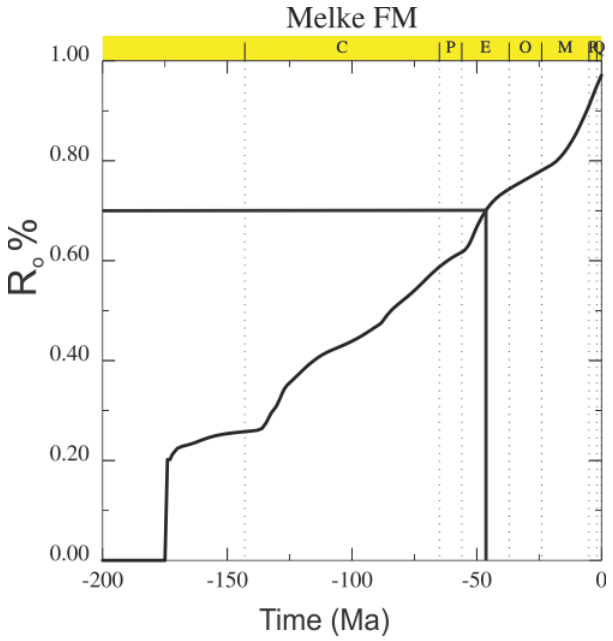

Figure 21: Time- Vitrinite reflectance cross-plot showing start of early oil generation at ca. -105 and peak oil generation is observed at -75 Ma and increases forward in time. An abrupt increase in the coke formation between -20 Ma -0 Ma can be noticed period. As discussed in the table 5.1, peak oil generation has been taken place recently and the Melke Formation is still in oil window.

Spekk Formation:

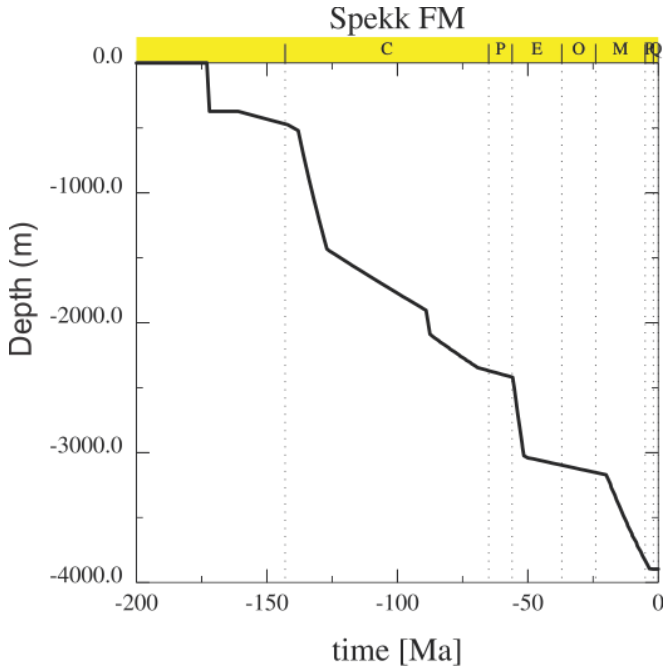

Figure 22: Time-Depth cross-plot for the Spekk Formation showing burial depth of the formation at different time intervals. Note the sudden drops in the burial curve at ca. -145 Ma, -90 Ma, -55 Ma and -20 Ma representing major tectonic subsidence at these times.

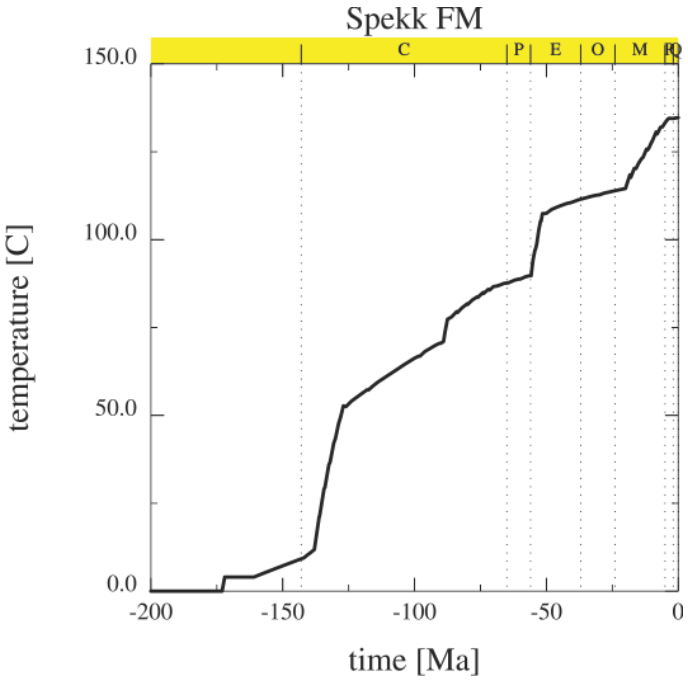

Figure 23: Time-Temperature cross-plot for the Spekk Formation showing temperature of the formation at different time intervals. A general increase in temperature with time is evident with abrupt rises at ca. -145 Ma, -90 Ma, -55 Ma and -20 M.Y.

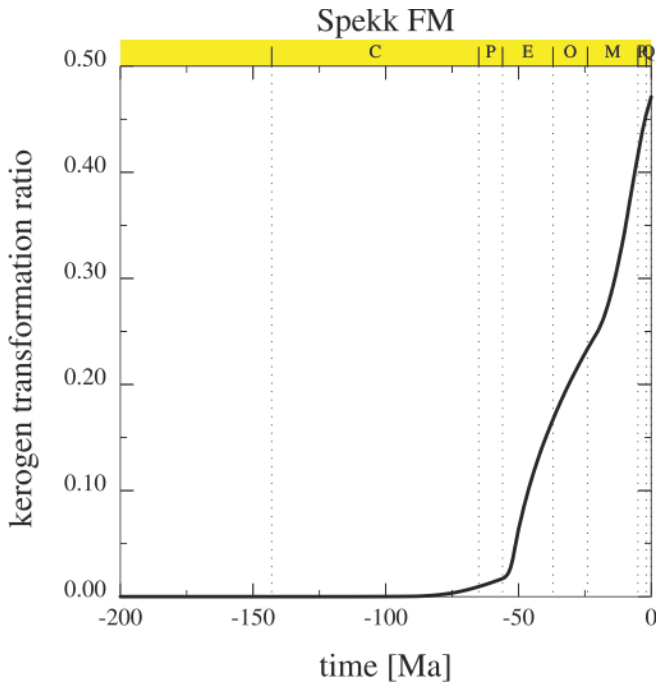

Figure 24: Time-Kerogen transformation cross-plot of the SpekkFormation showing start of bulk kerogen transformation at ca. -75 M.Y. while peak transformation can be placed at ca. -50 M.Y.

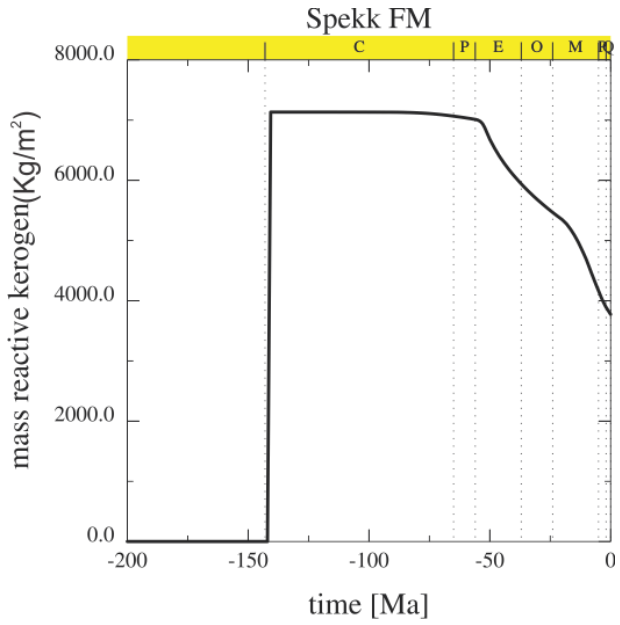

Figure 25: Time-Mass reactive kerogen cross-plot showing decrease in mass reactive kerogen with time at ca. -60 Ma transformation of reactive kerogen is evident while peak transformation can be placed at ca. -50 M.Y.

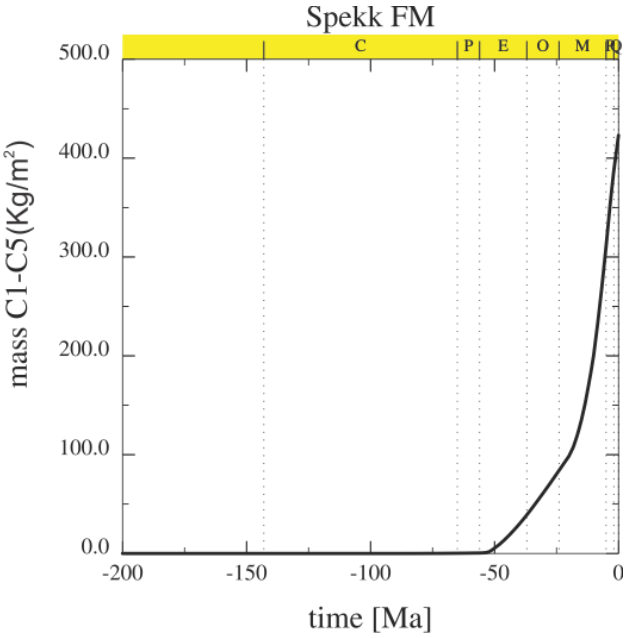

Figure 26: Time-Light HCs (gas) cross-plot showing start of generation at ca. -50 M.Y. Similarly, timing of peak generation can be placed at ca. -20 Ma, shown by the steep curve at this time after which the slope angle gradually decrease showing decline after the peak period.

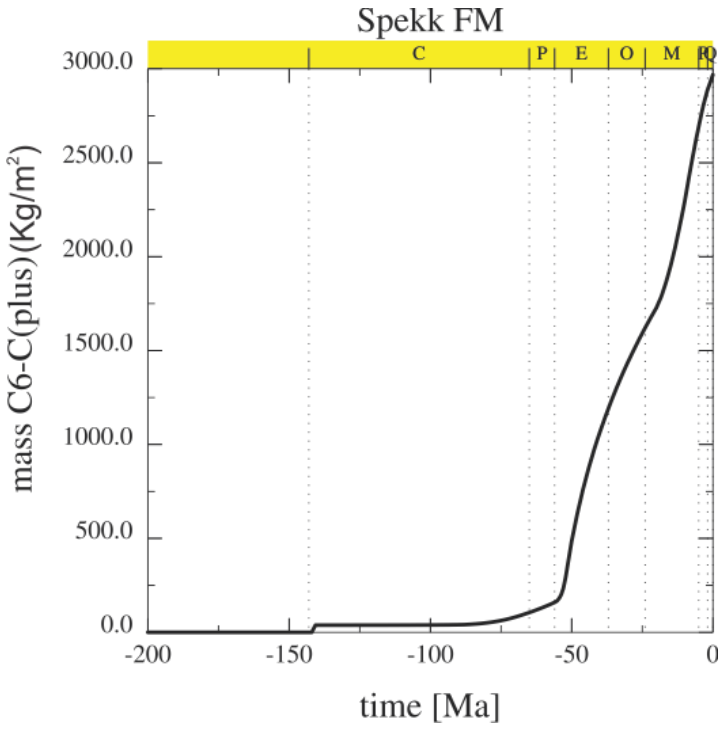

Figure 27: Time- HCs (oil) cross-plot showing start of generation at ca. -75 M.Y. Similarly, timing of peak generation can be placed at ca. -20 M.Y.

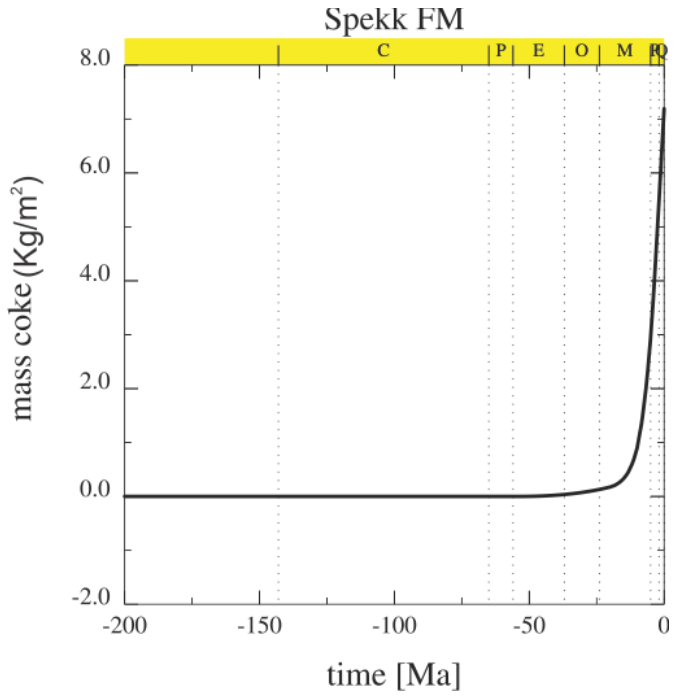

Figure 28: Time- Mass coke cross-plot showing start of coke generation at ca. -25 and increases forward in time. An abrupt increase in the coke formation between -20 Ma -0 Ma can be noticed period.

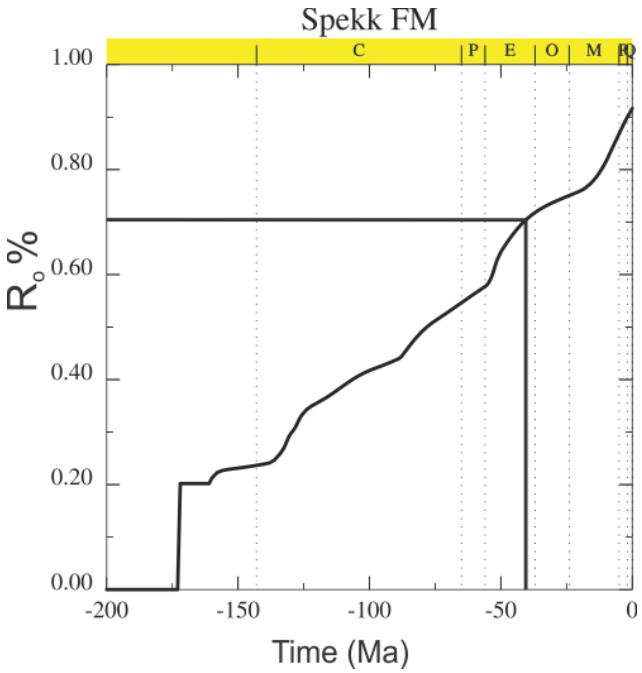

Figure 29: Time- Vitrinite reflectance cross-plot showing start of early oil generation at ca. -105 and peak oil generation is observed at -75 Ma and increases forward in time. An abrupt increase in the coke formation between -20 Ma -0 Ma can be noticed period. As mentioned in the table 5.1, peak oil generation has been taken place recently and the Spekk Formation is still in oil window.

Smørbukk (6506/12-9S)

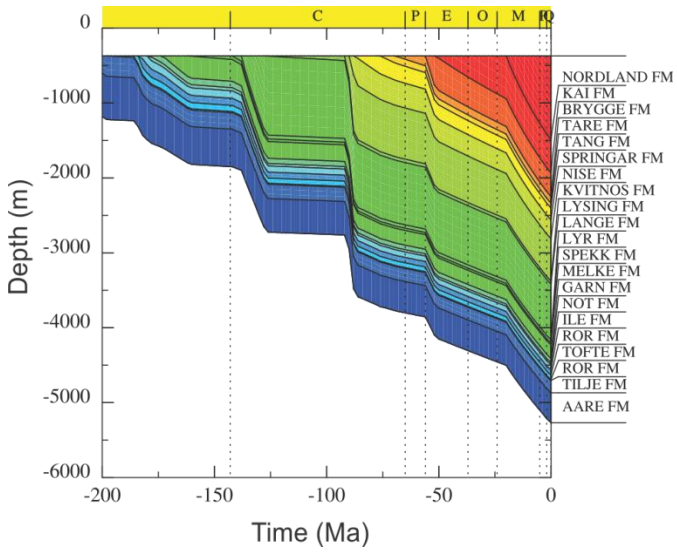

Figure 30: Burial reconstruction through time and depth for the Smørbukk (6506/12-9S) well which displays a relatively gradual burial trend, data used forCase-3 (by using Tissot / Espitallie kinetic model).

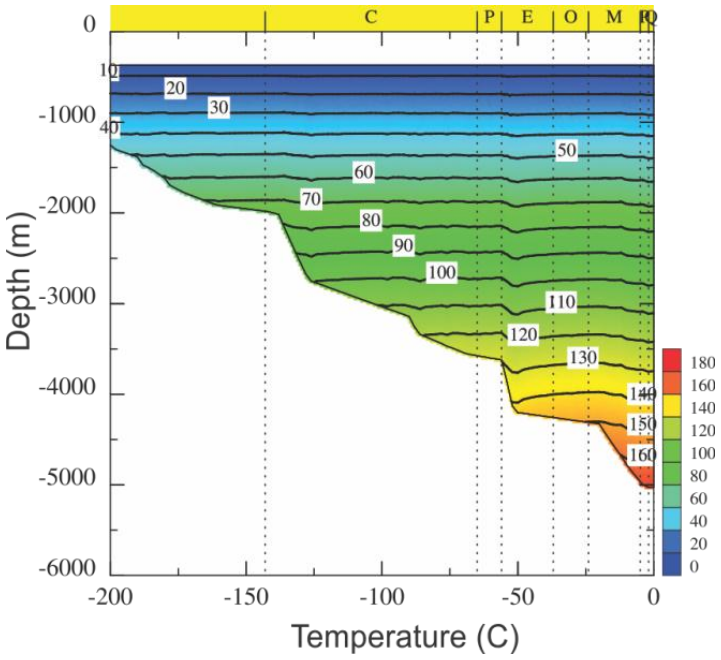

Figure 31: Temperature reconstruction through time and depth for the Smørbukk (6506/12-9S) well forCase-3.

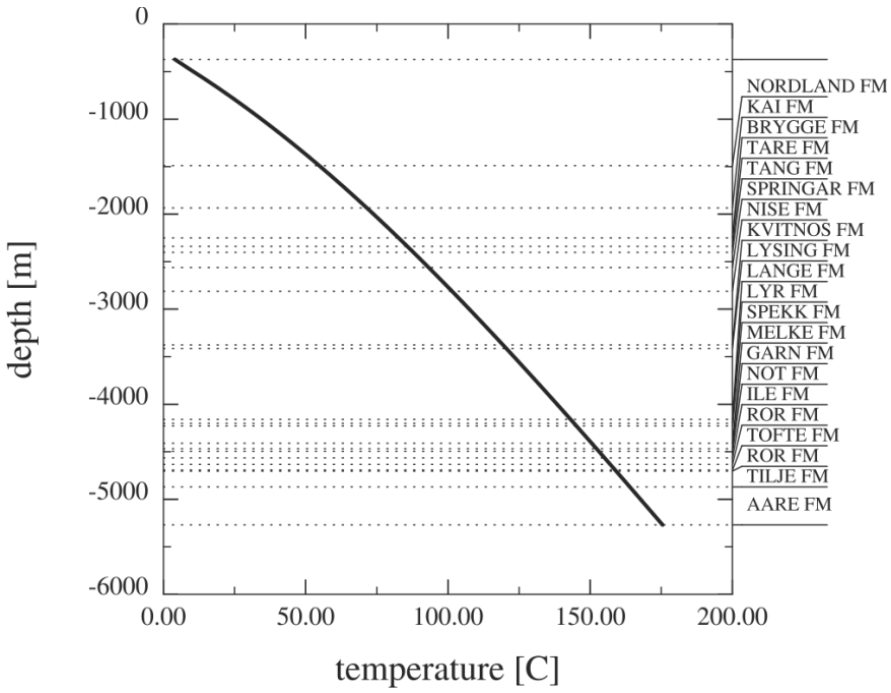

Figure 32: Temperature depth cross-plot for the Smørbukk (6506/12-9S) showing a linear relationship between the two values.

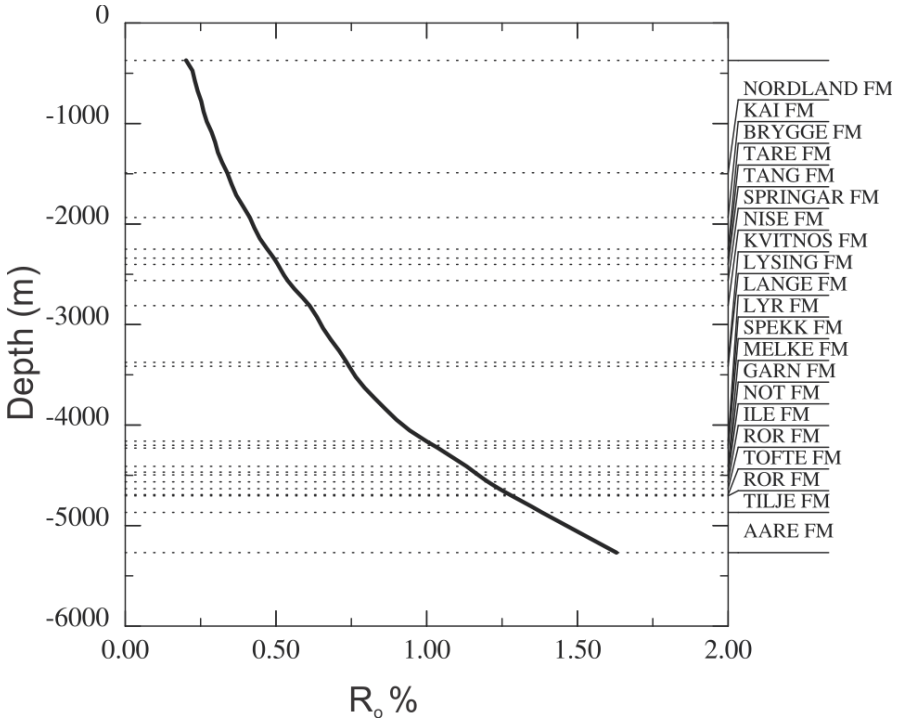

Figure 33: Plot of measured vitrinite reflectance against depth for the Smørbukk (6506/12-9S) well of modelled vitrinite reflectance against depth for the same well (using BAS software).

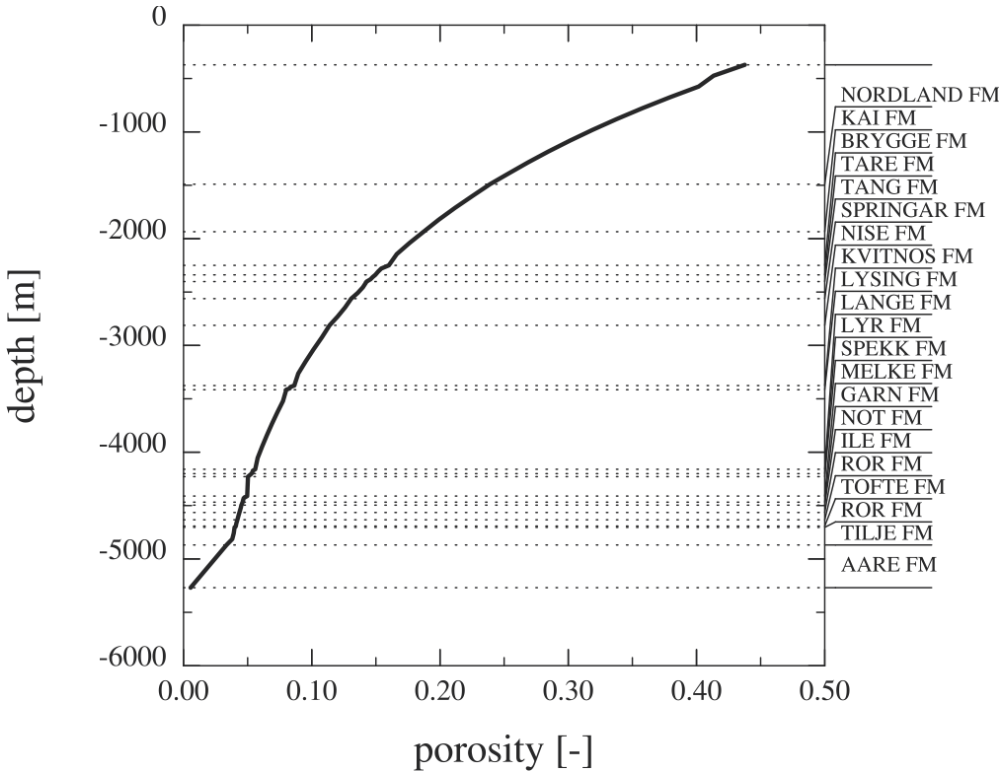

Figure 34: porosity versus depth cross-plot for the Smørbukk (6506/12-9S) showing decrease in porosity with depth. However, it is pertinent to note that decrease in porosity is a function of compaction, also above 80 C chemical compaction starts which disturbs the linear relationship of porosity lose with depth

Åre Formation:

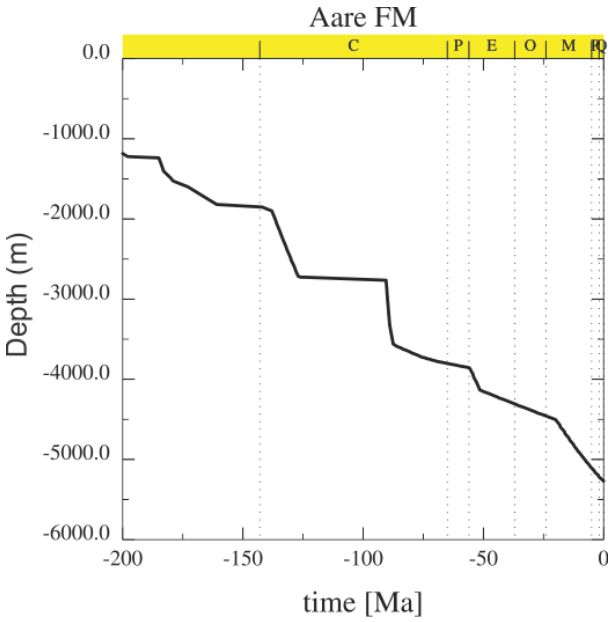

Figure 35: Time-Depth cross-plot for the Åre Formation showing burial depth of the formation at different time intervals. Note the sudden drops in the burial curve at ca. -145 Ma, -90 Ma, -55 Ma and -20 Ma representing major tectonic subsidence at these times.

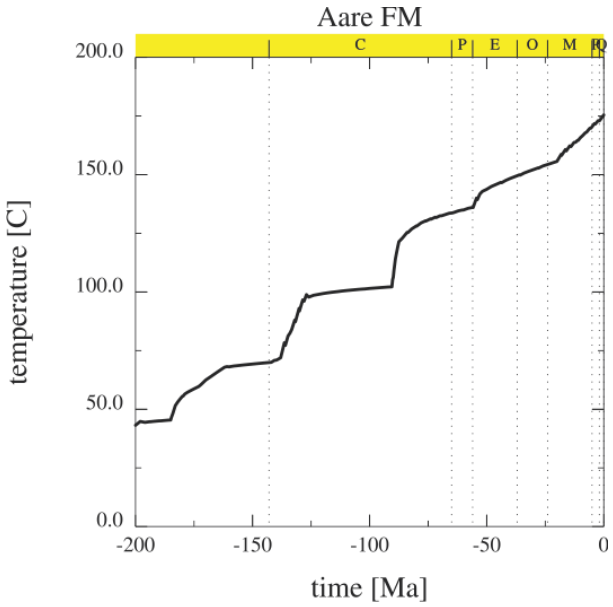

Figure 36: Time-Temperature cross-plot for the Åre Formation showing temperature of the formation at different time intervals. A general increase in temperature with time is evident with abrupt rises at ca. -150 Ma, -90 Ma, -55 Ma and -20 M.Y. Following Hunt (1996) Åre Formation remained in oil window between at ca. -170 Ma & -10 Ma and is currently in gas window.

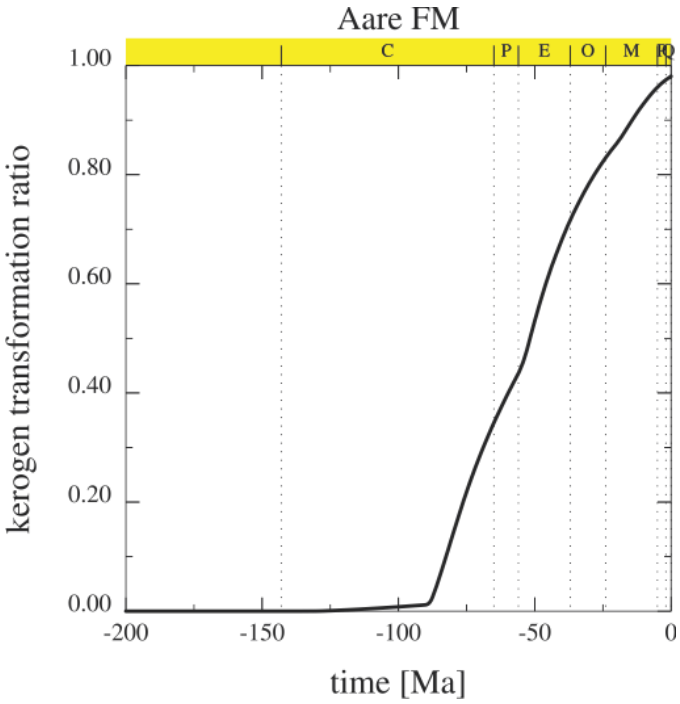

Figure 37: Time-Kerogen transformation cross-plot of the Åre Formation showing start of bulk kerogen transformation at ca. -110 M.Y. while peak transformation can be placed at ca. -50 M.Y. Presently however, less than 5% of the bulk kerogen is shown to be left within the Åre Formation as per modelling results.

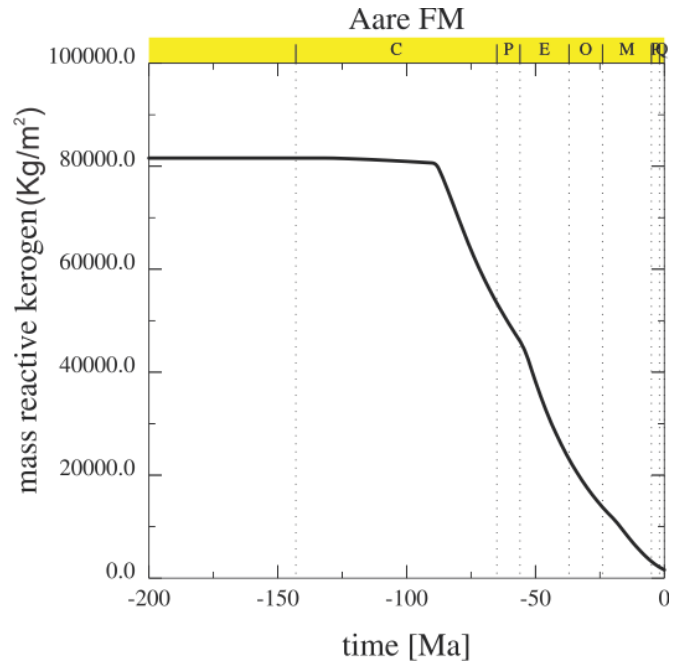

Figure 38: Time-Mass reactive kerogen cross-plot showing decrease in mass reactive kerogen with time at ca. -90 Ma transformation of reactive kerogen is evident while peak transformation can be placed at ca. -50 M.Y. Presently however, less than 10% of the reactive kerogen is shown to be left within the Åre Formation as per modelling results.

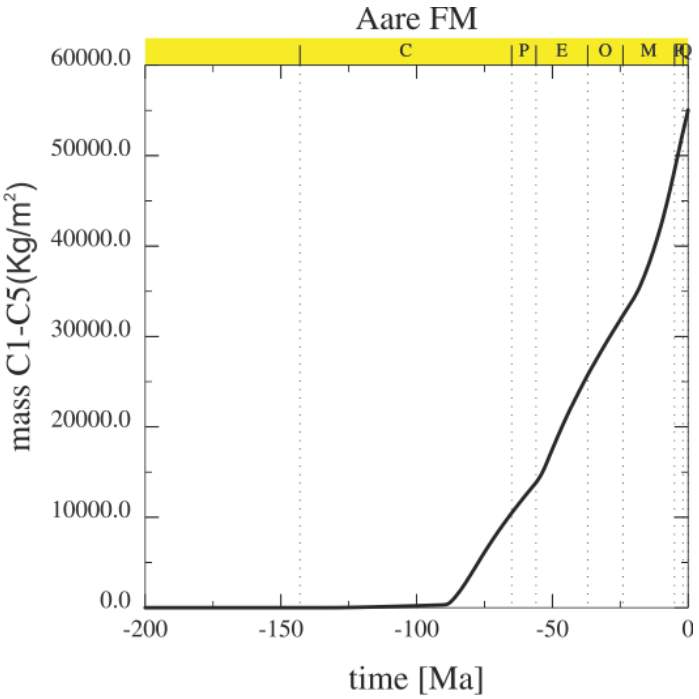

Figure 39: Time-Light HCs (gas) cross-plot showing start of generation at ca. -85 M.Y. Similarly, timing of peak generation can be placed at ca. -50 Ma, shown by the steep curve at this time after which the slope angle gradually decrease showing decline after the peak period.

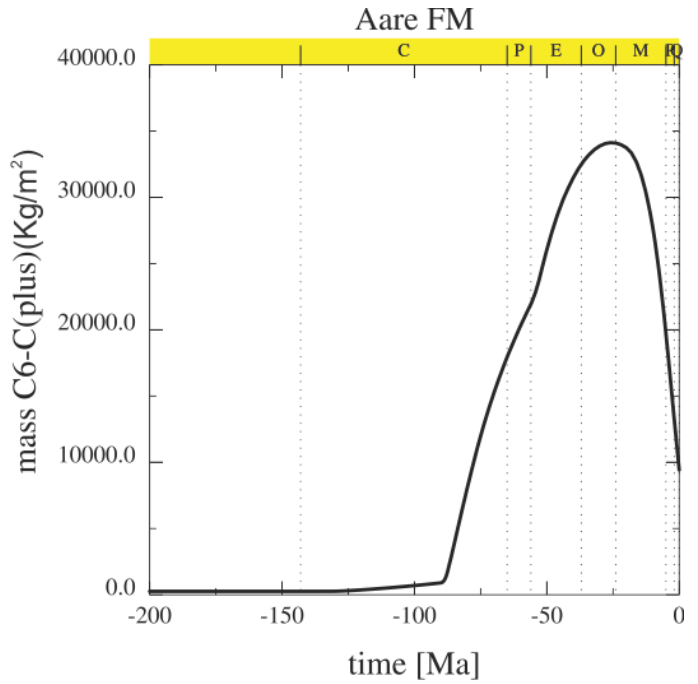

Figure 40: Time- HCs (oil) cross-plot showing start of generation at ca. -125 M.Y. Similarly, timing of peak generation can be placed at ca. -50 Ma, shown by the steep curve at this time after which curve flattens at the top between ca. -40 Ma and -20 Ma after which a clear decline in oil generation is observed.

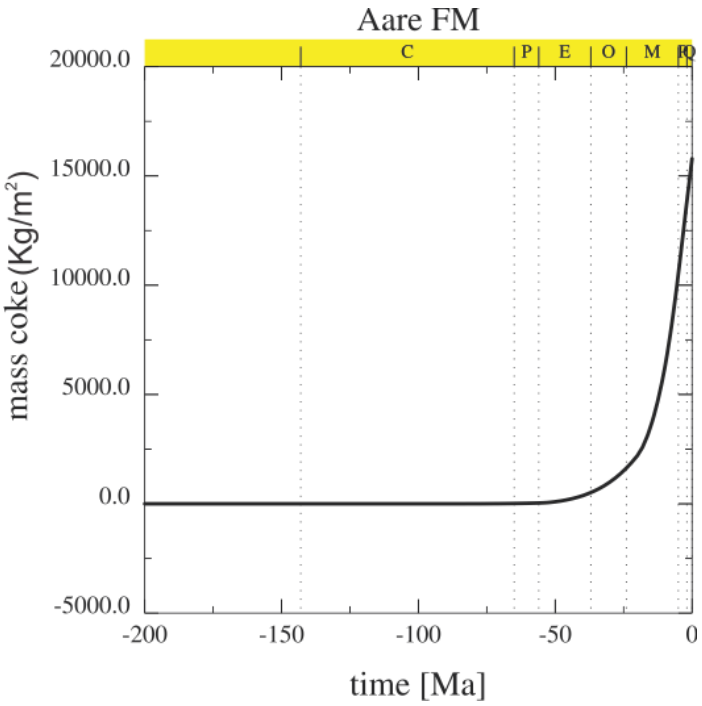

Figure 41: Time- Mass coke cross-plot showing start of coke generation at ca. -50 and increases forward in time. An abrupt increase in the coke formation between -20 Ma -0 Ma can be noticed period.

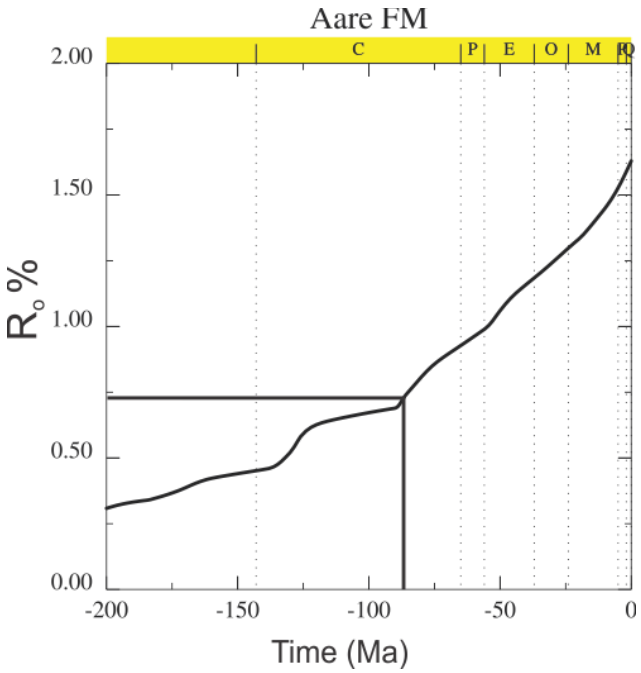

Figure 42: Time- Vitrinite reflectance cross-plot showing start of early oil generation at ca. -105 and peak oil generation is observed at -75 Ma and increases forward in time. An abrupt increase in the coke formation between -20 Ma -0 Ma can be noticed period. As mentioned in the table 5.1, peak oil generation is has been taken place ca. 55 Ma ago and Åre Formation is still in gas window.

Melke Formation:

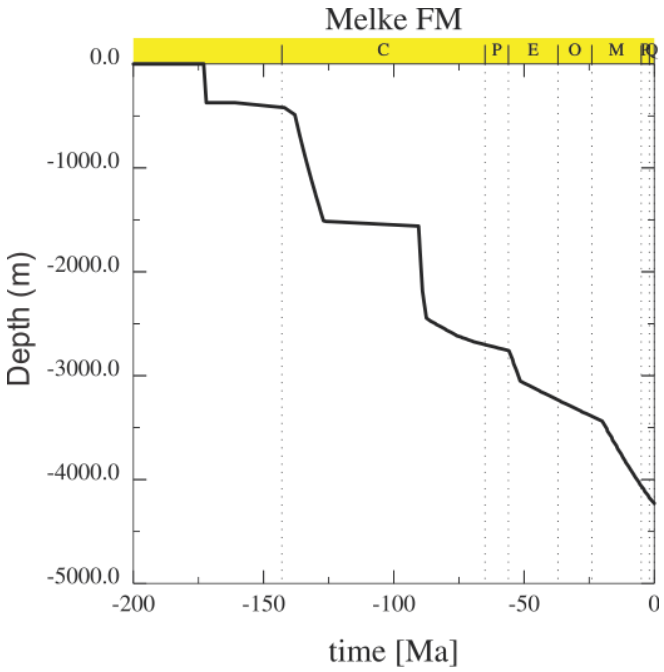

Figure 43: Time-Depth cross-plot for the Melke Formation showing burial depth of the formation at different time intervals. Note the sudden drops in the burial curve at ca. -145 Ma, -90 Ma, -55 Ma and -20 Ma representing major tectonic subsidence at these times.

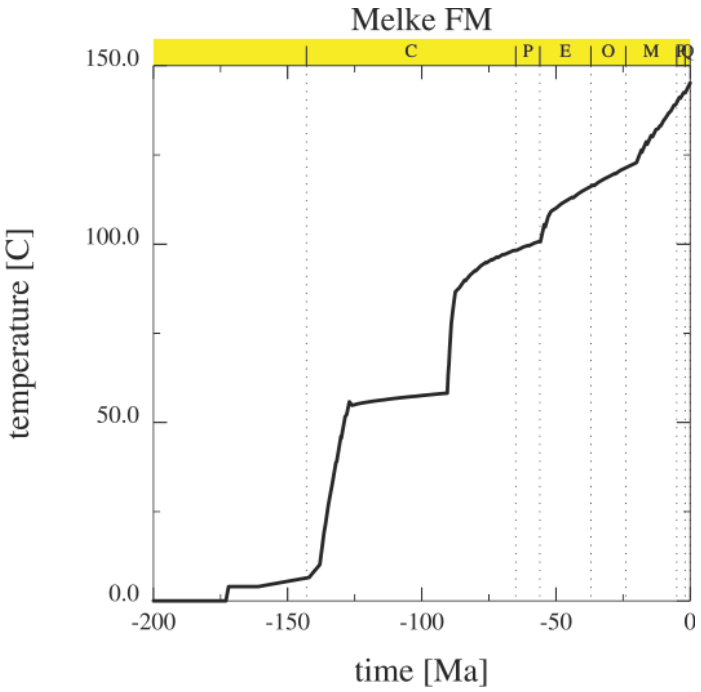

Figure 44: Time-Temperature cross-plot for the Melke Formation showing temperature of the formation at different time intervals. A general increase in temperature with time is evident with abrupt rises at ca. -145 Ma, -90 Ma, -55 Ma and -20 M.Y.

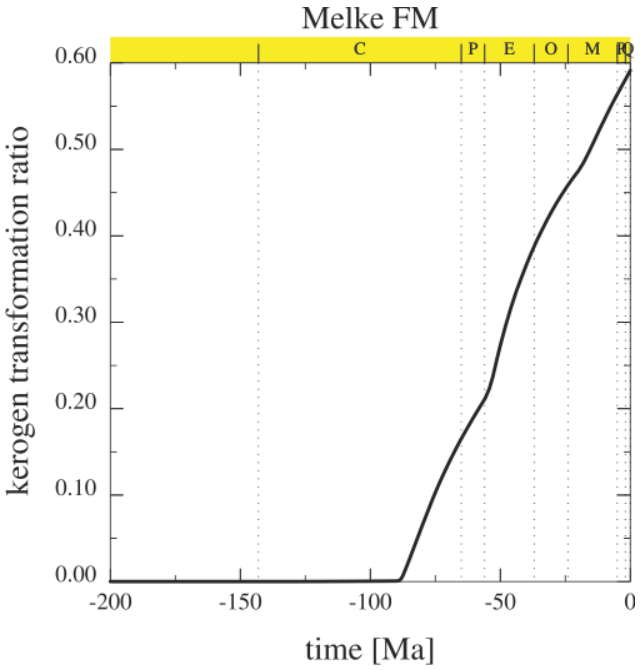

Figure 45: Time-Kerogen transformation cross-plot of the Melke Formation showing start of bulk kerogen transformation at ca. -80 M.Y. while peak transformation can be placed at ca. -50 M.Y.

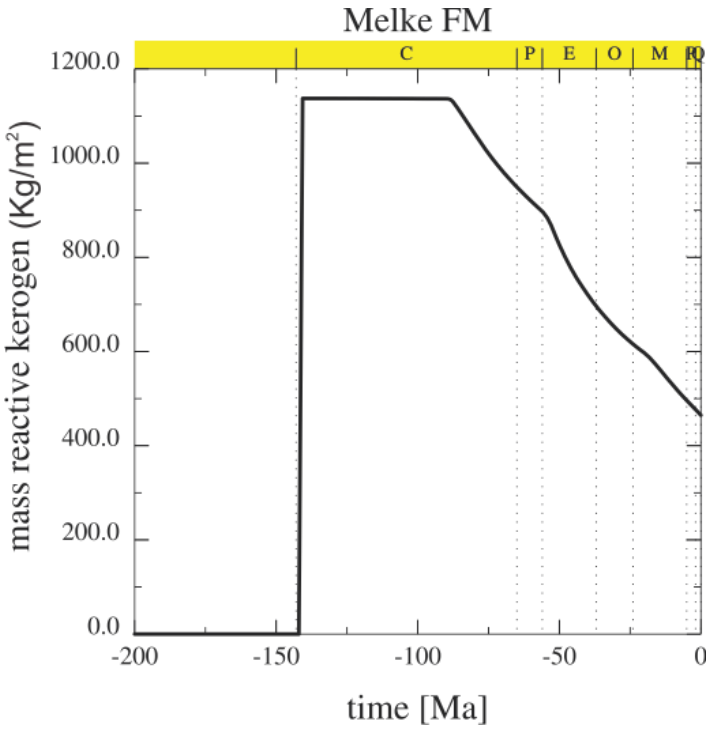

Figure 46: Time-Mass reactive kerogen cross-plot showing decrease in mass reactive kerogen with time at ca. -90 Ma transformation of reactive kerogen is evident while peak transformation can be placed at ca. -50 M.Y.

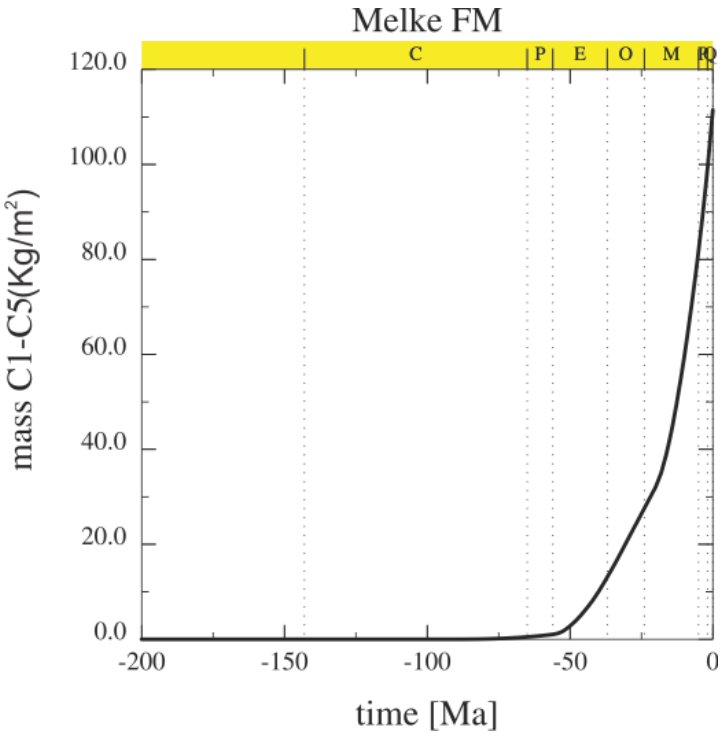

Figure 47: Time-Light HCs (gas) cross-plot showing start of generation at ca. -55 M.Y. Similarly, timing of peak generation can be placed at ca. -25 Ma, shown by the steep curve at this time after which the slope angle gradually decrease showing decline after the peak period.

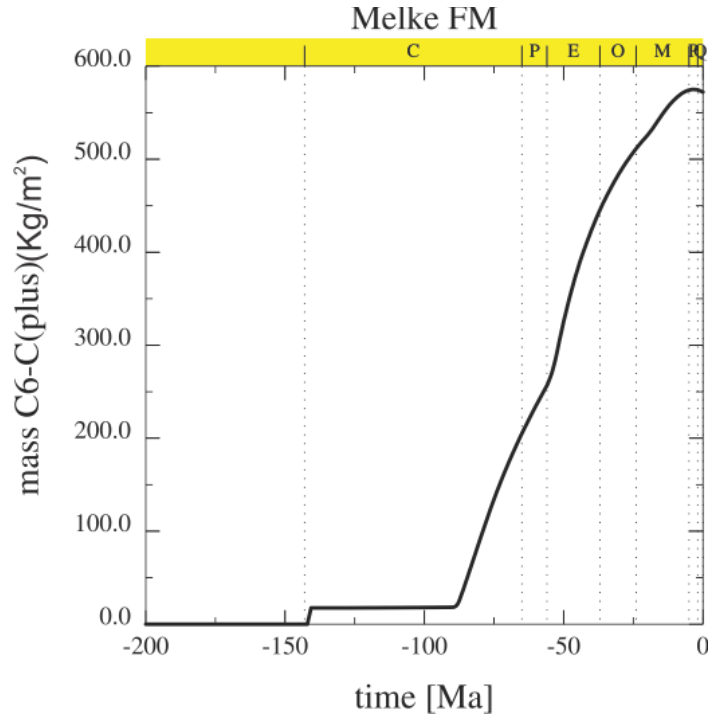

Figure 48: Time-Light HCs (gas) cross-plot showing start of generation at ca. -90 M.Y. Similarly, timing of peak generation can be placed at ca. -50 Ma, shown by the steep curve at this time after which the slope angle gradually decrease showing decline after the peak period.

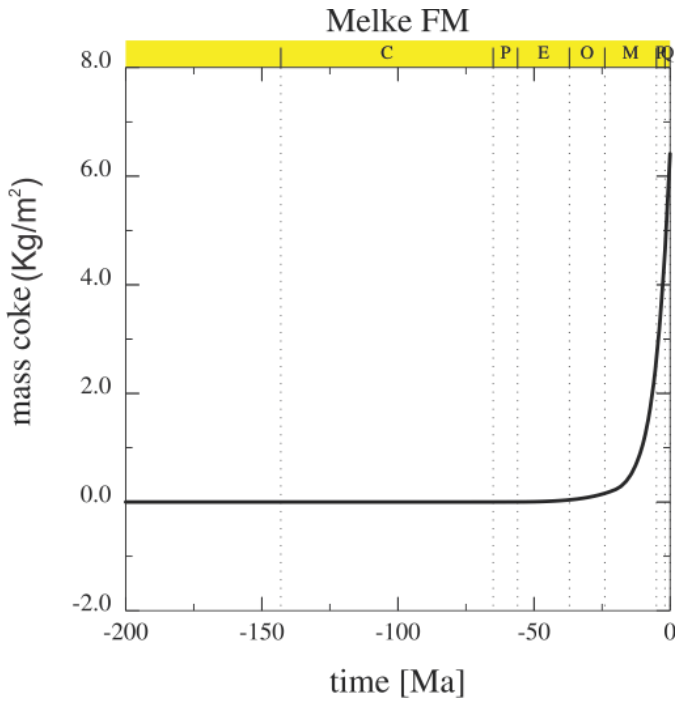

Figure 49: Time- Mass coke cross-plot showing start of coke generation at ca. -25 and increases forward in time. An abrupt increase in the coke formation between -20 Ma -0 Ma can be noticed period.

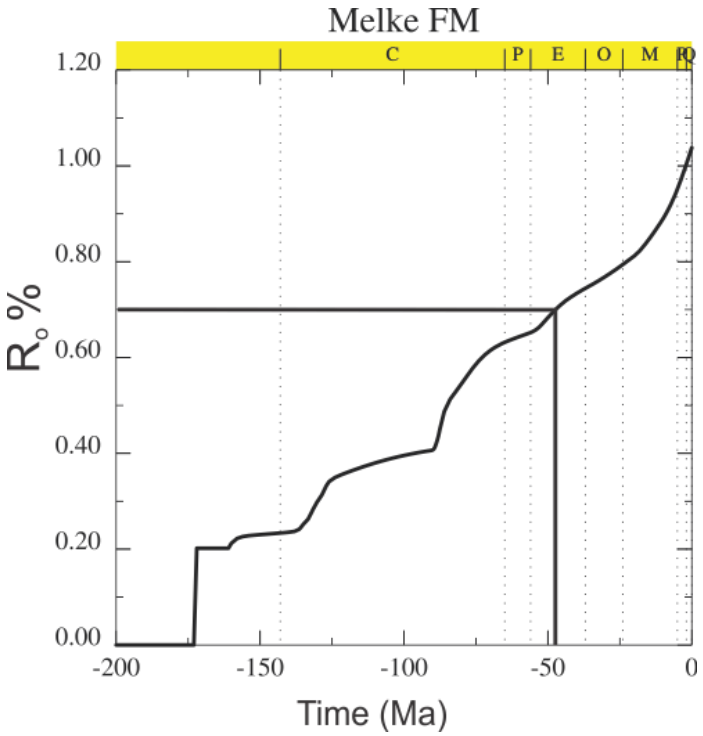

Figure 50: Time- Vitrinite reflectance cross-plot showing start of early oil generation at ca. -105 and peak oil generation is observed at -75 Ma and increases forward in time. An abrupt increase in the coke formation between -20 Ma -0 Ma can be noticed period. As mentioned in the table 5.1, peak oil generation has been taken place recently and the Melke Formation is still in oil window.

Spekk Formation:

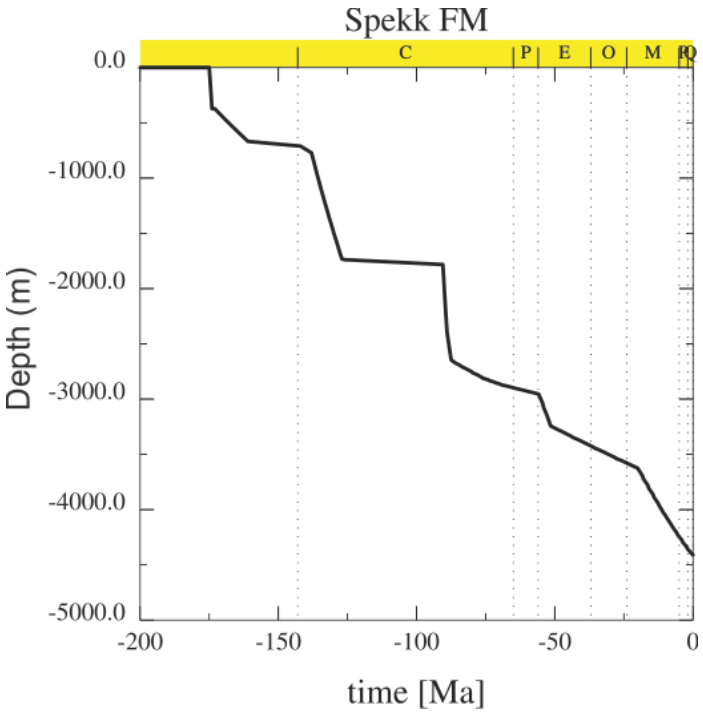

Figure 51: Time-Depth cross-plot for the SpekkFormation showing burial depth of the formation at different time intervals. Note the sudden drops in the burial curve at ca. -145 Ma, -90 Ma, -55 Ma and -20 Ma representing major tectonic subsidence at these times.

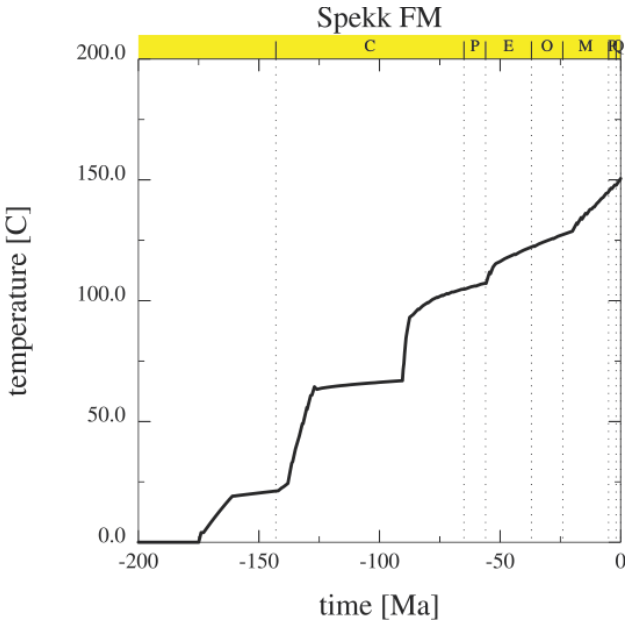

Figure 52: Time-Temperature cross-plot for the Spekk Formation showing temperature of the formation at different time intervals. A general increase in temperature with time is evident with abrupt rises at ca. -145 Ma, -90 Ma, -55 Ma and -20 M.Y.

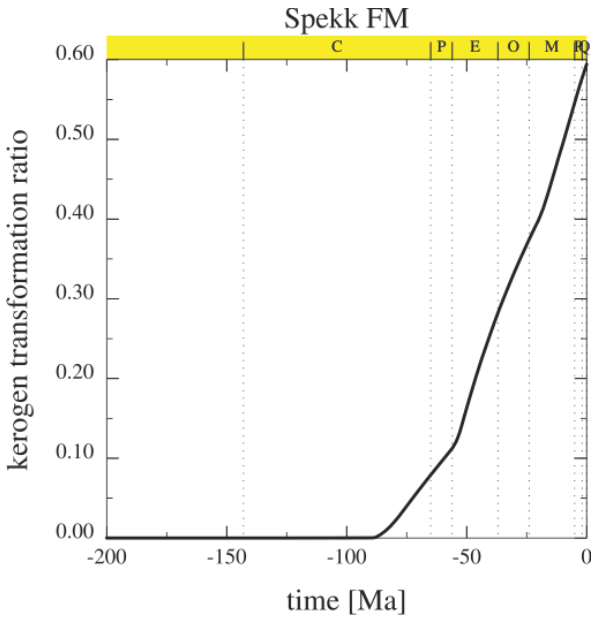

Figure 53: Time-Kerogen transformation cross-plot of the SpekkFormation showing start of bulk kerogen transformation at ca. -80 M.Y. while peak transformation can be placed at ca. -50 M.Y.

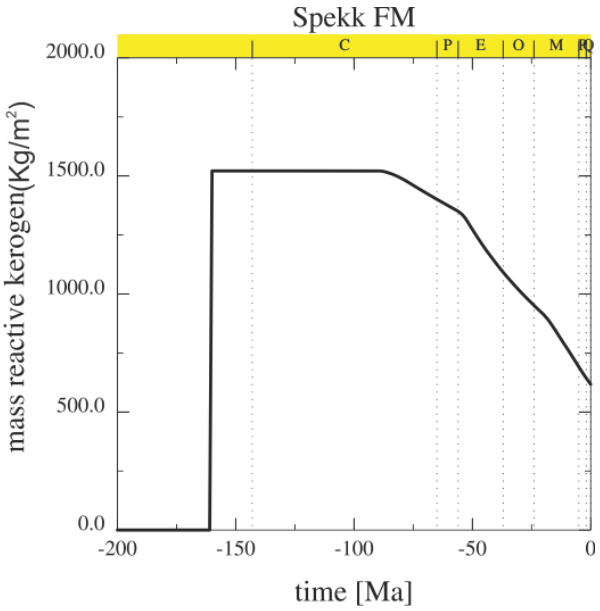

Figure 54: Time-Mass reactive kerogen cross-plot showing decrease in mass reactive kerogen with time at ca. -125 Ma transformation of reactive kerogen is evident while peak transformation can be placed at ca. -50 M.Y.

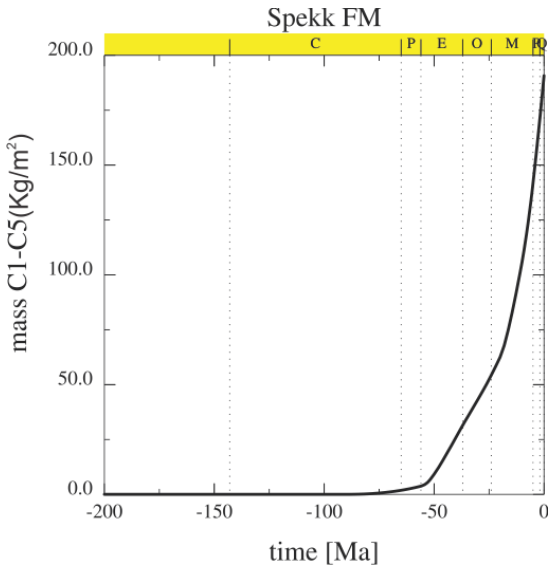

Figure 55: Time-Light HCs (gas) cross-plot showing start of generation at ca. -60 M.Y. Similarly, timing of peak generation can be placed at ca. -25 Ma, shown by the steep curve at this time after which the slope angle gradually decrease showing decline after the peak period.

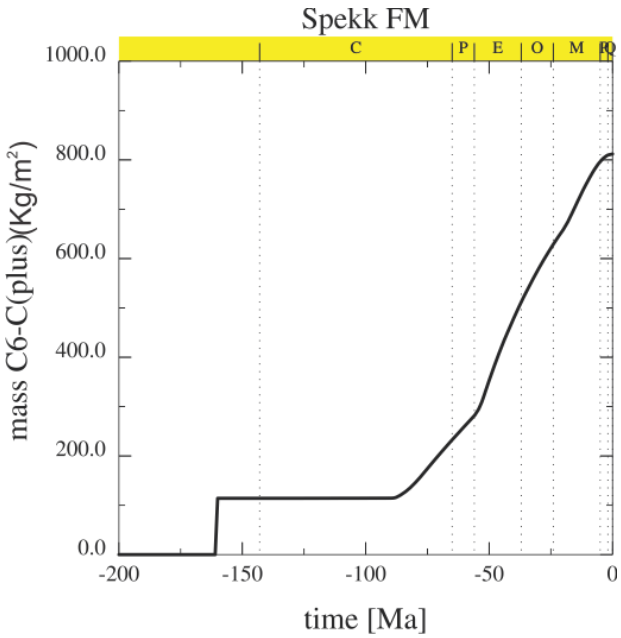

Figure 56: Time- HCs (oil) cross-plot showing start of generation at ca. -90 M.Y. Similarly, timing of peak generation can be placed at ca. -50 M.Y.

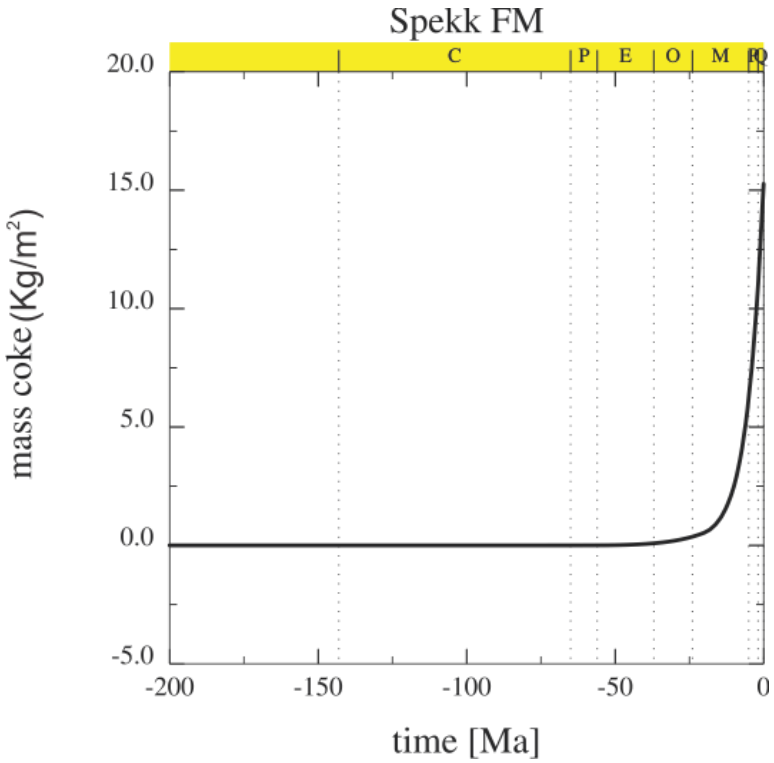

Figure 57: Time- Mass coke cross-plot showing start of coke generation at ca. -25 and increases forward in time. An abrupt increase in the coke formation between -20 Ma -0 Ma can be noticed period.

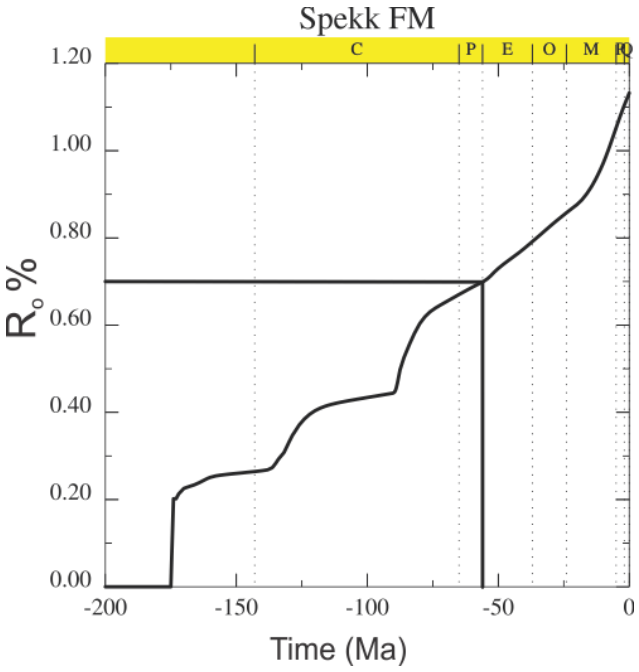

Figure 58: Time- Vitrinite reflectance cross-plot showing start of early oil generation at ca. -105 and peak oil generation is observed at -75 Ma and increases forward in time. An abrupt increase in the coke formation between -20 Ma -0 Ma can be noticed period. As mentioned in the table 5.1, peak oil generation has been taken place recently and the Spekk Formation is still in oil window.